Mapping and Landscape Interpretation of Al Madinah Province, Western Saudi Arabia

Thesis submitted for the degree of
Doctor of Philosophy
at the University of Leicester

by

Ghizayel Almuhammadi

Department of Geography
University of Leicester

2017

Abstract

Mapping and Landscape Interpretation of Al Madinah Province, Western Saudi Arabia

By

Ghizayel Almuhammadi

In relation to the Kingdom of Saudi Arabia, there is very little environmental and geomorphological information. This is especially so in the western region, represented by Al Madinah Province, which remains poorly understood. Therefore, in this study, the never before studied landscape in the east of Al Madinah Province was mapped and interpreted, using multiple approaches in the investigation, in what is considered an important and advanced step in mapping and interpreting landscape. Such approaches contributed to gathering the largest amount of data on this area relating to both the past and present, which provided a clearer and more comprehensive understanding than what had existed for this desert environment in the east of Al Madinah Province. These approaches included:

First, using remote sensing, ASTER GDEM and Landsat 8 multispectral image processing techniques (principle component analysis, band ratioing, and false colour composites) alongside field and laboratory reflectance measurements ASD HH2, helped in understanding the spectral characteristics of deposits, and as such describe composition and mixing of sediments in the image, and infer how sediment is weathered and transported around the study area. This contributed to interpreting the landscape, including provenance, sediment movement, and locations of deposition that have contributed to the principal geomorphological features found in the area. This study demonstrates the relationship between laboratory spectral reflectances, and that of Landsat 8 imagery showing a strong positive correlation (R2=0.84 to 0.89). Consequently, Landsat 8 surface reflectances data was used effectively in mapping different geomorphological units (sand dunes, sand sheets, sand ramps, wadi deposits, slopes, Qa, sabkha, intermountaneous basins, Sahuq plateau, and East Al Madinah plateau) on spectral bases using maximum likelihood supervised classification with overall accuracy of 80.84%. A spectral transect passing through East Al Madinah plateau showed the spectral characteristics of sediments regarding their grain size. Landsat 8 PCA colour composite was found to be the most effective for visual interpreting and describing sediments composition and mixing, and inferred the geomorphic processes

within the study area. In some cases, field spectral measurements might be more effective than laboratory measurements giving reliable spectral signature more comparable with satellite imagery, especially for dikes and similar longitudinal features.

Second, field observations with sediments analysis and OSL dating were used to identify the ages of palaeogeomorphic and palaeoenvironmental conditions. This allows the geomorphological history to be initially interpreted. Moreover, for this otherwise unstudied area, the extent of spatial and regional changes could be ascertained. The results of OSL dating support the existence of wet periods in Al Madinah at 34.2±2.5 ka in Marine Isotope Stage (MIS) 3, and in the early Holocene (9.9±0.6 – 11.6±1.0 ka). These results show that the monsoon rainfall belt extended to latitudes 25° N and 26° N, not just 23° - 24° N. The monsoon rainfall belt did not move from Southern to Northern Arabia over 1800 years, it took place at the same time, in southern, western, eastern, and central areas of the Arabian Peninsula.

Acknowledgements

Furthermore, my appreciation and love goes to my siblings, especially my brother Mohammed for his help and company during the field work phase, as well as my friends for their encouragement.

Table of Contents

List of Figures

List of Tables

Chapter 1. Introduction

The geology and geomorphology of Saudi Arabia are reviewed generally in this chapter. Similarly, the study area, i.e. the area of Al Madinah, western Saudi Arabia, is described, in terms of geomorphology, geology, soil, and climate. This information provides essential background to introduce the research. The research aims and objectives, the importance of the study as well as the thesis structure are also presented in this chapter.

1.1   Physical Characteristics of Saudi Arabia

The Kingdom of Saudi Arabia (KSA) is situated on the Arabian Peninsula, in the far southwestern edge of the Asian continent. Its territory is bounded by latitudes between 16° 22' 46" and 32° 14' 00" North, and longitudes 34° 29' 30" and 55° 40' 00" East (Figure 1.1). Hence, it lies within the dry tropical desert range. KSA covers an area of about 2 million sq. km, representing 70% of the Arabian Peninsula, which in itself is 2.8 million sq. km (Saudi Geological Survey, 2012).

Figure 1.1: Location of Saudi Arabia and Al Madinah; the green box represents the study area.

Source: Main map modified from: Saudi Geological Survey (2012).

Inset map modified from: Wikimedia Commons, *BlankMap-World6.svg*, Public Domain.

Available at: https://commons.wikimedia.org/wiki/Maps_of_the_world (Accessed 1/01/2016).

1.1.1 Geology of Saudi Arabia

From the geological perspective, KSA is divided into two large geological units, namely the Arabian Shelf and Arabian Shield.

1.1.1.1 Arabian Shield

The Arabian Shield is located in the western half of KSA, covering around 32% of the country's area, as shown in Figure 1.2 (Saudi Geological Survey, 2012). The Shield is narrow in its northern and southern extents, measuring around 100km and 200km wide, respectively. However, its central part extends for around 700km (Al-Welaie, 1997a). The Arabian Shield forms part of the Arabian-Nubian Shield. In the early Tertiary Period

(Paleogene), these land masses began to separate from each other due to a fault in the Earth's crust, forming the Red Sea (Al-Shanti, 1993). The Arabian Shield is composed of igneous and metamorphic rocks from the Precambrian. Basalt from the middle of the Tertiary and Quaternary Periods is widespread in the western extents of the Shield (Figure 1.2), resulting from the lava flows that accompanied the appearance of the Red Sea Rift, forming what are known as lava fields or Harrats. These are outflows of basalt formed from the liquid lava of melted rock, which flowed from the Earth's core to the surface at volcanic craters, due to tectonic movements or earthquakes. These lava fields are shown in Figure 1.2 and Figure 1.3. There are also some sedimentary rocks and sediments belonging to the Quaternary period (Saudi Geological Survey, 2012).

1.1.1.2 Arabian Shelf (Platform)

The Shelf is located to the east of the Arabian Shield, and covers around two-thirds or 68% of the area of KSA shown in Figure 1.2 (Saudi Geological Survey, 2012). The Arabian Platform was part of the Tethys Sea. Due to tectonic movements, intermittent transgression-regression cycles of sea water surrounding the Arabian Shield had occurred, leaving behind sedimentary layers. As a result of being buried, these transformed into rocks of increasing thickness, as one travels eastwards (Al-Saqqa, 2004). These sediments were deposited on top of the Arabian Shield rocks from Paleozoic Era, passing through the Mesozoic Era, up to the Cenozoic Era. The sediments formed during the Paleozoic Era (from the Cambrian to the Permian Eras) were distinguished by being consisting principally of sandstone and clays, deposted in a marine environment. In turn, those sediments formed during the Mesozoic and Cenozoic Eras were distinguished by consisting of gypsum rock resulting from evaporation of ancient seas, in addition to sand and valley sediments, as in Figure 1.3 (Saudi Geological Survey, 2012).
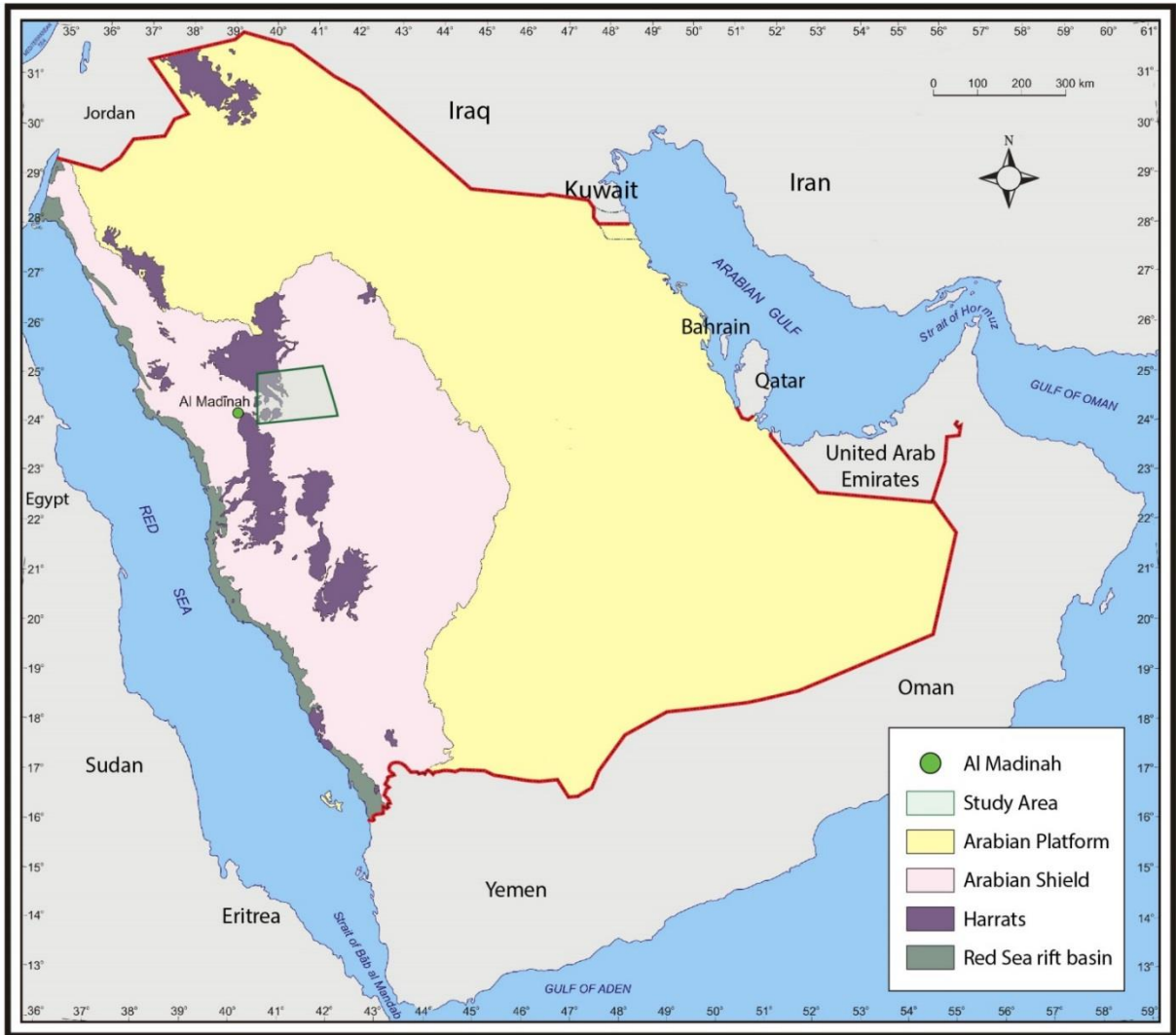
Figure 1.2: Arabian Shield (Platform) and Shelf in Saudi Arabia.

Source: Modified from: Saudi Geological Survey (2012).
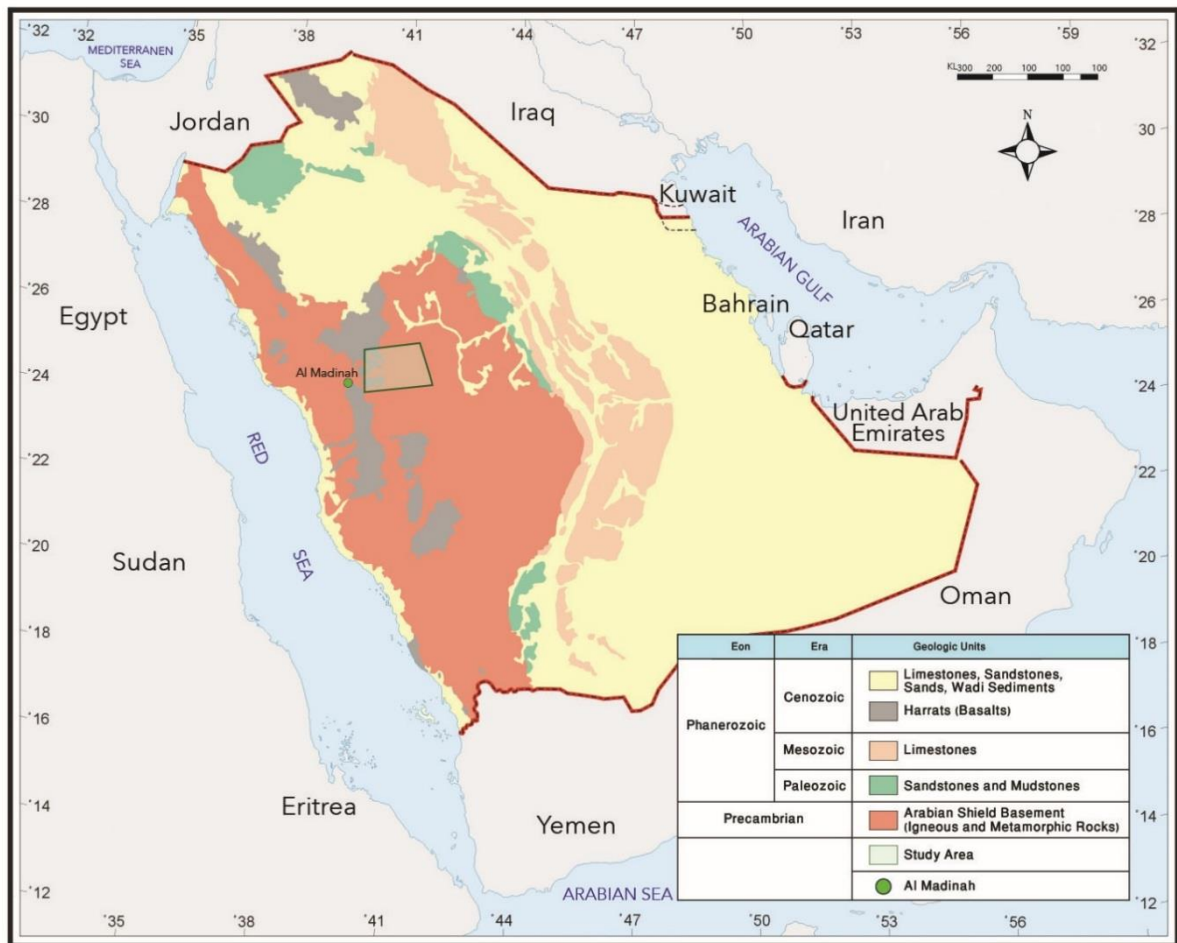
Figure 1.3: Geology map of Saudi Arabia.

Source: Modified from: Saudi Geological Survey (2012).

1.1.2 Geomorphology of Saudi Arabia

The geomorphological features of KSA are the outcome of complex interactions occurring throughout its geological and climatic history (Al-Welaie, 1997a). Indeed, it is possible to summarise the most important geographical surface forms in KSA, in Figure 1.4, as follows:

1.1.2.1 Tihamah Coastal Plain

These plains are level areas of land that do not have significant changes in elevation or many high points. The plains do not tend to be absolutely level, but any slopes are moderate, with few or widely dispersed hills (Al-Welaie, 1997a).

Tihamah Coastal Plain situated in the west of KSA, extends over the length of the Red Sea. It is composed of marine and continental sediments from the Tertiary (Paleogene to

Neogene) and Quaternary periods. It is graded in its slope towards the east. This coastal plain is penetrated by wadis distinguished by steep slopes, and deep channels flowing into the Red Sea. This plain is also distinguished by widespread sabkhas, commonly parallel to the coastline, as well as some sand formations near the coast, and the presence of some smaller lava fields or Harrats within them (Al-Saqqa, 2004).

A sabkha defines a closed depression with a saline surface in an arid environment; mostly composed of sand, silt and clay deposits that are mixed with evaporites. The sabkhas are divided into two types namely coastal or lagoonal that are located adjacent to coastal areas, and inland that are located in continental areas far from the coastal regions (Mahsoub et al., 1999).

1.1.2.2 The Western Escarpment

The Western Escarpment contains high areas that rise to a few hundred or thousands of metres, with extremely steep slopes, and many high peaks (Al-Welaie, 1997a). The Western Escarpment represents a mountainous belt that includes the Hijaz, Al-Sarawat, and Midyan mountain ranges, extending from the Gulf of Aqaba in the north to the border with Yemen in the south, alongside the Tihamah Coastal Plain. The Western Escarpment is distinguished by very steep slopes in the west, towards the Tihamah Coastal Plain, and gradual slopes eastwards, towards the interior of KSA. The Escarpment tilts upwards in the south, where the highest peak is 3015m at Al-Sawdah mountain (Mahsoub et al., 1999).

1.1.2.3 Plateaus

Plateaus are wide, flat topped highlands, with typical sudden height changes between the plateau surface and the adjacent terrain (Karbal, 2011). The plateaus in Saudi Arabia lie to the east of the Western Escarpment, and cover large tracts of KSA territory. These slope generally to the north and northeast. They are divided into the Western plateaus represented by Najran and Asir plateaus, the Hijaz plateau, and Hasmi plateau; the Central plateaus are represented by the Najd plateau; the Eastern plateaus are represented by the the As-Summan plateau and Al-Dibdibba plateau; and the Northern plateau is represented by the Al-Hajara plateau, and the Al-Hammad plateau (Saudi Geological Survey, 2012).

1.1.2.4 Sand Dunes

Ridge or mound features resulting from the deposition of wind-driven loose sand are called sand dunes. These could be a few metres in size, or may even stretch over a number of kilometres. Dunes may be found as isolated units or grouped to form dune fields (Tsoar and Pye, 2009). Such dune fields are referred to by the Arabic word, Nafud. In turn, a concentration of many dune fields results in a sand sea. Indeed, in KSA, sand is the most common surface sediment, present in four key sand seas (figure 1.4), namely (Al-Welaie, 1997b):

A. Al-Rub Al-Khali: This is found in the southeast of KSA, and is one of the largest contiguous sand fields in the world, as it covers an area of about 600,000 sq. km.

B. Al-Nafud: This is the second largest sand field in KSA, after Al-Rub Al-Khali desert. It is found in the northwest of KSA, covering an area of 64,630 sq. km approximately.

C. Al-Dahna: This is essentially a narrow belt of sand, in the form of a bow, extending 1200km from the Al-Nafud in the north to Al-Rub Al-Khali desert in the south.

D. Al-Jafurah: These extend from the northeast of KSA in the form of a strip paralleling the Arabian Gulf coast, and widening as one goes southwards, until it merges with the Al-Rub Al-Khali desert.

In addition to the sand seas there are large sand fields, in addition to Nafud Al Thuwayrat, Nafud As-Sirr, and Nafud Al Gamas, are mostly found in the east of KSA (the Arabian Shelf). In contrast, sand fields are notably less in the Arabian Shield in the west of the country, where they are smaller and cover less area, compared to those in the east (the Arabian Shelf). In addition, there are some dunes along the Tihamah Coastal Plain (Saudi Geological Survey, 2012; Al-Welaie, 1997b).

1.1.2.5 The Eastern Coastal Plains (the Coastal Plain of the Arabian Gulf)

The Arabian Gulf Coastal Plain is bounded by the Gulf coastline in the East and the As-Summan plateau to the West. This is a flat plain mostly covered by sand, with widespread sabkhas, especially near the coast (Al-Saqqa, 2004).

1.1.2.6 Wadi Systems

The Arabic term used to describe a valley is Wadi. Indeed, it is used to indicate a dry riverbed, where typically, water may be present as an irregular stream or substantial flow during severe rainstorms (Salama, 2013). Many wadi systems are found spread across the Kingdom's land surface. The majority were formed during the wetter climatic phases in the past; for example, Wadi Al-Rimah and Al-Batin (Figure 1.4), which is a grand wadi. The wadi's channel begins at the Harrat Khaybar lava field, situated to the east of Al Madinah region. The wadi runs eastwards and ends at Al-Asyah area, where it is blocked by Nafud Al Thuwayrat. On the other hand, Wadi Al-Batin runs towards the north east, continuing beyond the eastern border of Saudi Arabia with Iraq. In fact, Wadi Al-Rimah used to run towards the Arabian Gulf through its extension of Wadi Al-Batin. However, following dry phases in the past, sand (represented by Nafud Al Thuwayrat) closed the wadi's channel, separating Wadi Al-Batin from Wadi Al-Rimah (Al-Welaie, 1997a).

Wadi Al-Sahba and its tributaries, Wadi Hanifah and Wadi Nisah, comprise another large wadi system draining the central Arabian Shield, which also once reached the Arabian Gulf during the wetter phases in the past (Figure 1.4). At present, Wadi Al-Sahba's channel is buried under sand sediments that close it completely as it runs towards the southeast. In addition, Wadi Al-Dawasir and Wadi Al-Himd are considered among the key wadis in KSA (Figure 1.4) (Mahsoub et al., 1999). Indeed, Wadi Al-Dawasir's tributaries, such as Bishah, Raniyah, and Tathlith originate on the Asir plateau. This wadi runs to the east, passing through the Tuwayq plateau, until it terminates at the beginning of Al-Rub Al-Khali. During the wetter phases of the past, this wadi used to extend to the Arabian Gulf (Edgell, 2006; Mahsoub et al., 1999). As for Wadi Al-Himd, this is about 450km long, and originates at the escarpment near Al Madinah, and runs towards the northwest, until it ends in the Red Sea (Mahsoub et al., 1999).
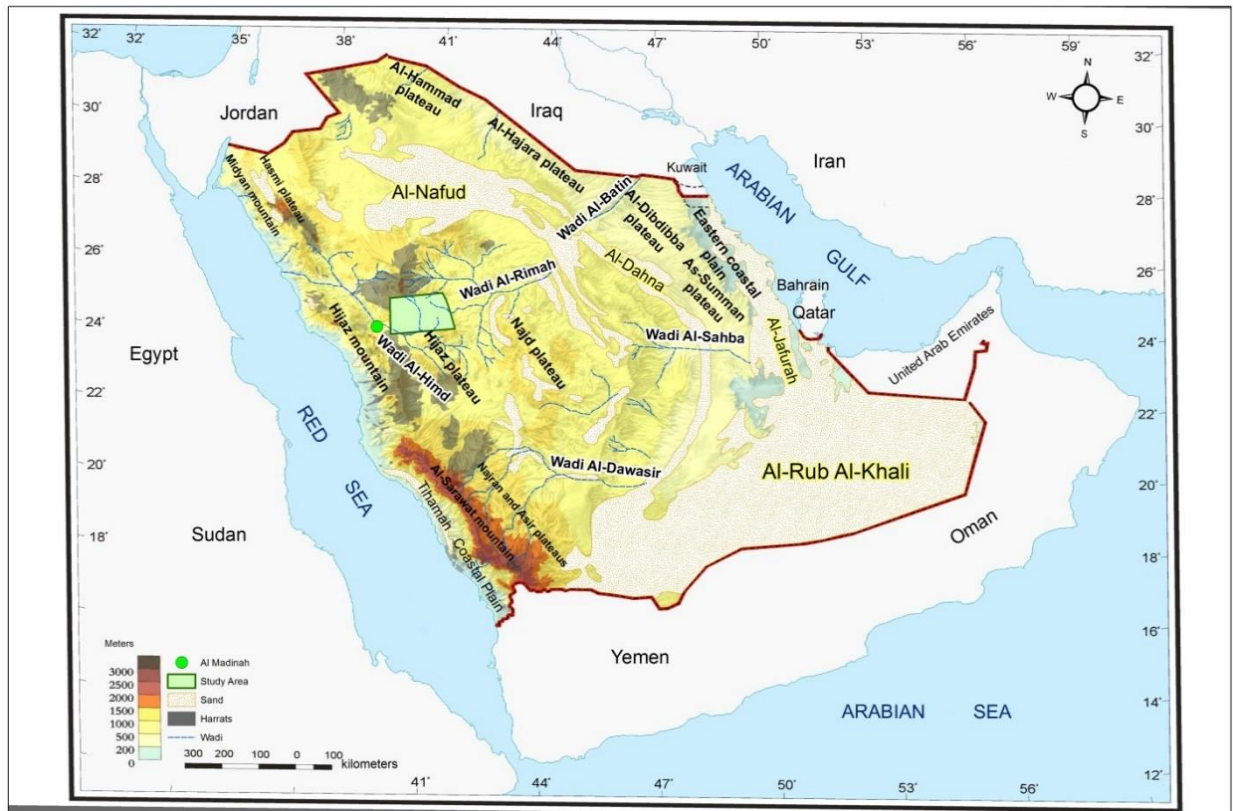
Figure 1.4: Geography of Saudi Arabia.

Source: Re-drawn and modified from: Saudi Geological Survey (2012).

1.2 Physical Characteristics of the Study Area

The Al Madinah Province is situated in the west of the Kingdom of Saudi Arabia. This study focuses on the eastern part of this province, which extends from the eastern area in the vicinity of Al Qassim 41° 38'15.33"E to Qa Hadawda to the West 39° 58' 49.99"E (Figure 1.1).

1.2.1 Geology of the Study Area

The study area lies in four quadrangles of 1:250,000 scale geologic maps that are Khybar (GM50), Nugrah (GM28), Al Madinah (GM52), and Al Hissu (GM58) (Kingdom of Saudi Arabia Deputy Ministry for Mineral Resources, 1981) (Figure 1.5). Table 1.1 shows a

9

compiled geologic column of the study area. A geologic map of the study area compiled from the pre-mentioned quadrangles along with field investigations and Landsat image classification is shown in Figure 1.6. The following statements discuss these rock assemblages chronologically arranged from older to younger.

1.2.1.1 Older Basement (**MIDDLE PROTEROZOIC**)

In the Precambrian the Middle Proterozoic is represented by an old granitic basement, large enclaves of granitized gneiss and amphibolite, and several belts of massive layered gabbro and serpentinized peridotite (Delfour, 1967; Dhellemmes & Delfour, 1980).

1.2.1.2 Ajal Group (**MIDDLE PROTEROZOIC**)

This group comprises alternating layers, decimeters to several meters thick, of fine-grained biotite-leptite, biotite-amphibole schist and feldspathic amphibolite. In many cases the rocks have undergone retrograde metamorphism resulting in the development of chlorite. Decimeters to meter size post-metamorphic folds are cut by veins of leucocratic granite and pegmatite-aplite (Delfour, 1976).

Table 1.1: Generalized lithostratigraphic divisions of the study area

GEOTIME	GROUP, FORMATION	
CENOZOIC	Quaternary	
	Tertiary	
LOWER PALEOZOIC	Cambrian-Ordovician	
UPPER PROTEROZOIC	Jibalah Group	Jifn Fm.
		Umm al Aisah Fm.
	Murdama Group	Hadiyah Fm.
		Hibshi Fm.
	Shammar Group	Malha Fm.
		Kuara Fm.
	Furayh Group	Dawnak Fm.
		Qidirah Fm.
		Murayr Fm.
	Al Ays Group	Difayrah Fm.
		Urayfi Fm.
		Farshah Fm.
	Hulayfah Group	Nuqrah Fm.
		Afna Fm.
	Urd Group	Ophiolitic Complex
MIDDLE PROTEROZOIC	Ajal Group	Rharaba Complex
	Older Basement	Granite &Orthogneisses

Source: Kingdom of Saudi Arabia Deputy Ministry for Mineral Resources (1981).
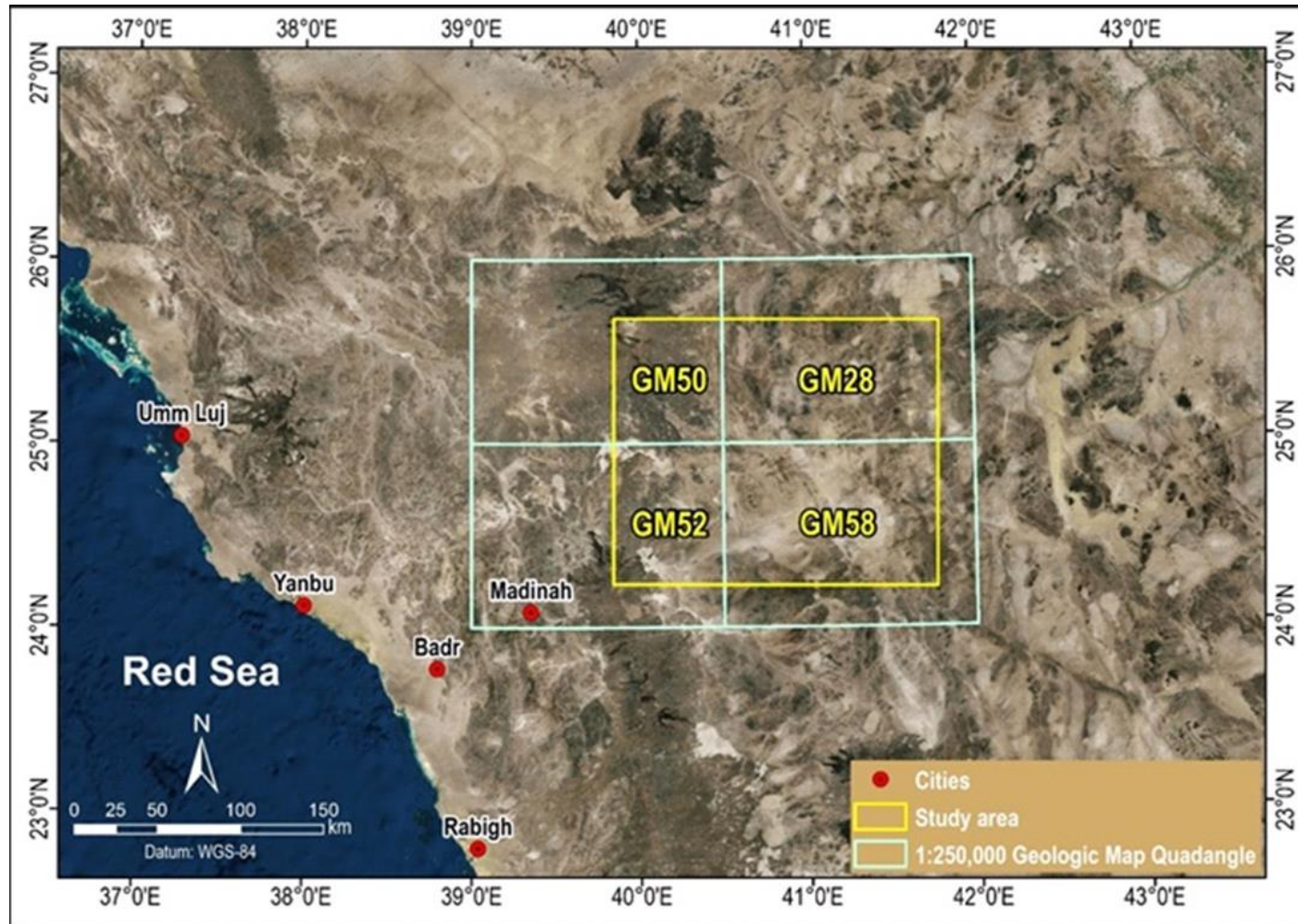
Figure 1.5: The study area location regarding to Kingdom of Saudi Arabia Deputy Ministry for Mineral Resources geologic maps quadrangles (GM50, GM28, GM52, and GM58) of scale 1:250.000.

Basemap from: ESRI World Imagery under ArcMap.
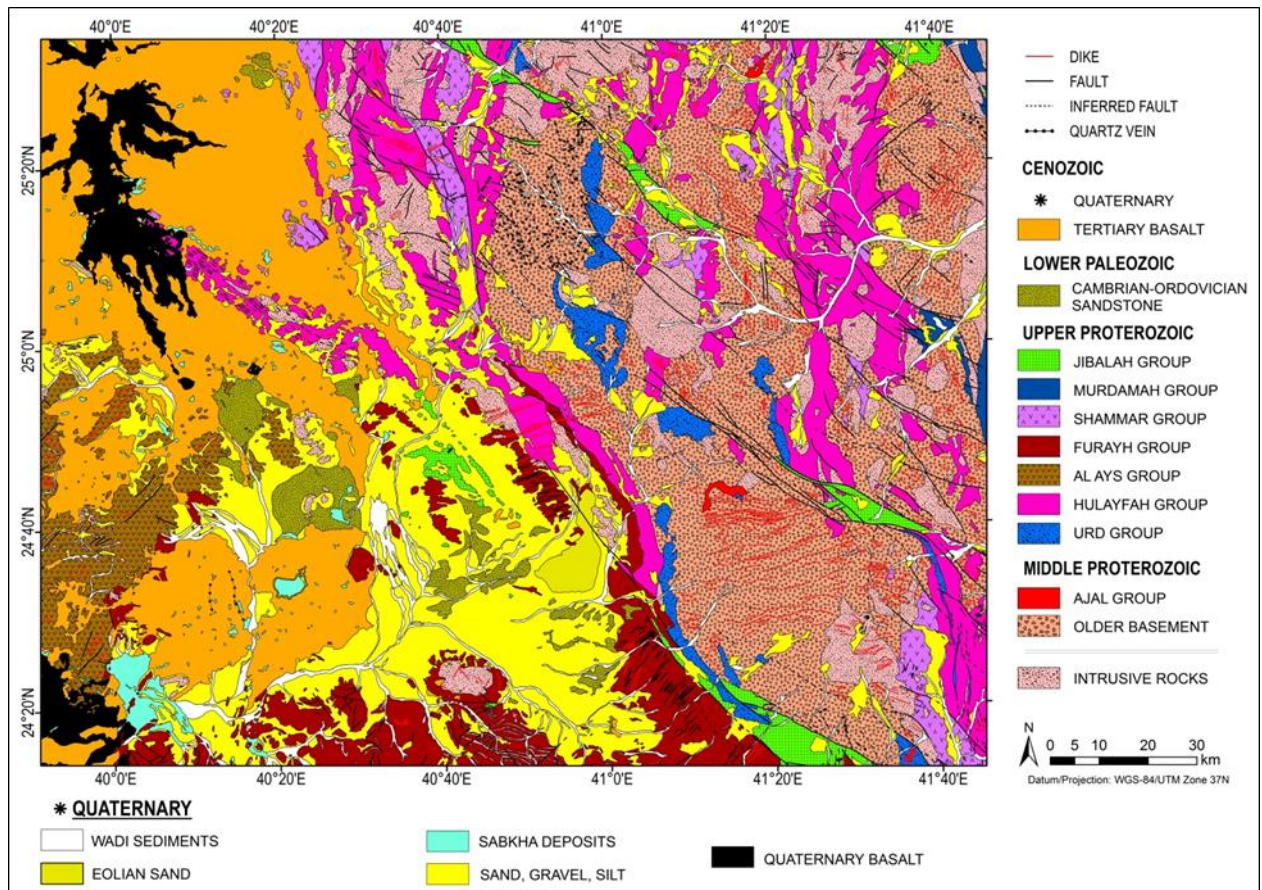
Figure 1.6: Geological map of the study area re-drawn and modified after the Kingdom of Saudi Arabia Deputy Ministry for Mineral Resources geologic maps quadrangles (GM50, GM28, GM52, and GM58), 1981, scale 1:250.000.

1.2.1.3 Rharaba Complex (**MIDDLE PROTEROZOIC**)

This is an ultramafic complex (generally layered gabbro with minor anorthosite and serpentinite) occurring as isolated outcrops a few meters across or as massifs up to several kilometres in size in more or less lenticular layers having thicknesses from a few decimetres to several tens of meters with weak evidence of metamorphism showing synclinal folding having a main northwest-striking axis (Delfour, 1976).

1.2.1.4 Urd Group Ophiolite Complex (**UPPER PROTEROZOIC**)

This is an alpine-type ophiolitic suite composed mainly of serpentinite, listuanite (quartz-carbonate rock), metamorphosed gabbro and basalt (Delfour, 1976).

1.2.1.5 Hulayfah Group (UPPER PROTEROZOIC)

According to Delfour (1976), the Hulayfah Group comprises steeply folded and subordinate sedimentary rocks characterized by important lateral facies variations, mostly in the volcanic assemblages that in places can be divided into.

1.2.1.5.1 Afna Formation

The lower part of Hulayfah Group (and can be locally absent) is composed of two subunits: the first is detrital and sedimentary with some pyroclastic deposits, and the second is essentially a sequence of basic and intermediate lava flows with related pyroclastics (Delfour, 1976).

1.2.1.5.2 Nuqrah Formation

The upper part of Hulayfah Group is represented by three subunits: the first is made up of acidic pyroclastics with some intermediate flows; the second consists of sedimentary deposits alternating with acidic, intermediate, and basic lava flows with related pyroclastics; and the third is composed of conglomerate and volcanic sandstone (Delfour, 1976).

1.2.1.6 Al Ays Group (UPPER PROTEROZOIC)

According to Pellaton (1981), the Al Ays Group consists principally of mafic to silicic volcanic rock and derivative epiclastic and detrital sedimentary rock. The Al Ays Group is generally intruded by younger igneous intrusions including layered gabbro complex, granite batholiths, granodiorite and diorite, and isolated gabbro stocks. Their chronologic relationships are unknown (Pellaton, 1981).

Three formations related to this Group have been recognized within the study area:

1.2.1.6.1 Farshah Formation

This formation comprises mostly andesitic volcanic rocks and pyroclastics. It consists of subordinate pyroclastic rock and andesitic lava measuring several thousand metres in thickness. The Urayfi Formation overlays this conformably, while showing gradational contacts (Pellaton, 1981).

1.2.1.6.2 Urayfi Formation

The Urayfi Formation consists of epiclastic rock and interbedded volcanic rock several thousand meters thick in which, in places, a detrital sedimentary member and a silicic

volcanic member can be mapped. The Urayfi Formation correlates with the Ghamrah and Mahaynah Formations in the khaybar quadrangle to the north (Dhellemmes and Delfour, 1980). The Mahaynah Formation represents the rhyolite-ignimbrite member of the Urayfi Formation (Pellaton, 1981).

1.2.1.6.3 Difayrah Formation

Alternating fine-grained detrital rock and rhyolitic volcanic rock are the principal constituents of the Difayrah Formation. The volcanic layers consist of beige rhyolite, ignimbrite, and rhyolitic tuff, intercalated in sedimentary layers, that were deposited under water. The sedimentary layers comprise fine-grained greywacke, siltstone, and epiclastic sandstone, with thin layers of chert and marble (Pellaton, 1981).

1.2.1.7 Furayh Group (UPPER PROTEROZOIC)

The Furayh Group unconformably overlies the Al Ays Group. The Group comprises, in ascending order:

1.2.1.7.1 Murayrr Formation

The formation is named from Jabal al Murayr, where an anticline exposes several hundred meters of polymictic conglomerate and sandstone strata conformably overlain by the Qidirah Formation on each side. The conglomerate contains pebbles and boulders, up to 60 cm in size, of rhyolite, andesite, granite and jasper in a sandy sized matrix interbedded with purplish-brown and green lithic sandstone with clear bedding (Pellaton, 1981).

1.2.1.7.2 Qidirah Formation

This formation consists of mafic volcanic (andesite and dark-gray to green amygdaloidal basalt containing chlorite and epidote) rocks, varying in thickness from several thousand to several hundred meters (Pellaton, 1981).

1.2.1.7.3 Dawnak Formation

This formation is represented by sandstone with conglomerate, tuff, and marble. The main outcrop in the southeast of the area is represented by thick sequences of several rocks including greywacke, siltstone, lithic sandstone, sandstone, conglomerate and marble. The Furayh Group is generally intruded by younger igneous intrusions represented by batholiths and plutons of calc-alkalic, alkali and peralkalic granite in addition to small intrusions of

diorite, microgranite, granophyre and rhyolite, together with dikes and stocks of microdiorite, micromonzonite and microgabbro (Pellaton, 1981).

1.2.1.8 Shammar Group (UPPER PROTEROZOIC)

The Shammar Group is distributed as a discontinuous north-trending band partly to the east of and partly within the Bir Abu Salim granitic terrain. It is composed mainly of ignimbrite, flows of amygdaloidal andesite, and andesitic tuff and breccia (Pellaton, 1981).

The Shammar Group comprises two Formations:

1.2.1.8.1 KuaraA Formation

This formation generally begins with a basal conglomerate, followed by alternating conglomerate, volcanic sandstone, rhyolite, and andesite (Pellaton, 1981).

1.2.1.8.2 Malhan Formation

This formation is mostly an accumulation of rhyolite flows or ignimbritic sheets with minor clastic rocks.

The Shammar Group is intruded by younger riebeckite granophyre stocks from which thick dikes of microgranite, with feldspar and amphibole phenocrysts, extend into the volcanic strata (Pellaton, 1981).

1.2.1.9 Murdama Group (UPPER PROTEROZOIC)

According to Pellaton (1981), the Murdama Group consists of sandstone, marble and andesitic volcanic including five formations:

1.2.1.9.1 Hibshi Formation

This formation comprises two subunits; a basal very poorly sorted polygenic conglomerate composed of well-rounded and packed cobbles and boulders of various rock types (commonly granite, granodiorite, rhyolitic tuff rhyolite, and porphyritic andesite) cemented by arenite cement. The conglomerates may reach a thickness of 4000 m in some places (Pellaton, 1981).

The upper subunit, with an average thickness of 3000 m, is composed of alternating layers (decimeters to meter thick) of sandstone with abundant detritus, siltstone, pelite and a conglomerate with pebbles of rhyolite and granite (Pellaton, 1981).

1.2.1.9.2 Hadiyah Formation

In Jabal Umm Sammah, the Hadiyah Formation is exposed in a 2,000 m thick succession of decametric to metric layers of volcanic sandstone, microconglomerate, and a conglomerate rich in granitic and rhyolitic pebbles. In the Al Humayliyah synclinorium, the Murdama rocks folded during the Ar Rimah orogenic phase were subsequently invaded by large intusions and numerous stocks of granite and diorite (Pellaton, 1981).

1.2.1.10 Jibalah Group (UPPER PROTEROZOIC)

In the Hissu quadrangle, the Jibalah Group is found largely in three belts and contains the largest exposure of Jibalah Group rocks presently recognized in the northern part of the Arabian Shield (Delfour, 1966). The Jibalah Group is the youngest unit of the Upper Proterozoic (Delfour, 1967, 1970). It includes two formations:

1.2.1.10.1 Umm AL Aisah Formation

The base of Umm Al Aisah Formation is represented by gray-pink coarse-grained arkosic sandstone and fine-grained conglomerate, followed by several amygdaloidal andesite and basalt flows with an overlay of cherty limestone and fine-grained sandstone. In several places, parent subvolcanic intrusions with compositions varying from diorite to gabbro invade the volcanic rocks (Delfour, 1967, 1970).

1.2.1.10.2 Jifn Formation

The Jifn Formation may exceed 2,000 m thick, and begins with light-colored fine-grained sandstone and siltstone, commonly siliceous, overlying the cherty limestone unit of the Umm al Aisah Formation. The formation then continues with an interbedded sequence of sandstone, tuffaceous sandstone and andesite flows (Delfour, 1967, 1970).

1.2.1.11 Cambrian-Ordovician Sandstone (LOWER PALEOZOIC)

Scattered table-like outcrops of horizontal sandstone beds of a Cambrian-Ordovician age (Brown et al., 1963), have been allocated near Nufud Al Qawz, Wadi Al Hinakiyah, around Sabkhat Hurumah and north Shaib Nijar. The strata consists mainly of reddish-purple to whitish-beige, commonly cross-bedded sandstone with a carbonate cement.

1.2.1.12 Tertiary Terraces (Paleogene to Neogene) (CENOZOIC)

Long terraces as much as 5 m thick of unconsolidated gravel, sandy clay, and gypsum beds lie a few meters above the present wadi floor scattered localities. Most of the gravel consists of well-rounded pebbles and cobbles of white quartz and other hard Precambrian rock types such as porphyritic rhyolite, microgranite, and quartz, and of Tertiary vesicular basalt in a sandy matrix (Pellaton, 1981).

1.2.1.13 Tertiary Basalt (Paleogene and Neogene) (CENOZOIC)

The western part of the Arabian Peninsula is one of biggest alkali basalt provinces in the world with an approximate area of 180,000 km^2 (Coleman et al., 1983). These lava fields (known as Harrats) were formed at the same time as the Red Sea rifting (Camp and Roobol, 1991). Generally, Harrats are composed of alkali olivine basalt typically derived from rift volcanism. Tertiary and Quaternary basalt in the Al Madinah quadrangle forms part of the north-south alignment of basalt plateau (Harrats) between lat 22° and 27° N in the western part of the Arabian Shield, covers an area of 500 km^2 (Pellaton, 1981). Tertiary basalts spread within the western fringes of the study area (east of Qa Hadawda).

1.2.1.14 Quaternary Deposits (CENOZOIC)

Quaternary deposits in the study area comprise surficial deposits of varied fluvial, aeolian, and lacustriane origin and are commonly closely intermixed. According to Kingdom of Saudi Arabia Deputy Ministry for Mineral Resources (1981), the Quaternary deposits include:

1-Wadi alluvium of gravel, sand and clay; these deposits follow the present-day drainage pattern and cover many parts of the study area. Also, terraces of poorly consolidated boulders, pebbles, and gravel occur in and around main wadis, and alluvial fans.

2-Extensive gravel mixed with gypsiferous clay and aeolian sand are commonly localized on pediments between the foothills and the wadi courses (for more information about these features see 1.1.2 & 1.2.2).

 3-Few areas of sabkha, essentially gypsiferous clay and Qa, appear in the west of study area. Qa is defined as a flat bottomed surface, closed depression (Plain) that is covered with fine silt and clay and is devoid of plant cover (this last feature distinguishes Qa from Sabkha which is defined in paragraph 1.1.2) (Al-Welaie, 1997a; Edgell, 2006). In addition, there is

a large system of sand dune (Nafud), and also small aeolian dunes and a thin layer of aeolian sand covered flat land (Pellaton, 1981).

1.2.2 Geomorphology of Study Area

Figure 1.7 presents a satellite image of the key landforms in the study area. In the western part, volcanic lava fields (Harrats) are wide spread, such as Harrat Hurumah, containing a wide volcano crater measuring 7000m in diameter, and a depth of around 50m. This volcanic crater occupies the Harrat Hurumah Sabkha, comprising sand, clay, and salt sediments. Moreover, small sabkhas are scattered across the Quaternary basalt flows.

The depression called Qa Hadawda lies to the southeast of Hurumah. It is a low-lying valley, into which flood waters from the Al Hinakiyah, Luwayy, Al Mahir, and Shaib Um Markhah wadi systems flow; these wadis together form one wadi system called Wadi Al Makhit, which flows into this depression. Shaib Nijar, situated to the west of Harrat Hurumah also flows into this depression. On the other hand, to the east of the study area, we find Wadi Sahuq, which begins at Al-Buwaybat mountains, and runs eastwards to connect with Wadi Al-Rimah.

Sand also covers parts of the study area, including the Nufud Al Qawz sand dunes that extend longitudinally in its northern part, and then widen in its southern part. In the area, 19km west of Nufud Al Qawz, we find sand dunes spread across an estimated area of around 3 sq.km. North of Nufud Al Qawz by about 30km, we encounter a sand accumulation spread over an estimated area of 2 sq. km. Sand ramps and sand sheets appear in different parts of the study area. Sand ramps are defined as sedimentary accumulations of a dune-scale usually found at mountain fronts and composed of a combination of aeolian sands and deposits resulting from hillslope and fluvial activities (Bateman et al., 2012). Indeed, sand sheets result from the accumulation of sand due to wind activity. Sand sheets exhibit an even or mildly wavy surface, and an absence of any significant dune topography (Tsoar and Pye, 2009).

Alluvial fans are geomorphological landforms which are usually formed where a valley channel emerges from mountainous uplands into lower and more gentler areas at the mountain front; sedimentary deposits in the fan form a radiating cone – like (or a triangular shape) with its apex (coarse grains) closer to the mountainous uplands, and its base (finer grains) closer to the lower flatter areas far away from the mountainous uplands (Thomas,

19

2011; Karbal, 2011). Desert pavement, also known as reg surface/ serir is found at different parts in the study area; and represents extensive sheets of gravel with little or no vegetation cover (Thomas, 2011). Formed by deflation; a thin and continuous sheet-like veneer of pebbles or gravels forms a surface armour, that demonstrates the erosional strength of the wind which can remove finer particles, and leave a residual (pebble or gravel) surface (Edgell, 2006).
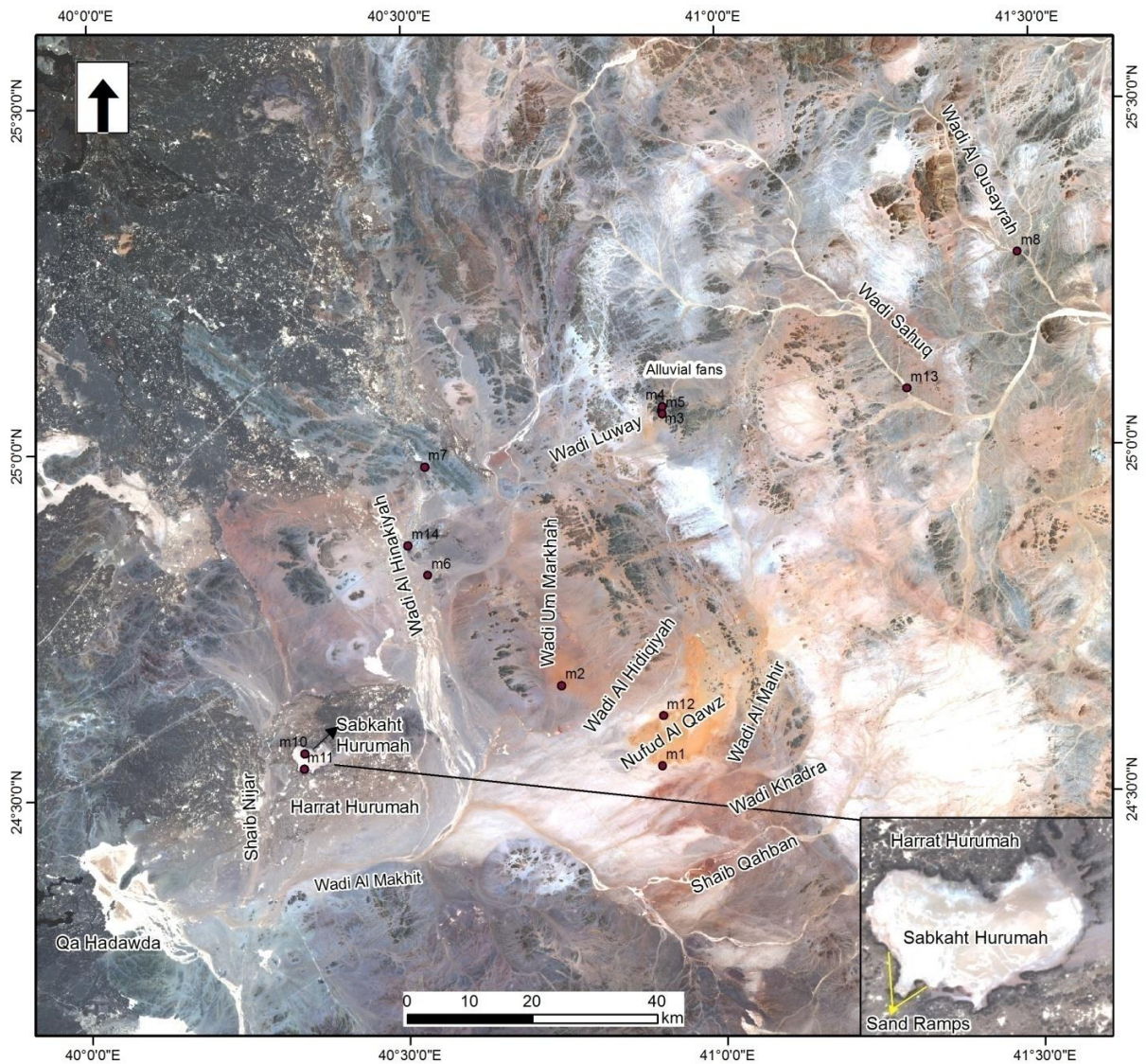
Figure 1.7: Satellite image of the main landforms in the study area, sample sites are marked with red markers.

1.2.3 Climate of the Study Area

According to Presidency of Meteorology and Environment Protection (2014), (Table 1.2), the current study area is located within the dry tropical climatic zone, distinguished by high temperature with an annual mean of 28.5°C. Temperatures are somewhat low in winter months and extremely high in the summer, with a monthly mean of 17.9°C for the coldest month, January, and 36.8°C for the hottest, August. Daily temperatures during the summer months commonly exceed 42°C. Relative humidity is very low, with an annual mean of

21

23%, due to high temperature, distance from water surfaces, low precipitation, and little plant cover. Relative humidity rises in winter months, reaching 39% in December, and drops to 12% in the summer month of June.

Table 1.2 below from Presidency of Meteorology and Environment Protection (2014) shows that the annual mean wind speed is 6 m/s, where the winter mean is 5 m/s and the spring and summer means are 7 m/s. Westerly winds prevail in the summer and Easterly winds in the winter. Annual mean rainfall is low at 4mm, as the study area lies within the Tropic of Cancer, and a continental region, and so is subjected to dry winds for the majority of the year. Precipitation is quite variable from year to year, and in any month. There may be sudden bouts of strong rainfall of short duration. However, it may be said that summer months are very dry, and any precipitation is the exception. However, rain may be expected in spring, where 11.6mm is recorded in November. Spring rainfall is convective type linked to rainy thunderstorms resulting from heating of the Earth's surface, and occurrence of instability in the surrounding air. The other seasons where rain may be expected are autumn and winter. Precipitation in these seasons are of the cyclonic type caused by low pressure zones passing over the Mediterranean Sea from west to east (Talbah, 2002).

Table 1.2: The annual climatological elements in the study area for the period 1970 to 2014

Month	Temperature	Relative Humidity	Wind speed	Wind direction	Rain (mm)
JAN	17.9	38	6	E	6.9
FEB	20.4	31	6	W	2.5
MAR	24	25	7	W	8.5
APR	28.5	22	7	WSW	9.9
MAY	32.9	17	6	W	5
JUN	36.1	12	7	W	0.3
JUL	36.4	13	7	W	0.8
AUG	36.8	15	7	W	2.6
SEP	35.3	14	6	W	0.2
OCT	30.2	19	5	E	3.1
NOV	23.9	33	6	E	11.6
DEC	19.4	39	6	E	6.2
Average	28.5	23	6	/	4.8

Source: Presidency of Meteorology and Environment Protection (2014).

1.2.4   Soil of the Study Area

In general, soils in the Al Madinah region are immature due to the arid climate and the slow processes of chemical and physical decomposition. Moreover, many parts of the study area are characterised by high salinity and contain a low percentage of organic matter (Al-Saharif, 1998).

According to the Atlas Soil Classification Map for Saudi Arabia (1984), the soils of the study area in sabkhas and depressions appear as loamy or clay, deep, high salinity soils with low porosity. In most areas there is salt layer on the surface, and the slope varies from 0-1%, and hence, is liable to flooding. In the volcanic lava fields, calciorthids and camborthids soils appear. These are loamy-skeletal, deep soils of 0-15% slope, ranging from low to high

salinity. Normally, gravel, large stones, and broken sharp-edged rocks are scattered over all parts. In the water channels and wadi terraces, calciorthids soils appear, which is loamy-sandy, deep calcareons, non-saline to medium salinity soil. This covers the desert pavement layer in some parts, with 0-5% slope and is liable to flooding. In the fluvial plains, and intermittent wadi water channels, torrifluvent soils appear. This is a deep soil, deposited in the form of loamy-sand layers, varying from non-saline to low salinity, and is liable to rare floods, with a slope of 0-5%. This soil, present in the wadi channels and terraces, and fluvial plains is considered the best soil type in Al Madinah region (Al-Saharif, 1998). A deep sandy soil appears in the sand dune areas. Moreover, in semi-flat and low slope plains (0-3%), calciorthid soils appear, representing a deep, loamy soil, which is highly saline in some areas. It is interspersed by rock outcrops, and small hills, and covers the desert pavement in most parts. The study area also contains areas of shallow, loamy, loamy-skeletal and deep, loamy, semi-flat soil, as well as rocky expanses found on escarpments, mountain edges, hills, and sedimentary fans. The soil consists of either calciorthids, i.e. calcareons, non-saline to medium saline soil, covering most parts of the desert pavement, or torriorthent type soils, present in small areas; this is a loamy, skeletal, shallow soil of low to medium salinity (Ministry of Agriculture and Water, 1984).

1.3   Study Area

The Al Madinah province lies in the west of the Kingdom of Saudi Arabia. The study will focus on the eastern part of Al Madinah province, which extends from its eastern boundaries to Qa Hadawda to the west (Figure 1.1, 1.7).

There are several reasons for choosing this particular area: first, the area is quite poorly mapped and has not been subject to any prior study, secondly, the area contains different landforms and deposits relating to the Quaternary period, which can be dated using OSL. As a result, been able to establish a new chronology of this region's late Quaternary landforms. For this purpose, thirteen sections were selected to study the Quaternary landforms spread over the study area (Figure 1.7). These comprise sections of fluvial deposits in Wadi Al Hinakiyah, Wadi Sahuq, and Wadi Luwayy. In addition, sections of palaeolake deposits preserved in Sabkhat Hurumah, and the interdune to the west of Nufud Al Qawz were investigated. Sections were made in aeolian deposits inside the wall of the crater of Hurumah

volcano, and a section in the slope wash deposits in the basin of Shaib Um Markhah west of Nufud Al Qawz.

This study was performed in the area east of Al Madinah province to contribute—in addition to what has been mentioned above—to achieving the following:

1- Produce geomorphological maps describing the surface, and to fill the gap in this type of data, and their use potentially as a primary tool in management of land, and risk management.

2- Gather the most data as practicable on the geomorphological processes that have acted on the landforms, and the evidence for environmental change witnessed in this area, east of Al Madinah province, which would enable better understanding of the past.

1.4 Aims and Objectives of the Study

This research has two key aims:

First, to employ data from remote sensing and field research to identify the type and map the distribution of the key geomorphological features and surface materials and identify sources of sediments, sediment transport pathways and depositional sites to subsequently interpret the landscape of the study area.

This aim addresses the relationship between Landsat spectral reflectance and ground based hyperspectral data of desert landforms and surface materials in the area of interest to help understand the spectral characteristics of deposits. This helps in understanding the use of image analysis and spectral information for mapping and describing the composition and mixing of sediments and inference as to how sediment is weathered and transported around the study area, as well as geomorphic processes occurring in this area.

Second, to employ the maps produced, field observations as well as laboratory results relating to the deposits preserved in the sectors of the study area, to determine the palaeogeomorphic and palaeoenvironmental conditions during the late Quaternary period that have prevailed in the area, and which have contributed to the development of the geomorphological features until they attained their current form. This aim seeks to deduce the effect and extent of the monsoon precipitation in the late Quaternary period over this part of Saudi Arabia, which is a contested point in the scientific literature.

In pursuit of this aim, both mineral and physical sediment properties are studied in order to establish an in-depth understanding of the conditions that prevailed during their formation, and to gain knowledge of the changes between aeolian and fluvial regimes, and the development of geomorphological features over time. Moreover, OSL dating allows the time of formation of these deposits to be deduced. In addition, comparing the sediment/ environmental results of the study area to published data from neighbouring regions and countries will allow determining the trend of environmental changes spatially, and also over time; this helps in determining the geomorphological processes that have occurred in the study area. Moreover, it allows deducing when and to what extent the monsoon rainfall in Al Madinah and Saudi Arabia occurred during the late Quaternary period.

1.5   Importance of the Study

Data describing the characteristics of the landscape are essential in providing indications as to the changes resulting from the varying conditions affecting the study area. Therefore, scientific study of the landscape aids in establishing knowledge of our current environment, which is a result of present and past conditions, and which can then be used to predict future processes and landscapes.

A fundamental tool in generating the data underpinning the study of the landscape and environment is geomorphological mapping. The characteristic maps generated through these techniques are graphical representations of the landscape, portraying the surface, sub-surface materials, and landforms. The geomorphological map is more than a data presentation tool, but also a research approach that is essential in understanding landscapes as well as the elements of landforms, in terms of the processes that act on them, and their consequent development. For this reason, fieldwork is an essential initial ground verifying step towards the production of a geomorphological map.

In relation to the Kingdom of Saudi Arabia (Figure 1.1), we find that there is very little environmental and geomorphological information, especially in the western part of KSA, represented by Al Madinah Province, which remains poorly understood (Figure 1.1, 1.7). The deposits preserved in the terrain of the region have never been studied until now and maps of the area do not contain much in the way of geomorphological information and details. These deposits preserved in the terrain of Al Madinah include wadis, alluvial fans,

sand dunes, sand sheets, slopes, Qa, and sabkha. In this regard, geomorphological mapping is a powerful scientific tool by which the constituents and distribution of the above-mentioned surfaces can be recorded. It can be used to determine both past and contemporary processes, and also identify the relative stratigraphic ordering of the landforms (Cooke and Doornkamp, 1990). The need for an accurate geomorphological map covering the study area and highlighting the different geomorphological units with a reasonable accuracy, wide coverage, created using a cost effective method and interpret the landscape were the principal motivations of the current study.

Remote sensing is currently considered as a highly effective and important tool for studying environmental and geomorphological changes. This has proven quite indispensable at this time, and its use with GIS systems has allowed the production of clear geomorphological maps for any area on the Earth's surface, large or small. In addition, other uses include identifying the nature of the landscape, monitoring changes, and establishing the relationships of the surface phenomena with each other (White et al., 2001; Al-Juaidi, 2003; Parker et al., 2006; Hamad, 2010; Al dughairi, 2011; Al-Juaidi, 1997).

The developments in GIS software applications leading to extensive use and powerful graphical features have been joined along with the wide availability of data provided by remote sensing platforms, such as satellites, in the form of images and digital elevation data, to enable detailed information to be extracted on landforms and surface features covering wide areas. This holds great promise in advancing geomorphological surveys, as such remote sensing data is brought into operational, day-to-day use (Otto and Smith, 2013).

Landsat is one of the key sources of geomorphological data available to workers in arid areas. Indeed, Al-Juaidi (1997) demonstrated that Landsat is considered the main source for geomorphological data and the production of geomorphological maps. Many geomorphological features were identified in the basin of Wadi Al-Harmaliah in Al-Quwaiayh region, Riyadh, using visual interpretation of Landsat images in the individual bands 1–7, and False Colour Composite (FCC) 234. Also, Al-wash et al. (1986) conducted a study to describe the arid geomorphological forms in Wadi Fatima using Landsat TM images and field survey. They concluded that Landsat TM images could be used successfully in mapping geomorphological features at medium map scale.

Moreover, numerous studies have employed Landsat data to map and investigate geomorphologic landforms. As such, Landsat has demonstrated its effectiveness as a principal information source in geomorphological research, including Al-Saleh (1999), White et al. (2001), Al dughairi (2011). However, no prior works have employed Landsat 8 data for geomorphological mapping relating to KSA.

As most of the previous studies in the Arabian Peninsula used Landsat MSS, TM and ETM imagery, the current study intends to make an integration and assess the effectiveness of using the modern Landsat-8 multispectral imagery data and field-lab spectral measurements in order to get a better knowledge about the spectral behaviour of different geomorphological units and determine the factors controlling this behaviour (essentially mineral composition and grain size). Consequently, this with applying image processing techniques to Landsat imagery and using geologic maps may lead to accurate spectral mapping and interpretation of the key geomorphological features and surface materials and identifying sources of sediments, sediment transport pathways and depositional sites leading to interpretation of the landscape of the study area. Relating this to the deposits preserved in the sections of the study area, to determine the palaeogeomorphic and palaeoenvironmental conditions during the late Quaternary period that have prevailed in the area, helps in providing a comprehensive and clear understanding (better than what is in existence) for this desert environment in the east of Al Madinah Province during the late Quaternary Period.

The methodological approach of using multi-pronged, interdisciplinary approach in the investigation (sediment analysis, luminescence dating, remote sensing, and geomorphological methods) to map, interpret and understand the landscape (sources of sediments, sediment transport pathways and depositional sites / provenance study) is in itself considered an advance in the discipline. This is the aim of the current study, since previous studies did not use high accuracy data in better interpretation of satellite (Landsat) imagery, as well as integrating these with the multidisciplinary approaches mentioned above and applying these to a provenance study.

1.6   Structure of the Thesis

Chapter 1: Includes an introduction to the subject of the research and a very brief overview of the physical characteristics of Saudi Arabia and the study area. It will also include the importance of the research, its aims and objectives, and the thesis structure.

Chapter 2: Reviews the literature on remote sensing for geomorphological research. It also, summarises the previous studies related to environmental changes in the Saudi Kingdom and neighboring regions and countries.

Chapter 3: Focuses on presenting a complete description of the research methodology chosen to achieve the aims of this research, and the methods used to gather data.

Chapter 4: Focuses on using remote sensing for geomorphological mapping and interpreting the landscape of the study area and determining the relationship between Landsat spectral reflectance and ground based hyperspectral data of desert landforms. It also, identifies the factors that influence the spectral reflectance of the surface geomorphology of the area of interest.

Chapter5: Presents the results of the analysis of Quaternary sediments coming from particle size analysis, X-ray diffraction analysis (XRD), Munsell colour charts, and optically stimulated luminescence (OSL) dating.

Chapter 6: Discusses and explains the results of the study.

Chapter 7: Presents the main findings and recommendations (conclusion of the study).

Chapter 2. Literature Review

The chapter consists of two main parts relating to the research aims. The first part covers remote sensing and geomorphological mapping. In the second, late Quaternary environmental changes in Saudi Arabia and adjacent areas are reviewed.

2.1 Remote Sensing and Geomorphological Mapping.

This section discusses previous research remote sensing of physical features, the distribution of the geomorphological environment, and methods for identifying and describing the surface features; to fill the gap in this type of data, and their future use as a primary tool in management of land, and risk management. The review will help in identifying research gaps for framing of the research questions and objectives for the thesis. The research focuses on the east of Al Madinah Province region using spectral techniques from remotely sensed data.

Vicente and de Souza Filho (2011) argued that traditional soil studies require field and laboratory analyses. Remote sensing involves obtaining information about an object without having contact with the object. In the last decade, remote sensing application involving the use of aerial photography for mapping vegetation, geological features etc. has proved to be useful for detailed mapping (Adam and Mutanga, 2009). It has been used for detection and classification of objects by electromagnetic radiation emitted from satellites (Schowengerdt, 2007). Remote sensing processes entail making observations from satellites at varying height from the earth surface to record the observed phenomena. The observed measurements are converted into information about the physical object that we are interested in for analysis. The basic concepts of energy interactions with different earth surfaces are very important for interpretation of satellite images (Curran, 1985). For example, the reflection properties of a given feature can vary with the wavelength. Thus, a combination of information recorded in the wavelength regions are used for the interpretation of an image. For example, environmental elements vegetation, soil and water each have a spectral signature that is unique to the object based on the target's surface on the incident radiation (Aggarwal, 2004; Curran, 1985).

The general term, geomorphological mapping is used to describe the process of mapping the different parts of a geomorphological system. According to Bishop et al. (2012), geomorphological mapping may include a number of themes, like chronology, surface materials and structure, surface-process regimes, sediment transfer, hydrology, land systems, and morphometry. It is a key tool in the study of processes occurring on land surfaces. This facilitates the analysis, identification, and ultimately, matching of landforms to the appropriate evolutionary mechanisms. The technique allows landforms to be fully and objectively described, and as such is an invaluable tool in practice, in relation to sustainable development initiatives, natural resources conservation, and environmental planning, according to Dramis et al. (2011). Geomorphological mapping, in its early days, was quite rudimentary, as information was typically general, and low in accuracy or detail, having been gathered by taking an aeolian, fluvial, glacial, or mass-wasting perspective. Indeed, it was rare for detailed field, technical, laboratory, or stratigraphic analyses to be incorporated. At the time, remote sensing was not available, while systematic methods and understanding of underlying processes were quite limited. The approach almost completely depended on interpretation of data gathered from the field (Bishop et al., 2012). However, today, the situation is remarkably different, given the appearance of remote sensing. Indeed, new developments in remote sensing and geographic information systems (GIS) have revolutionised the approach to geomorphological mapping, with remote sensing taking a core role in providing information from an increasing range of remote sensing datasources such as satellites, which are platforms orbiting the Earth and capture images from space of the surface using sensor arrays. Airborne platforms (those carried on aeroplanes), capture surface images from within the Earth's atmosphere, typically using a photographic camera (Muzein, 2006; Rao, 2002).

As a development in the domain of land-surface topographic models, digital elevation models (DEMs) accurately add the vertical dimension of altitude (Bishop et al., 2012). These are now capable of delivering high spectral, temporal and spatial data, landform distribution, surface distribution and composition, and land surface elevation information. Such developments have led to huge advances in building geomorphological maps, particularly in relation to quality, accuracy, and speed of execution. As a result, remote sensing has effectively facilitated understanding those natural processes that have caused the surface forms seen on the Earth's surface. Images of the surface captured by airborne and satellite sensors contain a wealth of useful and diverse data relating to the surface, landforms,

31

ecology, resources, and human impact (Rao, 2002). Moreover, comparison of repeated images taken over a span of time has allowed a dynamic record of changes and the rate of change to be kept. Imagery conveys a significant amount of information that can be appreciated by an untrained eye, but the professional practitioner is able to extract much more information, including features that are unknown or indiscernible in the field (Rao, 2002).

In addition, the use of remote sensing can help improve assessment of soil composition using classical methods (Mulder et al., 2011). The data derived from analysis of soil properties obtained using empirical methods may be incorporated into digital soil mapping models. These models may then be applied to facilitate mapping of inaccessible locations over a wider spatial domain using data captured by remote sensing (Ben-Dor et al., 2009; Slaymaker, 2001; Mulder et al., 2011). For a comprehensive management programme to deal with mapping and monitoring of geomorphological processes, remote sensing technology coupled with field data can provide an edge to analyse land surface processes (Rao, 2002). The study of geomorphology has greatly been improved by the use of space science such as remote sensing with influence in the environmental policy development in solving geomorphological problems. Slaymaker (2001) suggested that evolution of remote sensing applications to project planning, resource development planning terrain analysis, and land use, planning, and management has been greatly enhanced over time. Remote sensing allows for the monitoring of environmental changes over a larger area of interest over time, which would be difficult using field studies (Smith and Pain, 2009). Hervás et al. (2003) has emphasised the importance of remote sensing techniques for studying landslide hazards over wide areas compared to field investigations. Another importance of remote sensed imagery are the high spatial resolution images acquired at various points in time, and so representing a quite effective tool whenever field techniques cannot be applied to gather such data. It has also been applied for detection and monitoring the activity of existing landslides in some parts of Europe (Mantovani et al., 1996).

2.1.1 Hyperspectral and Multispectral Sensors for Geomorphological Research

Geomorphology is the branch of science dedicated to studying landforms in terms of parameters such as form, dimensions, origin/development processes, properties and material composition as applied to fixed characteristics of relief forms. In the past, in geomorphology,

the principal application of remote sensing was in interpretation of land relief. As such, it allowed geomorphologists to represent the landscape mentally and assisted in map-making (Hayden et al., 1986). In contrast, there has been a rapid growth in quantitative geomorphic studies where remote sensing has been applied. This has been especially facilitated by the rapid advances in remote sensing technologies and techniques. These now provide high resolution, high accuracy images that capture the Earth's surface in greater detail (Bishop et al., 2012).

Satellite systems may be classified into two types, namely: Hyperspectral and Multispectral sensors. Hyperspectral sensors are imaging spectrometers that collect spectral information within the spectral narrow bands. These imaging spectrometers from satellite and airborne platform could contain many spectral bands with a spectral resolution of 10 nanometres (nm). In contrast, broadband multispectral sensors, such as those of Landsat 8 with 11 bands, offer wider spectral resolution. The spectral resolution in hyperspectral image data allows the identification of surface materials, whereas broadband sensors such as Landsat data discriminate between materials. High accuracy, high spectral resolution devices called field spectroradiometers have appeared. These help in understanding the spectral behaviour of material (Shaw and Burke, 2003). Such field spectro-radiometers are very handy, and can be used to measure the spectral reflectance within a specific wavelength region electromagnetic spectrum (EMS) at a narrow sampling interval (~ 1000 or more) (ASD Inc, 2014). Field spectroradiometers may be used in either the field or laboratory to accurately determine reflectance of various substances, materials, etc. This opens up interesting opportunities for spectroscopy in the field, leading to greater understanding of the interactions between matter and energy, whether on a fine scale related to measurements on a single leaf, or undertaken for the wide and coarse scale study of a vegetation canopy (Clark, 1999).

According to Clark (1999), Abrams et al. (1983), Gaffey (1986.), Madani (2011), Robertson et al. (2016) and others, the principal motivations of using these instruments are:

a)   To understand the relationship between spectral features and Earth's surface nature.

b)   For data calibration and validation in earth observation studies.

c)   To acquire end-members for pixel unmixing analysis and related image classification techniques.

The magnitude of spectral radiance depends principally on the amount of incoming solar radiation (spectral irradiance) reaching the target surface. Indeed, this may vary greatly according to date and time of day during measutments; other effective conditions include atmospheric conditions, length of path, angle of solar zenith, topography, and shadowing (Clark, 1999). There are many types of field spectroradiometers; each has its specific spectral characteristics that make it suitable for specific targets, such as ASD FieldSpec® HandHeld 2 hand-held spectroradiometer (ASD Inc, 2014).

The field spectroradiometers, hyperspectral and multispectral data (airborne and space-borne) have been used in the areas of agriculture, ecology, oil and gas, oceanography and atmospheric for scientific investigations around the world. These sensors have provided scientists with data from regions of the world for identification and mapping of geomorphic physical features such as rocks and sediment types (Leverington, 2010). It has been used for mineral exploration and the study of geomorphological environments. The new developments in these technologies are used to obtained satellite and airborne hyperspectral data, thus providing detailed reflectance data at various scales (Hively et al., 2011). Soil properties were mapped using combined reflectance data derived from airborne imagery and high-resolution maps to minimise errors inherent in soil test data (Hively et al., 2011). Hyperspectral and multispectral data have been used for assessing the spatial properties of soil. Such data have become very important, and demonstrate the great potential of remote sensing approaches in the field of mapping the properties of surface soil (Selige et al., 2006). The advantages of Hyperspectral Imaging (HSI) have been discussed in Schowengerdt (1983). HSI spatial and spectral information on scene objects have aided detection and identification of features over multispectral data (Subramanian et al., 2000). For example, hyperspectral has demonstrated capabilities and means of measuring of soil characterised by their reflectance (Selige et al., 2006; Hively et al., 2011). The use of spectral reflectance from laboratory instruments for measurements of soil reflectance at visible, near infrared and mid-infrared wavelengths were shown to have great potential (Rossel et al., 2006). The technique is important in assisting traditional analysis of soil properties. For example, a comparative variation in the results from laboratory analysis and sensor methods were reported by Rossel et al. (2006), Demattê et al. (2010), Soriano-Disla et al. (2014). Also the effectiveness of combining hyperspectral and broadband multispectral (Landsat) datasets have been demonstrated. Spectral information obtained from Landsat datasets are capable of detecting and discriminating general land cover but may be unable to separate individual

soil classes (Leverington, 2010; Rowan et al., 1987). However, images from hyperspectral instrument are characterised with narrow spectral bands can be used to improve identification, separation of individual soil classes (Solomon and Rock, 1985; Goetz and Rowan, 1981; Goetz, 2009). Leverington (2010) has shown that Landsat TM and EO-1 Hyperion data can be used in combination for mapping individual of surface classes. Images from hyperspectral data have a greater advantage over multispectral data because of high spectral detail to identify high detail information. For example, a hyperspectral sensor is capable of discriminating between 3 minerals due to its high spectral resolution where a multispectral sensor could not. One short coming of the data from hyperspectral images is that it is expensive with limited area coverage. The multiple narrow bands in hyperspectral data can be difficult to deal with. The difference between the spectral bands in multispectral and hyperspectral image is shown in Figure 2.1.
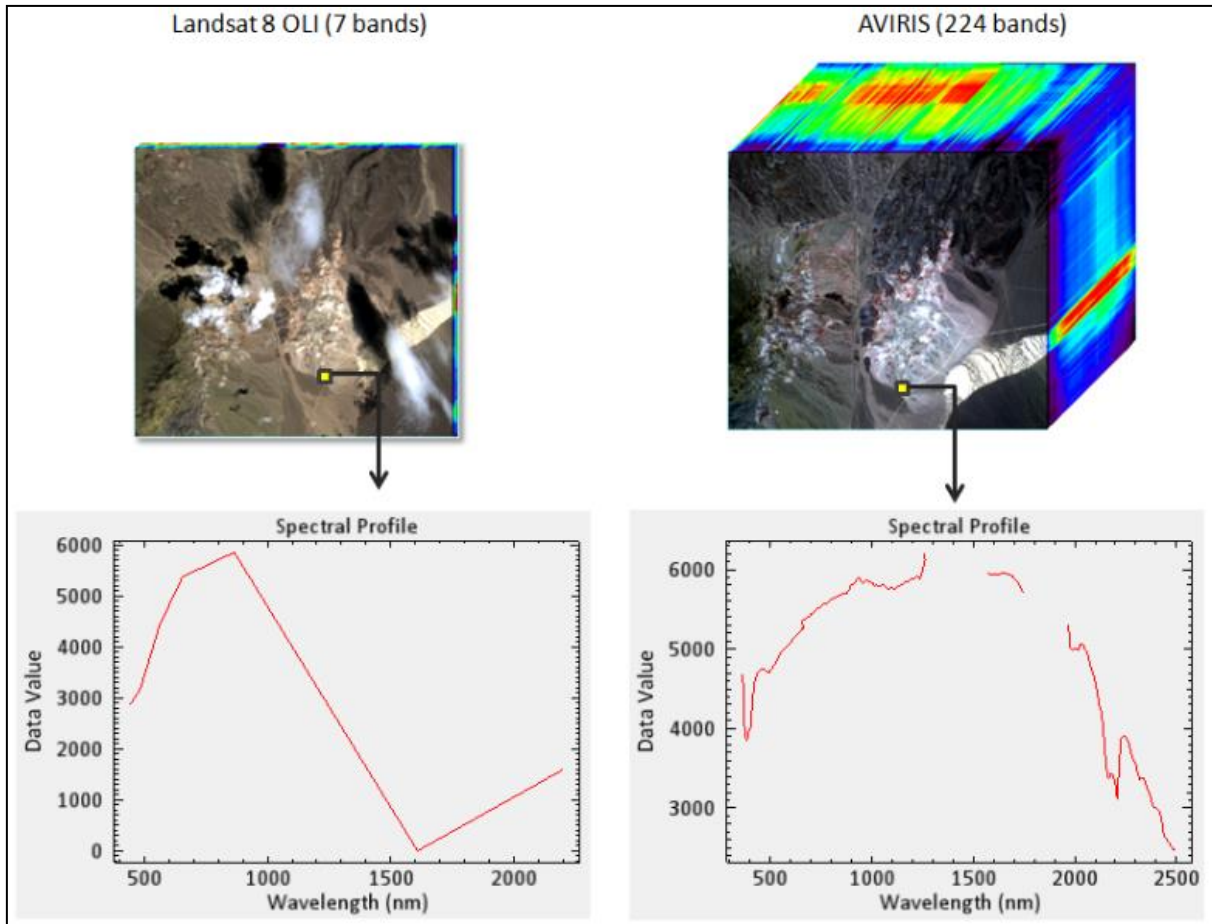
Figure 2.1: Discrete and continuous spectrum in multispectral and hyperspectral sensors respectively.

Image taken from: Harris Geospatial Solutions. (2018) *Basic Hyperspectral Analysis Tutorial*. Available at:

https://www.harrisgeospatial.com/docs/hyperspectralanalysistutorial.html (Accessed 05/04/2016).

2.1.2   The Use of Remote Sensing in Dryland Geomorphology

Drylands are characterized by high levels of aridity, reflecting low ratios between precipitation and potential evapotranspiration (Tooth and McCarthy, 2007; Tooth, 2000). Deserts or semi-deserts are commonly referred to as dryland regions found in cold, high latitude, high altitude environments to warm, low latitude and low altitude environments (Tooth, 2000). The global arid regions are characterised by sparse, unevenly distributed, or temporal variability of vegetation cover. The dryland regions located in the tropics and subtropics form the largest expanse of the drylands (Glennie, 1987; Cooke et al., 2006). In

recent times, dryland geomorphology has concentrated on the characterisation/classification of landforms, and process descriptions, as well as associating processes and landforms. Indeed, remote sensing has been useful in supplying data relating to landform position/distribution, surface/subsurface composition and surface elevation. Remote sensing has presented a new impact on the recent technologies in a wide availability of digital elevation models (DEM), hyperspectral imaging, radiometric and electromagnetic (Smith and Pain, 2009).

Geomorphologists strive to understand the processes that influenced past and present land surface features and thus predict future changes. Indeed, land surface remote sensing can prove valuable in further enabling this important work. There is a number of geomorphological researches around the globe that focuses on the application of remote sensing. The origins and development of aeolian sand dunes was both recorded and understood through the use of remote sensing images. In this context, sand dune mapping and classification was the subject of early studies. Advances in the application of space technology such as remote sensing and software have equipped researchers to carry quantitative investigations of the evolution and pattern development of sand dunes (Hugenholtz et al., 2012). For example White et al. (2001) applied multispectral remote sensing with reflectance spectral, linear mixture models and geochemistry analysis for mapping geochemistry of sand dunes in the northern Al-Rub Al-Khali in the United Arab Emirates. The study concluded that a multispectral remote sensing approach provides great potential for studying inaccessible large areas with better characterisation of the evolution of the northern Al-Rub Al-Khali.

The application of remote sensing in geomorphological research using digital elevation models represents the foundation of modern geomorphological studies for the extraction of data relating to the geomorphological, morphological, geometric, and hydrological characteristics of regions (Al- Husban and Zragat, 2011). The acquisition of mathematical values for the geomorphological description of surface landforms used to be performed through direct measurement in the field or directly from a map. This required significant effort. However, this type of work was greatly eased through the use of the DEM. With the widespread use of DEMs, many algorithms were developed to extract hydrological features, such as drainage basins, and surface flow direction, quite clearly, accurately, and easily. Hamdan and Abu Amrah (2010) used DEM technology to illustrate the fluvial network in

the upper part of Wadi Al-Rumaymin in Jordan, and to study the morphometric features rapidly and well, compared to traditional methods. Al- Husban and Zragat (2011) showed that the DEM played an effective role in geomorphological analysis. In their study of the Birayn area in Jordan, they were able to determine the geomorphological characteristics of the study area represented by the slope characteristics, in terms of directions and degree of slope, which varied from level areas to highly sloped. They were also able to determine the characteristics of the fluvial network, in terms of flow direction, and the form of basins, distinguished by the circulation pattern. Mohammad (2008) also determined and illustrated the palaeofluvial networks in current wadis, between Kuwait and Northeast Saudi Arabia using DEM and Landsat 7. Mohammad's study concluded that the fluvial networks in that area were formed during wet periods, and that these are an extension of the parent hydrological network in central Saudi Arabia (Wadi Al-Rimah), where the majority of tributaries had been buried with the passage of time due to climatic effects.

Despite its significant utility, the DEM alone does not provide all the information necessary for a detailed geomorphological analysis and description. However, linking the DEM to imagery captured from space is significant in providing the necessary data for detailed geomorphological analysis and description. Sahwan (2007) in his research conducted in north-west Syria preferred to connect and integrate DEM data with data from satellite imagery, in addition to the data from different maps, in order to have all the information necessary for detailed geomorphological analysis and description of the area of interest. He used Shuttle Radar Topographic Mission (SRTM) data to extract hydrological features such as drainage basins, height, slope, and direction of slope. He was able to distinguish and fully describe the form and morphology of the geomorphological units present in the area, in an integrated manner. Subsequently, Sahwan (2007) interpreted a number of satellite images of the study area, acquired by Landsat and Aster, using the False Colour Composite (FCC), band ratio, and Principal Components Analysis (PCA) techniques. He was able to formulate a number of deductions and conceptions on the geomorphological status of the area, especially regarding the formation of surface sediment materials and rocks.

Smith and Pain (2009) highlighted the application of remote sensing in geomorphological research using digital elevation models from satellites and hyperspectral imaging. In Brazil Zani et al. (2012) used SRTM, fieldwork and optical satellite images to analyse depositional landforms in alluvial areas of Taquarimegafan, Pantanal.

There are other potential applications of remote sensing for geomorphological investigations were detailed in Millington and Townshend (1987). It was reported in Mathieu et al. (2007) that a multi-scale approach was used to map regional and land degradation in Coastal Cordillera of central Chile. The results showed that surface colour and coarse fragment density are relevant indicators of erosion, and may be used as descriptors of a typical soil degradation sequence. Indeed, radiometric studies in the field have demonstrated that the reflectance of natural surfaces is influenced by both these factors. As such, radiometric indices have been applied successfully to the production of land degradation maps derived from SPOT images. White et al. (2007) mapped the Namib sand sea, in terms of iron-oxide content, using multispectral remote sensing. The reflectance of dune sands was measured in samples gathered from the field using spectrometric analysis. This data was then used to remotely sense the iron-oxide, and hence map it. Interestingly they have shown that the pattern of dune colour from a mixture of different distinct sources of sand due to aeolian transport processes can be characterised using remote sensing. Similarly, spectral reflectance curves from multispectral image were used to identify types of spectral mixture, quantify mineral abundances, and identify the effects of particle size (Smith et al., 1985). Radar images from the Spaceborne Radar Laboratory and visible wavelength images from the French SPOT satellite were utilised to determine the signatures of alluvial fan units in part of the Kun Lun Mountains of north-western China (Farr and Chadwick, 1996). The results in this study demonstrated how geomorphic processes affect alluvial fans, using field observations to compare surface processes and their influence on remote sensing signatures.

Naderi Khorasgani and De Dapper (2010) mapped the land surface features in the dry zones situated in south-eastern Isfahan in Iran, using Landsat MSS data. They found that the principle landforms were sand dunes, playas, valleys, mountains and piedmonts. In addition, they identified quite efficient differentiation of different areas in the Gavkhoni playa, namely the salt crust, pore water, saturation, and water zones. Their study concluded that integration of field observation and observer classification of Landsat images can compensate for the lack of detailed geomorphological maps of some areas. Moreover, Li et al. (2014) studied the Salar de Uyuni basin in Bolivia, which is a semi-arid, endorheic, internal drainage basin. They used Landsat data spanning multiple years, 1985 to 2011, to analyse the morphodynamics of the playa, as well as exploring the possibilities of sediment mapping using multi-temporal surface reflectance measurements from Landsat. Using the maximum likelihood classification technique, they were able to identify four playa surface material

types, namely pure salt, salty, clay-rich, and silt-rich surfaces. The results of this study illustrated the capability of using Landsat image data to identify and measure the distribution and grain size of sedimentary materials in endorheic basin playas. The results also illustrated that remote sensing is a powerful tool for gathering spatial information on, and monitoring playas. This is due to its ability to acquire data at different intervals in time, with synoptic coverage of the area of interest.

The most important tool in geomorphology is characterisation of physical properties of sediments such as variation in grain size, shape and density (Bullard and White, 2002). In a study conducted in an Australian desert (Simpson- Strzelecki dune fields) showed that the colour of sand dunes are determined by their variation in intensity in the UV band. In this study it was concluded that consistent measurements of redness and iron oxide levels can be provided by spectral measurements in the field (Bullard and White, 2002).

2.1.3   Spectral Characteristics of Land Surface

One technique exhibiting rapidly expanding use is reflectance spectroscopy. This is applied to the analysis of spectral data in the visible near infrared (VNIR) and short wave infrared (SWIR) wavelength regions (0.4 – 2.5 µm) to identify different materials according to their reflectance characteristics. A variety of analytical approaches that utilize remote sensing are applied to surface reflectance measurements in the field; for example, spectral mixture analysis, vegetation canopy reflectance modelling, and classification of airborne and satellite imagery, as well as in terrestrial ecology in terms of surface validation and predictive modelling (Gaffey, 1986; Strahler and Jupp, 1990; Adams et al., 1993; Franklin, 1995; O'Neil et al., 1997; Spinetti et al., 2009; Madani, 2011; Robertson et al., 2016).

Reflectance spectroscopy within the spectral bands (visible, near-infrared and shortwave infrared) could be used in the absence of spectral absorption features for determining soil mineralogy (Brady, 1983; Chang et al., 2001). The results from the soil analyses using reflectance spectroscopy and other optical sensors have shown to be effective technique in mapping in arid and semiarid climates (McCarty et al., 2002; Brady, 1983).

Remote sensing has been an efficient and meaningful source for source for spatial data in soil science studies. The advancements in remote sensing techniques and technologies provided a new dimension for researchers in soil-related fields (Anderson and Croft, 2009).

This has been evident in the soil curve with a less peak-and-valley variation in reflectance. Soil reflectance is affected by a number of factors, namely the surface roughness, moisture content, soil texture, (proportions of sand, salt and clay in Figures 2.2), organic matter and iron oxide content. For example, increased moisture decreases reflectance in the reflective portion of the EMS. Another example is the soil texture; increased particle size decreases reflectance, and an increase in iron oxide decreases reflectance (Anderson and Croft, 2009). Thus, the reflectance properties of a soil are consistent only within a particular range and familiarity with the conditions at hand is very essential. In recent times, optical and microwave remote sensing has been used to support segmentation of landscape for establishing soils composition (Mulder et al., 2011). This process can be supported by field data for the spatial interpolation of sampled soil properties. Remote sensing measures soil properties which include texture, soil iron, mineralogy, soil moisture etc (Mulder et al., 2011). Optically, soil surfaces that are rougher exhibit lower reflectance (Bowers and Hanks, 1965) and variations in individual grains size or aggregates and topography could also be influential factors (Romkens and Wang, 1987). Breunig et al. (2008) applied spectral reflectance techniques from ASTER data to determine the distribution of soil properties in relation to topography. The study showed that sandy soil surfaces are commonly found at lower elevations and clay soils at higher elevations.

Remote sensing of soil particle size was also demonstrated by Salisbury and D'Aria (1992) where particle size in soils was estimated using the ratio of ASTER bands 10/14, if providing confusion factors of vegetation cover, soil organic content, soil moisture, and the presence of quantities of minerals besides quartz was minimised using other ASTER bands. Crouvi et al. (2006) has evaluated the potential for using spectral reflectance from hyperspectral data for mapping the percentage of gravel coverage in alluvial fan surfaces in arid regions. The study was able to relate the specific absorption features depths and slope to field parameters, for example gravel coverage (%). Importantly, the study applied these correlations to demonstrate that gravel coverage (%) can be mapped fully over the surface of an alluvial fan. Mushkin and Gillespie (2005) study has shown that estimates of roughness of alluvial surfaces can be obtained by correlation with the ratio (RR) of two almost simultaneous measurements of surface-reflected solar radiance taken from two view angles. Rivard et al. (1992) have suggested that rock texture and mineralogy influence erosion and weathering of bedrock, and so in arid regions, reflectance properties of outcrops are

dependent on both. Figures 2.2 and 2.3 present spectral reflectance characteristics of soil classified by particle size and texture, respectively. Stoner and Baumgardner (1981) studied the characteristic variations in the reflectance of surface soils. Subsequently, reflectance spectral libraries were developed to help characterise soil properties (Shepherd and Walsh, 2002). Furthermore, the effectiveness of Landsat's Thematic Mapper (TM) sensor in distinguishing surface soils having comparable properties was evaluated using spectral radiance data. It has also been applied for the identification of the TM spectral band combination that may be useful in estimating soil properties. Coleman et al. (1993) evaluated the effectiveness of spectral reflectance from Landsat data to differentiate among various soils with similar properties. The study further identifies appropriate band combinations that could be useful in estimating soil properties. The result of Coleman et al's study concluded with uncertainty over the use of Landsat data with 30 meter resolution was effective for generating equation for predicting soil properties but adequate for differentiating among the similar types from the same soil order. Coleman et al.'s research suggested that the selection of Landsat bands is important and the order of the TM bands that was most effective were TM 6, 4, 5, 2, 7, 1, and 3 respectively. It has also been shown by (Nanni and Demattê (2006) that satellite spectral data correlates well with most of the soil attributes obtained Laboratory SR yielded. This has proved that studies have established links between soil properties and remotely sensed data and have been adjudged to be efficient at a regional scale.
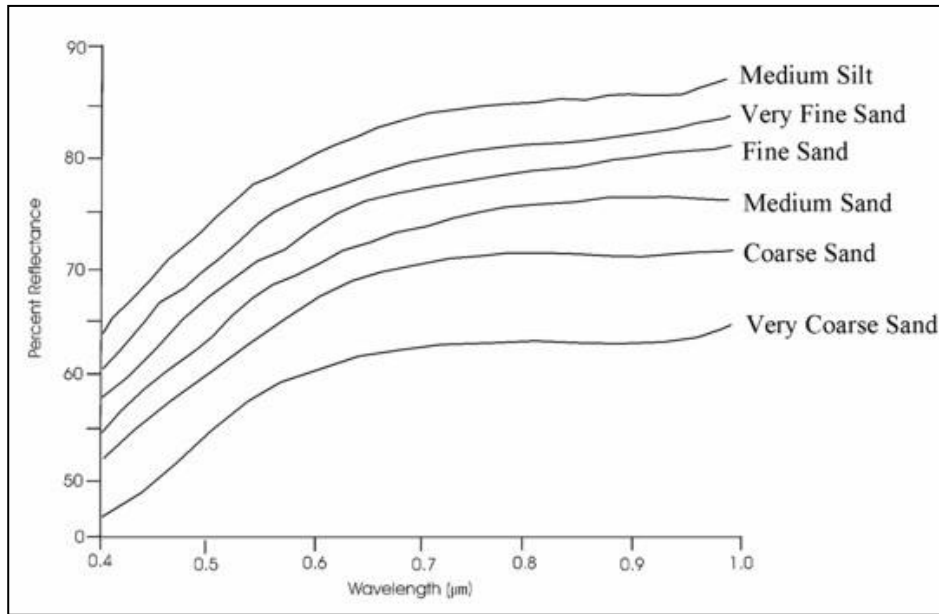
Figure 2.2: Variation in the spectral reflectance characteristics of soil according to particle size.

Image taken from: Department of Geology Aligarh Muslim University. *Spectral Reflectance of Land Covers.* Available at: http://www.geol-amu.org/notes/m1r-1-8.htm (Accessed 05/04/20 (16).
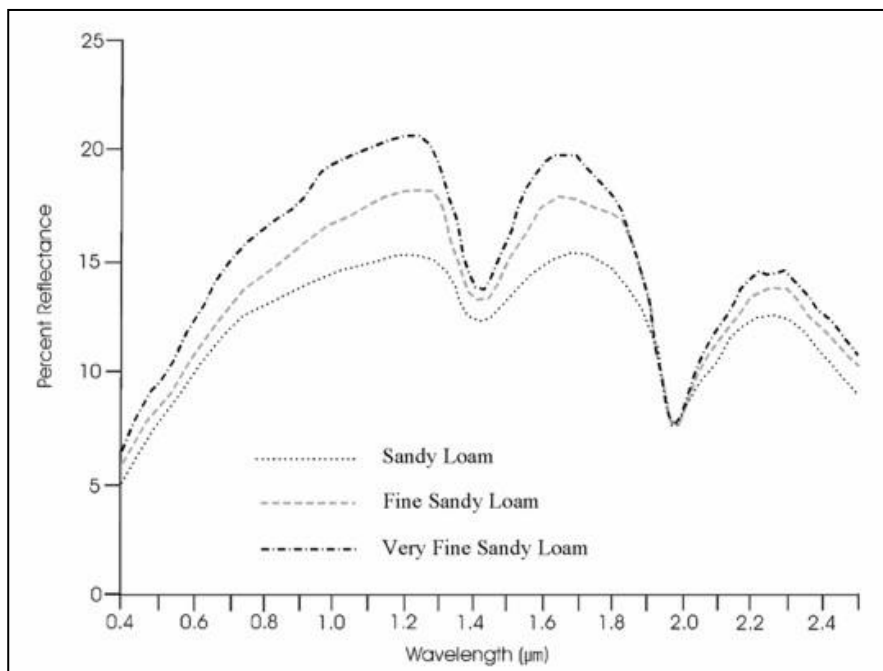
Figure 2.3: Variation in the spectral reflectance characteristics of soil according to soil texture.

Image taken from: Department of Geology Aligarh Muslim University. *Spectral Reflectance of Land Covers.* Available at: http://www.geol-amu.org/notes/m1r-1-8.htm (Accessed 05/04/2016).

43

2.1.4 The Use of Remote Sensing in Dryland Geomorphology in the Kingdom of Saudi Arabia

In this study a review of concepts and applications of remote sensing in dryland areas around world has been presented in section 2.1.2. This section provides a summary of work that has been done in Saudi Arabia as a case study. This research will examine how different researchers have used remote sensing in Saudi Arabia in order to monitor and map land forms.

Al-Juaidi (2003) has produced morphogenic maps that distinguish between fluvial landforms, aeolian landforms, desert pavements and gypsum crust, and a morpholo-chronological map of central Saudi Arabia from merging multispectral data (Landsat TM) and high spectral data (PAN).

Al-Juaidi (1997) demonstrated that Landsat is considered the main source for geomorphological data and the production of geomorphological maps. Many geomorphological features were identified in the basin of Wadi Al-Harmaliah in Al-Quwaiayh region, Riyadh, using visual interpretation of Landsat images in the individual bands 1 – 7, and False Colour Composite (FCC) 234.

Al-wash et al. (1986) conducted a study to describe the arid geomorphological forms in Wadi Fatima using Landsat TM images and field survey. They concluded that Landsat TM images can be used successfully in mapping geomorphological features at the medium map scale.

Al-Saleh (1999) used Landsat to reveal the fluvial network in the basin of Wadi Inan in the Arabian Shield, and Wadi Al-Muzayriah in the Arabian Shelf. Using various enhancement techniques, the results showed that a large proportion of the fluvial network (wadis) was revealed by the enhanced image, which was not shown by topographic maps. Therefore, using Landsat is the option preferred over topographic maps of scale 1:50,000 in revealing the fluvial network to be subjected to morphometric analysis.

The objective of Safi and Qari (1996) study of the area situated between Al-Sulimaniyah and Abhar, north of Jeddah city, were to identify the sabkhas covering that area. For this purpose, Landsat TM images were used. The most important findings of this study was that

the FCC-enhanced image helps in creating geomorphological maps of sabkha features, as well as distinguishing between sabkha and non-sabkha areas.

Qari and Basyouni (2003) studied Al-Majnunah Sabkha situated south-east of Al-Layth in western Saudi Arabia. They found that FCC helped in distinguishing sabkha areas from non-sabkha soil-covered areas, and in drawing maps of some geographical features, such as islands and coral reefs. On the other hand, images treated using PCA helped in distinguishing between the types of sabkhas present in the study area, as well as clarifying the changes in surface characteristics.

Al Sehri (2011) used data from Landsat and SPOT satellite to explore the spatial and temporal changes of the morphological characteristics of two types of sabkhas situated on the east coast of the Kingdom of Saudi Arabia. Al-Raqta Sabkha was selected to represent inland sabkhas while Al-Maslamiyah Sabkha was selected to represent coastal sabkhas. Different methods were used to identify these changes and prepare the related maps. These included image enhancement by using the best band combination, in addition to band ratio, image classification and finally exploring the changes using the post classification comparative technique. This study was able to distinguish five morphological units in both sabkhas. However, the morphological characteristics of the surfaces of both inland and coastal sabkhas differed in some morphological phenomena, and were similar in others. Some fine features on the surface of the sabkhas were not distinguished by the satellite images, such as surface shapes and salt ripples. This required a field visit to distinguish them.

Remote sensing techniques and Geographical Information Systems (GIS) allowed Al dughairi and Al Jaddani (2016) to study Wadi Al-Fuwaylig in Al Qassim in the period from 2000 to 2015. They employed 30 m SRTM to acquire the basin and network in WadiAl-Fuwaylig, as well as Landsat 7 and 8. They applied observer classification technology (selecting the maximum likelihood algorithm) and the Normalized Difference Vegetation Index (NDVI) to deduce the most important changes in the different surface covers, from fluvial sand, alluvial fans, sand dunes, sabkhas, and natural vegetation, as well as agricultural land. The most important results were related to the clear change and increase in fluvial sand, alluvial fans and sand dunes in the period 2000 – 2015. This is attributed to a number of factors, most importantly the role of the Shamal wind, urban growth, increased vegetation cover, and the increased flows in WadiAl-Fuwaylig during 2008 and subsequent years. On

the other hand, there was clear shrinkage in the area covered by natural vegetation, with least change registered in the sabkhas.

Al dughairi (2016) was able to map and reconstruct the water drainage systems and prevalent landforms in the Al-Rub Al-Khali over 43,500 years into the past using the DEM (SRTM). He linked this to intensive fieldwork and analysis and Radiocarbon dating of a set of samples taken from a set of palaeolakes in the Al-Rub Al-Khali, which contributed to building up a much clearer picture of the past of this area. The study concluded that the Al-Rub Al-Khali was covered by a shallow lagoon contiguous with the Arabian Gulf. This was affected by earth movements that led to the change in its system, which was diverted to a large group of wadis in the south, west, and north east, after its waters receded. This shallow sea was transformed into a group of neighbouring lakes, whose levels varied according to climatic change.

Al dughairi and Al Moqren (2016) used remote sensing techniques, represented by the DEM and Landsat 7 and SPOT images, in addition to field work, to reveal that Nafud Ash-Shuqayyiqah in Al Qassim included Holocene sand dunes with varying morphology (linear, transverse, dome, star, interdune, sand sheet, and nabkah), which also varied in their spatial distribution given the variation in geomorphological factors, and climatic conditions accompanying their formation and evolution.

Al dughairi (2011) used Landsat and Milton Multiband Radiometer technology, in addition to magnetic sensitivity technology and redness index, to study the differences in the distribution of sand in the Al Qassim region. Among the results of this study was a sand distribution map, including morphological forms and colour attributes. One of the most important factors that contributed to the sand acquiring this distribution is the mineral characteristics of the bed rock revealed around the sand, and the spatial topography surrounding the sand, such as sabkhas, palaeolakes, the morphological form of the sand, and the palaeo-wind systems.

Al -Azmi (2009) used images from the SPOT satellite for the period from 2003 to 2007 to measure the annual rate of advance in barchan dunes, which reached 9.7 m, and determined the directions of this advance. He drew maps that illustrated the rate and direction of sand dune migration, and identified the vital infrastructure that was affected, or would be affected by this movement of sand dunes.

Numerous researchers in the Kingdom have used DEM in the study of many river basins, and both drawing and determining the fluvial networks of wadis. For example, Al-Wuhabi (2013) used a DEM to illustrate the fluvial network of Wadi Al-Nisa in Al Qassim and studied the morphometric characteristics of the basin, linking this to current and future urban growth. The study concluded that urban growth had not taken into account wadi flows and land topography, which led to the risk of urban areas being affected by flash floods, especially during periods of heavy rainfall.

In summary, the studies conducted in Saudi Arabia all employed Landsat data (MSS, TM and ETM+). Moreover, no field studies were conducted using spectroscopy to understand sediment spectral characteristics as they appear in Landsat images, nor apply these to interpretation of the landscape (including sources of sediments, sediment transport pathways and depositional sites resulting in the current geomorphological features seen today). To map and interpret the landscape to the east of Al Madinah, the work in this thesis will employ both handheld spectroscopy for laboratory analysis of samples and satellite data (recently and freely available Landsat 8 data), to investigate and characterise surface reflectance from the two data gathering sources in a way that has not been conducted before. This contributes to a deeper understanding of the spectral characteristics of deposits within the study area, and find out the causes for the variation in reflectance characteristics of sediments throughout the study area. In addition, these spectral data are used along with other image processing techniques (PCA, Band ratios and FCC) to gather the most data on the landscape so as to describe composition and mixing of sediments and infer how sediment is weathered and transported around the study area also, geomorphic processes playing onto this area. This has never been done in previous studies by other scholars.

2.2 Late Quaternary Environmental Changes in Saudi Arabia and Surrounding Area.

This section reviews the history of the late Quaternary environmental changes that have occurred in the Arabian Peninsula.

2.2.1 Late Quaternary Precipitation in the Arabian Peninsula

Al the present day, the Arabian Peninsula is distinguished by low levels of precipitation, where typical mean annual rainfall is generally under 100mm a^{-1}. This is the case for most of Saudi Arabia; however, the exception is the south-western area of the Arabian Peninsula, which receives larger amounts of rainfall, reaching 200mm a^{-1}, and even 600mm a^{-1}. These levels of precipitation, seen in the summer, are caused by the moisture-laden south-westerly monsoon winds (Figure 2.5) (Edgell, 2006) blowing from the Indian Ocean colliding with the southwestern highlands of the Arabian Peninsula, resulting in seasonal summer rainfall over that area. This type of rainfall is called relief precipitation (Al Shaik et al., 2000).

In addition to these monsoon winds, the summer and winter Shamal winds are dominant in the wind system prevailing today. During the summer in northern Arabia, high pressure build up causes the Shamal wind. This wind is dry and hot, blowing in a predominantly northerly and northwesterly direction. In winter, it is extremely dry and cold, and takes a northerly and northeasterly direction. In winter, relatively warm northwesterly winds blow from the Mediterranean, causing some precipitation (Mahsoub et al., 1999; Kogaly and Al beshi, 1998; Edgell, 2006).

2.2.1.1 Monsoon Precipitation in the Late Quaternary Period in the Arabian Peninsula

During the late Quaternary Period, monsoon wind patterns witnessed significant latitudinal movement over time, such that their effect reached to North Oman during some intervals in that period. This contrasts with the situation in the present, where the influence of the monsoon wind is limited to the southwest area of the Arabian Peninsula, as can be seen in

Figure 2.5. The Intertropical Convergence Zone (ITCZ) has been shown to migrate seasonally. In the wettest phases of the late Quaternary, stronger monsoon winds were present along with rising sea levels and greater levels of evaporation in the tropical oceans, as a result of higher insolation levels and decreased snow cover affecting the Himalayan plateau (Fleitmann et al., 2004). Therefore, the ITCZ migrated northward, to reach the Arabian Peninsula (Fleitmann et al., 2004, 2007). This produced monsoon winds that were a more reliable source of seasonal rainfall (Glennie and Singhvi, 2002) (Figures 2.4, 2.5). This was confirmed by Burns et al. (1998), who studied the history of monsoon winds in the southern area of the Arabian Peninsula from evidence in Hoti Cave using stable isotope analysis of speleothems and U-Th dating. They concluded that heavy seasonal rainfall occurred in North Oman (23° 05' N) during the Pleistocene Marine Isotope Stage (MIS 5e). This confirms the findings of Fleitmann et al. (2011) in Mukalla Cave in south Yemen. They found that deposition of speleothem was limited to the periods of peak interglacial activity, i.e.MIS1 (6-10ka), MIS 5c, 5e, and MIS7, under the influence of seasonal monsoon precipitation, which was notably highest in MIS5e.

In this respect McClure (1976), Lézine et al. (1998) consider the early Holocene period, i.e. 10.5-6.5ka. At this time, Arabia saw a significant phase of lacustrine development, which corresponded with greater levels of solar heating over the Northern Hemisphere. The enhanced solar heating brought significantly greater fluxes of monsoon precipitation in Asia, North Africa, and Arabia (Gasse and Van Campo, 1994; Ortiz et al., 2000). The study by Fleitmann et al. (2007) demonstrated the existence of wet conditions in southern Oman during 10.3 ka as a result of monsoon winds penetration into this area. Neff et al. (2001) also documented the influence of these winds reaching Northern Oman dating back to 9.6 ka. Monsoon winds reaching Awafi in UAE as well according to Parker et al. (2004) as the beginning of lacustrine sedimentation did not take place until 8.5 ka. Al dughairi (2011) inferred the potential signal of great monsoon winds potentially at latitude 26° N in Al Qassim, central Saudi Arabia. This contrasts with Fleitmann et al. (2004) who emphasized that the monsoon precipitation belt did not migrate further than latitude $23 - 24°$ N . Moreover, Parker (2009) mentioned that the migration of monsoon winds from the south of the Arabian Peninsula (latitude 15° N) to the north of the Peninsula (latitude 25° N) took 1800 years between 10.3 ka and 8.5 ka. Al dughairi (2011) illustrated the existence of evidence for humid climate in Central KSA in the period 10 ka. This coincided with existing

evidence of humid conditions in the south of the Arabian Peninsula in the period 10.3 ka. As such, he explained that his results do not agree with Parker's (2009) conclusions. However, the western central region of KSA has not been studied by any worker, and as such there is no confirmation of the arguments posited by Parker (2009) and Fleitmann et al. (2004). In the Arabian Peninsula, most past studies concerning this period (early Holocene) have focused on the effects of monsoon winds on the south of that area (Fleitmann et al., 2011). Al Madinah is situated at latitude 25° N in the western central part of KSA, and no study has thus far focused on the migration of monsoon winds into the central western area of Saudi Arabia.

On the other hand, during glacial periods, there was no significant monsoon activity especially during the Last Glacial Maximum (LGM) where sea levels were low globally. The ITCZ was likely situated further to the south (Figure 2.4), taking the rainfall belt along with it. As a result, the prevailing climate in the Arabian Peninsula was predominantly arid. This was suggested by Glennie and Singhvi (2002), who found that significant phases of dune building took place in the Southeast Arabian desert, at 110-115 ka (MIS5d), 60-50 ka (MIS3) and 15-12 ka (MIS2). During MIS 2, an arid glacial climate prevailed, along with much lower global sea levels, which exposed the Arabian Gulf sea floor. Shamal wind activity was also greater, and so sand from the exposed Arabian Gulf floor dried out and was carried to the Al-Rub Al-Khali in the UAE.

Significantly higher precipitation occurred in the Arabian Peninsula in the early to middle Holocene (Figure 2.4, 2.5). This was caused by stronger monsoon winds, as well as the location of the ITCZ mean summer position being further north relative to its position currently (Fleitmann et al., 2004). Fleitmann et al. (2007) also add that the summer ITCZ, during the middle to late Holocene, migrated south constantly, with gradually less monsoon precipitation, until the ITCZ reached its current position, as in Figures 2.4, 2.5 , and as a result the dry Shamal prevailed in the Arabian Peninsula, and contributed prominently to dune building activity in this area (Edgell, 2006).

It is clear that the climate in the Arabian Peninsula during the late Quaternary period was influenced by the interaction between the monsoon winds and the Shamal wind. Therefore, it is important in this research to study this interaction in the area of Al Madinah during the late Quaternary period to determine the contribution of these winds to environmental changes occurring in the area at the time.

Figure 2.4: The expansion and retraction of monsoon during the late Quaternary.

Source: Re- drawn after Glennie and Singhvi (2002), McClure (1984), Fleitmann et al. (2004, 2007), Al-Juaidi (2003).
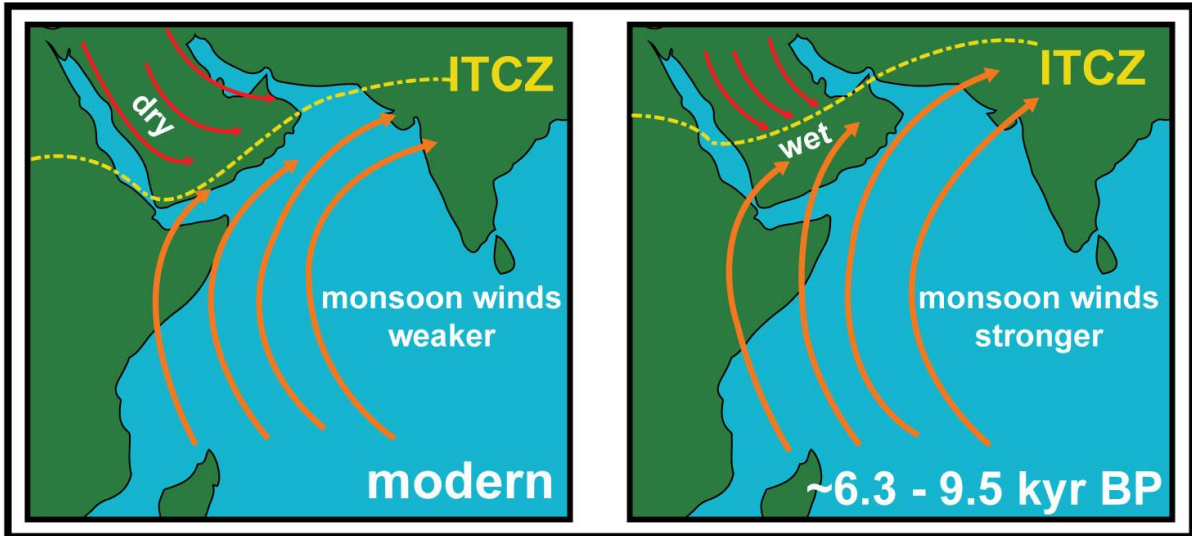
Figure 2.5: Monsoon circulation over Arabian Peninsula at 6.3 - 9.5 kyr B.P, present day. Source: Re- drawn from Fleitmann and Matter (2009).

2.2.2 Pleistocene Chronology of Environmental Changes

Figures 2.4 and 2.5 show evidence for many wet and dry periods witnessed by the Arabian Peninsula, including the kingdom of Saudi Arabia. Al dughairi (2011) studied the palaeoenvironments of Al Qassim region in central Saudi Arabia, and found evidence of increased moisture relative to present during MIS7 in the east of Buraydah region, specifically the Al Mistawi Plateau. This finding is in agreement with the study by Fleitmann et al. (2011) who studied the stalagmites in which Mukalla Cave, using $\delta^{18}O$ and Uranium-series and found that they grew during the interglacial period, around MIS7 (230-245 and 195-209 Ka). This indicates that in these time periods wetter conditions existed, which they emphasise was due to the migration of monsoon rainfall northward far from its current location. Also, Petit-Maire et al. (2010) studied Mudawwara lake situated in South Jordan using U/Th dating of shells. They found that the lake was inundated during MIS7, MIS6, and continued to be active during MIS5e, which is the period that witnessed heavy seasonal rainfall, especially during 120-125 ka, according to Burns et al. (1998). This supports the findings of Fleitmann et al. (2011), who studied speleothems in Mukalla Cave in South Yemen and Hoti Cave in Oman. They found that during MIS5e, specifically 130 -123ka, the highest monsoon rainfall was recorded. This is also corroborated by Burns et al. (1998, 2001), whose study in North Oman indicated prevailing moisture during MIS5e.

Al dughairi (2011) identified phases of significant precipitation during MIS5d (110.4 ka) in the lower part of Wadi Al-Rimah. Fluvial sand in the wadi terrace, in Wadi Bathah in Oman bear indications of a significant flow prevailing during the MIS5C phase (Juyal et al., 1998). In contrast, other parts of the Arabian Peninsula, during the same period, did not experience precipitation, but remained dry; Glennie and Singhvi (2002) found that during this time the sand dunes actively accumulated in south-east Arabia. The significantly drier climate that prevailed led to the Arabian Gulf seafloor becoming partially exposed. At the same time, the greater activity of the Shamal wind led to sand being transported south to the Al-Rub Al-Khali, and also to the UAE from the Arabian Gulf seafloor. This is in agreement with the findings of Preusser et al. (2002), who via OSL identified a phase of dune accumulation at approximately 100-120 Ka. Indeed, the dune building activity in that period had been the result of greater availability of sand sediment due to partial exposure of the continental shelf floor, greatly reduced rainfall, and the diminished plant cover as a consequence of the dry climate (Preusser et al., 2002, 2005). Al dughairi (2011) explained that the contrasting existence of a wetter conditions in the central area of the Kingdom during this period, as perhaps reflecting greater amounts of precipitation over the upper wadi in western Saudi Arabia. This led to sediment feeding down into the lower part of Wadi Al-Rimah in Al Qassim, where greater Shamal wind activity was contributing to the build-up of sand dunes. However, the area in the west of the Kingdom has not been studied yet, and therefore, there is no study with which to compare and confirm Al dughairi's results. Since Al Madinah is located to the west of Al Qassim, and in its eastern part, the upper sources of Wadi Al-Rimah are situated, represented by Wadi Sahuq, the current study will aim to find out whether wetness prevailed in Al Madinah as well, during that period, and hence whether Wadi Sahuq received large amounts of rain, which led to the lower parts of Wadi Al-Rimah being fed by rainfall, as mentioned by Al dughairi (2011). The subsequent, warmer MIS5c period evidence pointed to the formation of dunes in lower Nafud Burydah at 99.5 ka approximately. At the same time, other parts of the Arabian Peninsula witnessed a period of increased moisture availability. In eastern Jordan, Lake Mudawwara was active and stalagmites grew in the Oman cave during this time, i.e. 105-100 ka (Fleitmann et al., 2011; Petit-Maire et al., 2010). Moisture clearly prevailed in the Arabian Peninsula during MIS5a, where Petit-Maire et al. (2010) inferred that during MIS5a (77 ka) and MIS5b (91.1-88 ka) in southern Jordan, Lake Mudawwara was inundated. Wadi Al Butaun which is a tributary channel of Wadi Al-Rimah also witnessed high moisture during MIS5b,a, i.e. 77.2-85.5 ka.

Al dughairi (2011) states that this may probably have occurred due to the effect of seasonal rains. He also mentions that north-westerly Mediterranean systems possibly contributed to some extent to the winter precipitation occurring in northern Saudi Arabia in the same period. This also confirmed the results of Burns et al. (1998, 2001), who identified greater moisture availability to have prevailed during MIS5a (78-82ka) in Oman. In studying calcite speleothem found in a lava tube in Jordan, U/Th dating provided evidence from which Frumkin et al. (2008) inferred that the North Arabian desert had fallen under the influence of Mediterranean cyclones in the periods MIS5a and MIS4 (80-70 ka).

According to Preusser et al. (2002), significant amounts of aeolian sediment accumulated in the Wahiba Sand Sea dating to 64 to 78 ka in MIS4. However, Stokes and Bray (2005) notes that this differs with the record from the Southern Al-Rub Al-Khali, in the areas of Al Qafa and Liwa, where during the same period, there was less evidence of wind activity. In explaining this difference they outline additional factors controlling dune accumulation in this region, notably the level of groundwater, supply of sand, wind type, and change in sea levels. Therefore, wind-transported sand build-up cannot be considered a direct proxy for dry climate. Al dughairi (2011) confirmed this in his study, as he explained that at 99.5 ka, in the warmer MIS5c period, dune formation took place in the lower Nafud Burydah.

During MIS3, in which the sea levels were quite high, central Saudi Arabia experienced wetness, where the lake situated on the eastern part of Burydah became active between 33.2-34.5 Ka and 40.6-43.2 Ka (Al dughairi, 2011). McLaren et al. (2009) studied the outwash plains in Al-Quwaiayah in central KSA and found wetter conditions occurred at 54 Ka and 38.8 Ka which caused flooding. This is also in agreement with the palaeolake evidence in Al-Rub Al-Khali (McClure, 1976), and activity in Al Khayzaran palaeolake in the Al-Rub Al-Khali during 35.9 – 36.4 ka (Al dughairi, 2016). In Egypt, Warne and Stanley (1993) established that Maryut Lake in Alexandria had been active ca. 35 ka. By contrast, the early part of MIS3, between 60-50 Ka, was considered dry (Fleitmann et al., 2007). Dune build up was active in southeast Arabia, due to the dry Shamal wind activity according to Glennie and Singhvi (2002).

In the period, 32-24Ka, i.e. in MIS2, all parts of the Arabian Peninsula were affected by single or multiple pluvial episodes. In this period, greater precipitation or evaporation or both were typical. Whitney et al. (1983) conducted radiocarbon dating in al-Nafud, and concluded from calcareous lake deposits that wetter conditions prevailed between 32-24 Ka.

In addition, McClure (1976) also radiocarbon dated lakes in al-Nafud and Al-Rub Al-Khali, and concluded that wet conditions prevailed in 26-40 Ka. Furthermore, the discovery of lacustrine diatomite in northern Saudi Arabia dated 29.5-31 ka indicated a period of less evaporation along with the presence of perennial water (Garrard and Harvey, 1981; Garrard et al., 1981). The same results were obtained by Hötzl and Zötl (1978) in Wadi Raniya, where they found a ca-horizon at a depth of 1m below the surface, and dating determined it belonged to 26.4 and 29.8ka. Similarly, north of KSA, in eastern Jordan, a large lake was discovered within Lake Al Jafr. Dating of marl in the lake established that it was from 29.3-32.7 cal year BP (Huckried and Wieseman, 1968).

According to Anderson et al. (2007), a strong arid climate was commonplace during Last Glacial Maximum (LGM) period. This was due to the influence on the climate in Earth of ice sheets that covered extensive areas in the north, and which resulted in lower sea levels and drought, as well as weaker seasonal winds. Therefore, during this period, there is no evidence of significant moisture in parts of the Arabian Peninsula. Indeed, there is strong agreement among workers, such as Whitney et al. (1983), Garrard and Harvey (1981), that during the LGM, arid conditions prevailed across most of the Arabian Peninsula. Indeed, according to Preusser et al. (2005), the main build-up of sand dunes more recently occurred in the period 18-22 Ka. This is supported by evidence from a study of dunes in the Northwestern Negev, Israel, where OSL dating showed that dune building activity was occurring around 18-11.5 ka (Roskin et al., 2011). Another study of dune building activity in the UAE (northeast Al-Rub Al-Khali), by Atkinson et al. (2011), found that this had occurred in the same period. Dune formation had been influenced by northwesterly winds transporting. This is in agreement with the results of both McClure (1976), Glennie and Singhvi (2002). In the current study, we perhaps find evidence of this period, especially since Al dughairi (2011), Al-Juaidi (2003) did not find evidence of such climate prevailing in the LGM.

2.2.3 Holocene Environmental Changes

Arid climates continued for a short period from the start of the Holocene (notably during the Younger Dryas 13.0-11.5), in which sand accumulation continued until 11.5ka in the Northwestern Negv Desert (Roskin et al., 2011), and in Southeast Arabia, up to 12 Ka

(Glennie and Singhvi, 2002). In Al Qassim, ca. 11.9 ka, sand accumulated in Wadi Al-Rimah's lower channel at Nafud Al Thuwayrat (Al dughairi, 2011). Also, Awafi dune was active in the period between 10 - 13 ka (Goudie et al., 2000). Lacustrine deposits have developed in Yemen at approximately 11 ka (Parker et al., 2006; Lézine et al., 1998, 2007). Humid climate in the period 11.2 to 10.7 ka is also evidenced by the presence of tufa in this area (Al dughairi, 2011). Similarly in Africa, the same kind of evidence shows that in Lake Victoria, Holocene conditions prevailed; circa 11.2 ka, Lake Victoria was an open basin (Johnson et al., 2000). Also, the period 13 to 11 ka witnessed higher fluvial run-off, and savannah extended to its northernmost position (Hooghiemstra, 1988). At the beginning of the Holocene, around 10 Ka, studies are in strong agreement that moisture availability increased across Arabian Peninsula, as distinguished by shallow lakes developing in al-Nufud and Al-Rub Al-Khali, where dating of lacustrine deposits placed them in the period 10-5 Ka (McClure, 1976; Whitney et al., 1983). Deposits present in Wadi Al Watah reflect alternating low and high activity around 10 ka (Al dughairi, 2011). Moreover, according to workers Hötzl and Zötl (1978), during the period around 9-9.5 ka, Wadi Al Luhy (21°N) was active. Similar findings have been reported relating to Africa. In this respect, in southern Egypt, the effect of the enhanced monsoon led to the rise in Umm Akhtar Lake in the two periods,ca. 9.9 to 9.5 calyr BP and7.8 to 6.7 calyr BP (Nicoll, 2001). Furthermore, the shortest wet period seen in Africa was in ca. 9.9-7 ka (Stokes et al., 1997).This coincides with the rapid migration north of enhanced monsoon rainfall, and therefore, the profiles of oxygen isotopes in stalagmites in Oman showed rapid development between 10.6-9.7ka (Fleitmann et al., 2007). Neff et al. (2001) also revealed the presence of speleothems in the Oman cave dating to 9.6-6.1 ka using U/Th and oxygen isotope, which reflects a humid period in that period. In addition, the deposits present in Awafi Lake also reflect that this period was humid due to the domination of stratified marls accompanied by thin organic material layers (Parker et al., 2004). Also, Ash-Shuqqyyiqah palaeolake was inundated during 6.1 ka (Al Moqren, 2016). Although this period witnessed moisture and seasonal wind activity, sand accumulated in parts of Saudi Arabia. Indeed, Preusser et al. (2005) found that there were two short periods of increased aridity in Wahiba Sand field, Oman, at around 9 to 8 ka, and 8-5.5 ka. Moreover, Atkinson et al. (2011) found that sand in Northeastern Al-Rub Al-Khali continued to build up until 10ka. According to Al dughairi (2011) Both Nafud Uyun Al-Jiwa and Nafud Burydah were formed by deposits occurring in the periods, 9.8 ka and 9.4 – 10.7 ka, respectively. This strongly supports the view that sand

accumulation is not a good indicator of aridity, since sand may continue to build up even during periods of moisture.

Constant southward migration of the summer ITCZ occurred in the middle to late Holocene, while monsoon rainfall slowly reduced, which led to more arid conditions in the Arabian Peninsula (Fleitmann et al., 2007). In addition, the dry Shamal wind prevailed in the Arabian Peninsula (Edgell, 2006), and so when Parker et al. (2004) studied Awafi Lake, this revealed increased wind activity and reactivation of sand dunes in the period 5.5ka. Furthermore, at 4.1ka, an extreme arid event took place, in which the lake dried out and was filled with sand carried over by wind. Indeed, Preusser et al. (2002) also found that palaeodune occurred in Wahiba in 2000-700 BP. Moreover, at around 5.1ka Wadi Al Butaun was covered by an orange-coloured sand sheet that had been transported by the wind in addition, Wadi Al Watah was also covered by a large sand sheet. Nebaks expanded rapidly before 5.3 and 2.1 ka, as in Wadi Raghwah in Al Qassim. This coincided with the accumulation of aeolian sand in Nufud Uyun Al Jiwa 4.7 ka (Al dughairi, 2011). The flow channel of Wadi Al-Rimah was closed by Nufud Al Thuwayrat sand before 4.8 ka (Al dughairi, 2011). Evidence of arid climatic conditions in other parts of the Arabian Peninsula are found; for example, ceased activity in Ash-Shuqayyiqah palaeolake in Al Qassim ca. 4.6-4.7 ka (Al Moqren, 2016). There was also sand accumulation activity in Oman before 5.4 ka (Preusser et al., 2005), as well as Liwa region in UAE before 6 ka (Stokes and Bray, 2005).

In Summary, from the aforementioned, it becomes clear that studying the sediment sequences preserved in the landforms in the Arabian Peninsula has provided us with valuable information on palaeoenvironmental changes. Therefore, the sediment sequences preserved in wadis, palaeolakes, and dunes, sabkhas, slope wash deposits in Al Madinah will be studied. The purpose is to obtain credible evidence illustrating the environmental changes that occurred in the western part of Saudi Arabia, represented by Al Madinah, which has not been studied before. The majority of research studies were conducted in Yemen, UAE, Oman, and southern, central, and eastern KSA. However, the central western part of KSA, represented by Al Madinah has never before been studied. In addition, most studies performed in south and central KSA addressed the effects of seasonal monsoon winds. Yet, no previous work has concentrated on the development and also migration of the monsoon across central western KSA.

Therefore, this study will contribute to providing further data to the archive relating to the monsoon wind system, and will help in progressing the discussion and critique of hitherto uncorroborated opinions relating to the monsoon precipitation belt.

Chapter 3. **Data and Methodology**

This chapter presents and describes data and methods used for the analysis in the study. Field data collection and laboratory procedures for analysis are also described in this chapter.

3.1 Data Sources for Production of Geomorphological Maps of the Study Area

The methodological flowchart for remote sensing is shown in Figure 3.1.

The production of a geomorphological map of the study area is based, in the first instance, on the analysis using Environment for Visualizing Images (ENVI) and Earth Resource Development Assessment System (ERDAS) of remote sensing data represented by four neighbouring Landsat 8 images. Table 3.1 describes spectral specifications of Landsat 8 band. The four images were acquired in 2013 on WGS-1984/ UTM Zone 37 North with no cloud cover over the study area. Data pre-processing included geometric, radiometric and atmospheric corrections, and mosaicking of the multiple neighbouring images into one large scene. Supervised classification and reflectance characteristics techniques were applied to the images to reveal the different spectral surfaces in the study area (see section 3.3).

The Global Digital Elevation Model (ASTER GDEM 1 arc-second) was used to determine altitude variations, hydrological networks, drainage basin and other geomorphological features. The ASTER GDEM was computed to produce slope, topography, and contour for characterising the spatial distribution of sample sediments using spatial analysis tool extension in ArcMap.

In addition, topographic maps at 1:50,000, 1:250,000 and geological maps at 1:250,000 scale were utilised for identification and distribution of sediment types and landforms. These maps were scanned into raster format, and geographically corrected in ArcMap, so the maps could be overlain on the satellite scenes and ASTER GDEM imagery in a GIS environment. All of this data allowed for the development of a first stage geomorphological map.

Finally, observations were conducted during field visits in order to verify and revise the information obtained from the images and topographic maps. The field work is considered highly important in the production of any geomorphological map because it allows

59

geomorphological phenomena to be described clearly and precisely (see section 3.2 fieldwork).

Table 3.1: Landsat 8 spectral information on land surfaces

Band	OLI	Spectral Information on Land Surface
2	0.45-0.51 µm blue	Detection of water bodies and differentiates soil from vegetation
3	0.53-0.59 µm green	Green reflectance of vegetation and vigor.
4	0.64-0.67 µm red	Chlorophyll absorption region with strong reflectance region for soil.
5	0.85-0.88 µm NIR	To distinguish vegetation conditions and varieties.
6	1.57-1.67 µm SWIR1	Sensitive to the amount of water in plants and to separate water bodies from soils or barren lands.
7	2.11-2.29 µm SWIR2	Detects land-water interface based on high absorption in water and high reflectance on soil and rock.

Source: NASA (2013), Lillesand et al. (2008).

Table 3.1 illustrates information about each spectral band with respect to the land surface reflectance. This information is useful in making decisions on combining of the spectral bands in the identification of different geomorphological and geological surfaces for the study. Band ratios provided unique information between surface materials that were sometimes difficult to detect using standard band combinations on the image and was also suitable for mapping mineral deposits. Landsat 8 is better quality than previous Landsat data (Mann et al., 2012). For this reason, data from Landsat 8 was selected for use in this work.

In addition compared to other satellites, Landsat 8 provides both wide area coverage and temporal resolution.
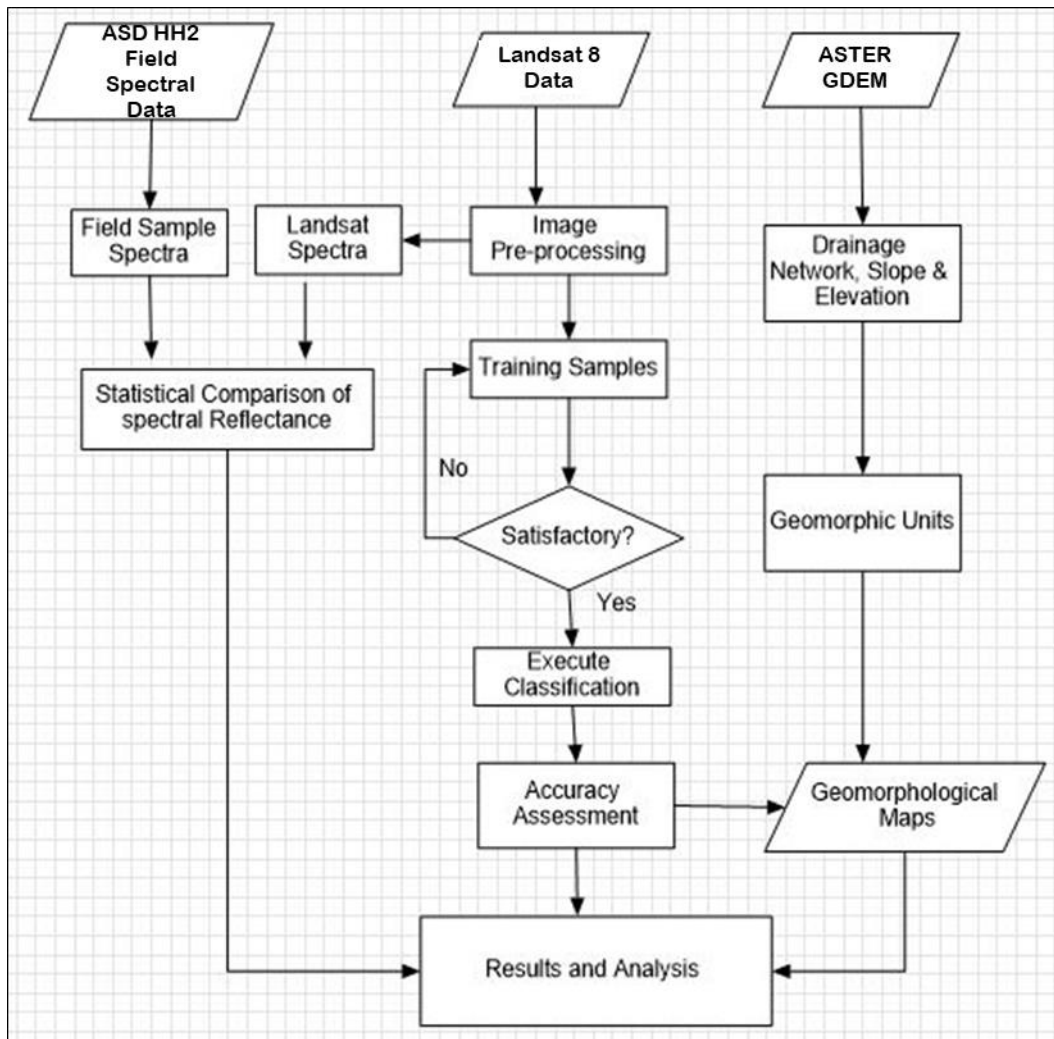
Figure 3.1: General methodological flowchart for remote sensing.

3.2 Fieldwork

Intensive field work was performed in the study area in the period between December 2012 and March 2013. It involved, ground verification, assessment of the study area around the sample sites, and surface samples collection.

3.2.1   Ground Verification

The verification was performed in stages; the first stage involved the initial interpretation of the image from field observations. On a hard copy, landforms that were not identified were noted on the images, as the various landforms were investigated. A GPS guided this process of verification, because geomorphic features were located accurately, and then compared with the images and maps. Ground control points (GCPs) were also collected to act as fixed reference points for geometric correction of the satellite images (section 3.3.1). In this regard, thirty GCPs were established, using specific man-made (e.g. roundabouts, road junctions) and natural features (e.g. small isolated hills, wadi junctions etc). In addition, the landforms in the vicinity of the sample sites were verified in relation to the preliminary geomorphological map produced by the Landsat 7 images, ASTER GDEM, topographic and geological maps.

3.2.2   Study Sites and Sample Collection.

Different surfaces and sections were sampled. There were two types of samples; stratigraphic sections and surface samples.

3.2.2.1   Stratigraphic Sections

Topographic and geologic maps, Landsat imagery, and Google Earth were used to generally identify the landforms present in the study area. These were represented by wadis, alluvial fans, sand dunes, sabkhas, interdunes, and slope sediment. In addition, the routes to travel to these landforms were also identified to facilitate visiting these areas, and thus search within these landforms for representative sections during the field trip (3.2 and 3.2.1). Care was taken to select representative section having well-preserved sediments and away from human activities.

Thirteen sections were chosen to represent the landforms within the study area (Figures 3.2 and 3.3).
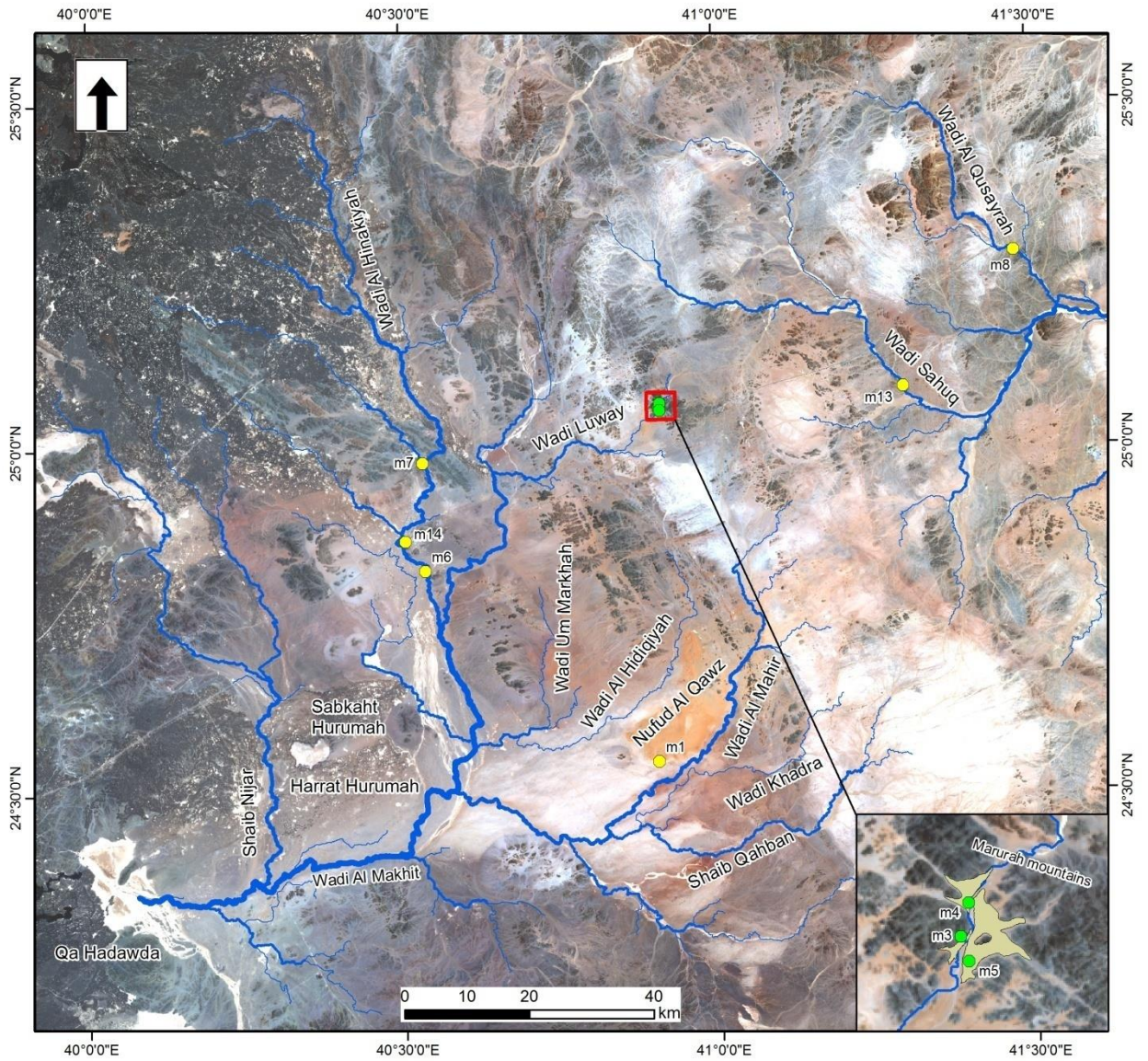
Figure 3.2: Suitable landforms and sections, the wadis' sample sites are marked with yellow markers, and the alluvial fans are marked with green markers.
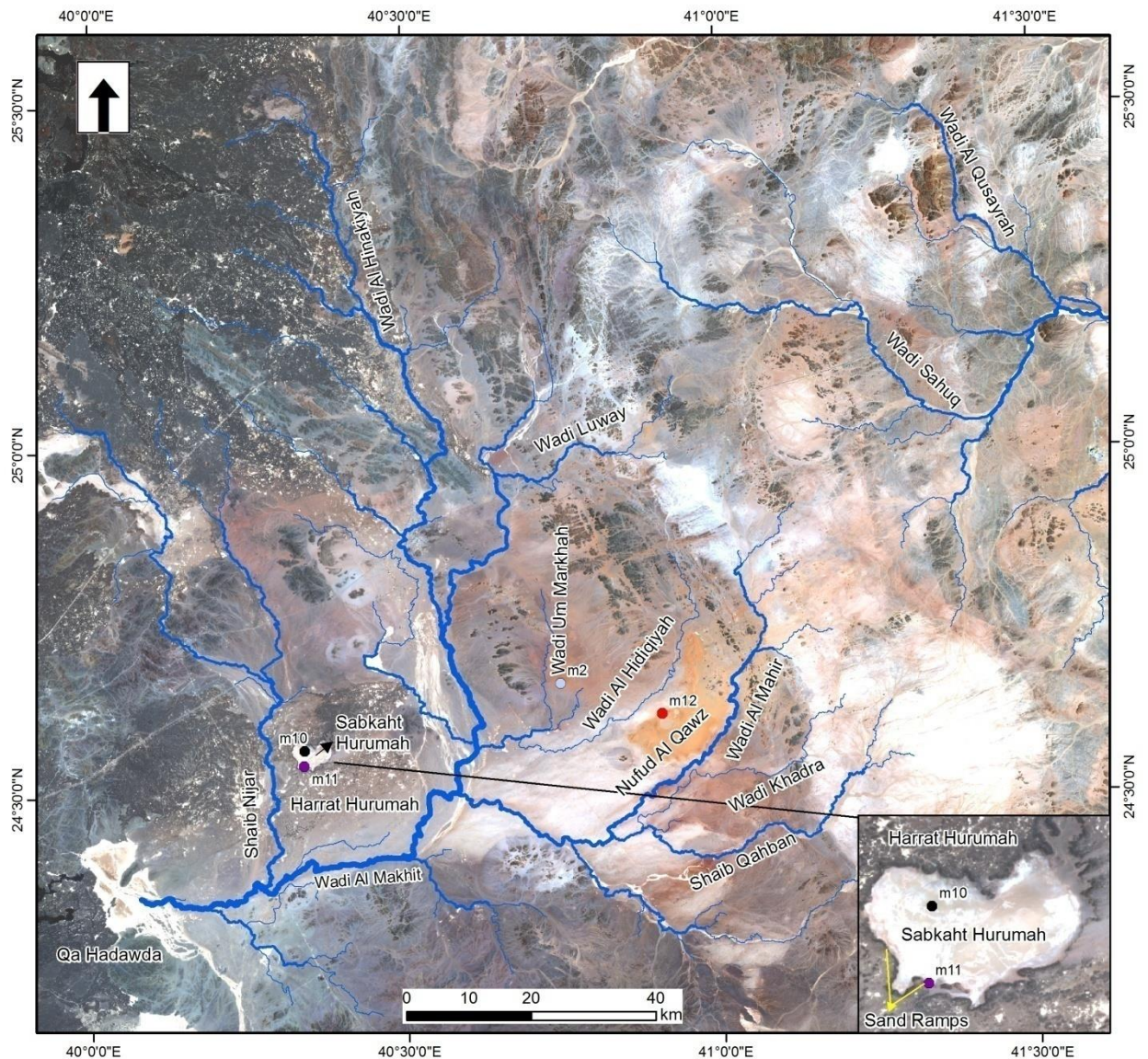
Figure 3.3: Suitable landforms and sections for study, the sand ramps' sites are marked with purple marker, the sabkha with black marker, the palaeolake with red marker, and the slope wash with blue marker.

All sections were prepared for sampling. The preparation of some of the sections required the use of an mechanical digger or mechanical drill while others were dug manually. Each section was then divided into several sub-units, based on the variation of sedimentation environments of that section, and the description and delineation of these sections were carried out in the field. In addition, all samples from the section units were collected in plastic bags for laboratory analyses e.g. particle size analysis, XRD analysis, Munsell colour classification. Some samples were collected for OSL dating in plastic tubes, and were

hermetically sealed using caps and tape, and wrapped in thick black bags to reduce possible contamination with light.

3.2.2.2 Surface Samples.

Many parts of the study area surface vary spectrally in the Landsat 8 scene, and their exact nature could not be ascertained from the image. The field visit was conducted in order to explore, identify, and describe the nature of these surfaces in the field, as well as to collect samples for analysis of the spectral reflectance of the surface samples. Seventeen samples were collected (Figure 3.4).

Sampling locations were carefully selected to be representative of each selected geomorphic surfaces within the study area. Care was taken to select open spaces having homogeneous surfaces, away from human activities like roads and urban areas, where possible. Each sample was collected within approximately 1m x 1m using a clean small trowel by scraping the upper few millimetres containing all surface materials (gravel, sand, clay etc). The sample was then placed in a labelled plastic bag and then stored tightly in a closed box for onward transit to the laboratory at Leicester for spectral analysis. Before leaving the sampling location, a photo of the sample area and the adjacent non-disturbed area was taken as a reference during laboratory spectral measurements. This was required to assist a simulating the natural surface pattern of the sample during reconstruction in the laboratory. The coordinates of each sample were recorded using a handheld GPS.
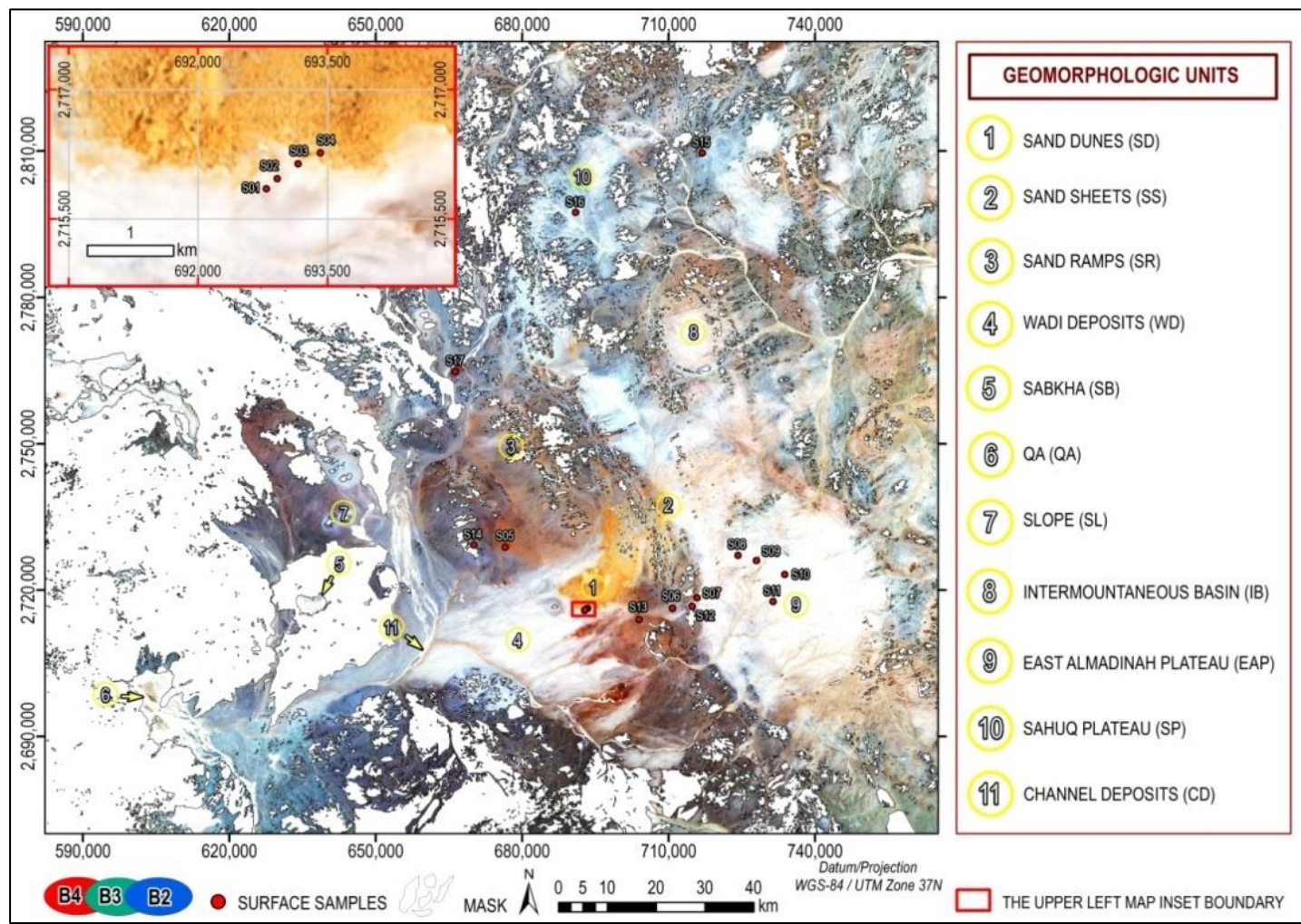
Figure 3.4: Location of surface samples.

3.3 Processing of Remote Sensing Data

3.3.1 Image Pre-processing

The image pre-processing stage prepares data for subsequent analysis. There are number of preprocessing operations that have been carried out on the Landsat 8 images including the following:

3.3.1.1 Image Enhancement

In order to increase the interpretation of Landsat 8 image by increasing apparent contrast between various features in the scene, image enhancement techniques were used. This included geometric, radiometric and atmospheric corrections.

3.3.1.1.1 Geometric Correction

In the current study, Landsat-8 imagery has been geometrically corrected using 110 ground control points (GCPs) extracted from topographic maps (scale 1:50.000) (Saudi Geological Survey), GPS location points through field visits, and a reference orthorectified ETM+ (Landsat-7) image at evenly spread points covering the entire study area in an image-image registration process. The GCPs included reliable positions (roads crossings, edges, desert tracks, small isolated hills etc) (Figure 3.5). The selected GCPs used for solving first order polynomial equations for geometric correction of Landsat-8 data attained a root mean square error (RMSE) less than one pixel, which is sufficient for the current study objectives. Nearest neighbour resampling was then applied to minimize the changes in DN values of Landsat-8 pixels (preserving the spectral information). Figure 3.6 shows the resultant geometrically rectified Landsat 8 imagery with coordinates (Datum: WGS-84, Projection: UTM Zone 37N).
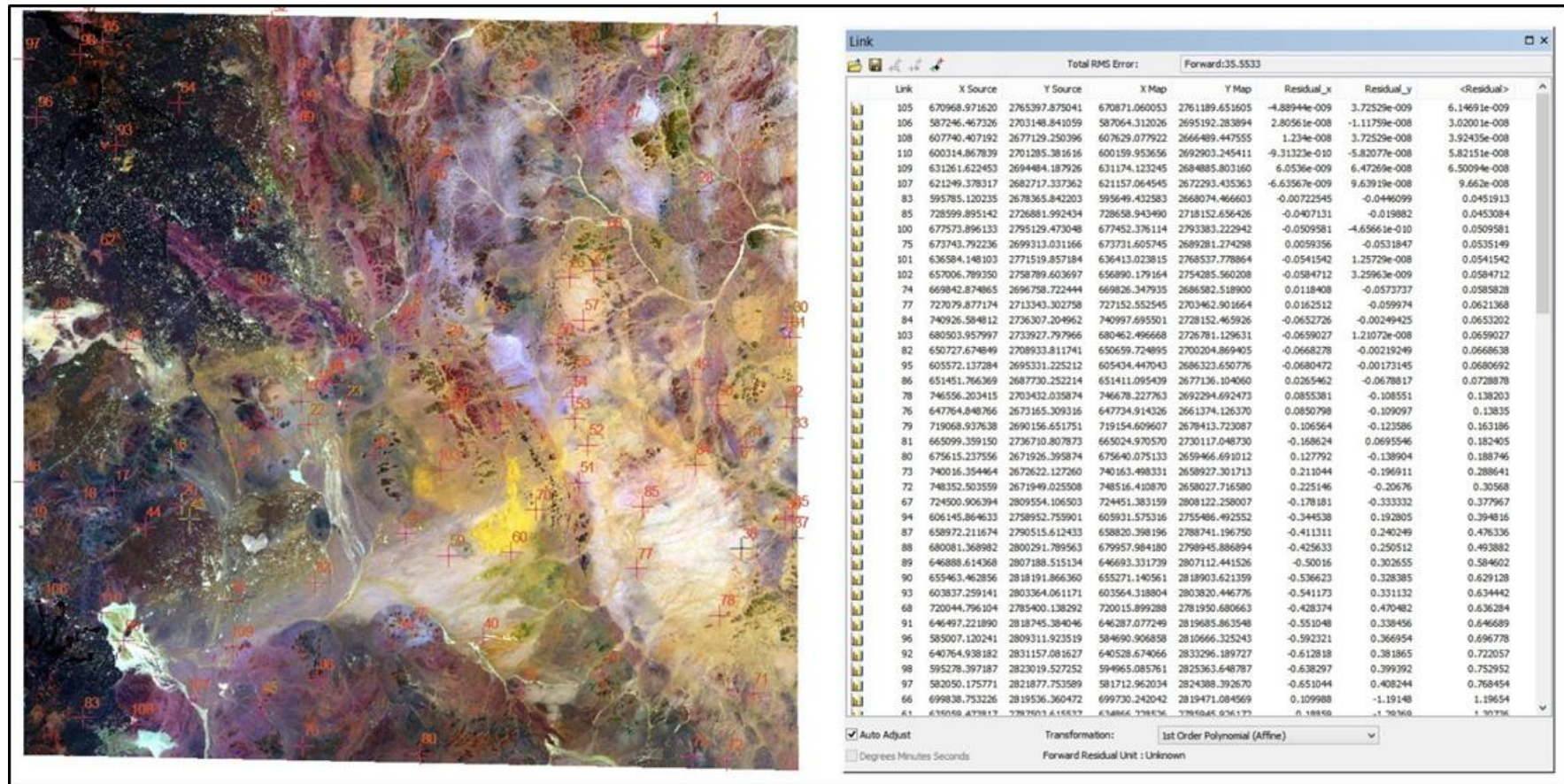
Figure 3.5: Points used for Landsat-8 geometric correction (image rectification) (ArcMap georeferencing interface).
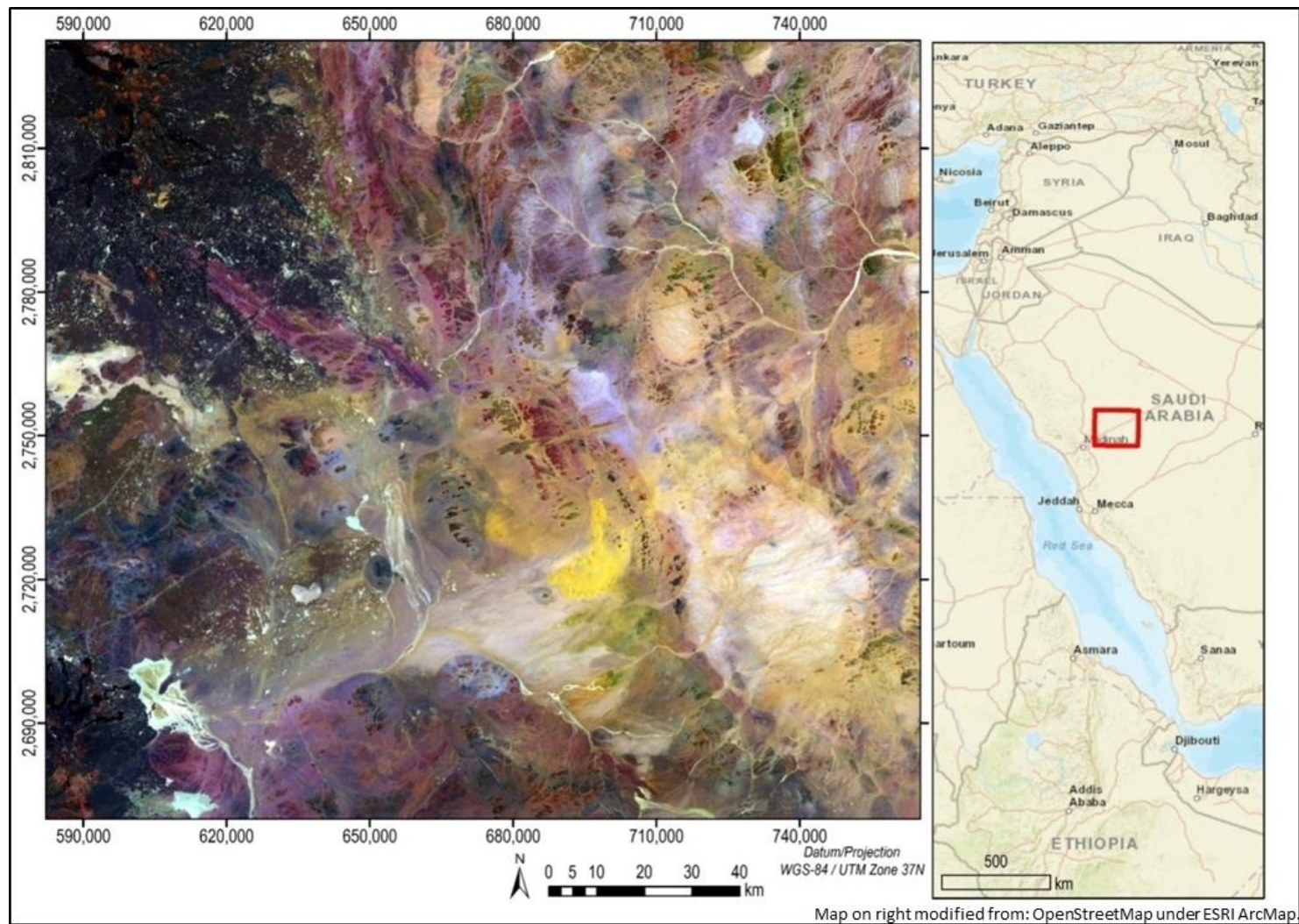
Figure 3.6: Landsat-8 image rectification result as a false colour composite (752 in RGB).

3.3.1.1.2 Radiometric Correction:

Landsat 8 imagery was downloaded from USGS EROS Center which includes quantized Digital Numbers (DN) that gained by both the Operational Land Imager (OLI) and Thermal Infrared Sensor (TIRS).The imagery data was then rescaled from its original 16-bit unsigned integer format into radiance at Top of Atmosphere (TOA) using radiometric rescaling coefficients involved in the associated metadata file (MTL file) Landsat (2016).

The radiance rescaling factors were used in the following equation USGS (2013):

$$L_\lambda = M_L Q_{cal} + A_L$$

Where:

L_λ = TOA spectral radiance (Watts/ (m2 * srad * μm))

M_L = Band-specific multiplicative rescaling factor from the metadata (radiance_mult_band_x, where x is the band number)

A_L = Band-specific additive rescaling factor from the metadata (radiance_add_band_x, where x is the band number)

Q_{cal} = Quantized and calibrated standard product pixel values (DN)

The ENVI radiometric correction module was used to rescale Landsat-8 data from quantized DNs to TOA radiance. The output TOA radiance was then converted from band sequential interleave (BSQ) to band interleaved by line (BIL) for the FLAASH atmospheric correction module (3.3.1.1.3).

3.3.1.1.3 Atmospheric Correction:

Sun illumination, weather disturbances and the production of shadows reduce the amount of extractable data from satellite images. This causes haze due to scattering or emission of electromagnetic radiation from the atmosphere that should be removed before any further processing. The most serious atmospheric impact arises from diffusion of light by particles suspended in air, as depicted by Rayleigh's law, which increments towards shorter higher energy wavelengths (Ye et al., 2017).

The current study used Fast Line-of-sight Atmospheric Analysis of Spectral Hypercubes (FLAASH) atmospheric correction module of the EXELIS ENVI 5.3 program in order to correct the reflected wavelengths up to 3 µm (VNIR-SWIR bands) getting the ground surface reflectance. The input data is BIL TOA radiance and ASTER GDEM topographic data (Figure 3.8, 3.9); other FLAASH parameters are tabulated in Tables 3.2 - 3.5 (Exelis E.N.V.I, 2012).

3.3.1.2 Image Mosaicking

In remote sensing image mosaicking includes assembling neighbouring images of the geographical area to form one combined image in order to delineate or subset the area of interest. The study area spans four scenes, and so this process was used to merge these into one scene of the whole area.

The mosaic was completed for the upper and lower left images, as shown in Figure 3.7A using Automatically Generated Seamlines for Intersections. Weighted seamline was used to generate the seamline. In this method the choice of initial seamline for weighted seamline generation is performed automatically. The same procedure was also completed for the upper and lower right images.

Mosaicking was then applied to the two mosaicked pairs of images (Figure 3.7B), which vary in colour (tonal differences). The automatically generated seamline process was performed to provide a starting point for further editing. The existing seamline was edited so that it follows a natural feature such as a road or wadis, mountains etc. Then colour correction was used to improve colour and tone consistency between the mosaic input scenes (ERDAS tutorial, 2010).

Image subsetting, during the pre-processing the four image scenes were carried out from one after the other before mosaicking into one single image. The mosaic image was then used for creating an area of interest (AOI) for ease of processing and analysis.
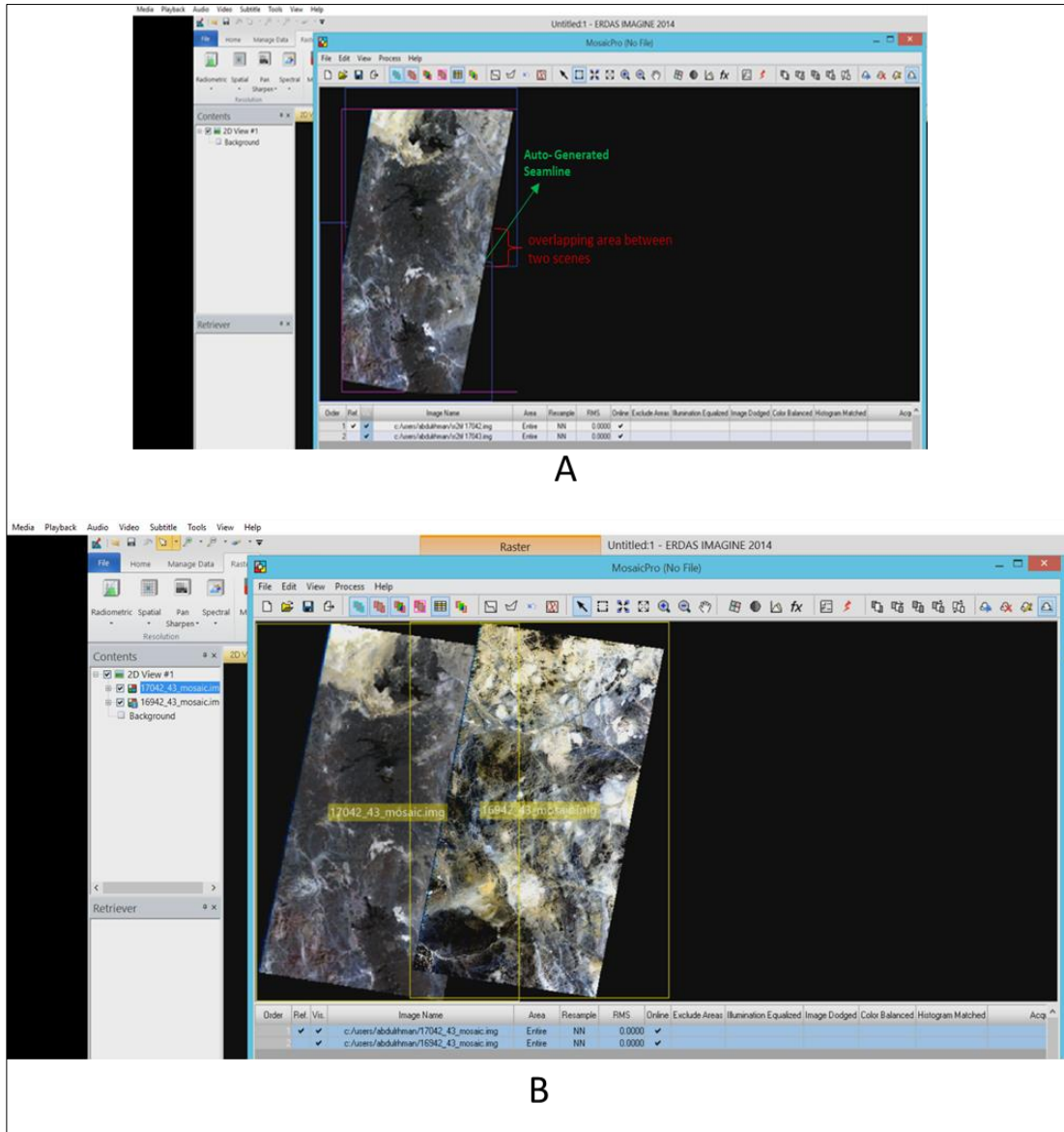
Figure 3.7: Image mosaicking.

3.3.1.3   Data Masking

As the main topic of the current study concentrates on the classification of geomorphological units related to detrital sediments including: Sand Dunes (SD), Sand Sheets (SS), Sand Ramps (SR), Wadi Deposits (WD), Channel Deposits (CD), Sabkha(SB), Qa (Qa), Slope (SL), Intermountaneous Basins (IB), East Al Madinah Plateau (EAP), and Sahuq Plateau (SP), harrats and mountains had to be excluded (masked) through each successive image processing method to remove redundant spectral information. Removing this data also helps

visually increase the contrast between the components within the study area, and save processing time and effort.

As there was an absence of a specific spectral signature of both mountains and harrats it was difficult to separate them from the adjacent sediments derived from these mountans and harrats so although time consuming, manual tracing of Landsat 8 panchromatic image mosaic was found to be the most effective way to form the mask.

Table 3.2: FLAASH atmospheric correction input parameters (scene1)

Input Parameter	Value	Source
WRS_PATH	169	Metadata file
WRS_ROW	42	
Scale Factor	1	Optional
Sensor Type	Multispectral – Landsat-8 OLI	Metadata file
Sensor Altitude	705 km	Metadata file
Av. Ground Elevation	0.946 km	ASTER GEDM
Pixel Size	30 m	Metadata file
Flight Data/Time	2013-05-14 "07:43:45.0710480Z"	Metadata file
Atmospheric Model	Tropical	Based on Geogrphic Location /Optional
Aerosol Model	Tropospheric	Optional
Aerosol retrieval	2-band KT	Optional
Initial Visibility	80 km	Madina Airport

Table 3.3: FLAASH atmospheric correction input parameters (scene 2)

Input Parameter	Value	Source
WRS_PATH	169	Metadata file
WRS_ROW	43	
Scale Factor	1	Optional
Sensor Type	Multispectral – Landsat-8 OLI	Metadata file
Sensor Altitude	705 km	Metadata file
Av. Ground Elevation	0.983 km	ASTER GEDM
Pixel Size	30 m	Metadata file
Flight Data/Time	2013-05-14 "07:44:08.9712562Z"	Metadata file
Atmospheric Model	Tropical	Based on Geogrphic Location/ Optional
Aerosol Model	Tropospheric	Optional
Aerosol retrieval	2-band KT	Optional
Initial Visibility	80 km	Madina Airport

Table 3.4: FLAASH atmospheric correction input parameters (scene 3)

Input Parameter	Value	Source
WRS_PATH	170	Metadata file
WRS_ROW	42	
Scale Factor	1	Optional
Sensor Type	Multispectral – Landsat-8 OLI	Metadata file
Sensor Altitude	705 km	Metadata file
Av. Ground Elevation	0.1107 km	ASTER GEDM
Pixel Size	30 m	Metadata file
Flight Data/Time	2013-06-06 "07:50:00.7402813Z"	Metadata file
Atmospheric Model	Tropical	Based on Geogrphic Location/ Optional
Aerosol Model	Tropospheric	Optional
Aerosol retrieval	2-band KT	Optional
Initial Visibility	80 km	Madina Airport

Table 3.5: FLAASH atmospheric correction input parameters (scene 4)

Input Parameter	Value	Source
WRS_PATH WRS_ROW	170 43	Metadata file
Scale Factor	1	Optional
Sensor Type	Multispectral – Landsat-8 OLI	Metadata file
Sensor Altitude	705 km	Metadata file
Av. Ground Elevation	0.866 km	ASTER GEDM
Pixel Size	30 m	Metadata file
Flight Data/Time	2013-06-06 "07:50:24.6362927Z"	Metadata file
Atmospheric Model	Tropical	Based on Geogrphic Location/ Optional
Aerosol Model	Tropospheric	Optional
Aerosol retrieval	2-band KT	Optional
Initial Visibility	80 km	Madina Airport
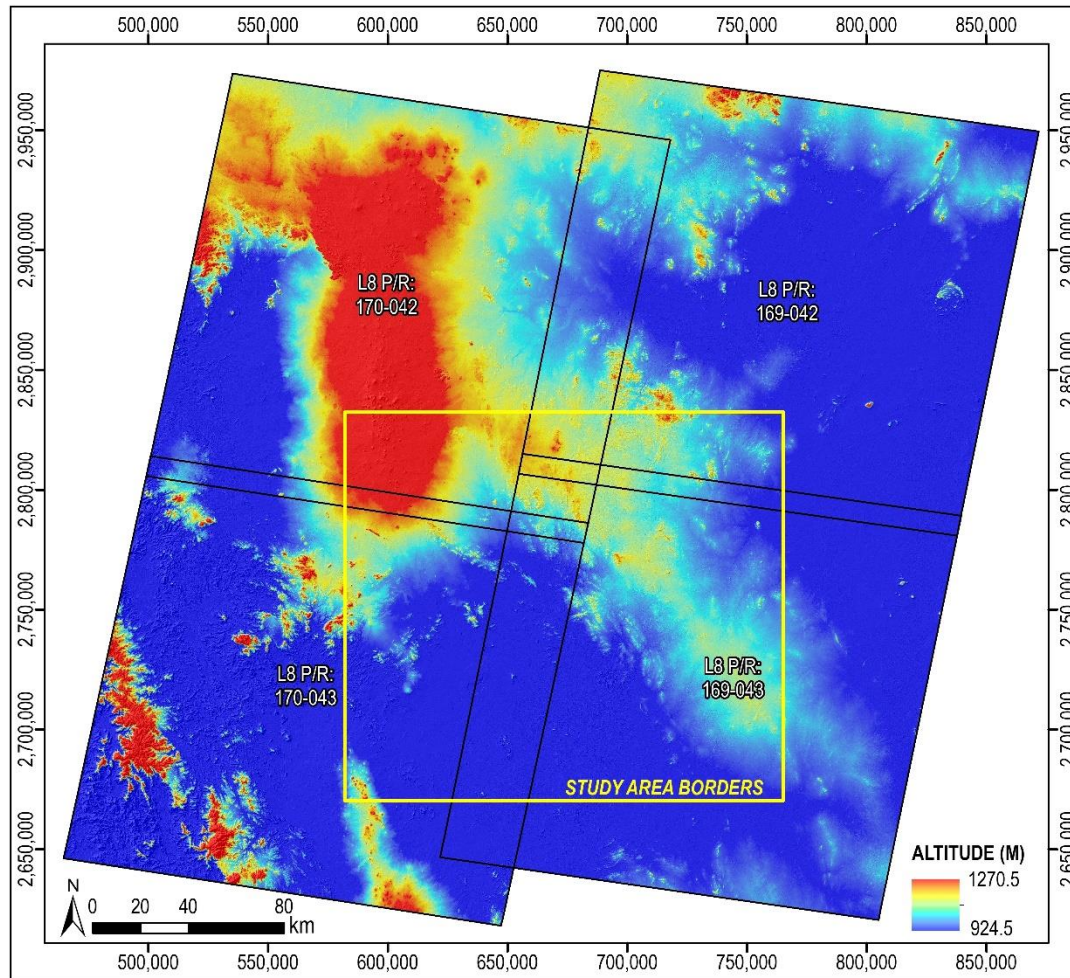
Figure 3.8: ASTER GDEM used in deriving average ground elevation in FLAASH atmospheric correction.
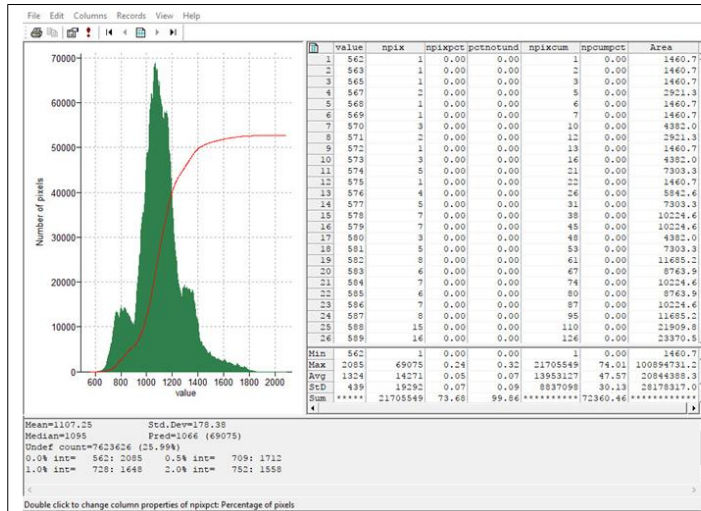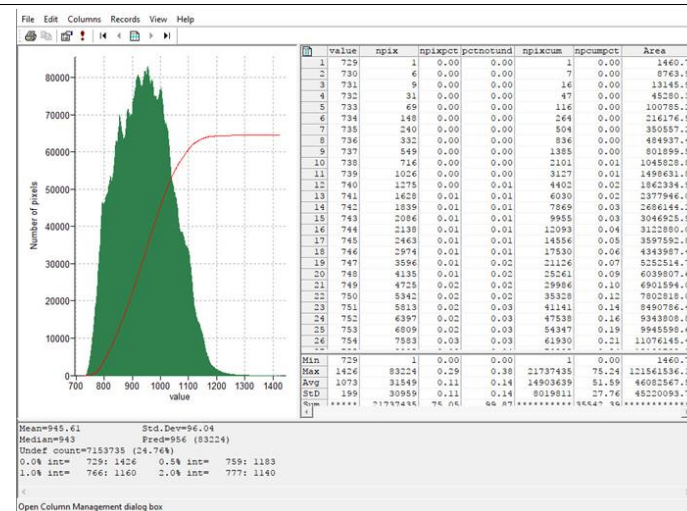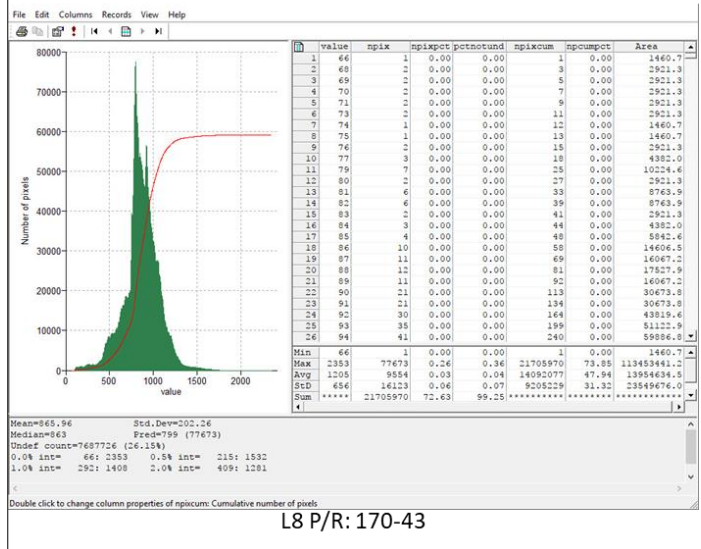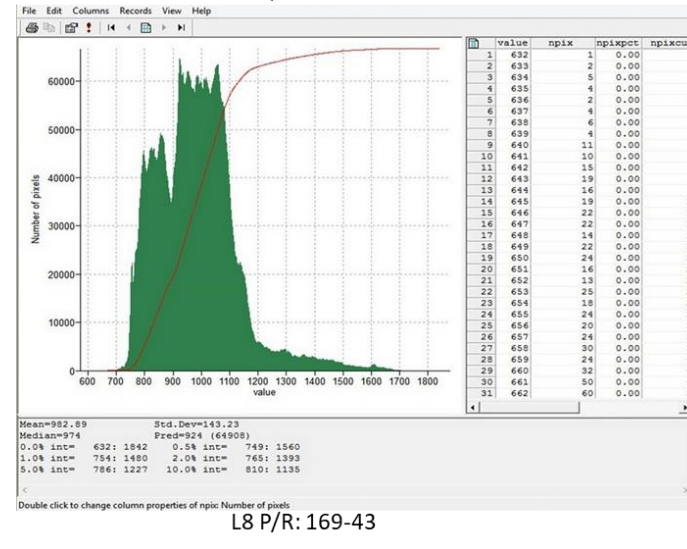
Figure 3.9: Elevations histogram of ASTER GDEM of the study area.

3.3.2 Landsat -8 Image Processing:

The Landsat 8 Image processing procedures were intended to convert multispectral image data into informative images, which increase the contrast between targets and produces information about certain pixels in the image. The processing techniques used in the current study include colour composites, band ratioing, principle component analysis, and supervised classification.

3.3.2.1 Colour Composite Images:

In a gray scale image, the distinction between different reflectance values may not always be clear. This was solved using colour composites of multiple bands, which give a better contrast in RGB display. Colour composite images are a blend of two or more bands according to known spectral properties of ground surface components.

The current study used colour composites in order to interpret the spectral behaviour of different geomorphologic units within the reflected portion of electromagnetic spectrum (0.4 – 2.5 µm). The band colour composite of Landsat-8 imagery that uses bands 4, 3, and 2 in Red, Green, and Blue (RGB) colour channels respectively is called a true colour image. Using adjacent bands usually gives a high correlation and a weak variance, and consequently cannot discriminate between most components.

Mathematically, the total number of possible colour composites (N) derived from Landsat-8 (7 bands) could be calculated from the following equation (ILWIS tutorial):

$$\binom{N}{3} = \frac{N!}{(3! * (N-3)!)} \rightarrow (1)$$

Where; N is the total number of bands in the map list

Thus, the total possible composites of the Landsat-8 (seven bands) will be 35 composites. The Optimum Index Factor (OIF) is a statistic value that can be used to select the most informative combination, which has highest sum of standard deviations with the lowest correlation among band pairs (Chavez et al., 1982). ILWIS Open software has been applied in the current study using the following algorithm to conclude the highest ranked OIF index:

$$OIF = \frac{Si + Sj + Sk}{|Ri,j| + |Ri,k| + |Rj,k|} \rightarrow (2)$$

Where;

Si, Sj, and Sk are the standard deviations for bands i, j, and k, respectively

Ri,j, Ri,k, and Rj,kare the correlation coefficients between any two of the three bands being evaluated.

Pearson correlation has been applied for correlating bands and determining the most informative combinations.

3.3.2.2 Band Ratios

Using band ratios is a type of image transformation, referring to processing multiple images from different bands into one single image (Gupta, 2003). Dividing reflectance values at peaks/maxima and troughs/minima in a reflectance curve will elevate the transformed reflectance values of specific geologic materials and may enhance the contrast between them. The choice of bands is based on their spectral reflectance and the absorption features of the mapped geomorphologic units.

Band rationing is advantageous because the effect of terrain and shadow is divided out in the calculations (Vincent, 1997).

Sultan et al. (1987) proposed a Lansdsat-7 false colour composite of ratios 5/7, 5/1, 5/4 * 3/4 in RGB for lithological mapping. The current study used the Landsat 8 equivalent of Sultan's ratio (6/7, 6/2, 6/5*4/5 in RGB) for lithologic mapping.

Abrams et al. (1983) used Landsat-7 band ratios 5/7, 4/5, 3/1 in RGB for lithologic mapping. Landsat-8 equivalent of these band ratios are 6/7, 5/6, 4/2 respectively. The band ratio 6/7 emphasizes the strong absorption feature of electromagnetic radiation in the $2.08 - 2.35$ µm spectral range (bands 7) that is directly related to Mg OH, AlOH, CO_3 minerals (chlorite, clays, mica, serpentine, amphiboles, and carbonates). The ratio 5/6 band of Landsat-8 highlights vegetation, while 4/2 band ratio highlights the absorption feature of iron oxides.

3.3.2.3 Principal Component Analysis (PCA)

Multispectral images often have similar visual appearance for different bands leading to high correlation between each other (Figure 4.8). Principal component analysis (PCA) is a common method of analysis for correlated multi-variable datasets by mathematical transformation of the original data to be arranged according to the axis of greatest variability

for creating new non-correlated components. Mathematically, this means that the covariance matrix in the new system is diagonal with all elements equal to zero, except the first diagonal where the elements are in decreasing order. The transformation coefficients of the covariance matrix are the eigenvector values. So, PCA displays the maximum contrast from several spectral bands with just three primary display colours (Vincent, 1997).

The number of output PCs is the same as the number of the input spectral bands. Often the first three PCs usually contain more than 98% of the data variance. Liu and Mason (2016) stated that PC1 concentrates features common to all input bands (essentially topography) displaying important structural information. PC2 is orthogonal to PC1 in n directional space and highlights the spectral differences between visible and the infrared spectral bands. PC3 includes the third most variability and is orthogonal to the other two PCs.

3.3.2.4 Image Classification

The current study used a Maximum likelihood supervised classification method based on training sites selected according to the geologic maps, field investigations, 2D scatter plots of non-correlated reflectance bands, and visual assessment of the colour composites.

Eleven geomorphologic units were selected to be classified: sand dunes, sand sheets, sand ramps, wadi deposits, channel deposits, slope, Qa, sabkha, intemountaneous basins, Sahuq plateau, and East Al Madinah plateau. Each unit was represented with a number of training sites containing between 300-2000 pixels. As a geomorphologic unit usually contains materials of different composition and different spectral characteristics, (this was clear especially within slopes, and wadi deposits), a number of training sites were selected as subclasses belonging to the same geomorphologic unit. Consequently, the number of input endmembers increased to be 21, this reduced the standard deviation of the average reflectances and the classification results became more reliable (all subclasses then merged to their unit through the postclassification process).

The mean reflectance value of each was calculated and finally the end-members spectral library created.

Postclassification processes were applied to the classification these were:

- Sieving; to solve the problem of isolated pixels occurring in classification images.

- Clumping adjacent pixels. A dilate kernel value was used to expand shapes containing the input classes. An array of 3*3 and element value of 1 were used for the clumping process.
- Majority-Minority analysis; to change spurious pixels within a large single class to that class.

A Confusion matrix was then applied to the classification results to assess the overall accuracy based on an independent validation ground truths (73 sites) representing the different 11 geomorphologic units.

3.3.3 Spectral Measurements of Surface Samples

The proportions and distribution of grain sizes exposed on the sediment surface of the 17 sites were determined using surface samples, recorded field observations and pictures captured on location. Sediment surface colour was also determined using a Munsell soil colour chart.

The 17 surface samples were spectrally analysed with an ASD Field-SpecR Hand Held2 TM Spectroradiometer, with an operating wavelength range of 325-1075nm, to ±1nm accuracy, and spectral resolution <3 nm at 700 nm, according to the manufacturer's specification (ASD Inc, 2014). The majority of the samples contained both fine and coarse clasts. Fine clasts were classified as those less than 1mm, namely silt, sands, and clay, while coarse clasts were greater than 1mm, such as gravels, cobbles and boulders. In order to properly analyse the spectral signatures of the 17 surface samples a two-stage process was performed.

First, for all samples, the original sample surface was reconstructed using the photographic record taken in the field (section 3.2.2.2), and recorded the spectra of the reconstructed surface. In the second stage, all samples were divided using a 1mm sieve, into fine (less than 1mm particles) and coarse components (greater than 1mm particles). A two-stage measuring of the spectral signatures of the samples was performed to determine the role of spatial variation in the extremes, e.g. fine and coarse components on the reflectance of satellite images.

The measurements of sample spectral response were performed in a dark room. Following Bullard and White (2002), each sample was placed in a matt black dish and illuminated by

a lamp at an angle of 45° and a distance of 36cm. The sample and white reference panel were viewed at nadir 90°.

The reflectance measurements were taken for each sample five times, and the average of these values calculated. The measuring device, ASD Field-SpecR Hand Held2 TM Spectroradiometer, captured the spectral data, and provided it in .asd file format. The ViewSpec Pro Version 6 software, was used to convert the .asd file to ASCII (.txt) format, in Microsoft Excel. The ASCII (.txt) file was then used for calculating the average spectral reflectance value from sample data.

3.3.4 Comparison of Images to Surface samples

The reason for converting the Landsat image raw DN (radiance) to ground reflectance or surface using the FLAASH module is to allow direct comparison between multispectral and hyperspectral data obtained using the instrument (ASD Field-SpecR Hand Held2 TM Spectroradiometer). In this study, Landsat 8 bands 1 to 7 were chosen based on their spectral characteristics and ability to enhance geomorphological features (Table 3.1). The aim of using this imagery was to investigate the reflectance means and what surface conditions caused changes in reflectance along the sediment surface within the study area.

In the current study, it has been attempted to find out if the relative proportion of fine and coarse material could be determined on the images with a comparison between laboratory surface reflectance of collected samples (hyperspectral data) and the Landsat 8 surface reflectance of their pixels. As the ASD HH2 spectral range falls between (325 − 1075 nm) that is correlated with Landsat 8 bands (2 to 5), only bands 2, 3, 4 and 5 were used due to the limited wavelength range of ASD HH2. Therefore, the ASD HH2 spectra were been resampled to Landsat spectral resolution before carrying out the comparison process. By doing this, the comparison provided information as to why there were variations in reflectance of the surface sediments and also spatial contrasts in the fine and coarse components of the sediments.

The seventeen field samples' coordinates were converted to a shapefile for extracting the reflectance from the image (Landsat data). To ensure the sample area was well represented, eight neighbouring pixels were also sampled around the sample pixel so that the average

value could be calculated, thus reducing the impact of a pixel that may have an abnormal reflectance.

3.3.5 Spectral Transect

A spectral transect was carried out in order to describe how the distribution of sediments varies at different locations in the field using Landsat 8 imagery and laboratory ASD HH2 spectral reflectance, and to assess the ability of Landsat 8 data in mapping the distribution of the detrital sediments with different grain size over large areas. The current study selected four pixel samples (1, 2, 3, 4) across East Al Madinah Plateau and a reference pixel sample (S8) that is measured using ASD HH2. The reference sample (S8) was used to interpret the spectral behaviour of the four pixel samples along the transect line.

3.4 Laboratory Analysis

Laboratory analyses were undertaken on the samples collected from the field, in order to obtain the environmental information preserved in the deposit sequences, and buildup a picture of the palaeoenvironment in the east of Al Madinah. These analyses include:

3.4.1 Particle Size Analysis

Particle size analysis is used to measure the size of particles in the collected samples. The distribution of particle sizes represents a key property defining all sediments, and also provides valuable indications regarding the origin, history of transport, and the conditions under which the sediment was deposited (Tucker, 1988).

In this research, samples were split into representative subsamples using a riffle box. Samples were then sectioned into two parts: the first one is the fine fraction (less than 2 mm), and the second one is the coarse fraction (2 mm and above). The weight of both parts were measured using a balance.

Organic materials have been removed if present, by placing the samples in the furnace overnight. Also carbonates have been removed from the samples, if any, where the sample was placed in a beaker and added to 10% HCI until no reaction was visible, then the beaker was filled with distilled water and then the distilled water was disposed after three nights in order to eliminate the loss of sediment particles. Then the sediment particles in the beaker was placed in an oven to dry completely at a temperature of 110°C. This procedure was carried out three times.

For the first part (fine fractions less than 2 mm), was measured by using the laser diffraction method by placing the sample into a beaker and mixing it with Calgon and boiling it for 5 minutes. Then the sample was added into the fluid reservoir in the laser equipment Beckman Coulter LS230. Coarse fractions were measured using stacked sieves (-1 φ= very fine pebbles; -1.4 φ = very fine pebbles; -2 φ= fine pebbles; -2.4 φ= fine pebbles; -3 φ= medium pebbles; -3.4 φ= medium pebbles; -4 φ= coarse pebbles. Particles which were bigger than -4 φ, were measured using a caliper.

3.4.2 X- Ray Diffraction Analysis (XRD)

This technique allows the different mineral proportions present in the sample to be identified, and hence, shed light on the varying conditions during formation (Tucker, 1988). A total of 34 samples were subjected to XRD analysis.

The experimental procedure is in brief as follows:

Stage 1: Each sample was crushed into powder using a centrifuge mill.

Stage 2: Next the wet mill method was used which includes:

- Placing pink beads into a container, with beads carefully aligned parallel to side, and fill to the brim of the grey container.
- Next (about 4 g of the sample and 10mL of IMS) were added into the container with beads.
- Then the mixture was milled (on a vibrating shaker) for 15 minutes.
- After the sample was poured out (the residue was washed with IMS) into a petri dish.
- Then the sample was left to dry in the cool oven for overnight.
- Finally the sample was packed into a bag after drying.

Stage 3: Preparation in this stage includes:

- The Perspex disk which holds the sample was scratched longitudinally before the XD run.
- Putting the XRD sample into the Perspex disk.
- Levelling, smoothing, (with no pits) and flattening the surface of the sample as required.
- Finally the sample in the disk was inserted into the XRD equipment, and is ready to be analysed.

3.4.3 Munsell Soil Colour Charts

In this research all the units in the sections (numbering 13) selected in the study were described according to sediment colour based on the Munsell soil colour book, as illustrated in Figure 3.10.

Figure 3.10: Matching the colour of a sediment sample against the standardised swatches for brown shades within the Munsell soil colour.

3.4.4 Optically Stimulated Luminescence (OSL) Dating

A number of geochronological methods are available for dating sediment, of which optically stimulated luminescence (OSL) is a commonly-used technique for the dating of sediment samples. As described by Duller (2008b), this technique determines the last time a mineral (quartz or K-feldspar) grain was exposed to sunlight. Exposure to heat or light resets the luminescence signal to zero, which then progressively increases over time as a result of the exposure to radioactive isotopes present within the sediments following burial. This radiation is provided by natural radioactive isotopes, as well as cosmic rays. According to Duller (2008a) the process of dating using OSL relies on measurement of both the total radiation dose (D_e) received by the mineral (also known as palaeodose or equivalent dose), and the environmental dose rate (Dr). The latter is sum of alpha, beta and gamma radiation doses, plus cosmic ray contributions, as derived from and radioactive elements, namely Potassium (^{40}K), Thorium (^{232}Th), and Uranium (^{238}U), present within the sediment. The sample age is calculated by dividing equivalent dose (De, measured in Grays) by the annual environmental dose rate (Dr, Grays per annum).

In this work, OSL dating was applied to four samples. The samples were prepared for coarse grain (90-250 μm) quartz analysis under red light conditions following the methods outlined in Bateman and Catt (1996). In brief this comprised:

- Removal and retention of sample tube ends. This material provided an estimate of the sample water content and a sub-sample of this was used to obtained ICP-MS and ICP-OES estimates of the uranium, thorium and potassium contents of the samples, which are required for dose rate estimation.
- HCl treatment to remove carbonate.
- H_2O_2 treatment to remove organics.
- Wet sieving to isolate a single size fraction for analysis within the range 90 and 250 μm.
- Density separation to isolate the fraction < 2.7 g cm^{-3}
- A second density separation to remove feldspar grains <2.58 g cm^{-3} (the feldspar fraction was retained).
- 45 minutes of 48% hydrofluoric acid treatment to etch the outer 10 μm of the quartz grains and to remove any remaining feldspar grains.
- Dry sieving to remove heavily etched grains/feldspars and to re-isolate the originally sieved size fraction.

Sample properties and analysis protocols

All luminescence measurements were performed on a Risoe DA20 TL/OSL reader. Stimulation (40 s at 125°C) was provided by blue LEDS (stimulation wave length 470 nm) at 70% power (delivering c. 72 mW cm^{-2} to the sample). OSL signals were detected with an EMI 9235QA photomultiplier tube with a U-340 detection filter. Laboratory irradiations were delivered by a ^{90}Sr beta source with a dose rate (at the time of measurement) of 8.54 Gy min^{-1}. This was calibrated against the Risoe calibration quartz and has been validated via comparison with an external luminescence dating laboratory. Single aliquot equivalent doses were determined using the Single Aliquot Regeneration (SAR) protocol [See for details Murray and Wintle (2000, 2003); Wintle and Murray (2006)]. All measurements were made on small (2 mm) aliquots containing c. 150-200 grains within the 180-250 μm range. All of the SAR analyses comprised a 6 or 7 regeneration point sequence, and in all cases included

a (repeat) recycling dose, a zero dose and an IR ratio dose (Duller, 2003) to check for feldspar contamination. Appropriate measurement (preheating) conditions were determined using dose recovery experiments (Murray and Wintle, 2003). Analyses were carried out in the Analyst software (version 4.14.6). Dose response curves were fitted with saturating exponential curves and equivalent dose uncertainties were estimated using a Monte Carlo simulation method (Duller, 2007). The associated uncertainty in final equivalent dose estimates incorporated beta source calibration uncertainty (3%), curve fitting uncertainty, counting statistics and a systematic instrumental uncertainty of 1.5%.

Sample OSL properties

The first measurements taken showed that all of the four samples were sensitive (i.e. substantial production of OSL per unit applied dose). These samples showed rapid decay in the first two seconds of stimulation. Furthermore, a strong 110°C TL peak was observed, along with very little indication of feldspar grains or inclusions; all implying that the samples are suitable for analysis with the standard quartz single aliquot regeneration (SAR) method.

Dose recovery experiments

A dose recovery (DR) experiment was employed for every collected sample. This was done to further evaluate the samples' suitability with regards to the SAR protocol (Murray and Wintle, 2003). Samples were first bleached twice at room temperature, after which a known beta dose was administered. This is treated as the "natural" signal.

The dose recovery protocol assesses the performance of the SAR protocol by assessing whether the measured "equivalent dose" matches the administered laboratory beta dose. The dose recovery experiments utilised a range of preheating temperatures in order to find the optimal temperature conditions for the analysis of the naturally occurring equivalent doses. Table 6.3 includes data from the dose recovery experiments. Additionally, the recuperation measurement is shown, which is the size of the sensitivity-corrected zero dose relative to the sensitivity-corrected natural signal. This measurement should be less than 5 % of the natural signal. Overall, it was found that De had little sensitivity to the varying preheating temperatures. Moreover, a plateau was seen for the natural/regeneration dose preheating temperatures between 180 and 240°C.

Table 3.6: Summary of the dose recovery experiment (n= 24 for each) with varying preheating temperature combinations

Sample	Average dose recovery ratio	Average recycling ratio	Average recuperation (%)	Chosen preheat/test dose preheat temperature (°C)	DR ratio for chosen preheat combination
MAD 13/4/1/1	1.01 ± 0.04	1.00 ± 0.03	0.51 ± 0.48	220/160	1.00 ± 0.02 (n=3)
MAD 13/4/1/2	1.01 ± 0.04	1.01 ± 0.03	0.37 ± 0.33	220/160	1.00 ± 0.01 (n=3)
MAD 13/5/1/1*	1.06 ± 0.03	nd	nd	240/160	1.01 ± 0.02 (n=3)
MAD 13/14/1	1.00 ± 0.06	0.98 ± 0.02	0.62 ± 1.24	220/160	0.98 ± 0.03 (n=3)

*Run crashed and points for recycling and recuperation were not obtained. When factoring in the general well behaviour of this sample, and accounting for the SAR response measurements obtained later on, this is not significantly problematic.

Equivalent dose determination

Between 20 and 24 aliquots were analysed for each sample. Aliquots with recycling values outside 10% of unity, recuperation >5% of the natural signal, IR ratios < 0.9, or equivalent doses > $2D_o$ (D_o is a fitting parameter for the saturating exponential growth curve and is indicative of the dose at which there is an onset of signal saturation) were removed from the analysis of the SAR runs. With the exception M5 unit1, few aliquots failed any of these criteria, resulting in yields of 16-24 aliquots for the estimation of the sample equivalent dose.

Over-dispersion was present within each sample, this being the inter-aliquot scatter beyond that which is not accounted for by individual De measurement uncertainties. MAD13/5/1/1 produced aliquots with equivalent dose estimates similar to and frequently well beyond the point of saturation that is usually observed for the quartz fast component (this being the thermally stable and rapidly bleached signal that the SAR protocol seeks to measure). Despite the fact that the samples registered regeneration doses of up to 270 Gy, an equivalent dose could only be interpolated using a saturating exponential fit for 10 samples out of the 24 analysed aliquots. Therefore, adhering to the approach described in Joordens et al (2014), the 2Do parameter obtained from the saturating exponential fit from every aliquot

(irrespective of whether the natural signal intercepted the growth curve) was used to estimate the minimum age. Based upon this, a minimum De estimate of 162 ± 7 Gy was obtained.

Dose rate estimation

Dose rates were determined via inductively coupled plasma mass spectrometry (ICP-MS) for U and Th and for K, ICP-OES carried out at SGS laboratories, Canada. The concentrations of U, Th and K were converted to annual dose rates following Guérin et al. (2011) with corrections for grain size Mejdahl (1979), water content Aitken (1985) and HF etching Bell (1979). It is important to determine sample water content, because environmental radiation is absorbed by water, which would otherwise contribute to the dose rate (Duller, 2008a). Cosmic dose rates were determined following Prescott and Hutton (1994) with a 5% uncertainty included, and assume the modern sample depth is representative of the average burial depth.

Nathan and Mauz (2008) demonstrated that a sample's dose rate may evolve through time by precipitation/accumulation of inert non-radioactive interstitial material, such as carbonate and/or water, provided it is not represented in the activity measurement. This occurs in two ways:

1)   Dilution of environmental activity in proportion to the mass per unit volume change.

2)   The intrusive body that contains the radioactive elements might have characteristic energy absorption cross-sections that will differ from those found in deposited sediments.

In the current study, all OSL samples contained a minor carbonate cement content (5–9%). This is relatively low compared to other cases modelled or analysed. For instance, Nathan and Mauz (2008) demonstrated that for marine carbonate rich (i.e. 17-83% carbonate content) coastal sediments there were, in the most extreme cases, 30% differences between onset and final dose rates. This impacted on conventional and modelled optical ages by between 2% and 15%, varying according to the final (current) carbonate and water content. These scenarios however involve substantially larger carbonate contents than observed in the present study. More recently, Nash et al. (2018) also working on clastic sediments in coastal areas, concluded that despite the fact that the carbonate cement percentage ranged between 17 to 44 %, the change in dose rate was usually less than 0.1 Gy kyr^{-1}. This made

the resulting ages as determined by OSL older by 13% on average. On this basis, given the substantially lower carbonate contents is unconstrained for the present study, no dose rate corrections were made.

Chapter 4. Results of Remote Sensing

This chapter focuses on the presentation of results based on the following structure: section (4.1) covers remote sensing and geomorphological mapping, which comprises of the morphologic identification of landforms using a digital elevation model (ASTER GDEM) (4.1.1), a geomorphological description of the study using Landsat 8 data and the ASD Hand-Held2 device (4.1.2), a mapping of the study area using Landsat 8 spectral data (4.1.3) as well as identifying the factors influencing the spectral reflectance of the surface geomorphology (4.1.4).

4.1   Remote Sensing and Geomorphological Mapping

4.1.1   Landscape Characteristics Derived from Digital Elevation Model (ASTER GDEM)

In this section, ASTER GDEM was used to generate the elevation map, slope, drainage networks, drainage and sub-basins of the study.

4.1.1.1 Elevation

In the elevation map (Figure 4.1), the terrain was divided into seven categories:

- 603 – 750 m: this category is situated in the low Qa areas, which is a flat bottomed surface, a closed depression (Plain) that is covered with fine silt and clay, and is devoid of plant cover or evaporated salts.

- 751 – 850 m: this category is found mostly in the lower parts of wadi drainage basins, as well as the Harrats (lava fields) situated to the south west of the study area.

- 851 – 1000 m: this category is found mostly in plateau areas.

- 1001 – 1100 m: this category is situated principally in the mountainous areas, in the upper catchment of the wadis, and the drainage divide line between Wadi Sahuq and Wadi Al Makhit, in addition to some scattered mountains within the two basins.

- 1101 – 1250 m, 1251 – 1450 m, 1451 – 2088 m: these categories are found mostly in the mountains and Harrats (lava fields) situated to the North West.
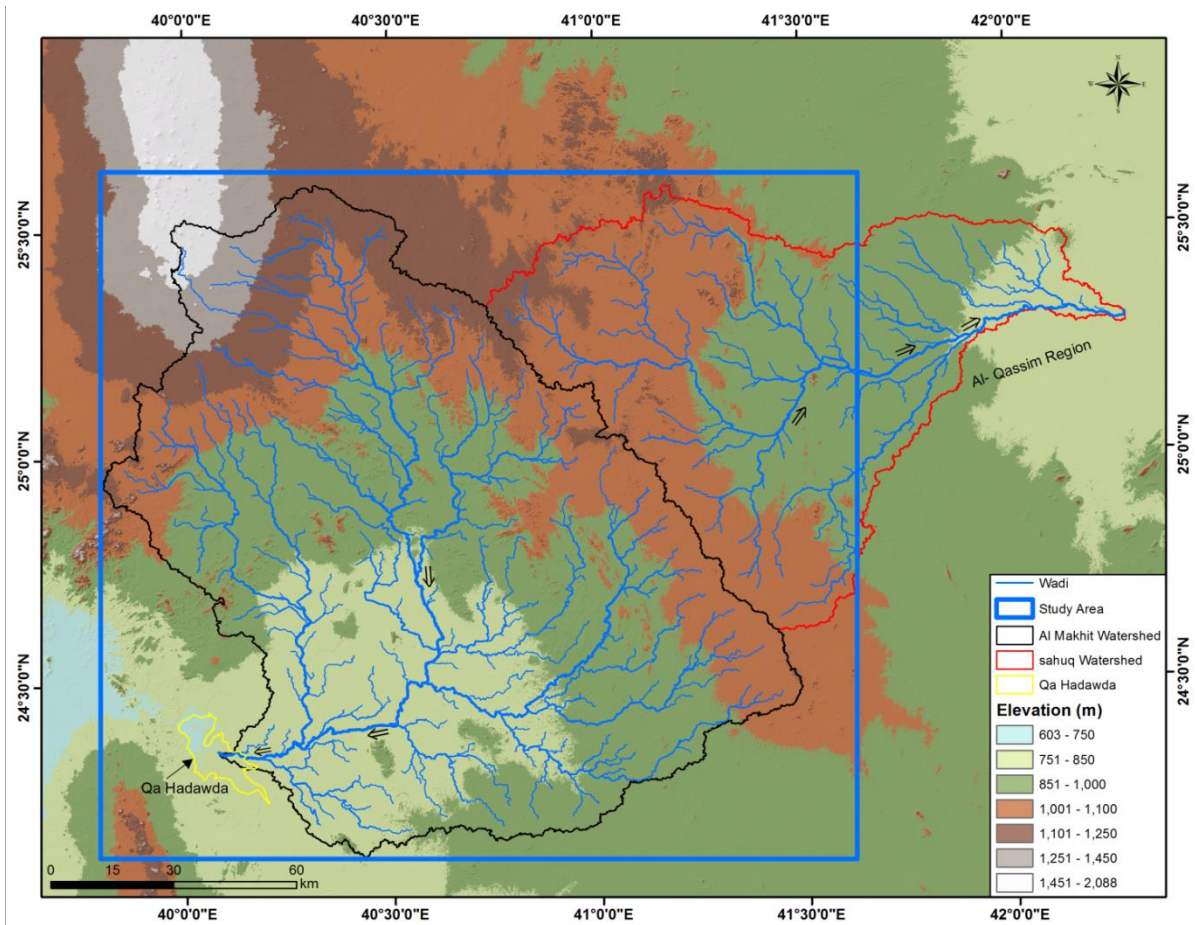
Figure 4.1: The seven elevation categories of the study area in relationship to the wadi drainage networks.

4.1.1.2 Slope

The degree of slope differs from one place to another within the study area, varying from 0° to 63°. The study area was divided into seven slope categories (Figure 4.2), and their most likely location is described in Table 4.1.
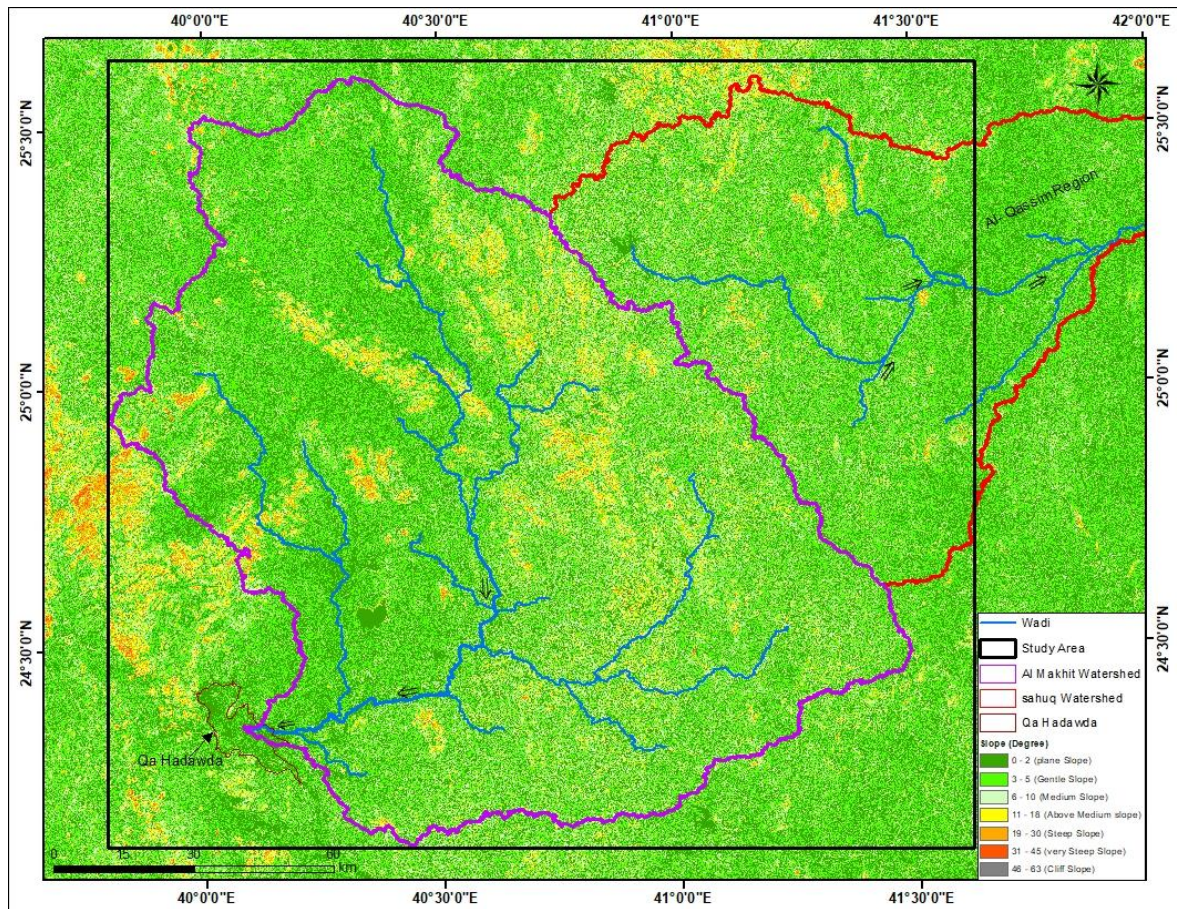
Figure 4.2: Slope categories of the study area in relationship to the wadi drainage networks

Table 4.1: Slope categories and where they are most likely to be encountered in the study area

Description	Degree of slope	Location
Plane Slope	0 – 2	Found in the low areas, such as Qa and sabkhas, as well as interdunes, alluvial fans, and wadi channels.
Gentle Slope	3 -5	The distribution corresponds to areas of Harrats (lava fields) and alluvial fans.
Medium Slope	6 - 10	These areas represent the transition between gentle slope and steep slope areas. Their distribution corresponds to escarpments and plateaus.
Above Medium Slope	11 - 18	Highland areas (mountainous and volcanic), as well as sand dunes.
Steep Slope	19 – 30	
Very Steep Slope	31 - 45	
Cliff Slope	46 - 63	

4.1.1.3 Drainage Network

The study area contains a large number of streams/wadis (Figure 4.3). The streams have reached the sixth order in the Al Makhit drainage basin (according to the Strahler classification), and the fifth order in the Sahuq drainage basin. The process of ordering streams is important in that it is directly and intimately linked to the size of the drainage network, where a higher order signifies potentially higher flows.
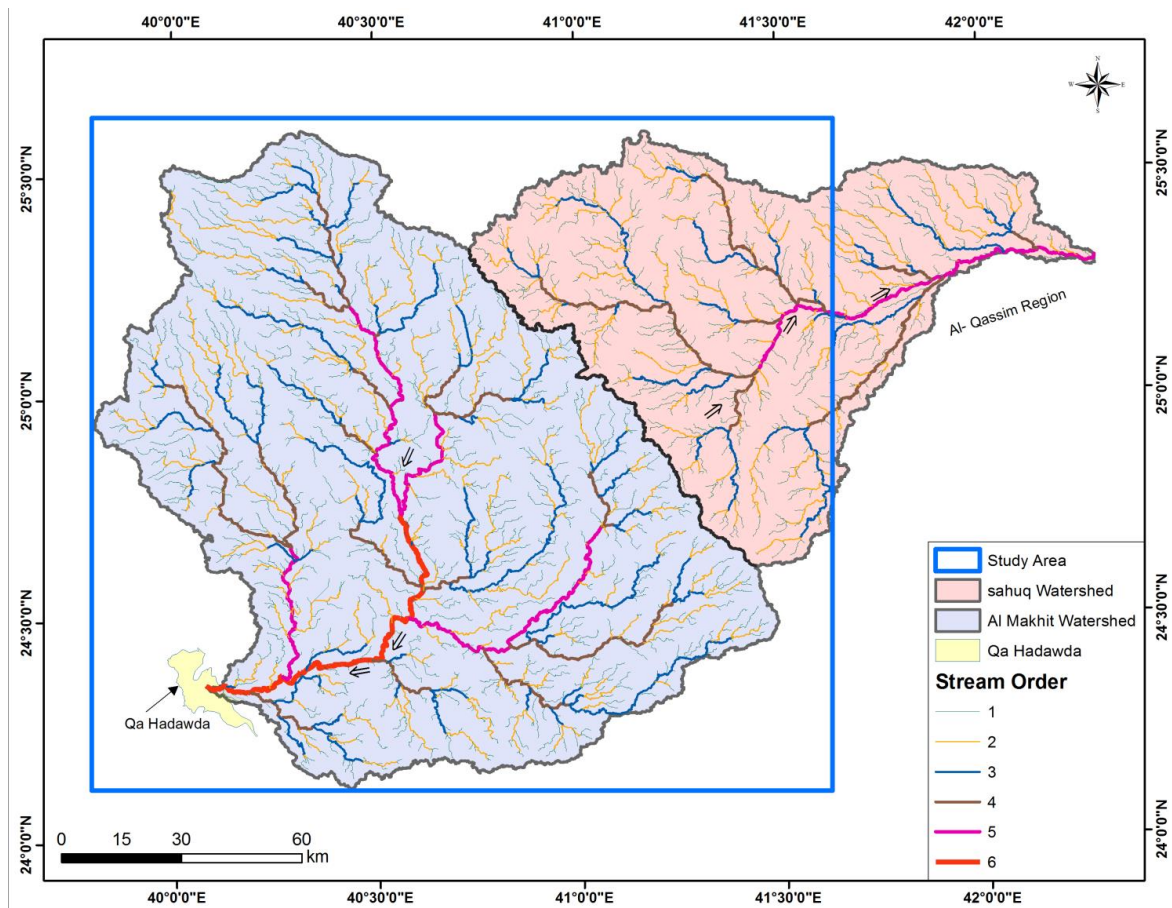
Figure 4.3: Wadi drainage network in the study area with stream ordering according to the Strahler classification.

4.1.1.4 Main and Sub-Drainage Basins

The study area is divided into two main drainage basins (Figure 4.4). Draining in opposite directions, the first is Wadi Sahuq, an open system which exits the study area to the east, and connects to the Wadi Al-Rimah that drains into the Arabian Gulf. The second drainage basin is in Wadi Al Makhit, a closed system which drains to the south-west, into Qa Hadawda.

Wadi Sahuq is 7889.6 sq.km in area; its upper catchment is situated in the eastern part of the Al Madinah region, while the lower part is found in the Al Qassim region. The part of Wadi Sahuq found in the Al Madinah region contains five sub-drainage basins, namely Wadi Al Qusayrah, Wadi Sabha, Upper Wadi Sahuq, Wadi Al Amirah, and Wadi Mabuj.

The Wadi Al Makhit drainage basin is 16035.1 sq.km in area, and contains eight sub-drainage basins, namely Wadi Al Hinakiyah, Wadi Luwayy, Shaib Um Markhah, Wadi Al Mahir, Shaib Farhah, Shaib Al Dawnak, Shaib Nijar, and Shaib Al Hamad.
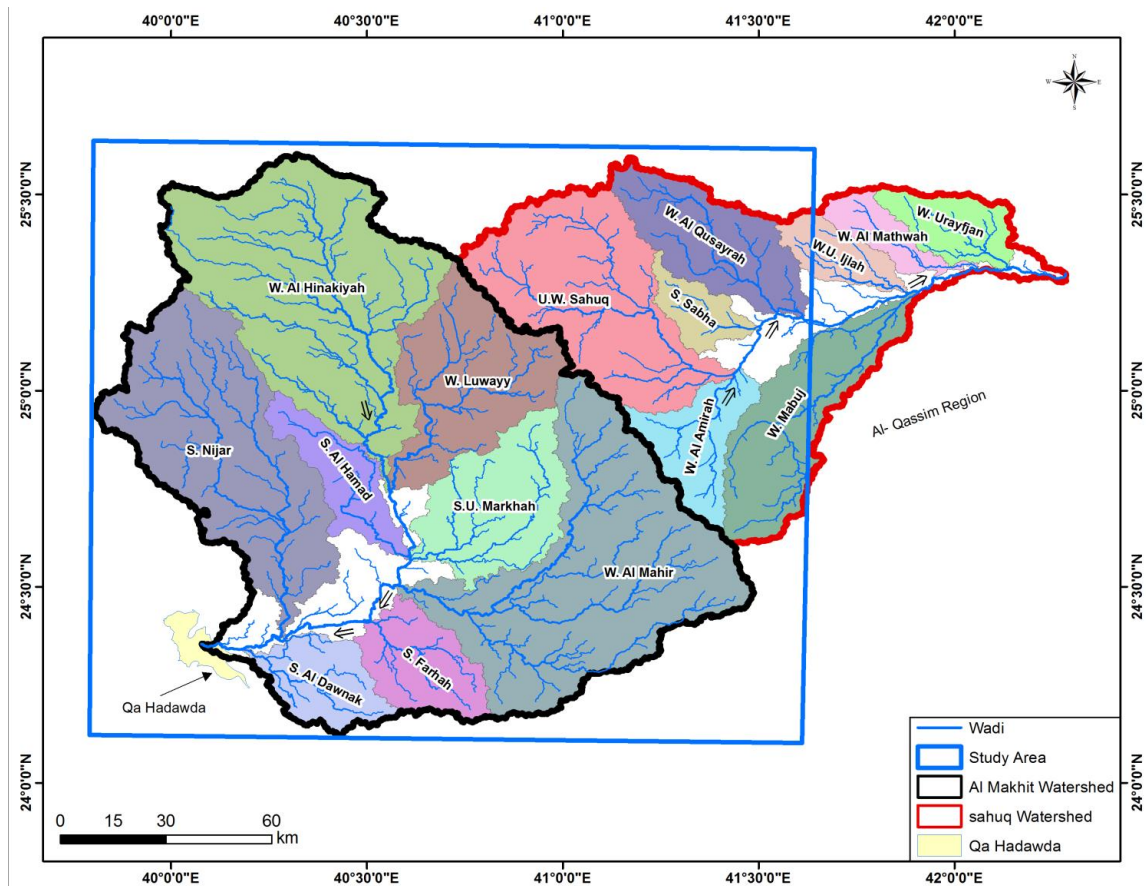
Figure 4.4: Drainage network in and around the study area, showing the direction of flow, extent of the watersheds and the component drainage basins.

4.1.2 Geomorphological Description of the Study Area using Remote Sensing

Input Landsat 8 corrected data

After radiometric and atmospheric corrections of Landsat 8 imagery the following (Figures 4.5, 4.6) show the descriptive statistics of these corrected data. The resulted ground surface reflectance bands were then used in further image processing techniques.

The final mask of harrats and mountains is shown in Figure 4.7. The results of the Pearson correlation matrix depict the correlation between reflectance bands (Figure 4.8), which helped in selecting appropriate band combinations and ratios in the following sections.

	Band 1	Band 2	Band 3	Band 4	Band 5	Band 6	Band 7
Min	0.0122	0.0179	0.0817	0.0982	0.0659	0.0357	0.043
Max	0.532	0.5312	0.5884	0.6458	0.6518	0.8937	1
Mean	0.126591	0.133154	0.194824	0.276443	0.320707	0.387263	0.378515
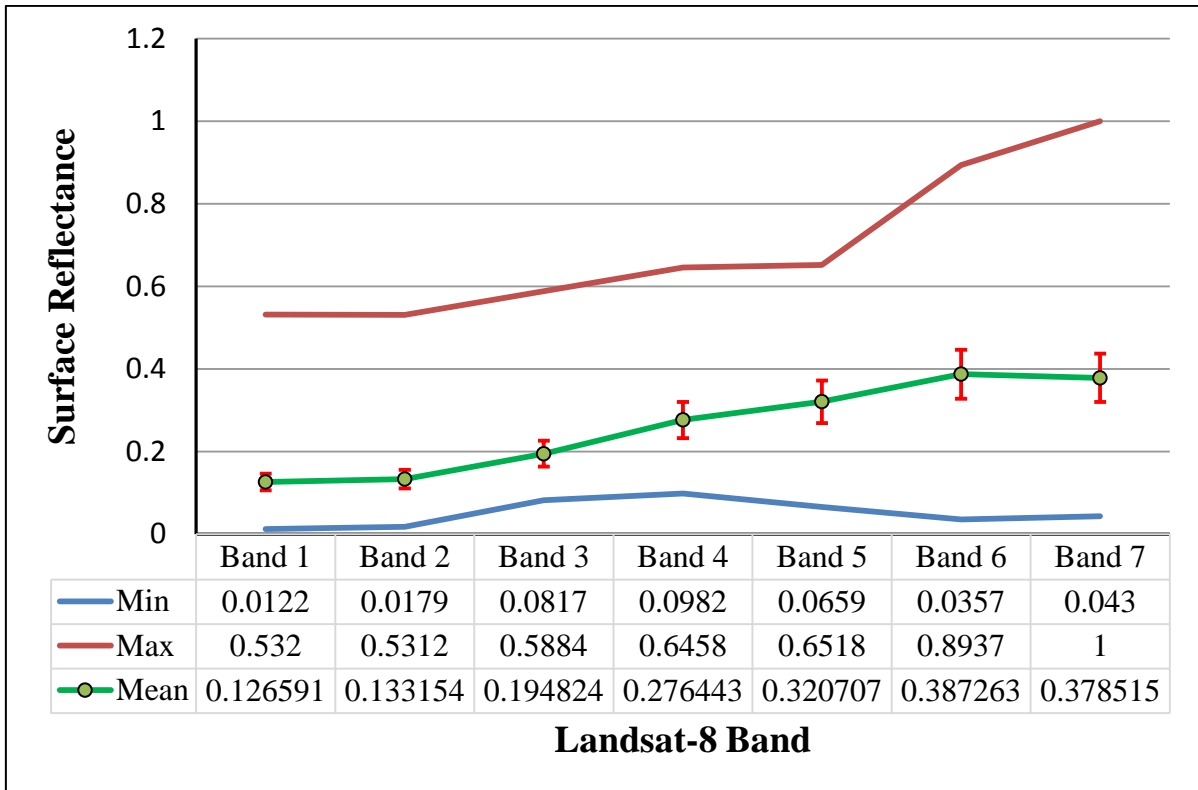
Landsat-8 Band

Figure 4.5: Statistical analysis chart of the reflectance values (error bars represent the standard deviation from the mean).
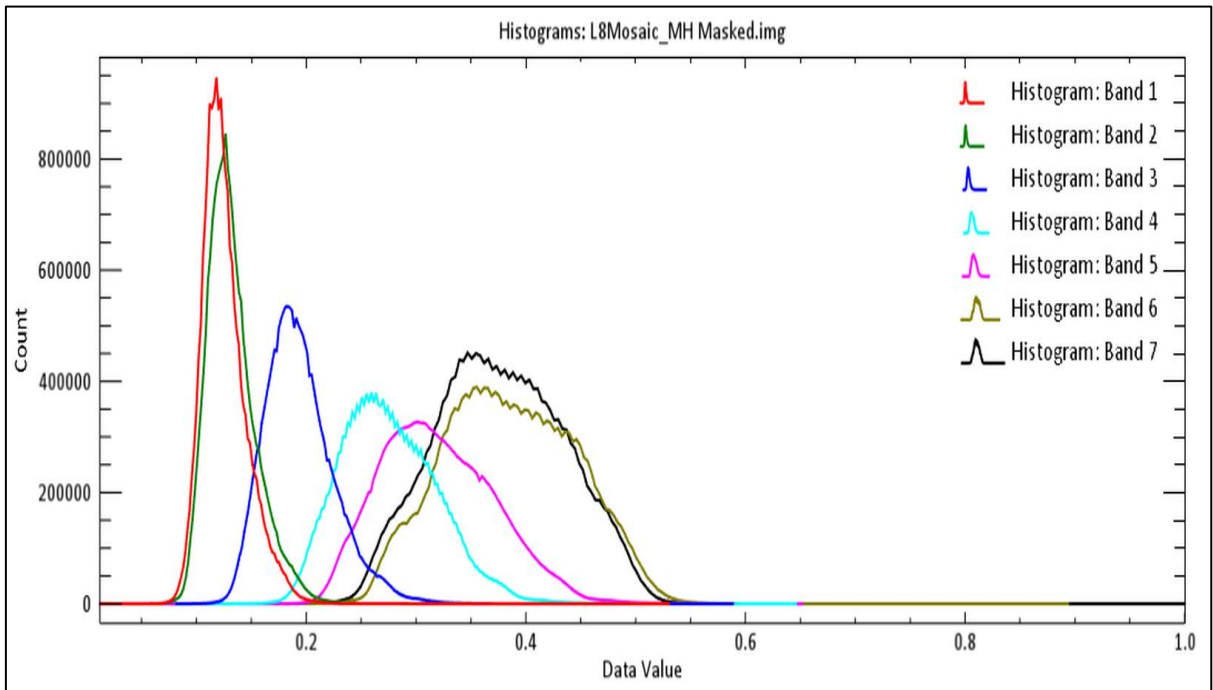
Figure 4.6: Frequency distribution of reflectance values of Landsat-8 bands.
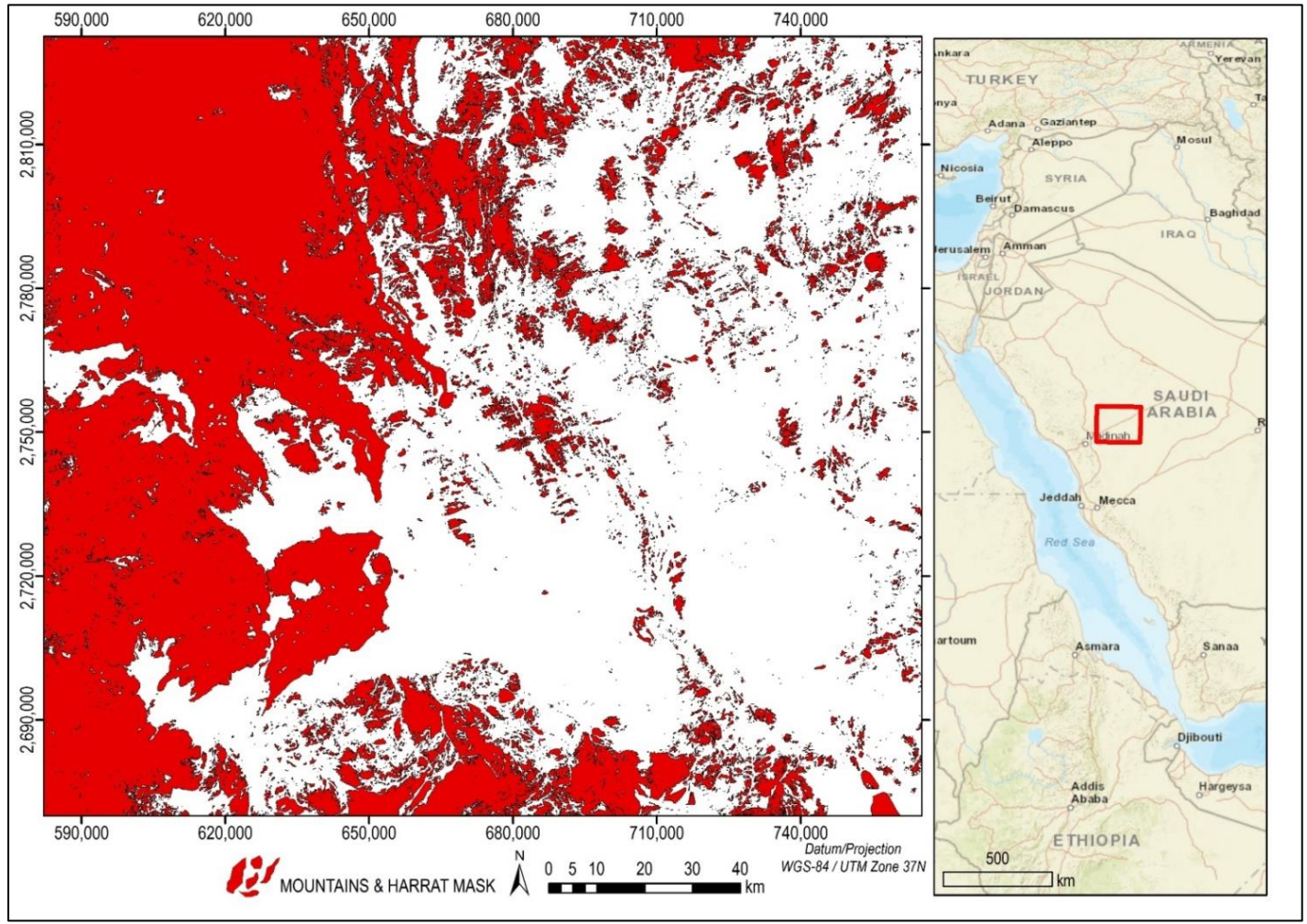
Figure 4.7: Mountains and Harrat volcanics zero mask used in the current study.
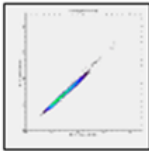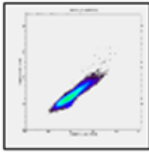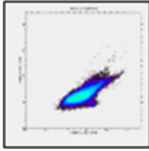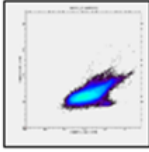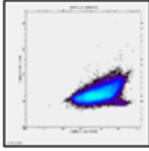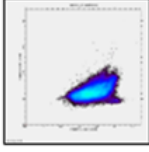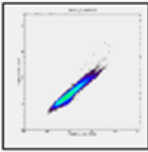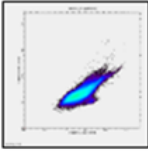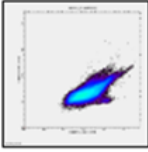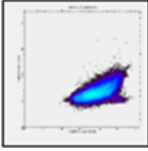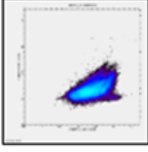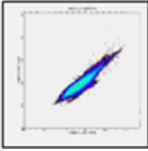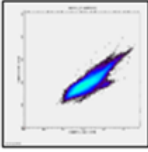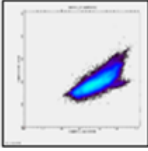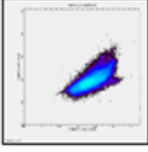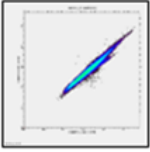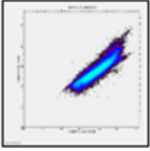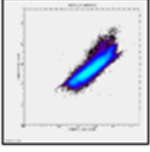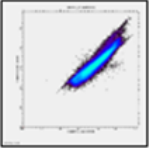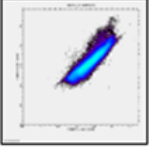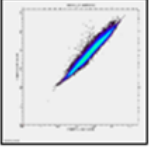
	Band 1	Band 2	Band 3	Band 4	Band 5	Band 6	and 7
Band 1	1						
Band 2	0.992823	1					
Band 3	0.924474	0.957122	1				
Band 4	0.764547	0.812543	0.932479	1			
Band 5	0.671265	0.72492	0.872988	0.986625	1		
Band 6	0.569974	0.630804	0.794783	0.924291	0.944026	1	
Band 7	0.516271	0.575299	0.741207	0.887103	0.913595	0.985362	1

Figure 4.8: Pearson correlation matrix and 2D scatter plots of Landsat 8 reflectance bands.

4.1.2.1 Field Samples and Laboratory Spectra

This section provides the details of sampled locations (Figure 4.9) and how the percent of gravel content varies with the sample sites (Table 4.2).
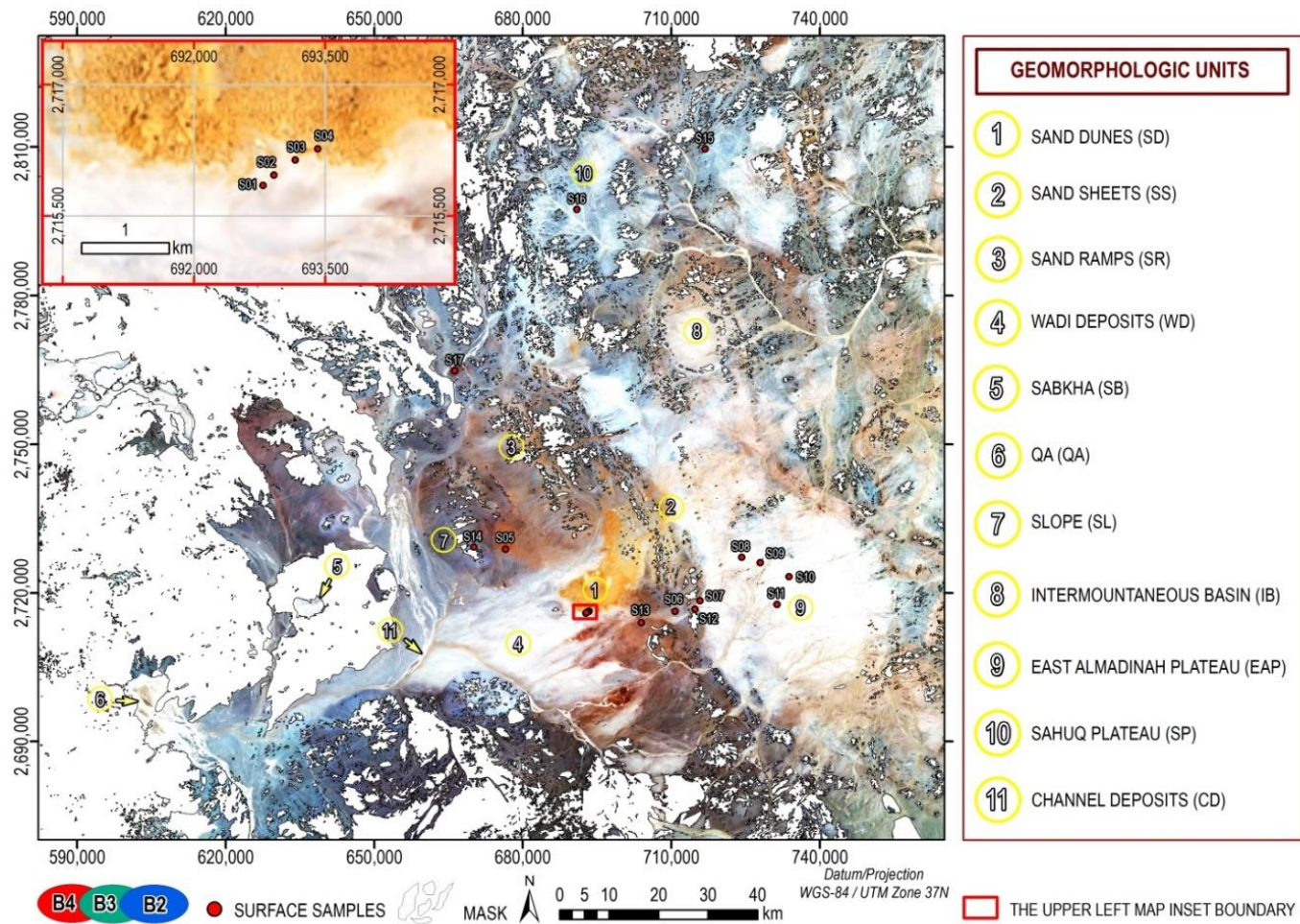
Figure 4.9: Map with the key sample locations (inset).

The spectral reflectance of each collected sample is shown in Figure 4.10. The lines in the illustration are average reflectance curves.

Table 4.2: Percentage of gravel within collected surface samples

Sample No.	Name of Unit	ID	% of gravel
S01	Wadi deposit	WD	80
S02	Wadi deposit	WD	80
S03	Wadi deposit	WD	80
S04	Sand dune	SD	0
S05	Slope deposit	SL	40
S06	Slope deposit	SL	80
S07	East Al Madinah Plateau	EAP	85
S08	East Al Madinah Plateau	EAP	35
S09	Channnel deposit	CD	35
S10	Dike	DK	100
S11	East Al Madinah Plateau	EAP	85
S12	Channnel deposit	CD	0
S13	Slope deposit	SL	85
S14	Slope deposit	SL	85
S15	Sahuq Plateau	SP	70
S16	Sahuq Plateau	SP	70
S17	Slope deposit	SL	80

In general, the spectral reflectance of all the studied samples ranged from 5.09% at the wavelength 450 nm to 44.1% at 850 nm. The common sample site 14 (Slope) with 85% gravel maintained consistence and distinct characteristics in terms of reflectance. This sample was used as reference to other samples because of its unique spectral characterstics. The spectral reflectance of individual samples at 450 nm revealed that the reflectance of the Channel deposits (Figure 4.10a) is about 12 – 15 % and between 600 – 900 nm with 35 – 39 % for both samples. However, samples vary in terms of gravel composition, with 0% for sample 12, and 35% for sample 9. At the Wadi deposit (Figure 4.10b), reflectance of 15% at 400 nm and 33-39% between 600-900 nm were recorded. The same proportion of gravel (80%) for each of the three samples (1, 2 and 3) were observed at the sample unit. The sand dunes (Figure 4.10c) unit is characterised by 0% gravel composition with a reflectance of

8% at 400 nm and 44.1% at 900 nm. The slope deposits (Figure 4.10d) unit (samples 6, 13 and 17), have a gravel composition between 80 – 85%, while the other sample (5) has 40% percent. The reflectance of these samples 5, 13 and 17 at 400 nm is less than 10% and higher reflectance of 25% at 900 nm and 31% for sample 17. The sample unit of Al Madinah (Figure 4.10e) shows that the reflectance curves of sample 7, 8 and 11 is 14% and 18% at 400 nm, and a maximum reflectance of 38% at 900 nm. Even though, the sample varation in terms of reflectance may be due to gravel composition of 85% for samples 7 and 11, and 35% for sample 8. The remaining two sample units (Sahuq [Figure 4.10f] and Dike [Figure 4.10g]) have distinct reflectance compared to the previous 5 units. For example, the Sahuq Plateau reflectance at 400 – 900 nm ranges between 10 to 16% with 70% gravel contents. Similarly, the Dike unit has sample reflectance between 7 – 15% in both the wavelength spectrum at 400nm and 900 nm respectively. The Dike sample units is 100% gravel.
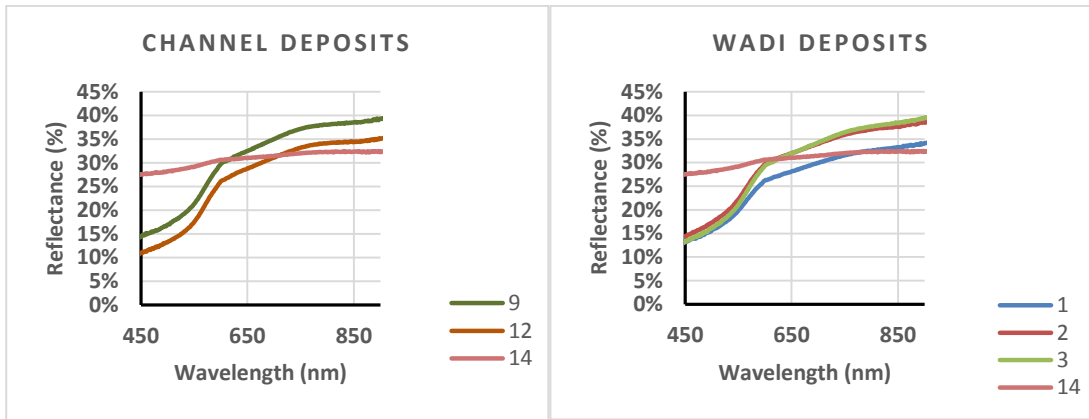
(a)

(b)
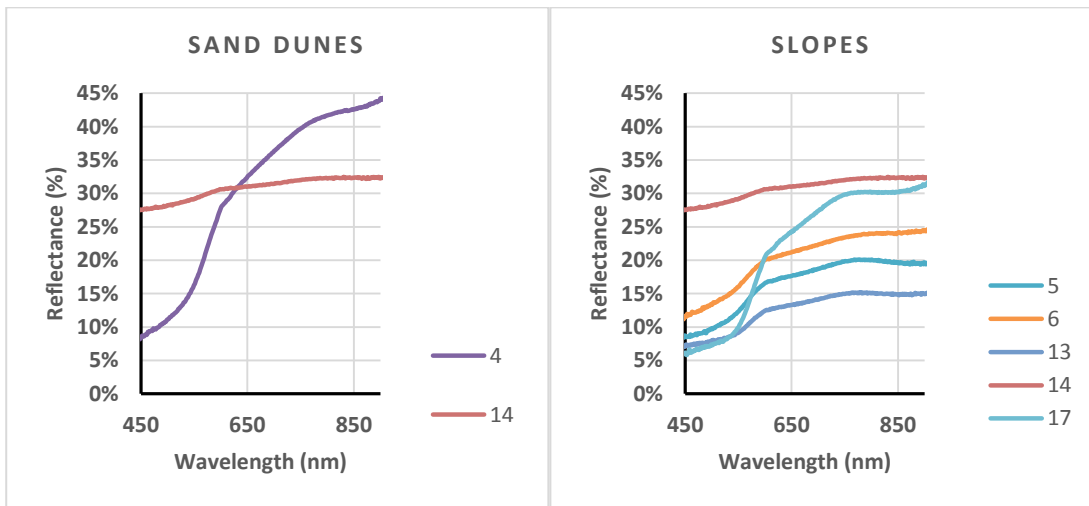
(c)

(d)
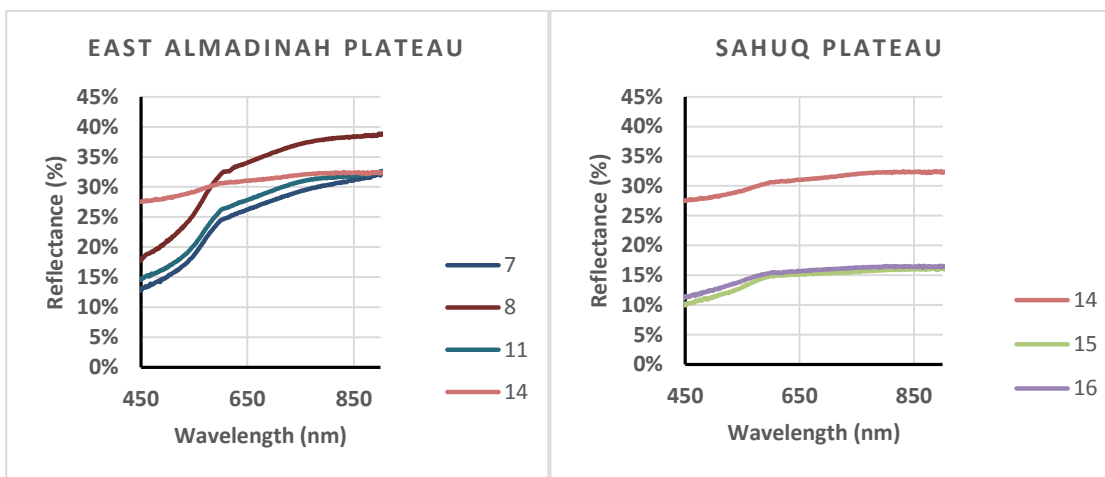
(e)

(f)
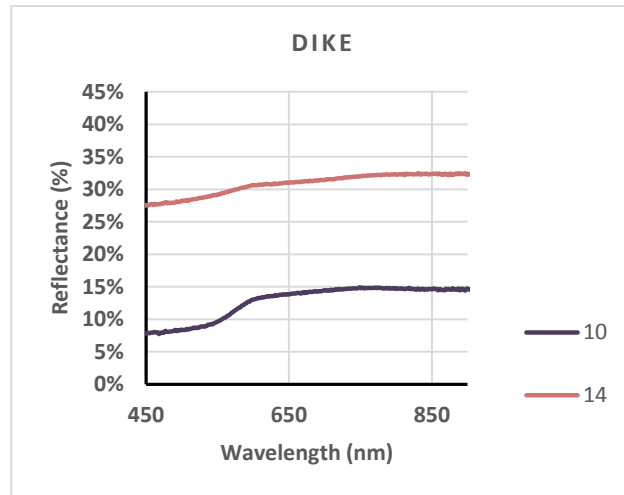
(g)

Figure 4.10: (a-g). ASD measurements of the spectral reflectance of 17 surface samples collected during the field study, grouped into, (a) Channel deposits unit, (b) Wadi deposits unit, (c) Sand dunes unit, (d) Slopes unit, (e) East Al Madinah plateau unit, (f) Sahuq plateau unit, (g) Dike unit. Sample 14, a slope deposit, is place on all groups as a reference.

Overall, the field spectra (Figure. 4.10) have similar reflectance showing in the visible blue-green band while the reflectance difference appears in red and IR bands (i.e. 600 to 900 nm). The difference could be due to mineral content, grain size, and the thickness of the sand distributions which influences the spectral reflectance. For example, wadi deposit samples S01, S02 and S03, dominated with felsic minerals and a high gravel percentage (80%), show reflectances around 33-39%. This is in contrast to the Sahuq Plateau which contains mafic minerals with 70% gravel, and has the lowest reflectance below 17%. The highest reflectance above 44% is found in sand dunes with 0% gravel, while the Dike which contains 100% gravel has reflectance of around 15%. At slope location, it appears that reflectance is low, due to the influence of source of rock characteristics.

4.1.2.2 Landsat-8 data and Spectral Reflectance

The spectral profiles extracted from the Landsat 8 image for each of the 17 surface samples are shown in Figure 4.11 (a-g). The spectra varied between 10 % in the blue region (Band 2) to 52% at SWIR region (Band7). The reflectance values increased between B2 and B6,

and levelled off between B6 and B7. Spectral reflectance of sampled pixels varied across the landsat-8 bands. In the case of band 2, there is a distinct deviation between sample 17 and sample 8, with a reflectance of 11% and 25% respectively. Reflectance spectra at green region (Band 3) were interlinked, and difficult to differentiate between the sampled locations. There is a distinct deviation in refelectance curves among the samples at Band 4, Band 5 and Band 6. Consequently the specifice spectral signature of ground materials helped in discrimnating rock types and geomorphologic units, even if they look the same at visible wavelengths (i.e. 400 to 600 nm). Moreover, with the observations of spectral reflectance beyond 600 nm, all the collected samples can be classified into 7 units. The 7 units from Landsat are explained based on the wavelength between 400 -900 nm, which corresponds to the hand-held hypersectral reflectance. This will provide logical comparison between the two data because hyperspectral reflectance did not go beyond 900 nm.

For example, the channel deposits unit reflectance is around 13.3% in band 2 between 600 – 900 nm, with 36% and 37% in band 5 for both samples 9 and 12. The Wadi deposit unit showed the reflectance of 14.3% in band 2 and 41%, 40% and 39% in band 5 were recorded for the three samples (3, 2 and 1 respectively). The sand dunes unit (sample 4) is characterised by the reflectance of 11.2% in band 2 and 43% in band 5. The reflectance characteristics at the slope deposits unit (samples 5, 6, 13 and 17) show that band 2 reflects 11.2%, while there is amaximum reflectance of 33% in band 5. At the sample unit of Al Madinah, the reflectance curves of sample 7, 8 and 11 is 15.9% in band 2, with the maximum reflectance of 40% in band 5. Sahuq Plateau surface reflectance shows lowest reflectance (14.9% in band 2 and 27 % in band 5) compared to other geomorphologic units witin the study area. Similarly, the Dike unit has sample reflectance of 15.1% in band 2 and 38.8% in band 5. The Dike appears to be distinct compared with what was obtained in ASD HH2 hyperspectral reflectance. The common sample site 14 (slope sample) in all units maintained consistent characteristics in terms of reflectance and was used as a reference for other samples.
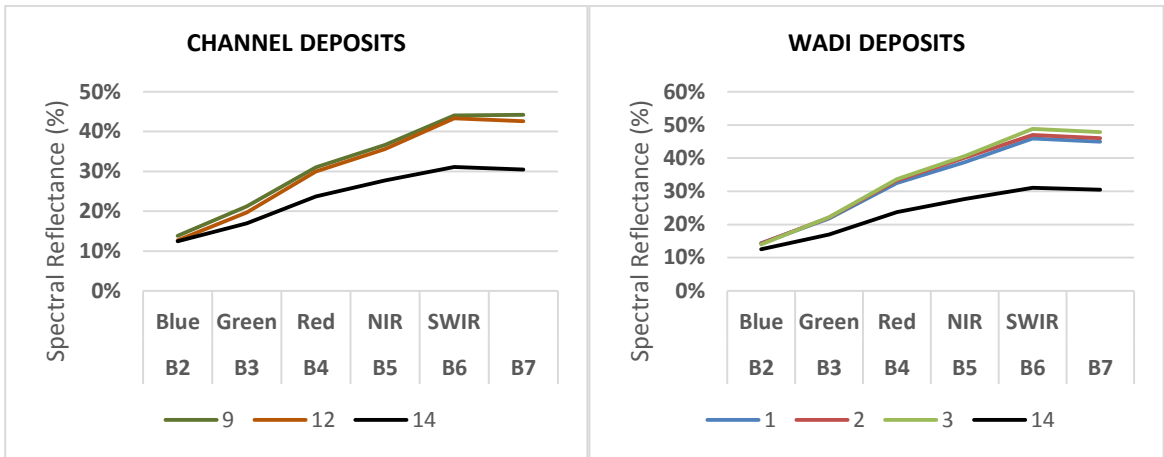
(a)

(b)
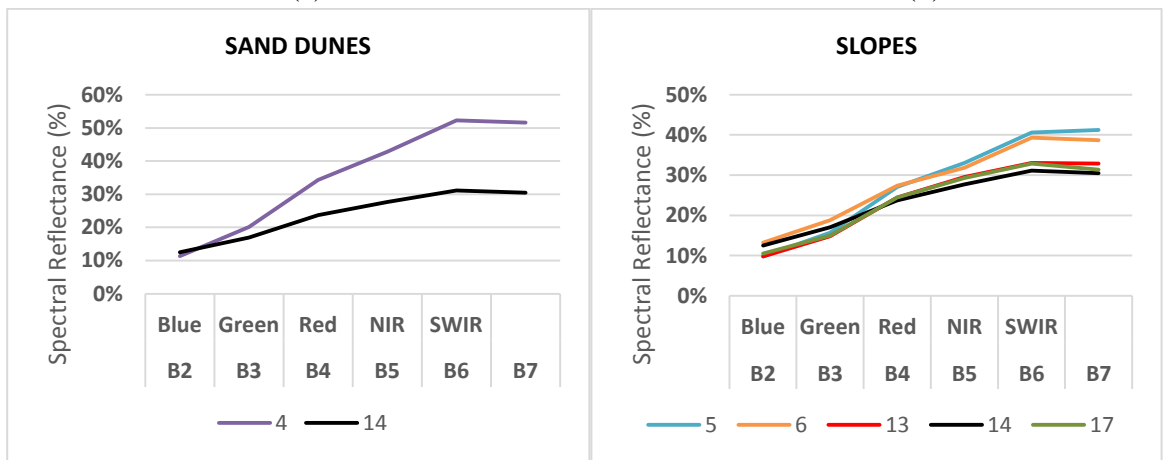
(c)

(d)
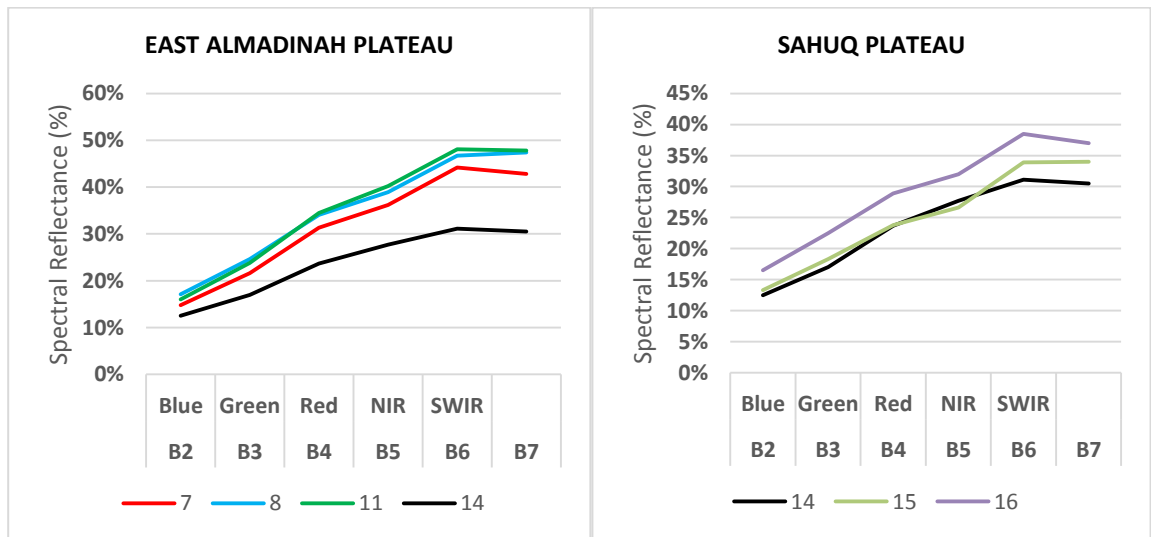
(e)

(f)
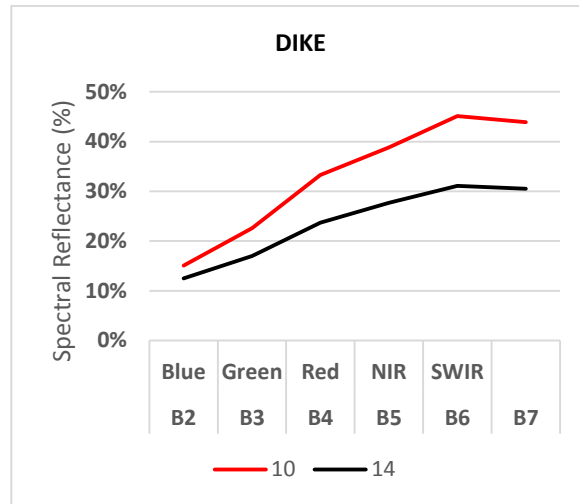
(g)

Figure 4.11 (a-g) Landsat-8 detected spectral reflectance of sampled surfaces, grouped into, (a) Channel deposits unit, (b) Wadi deposits unit, (c) Sand dunes unit, (d) Slopes unit, (e) East Al Madinah plateau unit, (f) Sahuq plateau unit, (g) Dike unit. Sample 14, a slope deposit, is place on all groups as a reference.

4.1.2.3 Landsat-8 Vs. ASD Spectral Reflectance

Sand Dunes

Sand Dunes	**S04**			

S04

	B2	B3	B4	B5
Landsat-8	0.11	0.20	0.34	0.43
ASD-HH2	0.10	0.19	0.33	0.43

S04

1-Sand dunes has the highest reflectance among the samples of geomorphological units. This is because of the high homogeneity in both the mineral composition (quartz represents more than 90% of the total mineral composition) and grain size (fine sand exceeds 92% of all grain sizes as an aeolian well-sorted deposit). This increases pixel purity and produces a more stable spectral signature, and a highest reflectance (43%) compared to other units within the study area.

2- Reflectance increases as wavelength increases.

Grain Size	Volume %
Coarse pebbles	0.00
medium pebbles	0.00
fine pebbles	0.00
very fine pebbles	0.00
very coarse sand	0.00
coarse sand	0.00
medium sand	5.36
fine sand	92.19
very fine sand	1.34
silt and clay	1.12
Total	**100**

3- The measured spectra of sand dune sample from both image and laboratory analysis closely coincide as a result of the presence of fine grain size (fine sand exceeds 29% of all grain size). 4- Sample S04 represents the sand dune of the geomorphologic unit, revealing absorption features within Landsat-8 bands 2 and 3 (blue and green). These characteristics may be related to the electronic absorption processes in ferric iron oxides contained (in trace amounts) within sand dunes. Similarly, it is the same behaviour that interprets the high reflectance in the band 4 (red band).		

Figure 4.12: Image spectrometry vs ASD laboratory spectral measurements of sand dunes S04.

Wadi Deposits

Wadi deposits have the second highest reflectance compared to other units within the study area. This could be related to its composition, which essentially comprises of felsic minerals (quartz and feldspar) and felsic rock fragments (essentially rhyolite and rarely basalt) that reflects the higher reflectance. There are slight variations in the reflection of the three samples (S01, S02, S03) within the Wadi deposits, despite the composition of 80% gravel coverage.

Wadi Deposits

S03

	B2	B3	B4	B5
Landsat-8	0.14	0.22	0.34	0.41
ASD-HH2	0.15	0.23	0.32	0.39

S03	Grain Size	Volume %
	Coarse pebbles	0.00
1-Reflectance increases as the wavelength increases.	medium pebbles	0.00
	fine pebbles	0.00
2-Both bands 2 and 3 are characterized by absorption features, while band 4 shows a relatively high reflectance due to the presence of iron oxides	very fine pebbles	2.93
	very coarse sand	41.35
which comprises different absorption processes.	coarse sand	6.74

3-The sample has the least grain size variability within the Wadi deposits (as the majority of the grain size does not exceed the very coarse sand). Consequently, the highest reflectance (41%) and the better coincidence between image and measured reflectance was observed.	medium sand	10.56
	fine sand	34.90
	very fine sand	0.59
	silt and clay	2.93
	Total	**100**

Figure 4.13 : Image spectrometry vs ASD laboratory spectral measurements of Wadi deposits S03.

S02

	B2	B3	B4	B5
Landsat-8	0.14	0.22	0.33	0.40
ASD-HH2	0.16	0.23	0.31	0.37

Wadi Deposits

S02

1-As the reflectance increases, the wavelength also increases.

2-Both bands 2 and 3 have absorption features, while band 4 shows relative high reflectance due to the presence of iron oxides of different absorption processes that occurred.

3-The divergence between image and measured reflectance become clearer in bands 4 and 5 as a result of a slight increase in grain size variability compared to S03.

4- The grain size variability in sample S02 is less than that of sample S01, thus, the reflectance in S02 appears higher (with 40%) than in S01.

Grain Size	Volume %
Coarse pebbles	0.00
medium pebbles	0.00
fine pebbles	6.32
very fine pebbles	20.31
very coarse sand	29.21
coarse sand	3.26
medium sand	11.21
fine sand	22.51
very fine sand	2.20
silt and clay	4.98
Total	**100**

Figure 4.14: Image spectrometry vs ASD laboratory spectral measurements of Wadi deposits S02.

Wadi Deposits

S01		
	B2	B3	B4	B5

Chart: S01 — Reflectance (y-axis 0%–45%)

	B2	B3	B4	B5
Landsat-8	0.14	0.22	0.32	0.39
ASD-HH2	0.15	0.22	0.30	0.35
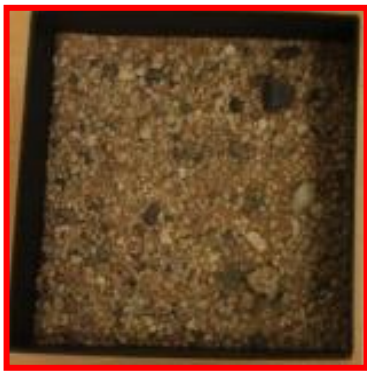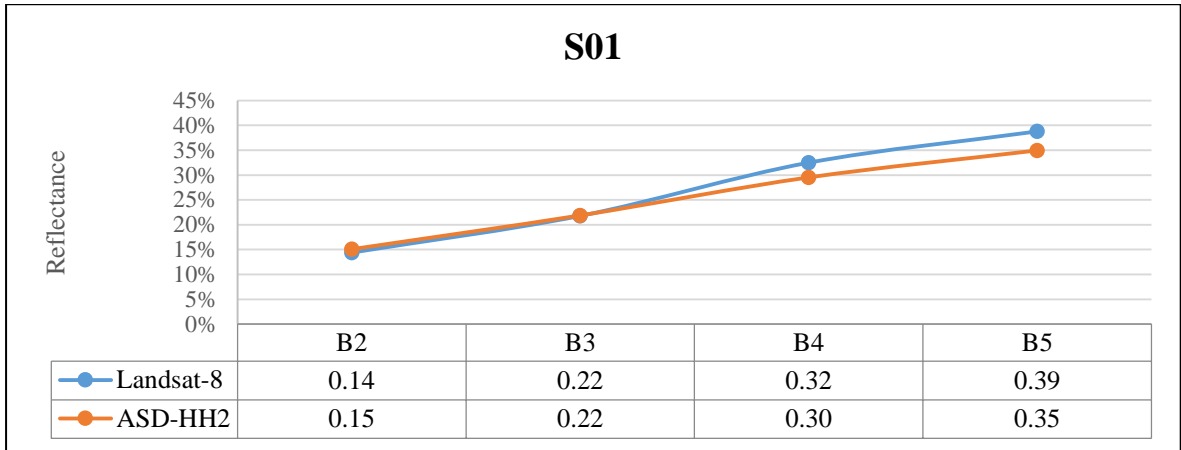
S01

1- Reflectance increases as the wavelength increases.

2- Both bands 2 and 3 have absorption features, while band 4 shows relative high reflectance due to the presence of iron oxides of different absorption processes that occurred.

3- The divergence between image and measured reflectance becomes clearer in bands 4 and 5 due to the increase in grain size variability.

4- Sample S01 has the highest grain size variability within the Wadi deposits unit, due to the content of fine pebbles compared to the other two samples, thereby exhibiting the lowest reflectance (39%).

Grain Size	Volume %
Coarse pebbles	0.00
medium pebbles	0.00
fine pebbles	22.56
very fine pebbles	24.62
very coarse sand	16.92
coarse sand	0.77
medium sand	5.38
fine sand	19.49
very fine sand	2.56
silt and clay	7.69
Total	**100**

Figure 4.15: Image spectrometry vs ASD laboratory spectral measurements of Wadi deposits S01.

Sometimes, some of the sediments in the Wadi deposits in the study area appear with somewhat low reflectance. This is because the source of these sediments are dark rocks such as basalt and andesite, as is the case in Wadi AI Hinakiyah.

East Al Madinah Plateau

East Al Madinah Plateau has the third highest reflectance compared to other units within the study area, which can be explained by its composition of essentially felsic minerals (quartz and feldspar). The samples also vary in terms of reflectance, with a gravel coverage of 85% (samples 7 &11) and 35% (sample 8).

S11

	B2	B3	B4	B5
Landsat-8	0.16	0.24	0.34	0.40
ASD-HH2	0.16	0.23	0.31	0.36

S11

1- Reflectance increases as the wavelength increases.

2- Both bands 2 and 3 are characterized by absorption features, while band 4 has a relatively high reflectance due to charge-transfer spectral absorption of ferric Fe-oxides.

3- The difference in reflectance between image and measured data were clearly observed in bands 4 and 5 due to the increased grain size variability.

4- Sample S11 exhibits highest reflectance (40%) within the East Al Madinah Plateau samples. This is due to its essential composition of felsic

Grain Size	Volume %
Coarse pebbles	0.00
medium pebbles	0.00
fine pebbles	17.95
very fine pebbles	27.44
very coarse sand	13.59
coarse sand	0.77
medium sand	10.00
fine sand	20.00
very fine sand	3.08
silt and clay	7.18

minerals (quartz and feldspar), where the grain size does not exceed fine pebbles.	**Total**	**100**

Figure 4.16: Image spectrometry vs ASD laboratory spectral measurements of East Al Madinah Plateau S11.

East Al Madinah Plateau

S08

	B2	B3	B4	B5
Landsat-8	0.17	0.25	0.34	0.39
ASD-HH2	0.20	0.27	0.35	0.40

S08

1- As reflectance increases, the wavelength increases as well.

2- Absorption features are properties of band 2 and 3, meanwhile a relative high reflectance is exhibited in band 4 due to charge-transfer spectral absorption of ferric Fe-oxides.

3-This sample has the least grain size variability within the East Al Madinah Plateau samples, where the reflectance in the image coincides with that of the measured data.

4- It has 39% reflectance, though the sample is generally containing finer grain size compared to the sample S11 which has higher reflectance. The low reflectance in sample S08 may suggest the higher content of mafic components that originates from mafic dike around the sample site.

Grain Size	Volume %
Coarse pebbles	0.00
medium pebbles	0.00
fine pebbles	4.31
very fine pebbles	5.10
very coarse sand	15.69
coarse sand	1.57
medium sand	29.41
fine sand	32.94
very fine sand	3.92
silt and clay	7.06
Total	**100**

Figure 4.17: Image spectrometry vs ASD laboratory spectral measurements of East Al Madinah Plateau S08.

	S07			
	B2	**B3**	**B4**	**B5**
Landsat-8	0.15	0.22	0.31	0.36
ASD-HH2	0.15	0.21	0.29	0.33

East Al Madinah Plateau
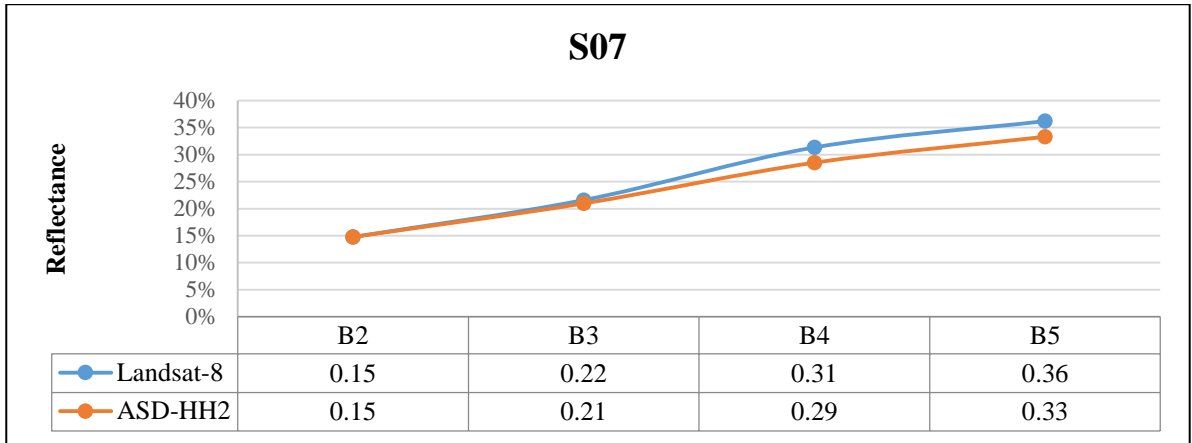
S07

1- Reflectance increases as the wavelength increases.

2- Both bands 2 and 3 have absorption features, while band 4 shows relative high reflectance, due to charge-transfer spectral absorption of ferric Fe-oxides.

3- The difference in reflectance between image and measured data is more apparent in bands 4 and 5 due to the increase in the grain size variability.

4- This sample has the coarser grain size within the East Al Madinah Plateau deposits compared to other samples (the grain size contains medium pebbles), given the lowest reflectance value of 36%.

Grain Size	**Volume %**
Coarse pebbles	0.00
medium pebbles	3.61
fine pebbles	28.13
very fine pebbles	13.70
very coarse sand	11.54
coarse sand	1.68
medium sand	7.45
fine sand	14.90
very fine sand	3.61
silt and clay	15.38
Total	**100**

Figure 4.18: Image spectrometry vs ASD laboratory spectral measurements of East Al Madinah Plateau S07.

Channel Deposits

Channel deposits are essentially composed of felsic minerals (quartz and feldspar). This section has the fifth highest reflectance compare to other units within the study area. This could be due to soil moisture that may be responsible for the overall reduction in reflectance. The samples vary in terms of reflectance and gravel coverage of 35% for samples 9, and 0% for sample 12.

S09

	B2	B3	B4	B5
Landsat-8	0.14	0.21	0.31	0.37
ASD-HH2	0.16	0.24	0.34	0.40

S09

1- There is a proportional increase between reflectance and wavelength.

2- Both bands 2 and 3 are characterized by absorption features, while band 4 has high reflectance due to charge-transfer spectral absorption of ferric Fe-oxides.

3- The sample has less grain size variability, and as a result, image and measured reflectance coincided.

Grain Size	Volume %
Coarse pebbles	0.00
medium pebbles	0.00
fine pebbles	2.89
very fine pebbles	9.50
very coarse sand	19.83
coarse sand	3.72
medium sand	21.07
fine sand	24.79
very fine sand	4.13

| 4- S09 has the highest reflectance (37%) within the Channel samples. The sample is essentially composed of felsic minerals (quartz and feldspar), where the grain size does not exceed fine pebbles. | silt and clay | 14.05 |
| | **Total** | **100** |

Figure 4.19: Image spectrometry vs ASD laboratory spectral measurements of Channel deposits S09.

Channel Deposits

S12

	B2	B3	B4	B5
Landsat-8	0.13	0.20	0.30	0.36
ASD-HH2	0.12	0.19	0.29	0.35
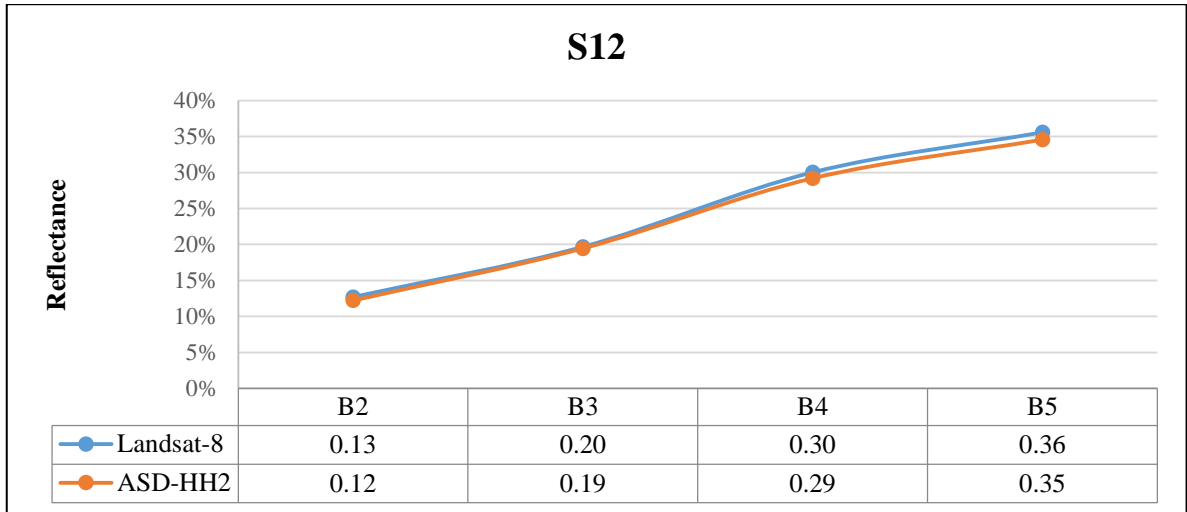
S12

1- As the reflectance increases, the wavelength also increases.

2- Both bands 2 and 3 have absorption features, while band 4 exhibits high reflectance due to charge-transfer spectral absorption of ferric Fe-oxides.

3- S12 has the finer grain size (with less variability within the Channel deposits), where the very high reflectance in image coincides with that of measured data.

4- This sample has the least reflectance (36%) among the Channel samples, although it has a finer grain size than S09, which may be as a result of soil moisture content.

Grain Size	Volume %
Coarse pebbles	0.00
medium pebbles	0.00
fine pebbles	0.00
very fine pebbles	0.23
very coarse sand	0.70
coarse sand	0.47
medium sand	52.80
fine sand	35.75
very fine sand	3.27
silt and clay	6.78
Total	**100**

Figure 4.20: Image spectrometry vs ASD laboratory spectral measurements of Channel deposits S12.

In some Wadi channels, the proportion of very fine sediments, namely silt and sand, is quite high. This results in higher reflectance, where the sediments appear in the image light in colour. This is the case in the lower flow channel of Wadi Al Hinakiyah, where the wadi slope is reduced, and as a result the quantity of very fine sediments increases.

Dikes

The dikes' composition is essentially of felsic minerals (quartz and feldspar), and has the fourth highest reflectance within the units in the study area.

Dikes

S10

	B2	B3	B4	B5
Landsat-8	0.15	0.23	0.33	0.39
ASD-HH2	0.08	0.10	0.14	0.15

S10 1- There is a proportional increase in both reflectance and wavelength.

2- Both bands 2 and 3 have absorption features, while band 4 shows relative high reflectance due to charge-transfer spectral absorption of ferric Fe-oxides.

4- Dike sample shows the highest divergence between reflectance in the image and measured data, due to natural surface in the field. It is not composed of pure, size-sorted minerals, and has nonhomogeneous minerals. It contains some sand sheets, as observed in the laboratory where the sample is more homogeneous without the sand sheets, which reduces the overall reflectance.

Grain Size	Volume %
Coarse pebbles	100
medium pebbles	0.00
fine pebbles	0.00
very fine pebbles	0.00
very coarse sand	0.00
coarse sand	0.00
medium sand	0.00
fine sand	0.00
very fine sand	0.00
silt and clay	0.00
Total	**100**

Figure 4.21: Image spectrometry vs ASD laboratory spectral measurements of Dikes S10.

Slopes

Slopes have low reflectance and it is the sixth highest reflectance within the units. The presence of slope samples near their different source of rocks leads to bad sorting and coarse grain size, which decreases their overall reflectance. The slope samples vary in terms of reflectance and gravel coverage of 85% for samples S13 and S14, 80% for samples S06, S17 while the other sample S05 has 40% percent.

S05

	B2	B3	B4	B5
Landsat-8	0.10	0.16	0.27	0.33
ASD-HH2	0.09	0.14	0.21	0.26

Reflectance

Slopes
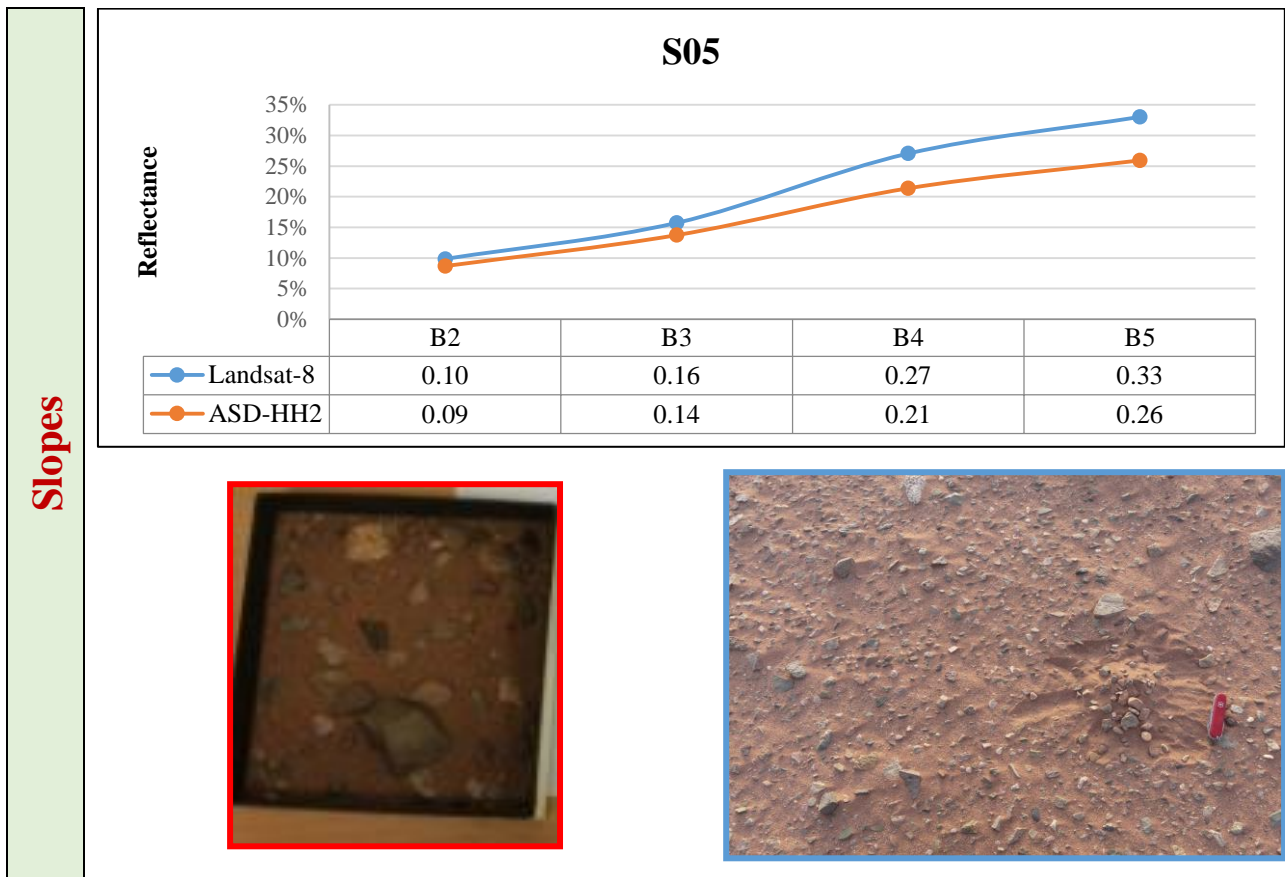
S05

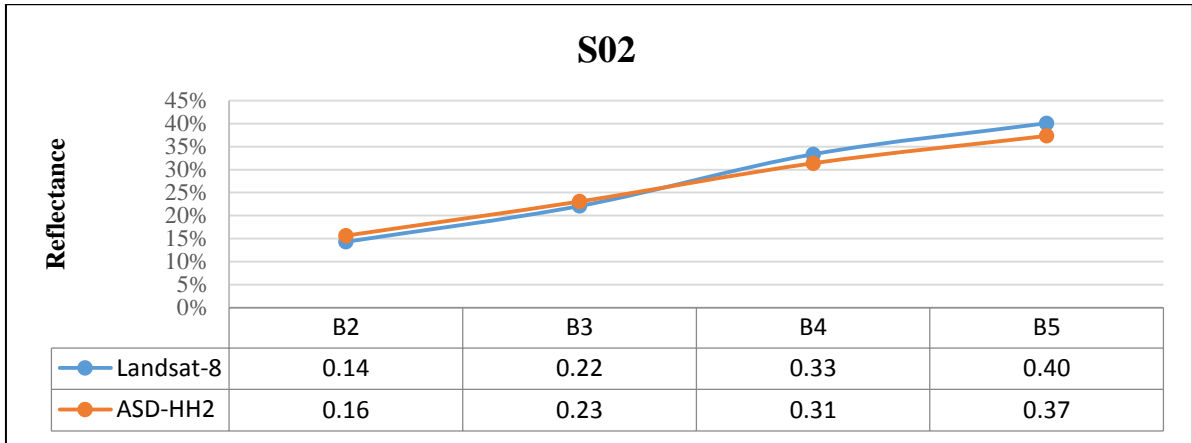1- As reflectance increases, wavelength increases too.

2- Both bands 2 and 3 have absorption features, while band 4 show relatively high reflectance due to charge-transfer spectral absorption of ferric Fe-oxides.

3- The divergence between image and measured reflectance becomes clearer in bands 4 and 5, as a result of increased grain size variability.

Grain Size	Volume %
Coarse pebbles	0.00
medium pebbles	36.84
fine pebbles	23.98
very fine pebbles	0.58
very coarse sand	0.39
coarse sand	0.39
medium sand	9.16
fine sand	12.48
very fine sand	2.53

4- The majority of surfaces in S05 are covered by fine grain size (60% sand and less than sand size with 40% gravel coverage), as this sample is located at the end of a slope. Therefore, the overall reflectance of S05 is the highest within the Slope samples (reflectance of S05 is 33%).	silt and clay	13.65
	Total	**100**

Figure 4.22: Image spectrometry vs ASD laboratory spectral measurements of Slopes S05.

Slopes

Figure 4.23: Image spectrometry vs ASD laboratory spectral measurements of Slopes S06.

	B2	B3	B4	B5
Landsat-8	0.13	0.19	0.27	0.32
ASD-HH2	0.11	0.16	0.22	0.27
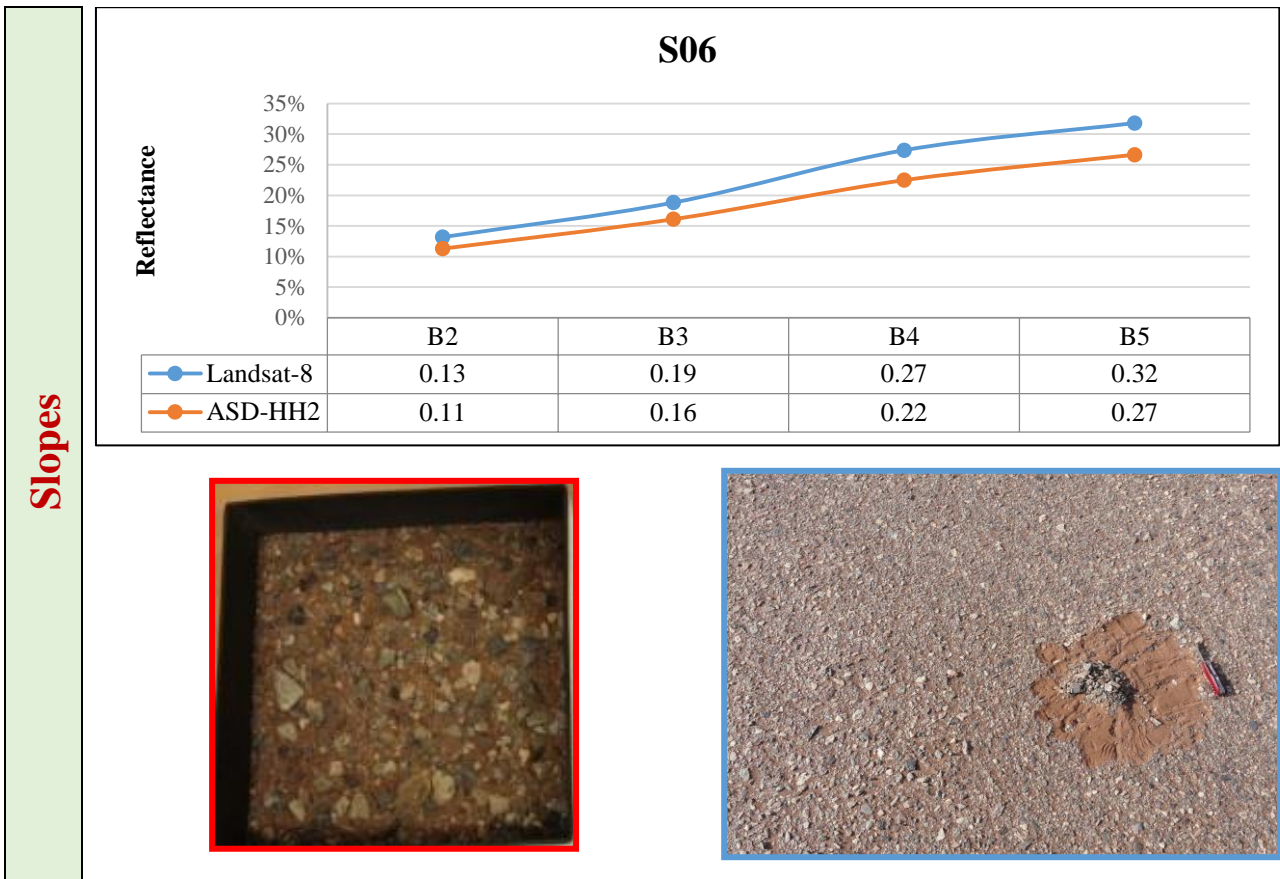
S06

1- Reflectance increases as the wavelength increases.

2- Both bands 2 and 3 have absorption features, while band 4 shows relatively high reflectance due to charge-transfer spectral absorption of ferric Fe-oxides.

3- The heterogeneity of grain size leads to the divergence between image and measured reflectance.

4- As the majority of the surface in S06 is covered by coarse grain size (80% gravel), and the presence of mafic minerals, decreases the overall reflectance of sample S06 (32%).

Grain Size	Volume %
Coarse pebbles	0.00
medium pebbles	12.39
fine pebbles	40.37
very fine pebbles	7.57
very coarse sand	6.42
coarse sand	0.46
medium sand	4.59
fine sand	15.37
very fine sand	2.52
silt and clay	10.32
Total	**100**

Slopes

S13

	B2	B3	B4	B5
Landsat-8	0.10	0.15	0.24	0.29
ASD-HH2	0.09	0.13	0.20	0.23

S13

1- Reflectance increases as the wavelength increases.

2- It has a high content of iron oxide that absorbs both bands 2 and 3, through the electronic absorption process, and reflects the red wavelength in band 4.

3- The divergence between image and measured reflectance becomes clearer in bands 4 and 5 as a result of increased grain size variability.

4- As the majority of the surface in S13 is covered by coarse grain size (85% graves) and the presence of mafic minerals decreases the overall reflectance of sample S13, which is 29%.

Grain Size	Volume %
Coarse pebbles	0.00
medium pebbles	5.85
fine pebbles	42.41
very fine pebbles	9.87
very coarse sand	5.85
coarse sand	0.55
medium sand	4.39
fine sand	12.61
very fine sand	5.30
silt and clay	13.16
Total	**100**

Figure 4.24: Image spectrometry vs ASD laboratory spectral measurements of Slopes S13.

Slopes

S17

	B2	B3	B4	B5
Landsat-8	0.11	0.15	0.24	0.29
ASD-HH2	0.07	0.12	0.24	0.30

S17

1- Reflectance increases as the wavelength increases.

2- It has a high content of iron oxide that absorbs both band 2 and 3 through an electronic absorption process and reflects red wavelength band 4.

3- As the majority of the surface in S17 is covered by (80%) gravels and the presence of mafic minerals decreases the overall reflectance of sample S17, giving the result of 29%.

Grain Size	Volume %
Coarse pebbles	0.00
medium pebbles	0.00
fine pebbles	6.13
very fine pebbles	2.14
very coarse sand	4.70
coarse sand	1.71
medium sand	23.93
fine sand	36.47
very fine sand	14.10
silt and clay	10.83
Total	**100**

Figure 4.25: Image spectrometry vs ASD laboratory spectral measurements of Slopes S17.

Slopes

	B2	B3	B4	B5
Landsat-8	0.13	0.17	0.24	0.28
ASD-HH2	0.11	0.14	0.18	0.21
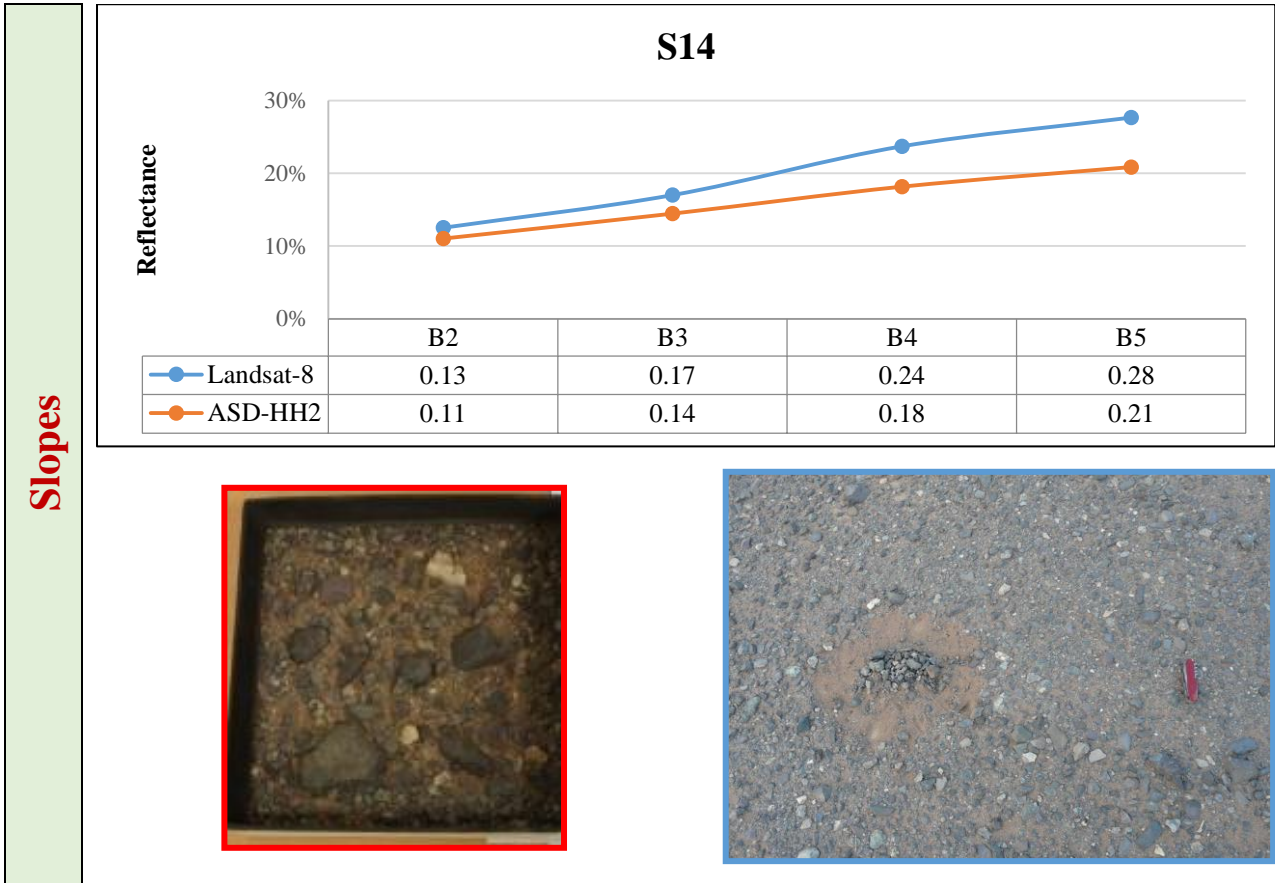
S14

1- Reflectance increases as the wavelength increases.

2- Both bands 2 and 3 have absorption features, while band 4 shows relative high reflectance due to charge-transfer spectral absorption of ferric Fe-oxides.

3- The divergence between image and measured reflectance become clearer in bands 4 and 5 as a result of increased grain size variability.

4- Sample S14 has the highest grain size variability within the Slope deposits samples (as more grain size reach to coarse pebbles compared to other slope samples) and the presence of mafic minerals and 85% gravel coverage this consequently gives the lowest reflectance (28%).

Grain Size	Volume %
Coarse pebbles	4.35
medium pebbles	24.35
fine pebbles	37.39
very fine pebbles	5.74
very coarse sand	3.48
coarse sand	0.70
medium sand	7.83
fine sand	9.57
very fine sand	1.39
silt and clay	5.22
Total	**100**

Figure 4.26: Image spectrometry vs ASD laboratory spectral measurements of Slopes S14.

Sahuq Plateau

The Sahuq Plateau has low reflectance, and the seventh highest reflectance compared to the other units within the study area. This reflectance relates to the samples' source of rocks (diorite and migmatite) which contain relative higher ratios of mafic minerals (pyroxenes, amphipolis and alornorthit plagioclase). There is a variation in reflection between the Sahuq Plateau samples, although they (S15 and S16) have 70% gravel coverage.

Sahuq Plateau

S16

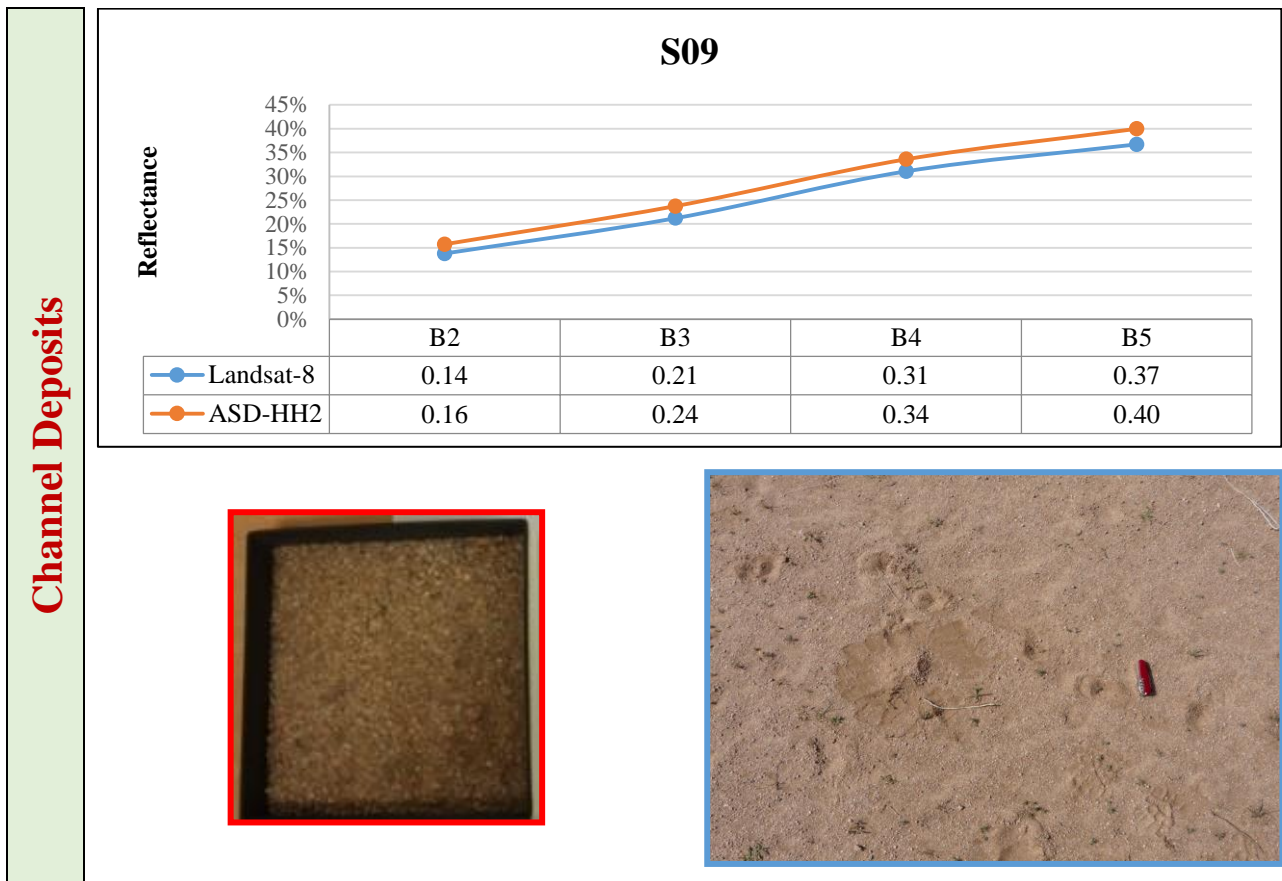|	B2	B3	B4	B5
Landsat-8	0.16	0.22	0.29	0.32
ASD-HH2	0.14	0.19	0.23	0.26

S16

1- Reflectance increases as the wavelength increases.

2- Both bands 2 and 3 have absorption features, while band 4 shows relative high reflectance due to charge-transfer spectral absorption of ferric Fe-oxides.

3- The divergence between image and measured reflectance becomes clearer in bands 4 and 5 as a result of increased grain size variability.

Grain Size	Volume %
Coarse pebbles	0.00
medium pebbles	0.00
fine pebbles	6.32
very fine pebbles	20.31
very coarse sand	29.21
coarse sand	3.26
medium sand	11.21
fine sand	22.51

4- Sample S16 has the highest reflectance (32%) within the Sahuq Plateau; this is related to it originating from diorite igneous rock, which has a lower mafic minerals content, implying that there is a higher reflectance than in S15 (which originates from migmatite metamorphic rocks).	very fine sand	2.20
	silt and clay	4.98
	Total	**100**

Figure 4.27: Image spectrometry vs ASD laboratory spectral measurements of Sahuq Plateau S16.

Sahuq Plateau

S15

	B2	B3	B4	B5
Landsat-8	0.13	0.18	0.24	0.27
ASD-HH2	0.13	0.17	0.21	0.23
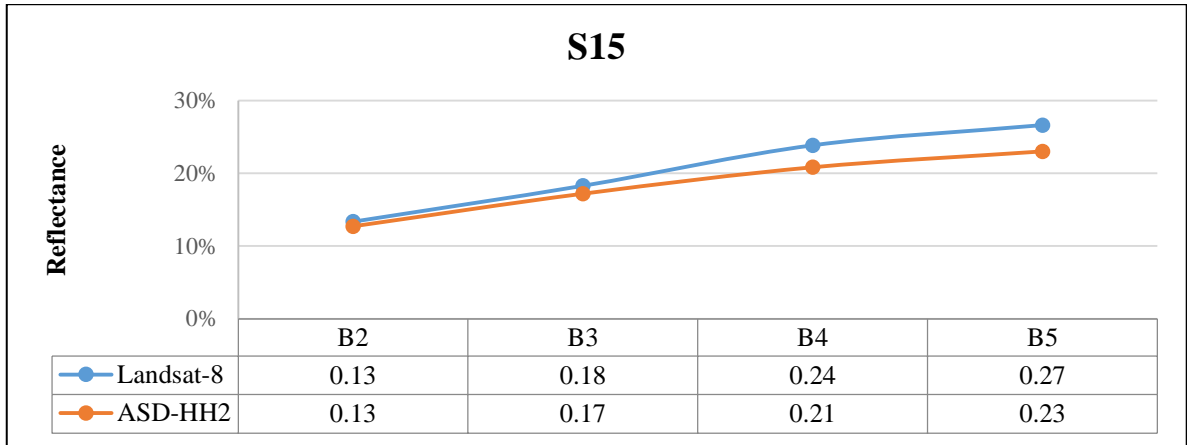
S15

1- Reflectance increases as the wavelength increases.

2- Both bands 2 and 3 have absorption features, while band 4 shows relative high reflectance due to charge-transfer spectral absorption of ferric Fe-oxides.

3- The divergence between image and measured reflectance become clearer in bands 4 and 5 as a result of increased grain size variability.

4- S15 has the low reflectance (27%) within the Sahuq Plateau, as the sample originated from migmatite metamorphic rocks with high mafic minerals content, which implies a lower reflectance than S16. Also, the grain size in S15 is coarser than in S16 as (the grain size in S15 reaches that of medium pebbles, while in S16 the grain size does not exceed fine pebbles), and consequently results in lower reflectance in S15.

Grain Size	Volume %
Coarse pebbles	0.00
medium pebbles	52.58
fine pebbles	28.78
very fine pebbles	1.48
very coarse sand	2.21
coarse sand	0.74
medium sand	4.61
fine sand	5.17
very fine sand	1.11
silt and clay	3.32
Total	**100**

Figure 4.28: Image spectrometry vs ASD laboratory spectral measurements of Sahuq Plateau S15.

The following table (4.3) summarizes the spectral comparison between Landsat 8 imagery and ASD HH2 laboratory measurements for all the surface samples of the study area (classified geomorphic units).

Table 4.3: Surface samples of the study area and their spectral reflectance in both Landsat 8 and ASD HH2 laboratory measurements

| Unit | Sample | Spectral Reflectance (µm) | | | | | | | |
| | | Landsat-8 Pixel | | | | ASD HH2 | | | |
		B2	B3	B4	B5	B2	B3	B4	B5
Wadi Deposits	S01	0.14	0.22	0.32	0.39	0.15	0.22	0.30	0.35
	S02	0.14	0.22	0.33	0.40	0.16	0.23	0.31	0.37
	S03	0.14	0.22	0.34	0.41	0.15	0.23	0.32	0.39
Sand Dunes	S04	0.11	0.20	0.34	0.43	0.10	0.19	0.33	0.43
Slope	S05	0.10	0.16	0.27	0.33	0.09	0.14	0.21	0.26
	S06	0.13	0.19	0.27	0.32	0.11	0.16	0.22	0.27
	S13	0.10	0.15	0.24	0.29	0.09	0.13	0.20	0.23
	S14	0.13	0.17	0.24	0.28	0.11	0.14	0.18	0.21
	S17	0.11	0.15	0.24	0.29	0.07	0.12	0.24	0.30
East Al Madinah Plateau	S07	0.15	0.22	0.31	0.36	0.15	0.21	0.29	0.33
	S08	0.17	0.25	0.34	0.39	0.20	0.27	0.35	0.40
	S11	0.16	0.24	0.34	0.40	0.16	0.23	0.31	0.36
Channel Deposits	S09	0.14	0.21	0.31	0.37	0.16	0.24	0.34	0.40
	S12	0.13	0.20	0.30	0.36	0.12	0.19	0.29	0.35
Dike	S10	0.15	0.23	0.33	0.39	0.08	0.10	0.14	0.15
Sahuq Plateau	S15	0.13	0.18	0.24	0.27	0.13	0.17	0.21	0.23
	S16	0.16	0.22	0.29	0.32	0.14	0.19	0.23	0.26
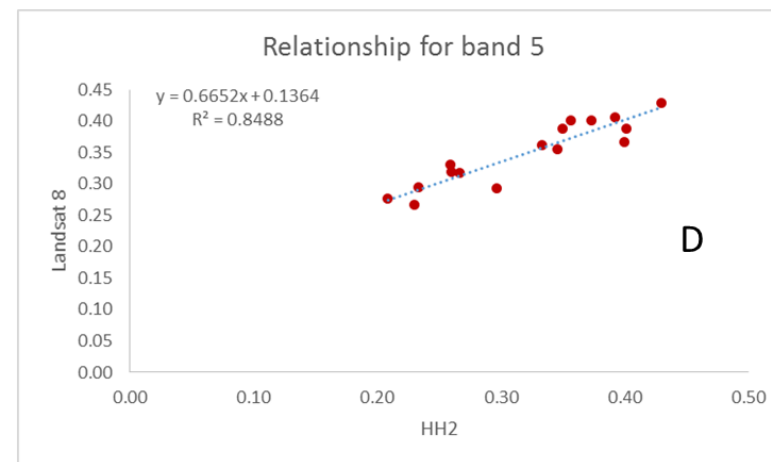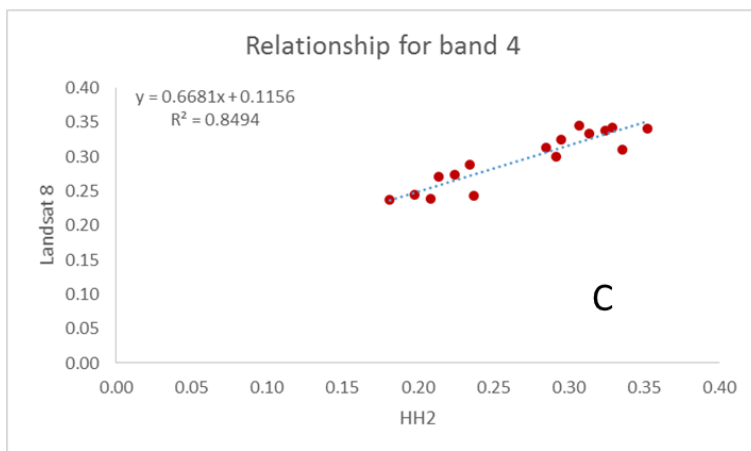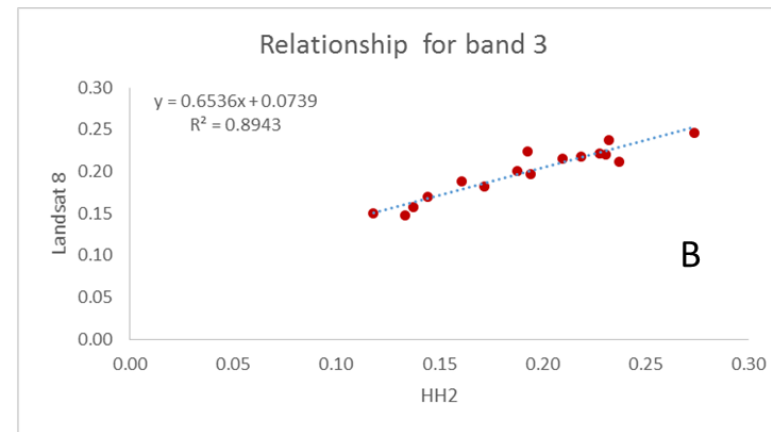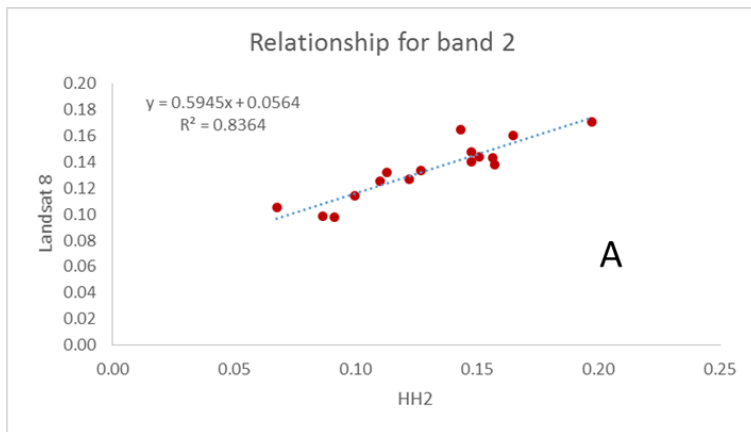
Figure 4.29: Relationship between ASD spectral reflectance and that of Landsat-8 image, (a) band 2, (b) band 3, (c) band 4, and (d) band 5.

Based on the previous samples, other landforms are present in the study area, with different reflectance compared to previous samples, as is the case with sabkhas and Qa. These appear with high reflectance and very light colour in the image, as they contain very fine sediments of silt and clay.

Finally, based on the results presented in sections 4.1.2.1, 4.1.2.2 and 4.1.2.3, regression analysis between ASD HH2 spectral reflectance and Landsat 8 image shows a positive and strong correlation, as demonstrated in Figure 4.29. For example, the correlation coefficient (R^2) between Landsat 8 and ASD HH2 spectral reflectance is in B2 ($R^2=0.84$), B3 ($R^2=0.89$), B4 ($R^2=0.85$) and B5 ($R^2=0.85$). In other words, the results from measured samples have a similar spectral behaviour, especially within bands 2, 3, 4 and 5. The good correlation suggests the suitability of Landsat-8 data in mapping geomorphological units based on their spectral behaviour in visible-NIR spectral regions.

Note: according to field check, dikes are longitudinal bodies of mafic to felsic mineral composition, partly covered by sand sheets and sparsely distributed vegetation cover, which alter their surface reflectance within Landsat imagery. Conversely, the laboratory samples of dikes did not contain these components, and this explains the weak correlation between Landsat8 and HH2 lab reflectance (Figure 4.21). Therefore, field spectral measurements were found to be more effective than laboratory ones, giving reliable spectral signatures for dikes and similar longitudinal features. Because of this, it was decided to exclude dikes from the spectral correlation.

Differences between image and laboratory reflectances are common due to the following:

1- Even after applying the most comprehensive atmospheric corrections modules, atmospheric components (essentially water and carbon dioxide) attenuate energy and restrict the wavelength range of satellite data to the limit of excluding most useful data. Conversely, laboratory reflectance measurements overwhelmed nearly all these effects.

2- Natural surfaces are rarely composed of pure, size-sorted minerals; they are commonly nonhomogeneous mineral assemblages in a wide spectrum of shapes and sizes with weathered and/or altered surfaces. This becomes more obvious within pixel reflectance (pixel area in Landsat-8 is about 900 m^2).

3- Soil moisture, organic materials, and vegetation cover contribute to the total spectrum, often dominating it.

4- The smallest particle size range gives the least spectral contrast and the highest relative reflection (Hunt, 1977).

5- The major constituents of most minerals (silicon, aluminium, magnesium, and oxygen) have no absorption features in the VNIR spectral range (Hunt, 1977; Hunt and Salisbury, 1970; Hunt and Salisbury, 1971).

6- Most common electronic absorption features in the VNIR spectra of minerals (rocks an soils) caused by iron as Fe^{2+} and/or Fe^{3+} valence states through crystal field and charge transfer processes (Clark, 1999).

7- OH- group minerals (clay minerals, gypsum, zeolites, milky quartz, etc) carbonates, borates, and phosphates imply their specific absorption beyond the VNIR spectral region (within SWIR one) due to vibrational absorption processes and their overtones (Hunt, 1977).

4.1.2.4 Landsat 8 Vs. ASD Spectral Reflectance (mix, C,F)

The spectral relationship between ASD HH2 and the image was determined in section 4.1.2.3 and 4.1.2.4; this has helped in understanding how imagery can be used for mapping and estimation of the fine and coarse material spectral properties. It was done by an estimate of a large area coverage from image (pixel size is about 900 m^2), since the ASD HH2 field of view is restricted to a few centimetres.

The convoluted reflectance values for the hand-held radiometer (ASD) bulk samples fine and coarse fractions are presented with the equivalent reflectance values extracted from the Landsat-8 image (Figure 4.30).

The reflectance values for the fines, shown in purple, are high. In most cases, the reflectance values for the fine material is slightly higher than with the Landsat 8. The field measurement of reflectance for the coarse material, in green colour, has the lowest reflectance values in most of the samples, with the exception of slope deposits 14. The red line indicates the reflectance values for the mixed sediments. The behaviour of the reflectance over these samples formed a transition between the fine and the coarse material in most samples.

In laboratory spectral measurements, it is found that the limited grain size variability within the same sample leads to similar spectral profiles, as shown in samples 1, 2, 3, 8 and 9. Conversely, more grain size variance leads to highly contrasted spectra as in samples 5, 6, 13, 15 and 16.

Overall, the variability of reflectance in field measurements with Landsat data is high where the samples are heterogeneous (sample 5, 11, 14, 15, 16) and the direct opposite is true when the sediments are homogeneous (e.g. samples 4 and 12).
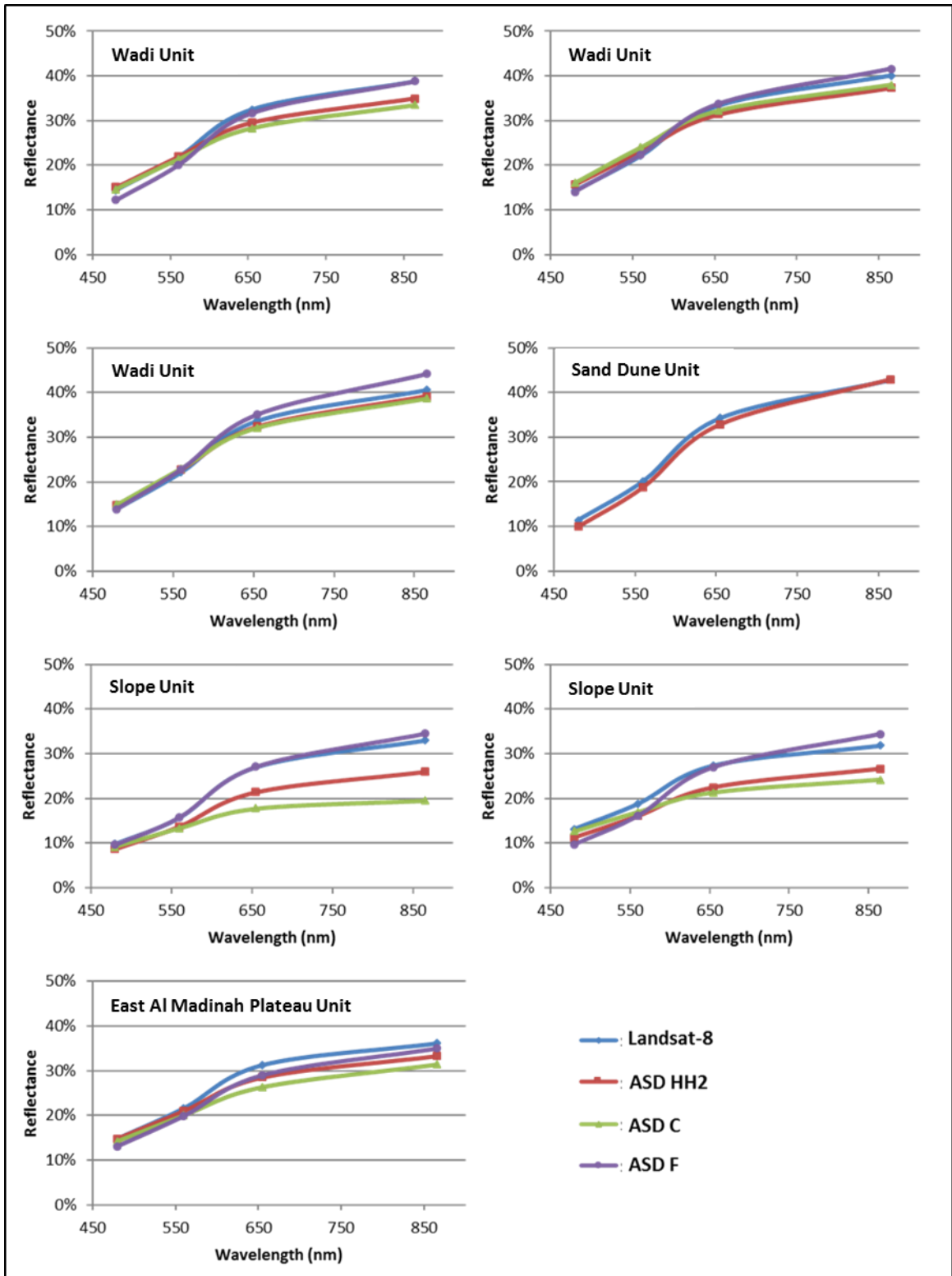
Figure 4.30: Spectral reflectance of Landsat-8 v. convoluted hand held radiometer readings of studied samples (1 to 7). ASD HH2 (Hand Held bulk sample), ASD C (Coarse fraction), ASD F (Fine fraction). To be continued.
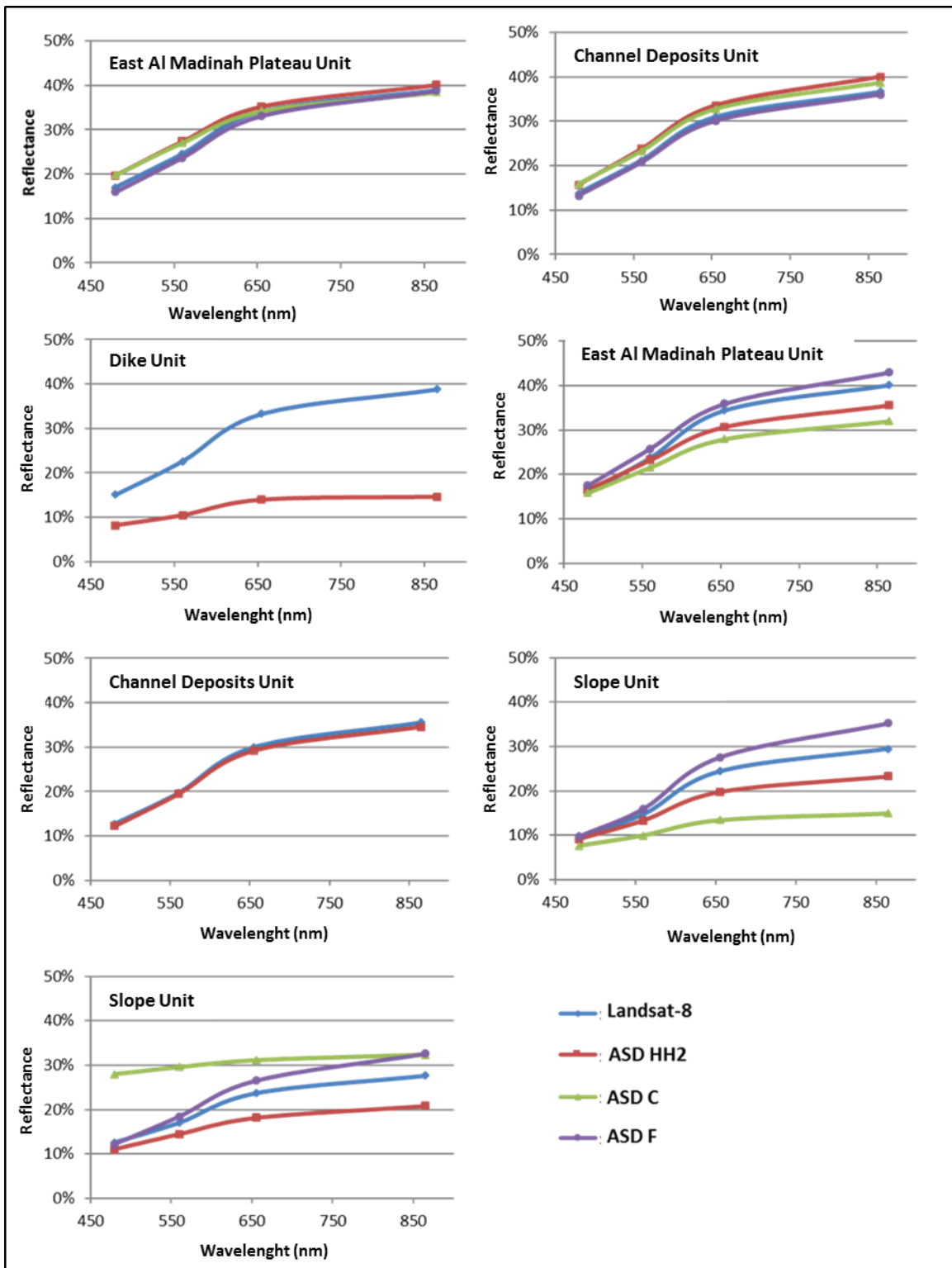
Figure 4.30: Spectral reflectance of Landsat-8 v. convoluted hand held radiometer readings of studied samples (8 to 14). ASD HH2 (Hand Held bulk sample), ASD C (Coarse fraction), ASD F (Fine fraction). To be continued.
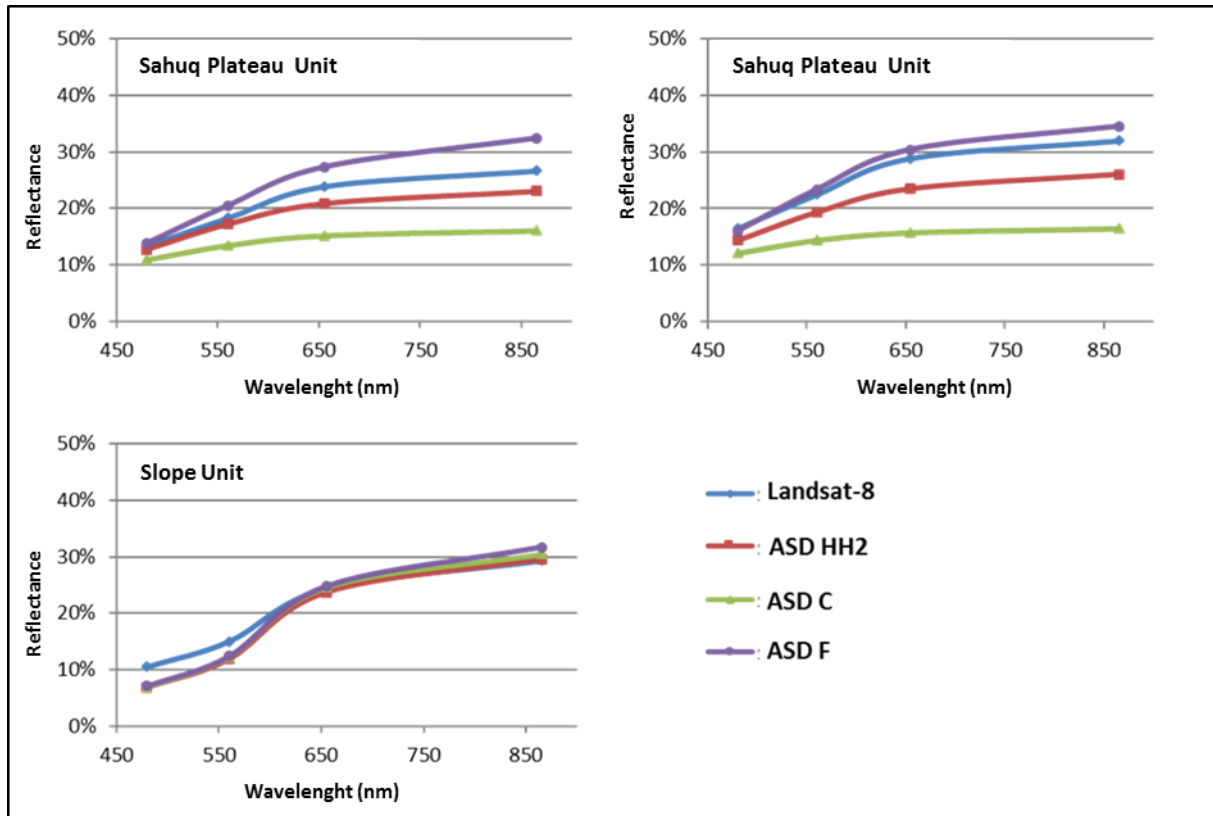
Figure 4.30: Spectral reflectance of Landsat-8 v. convoluted hand held radiometer readings of studied samples (15 to 17). ASD HH2 (Hand Held bulk sample), ASD C (Coarse fraction), ASD F (Fine fraction).

4.1.2.5 Spectral Transect Mapping and Estimate of Fine and Coarse Material Proportion

Figures 4.31 and 4.32 show a gradational increase of surface reflectance from upstream (pixel 1) towards downstream (pixel 4), clearly represented by Landsat bands 3 and 4. This reveals a good matching with grain size decrease from upstream (near the source rocks and dike swarms near sample 1) to downstream (where pixel 4 is located away from the source rocks near to a sand sheet of finer grain size). Pixels 1 and 2 show lower reflectance than the reference pixel (sample S8 in Figure 4.17), which may be related to their higher content of coarse grain sediments. On the other hand, pixels 3 and 4 have higher reflectance, implying finer grain sizes.
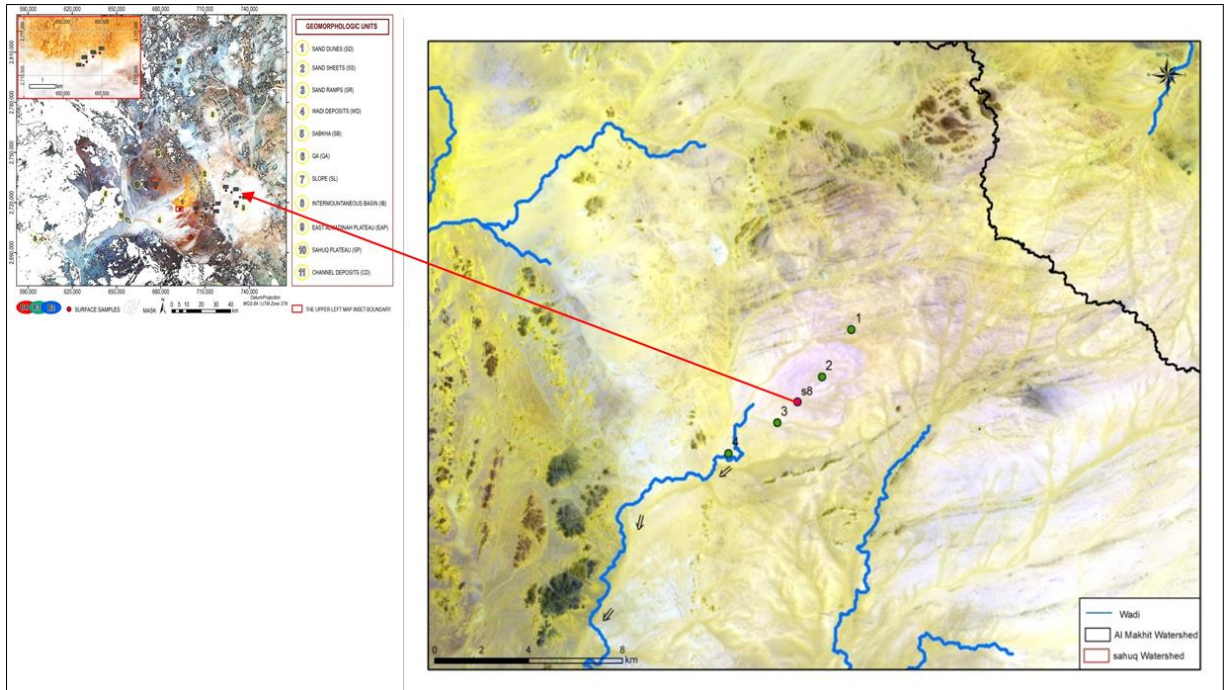
Figure 4.31: Surface reflectance transect along four pixel samples; sample S8 was used as a reference.
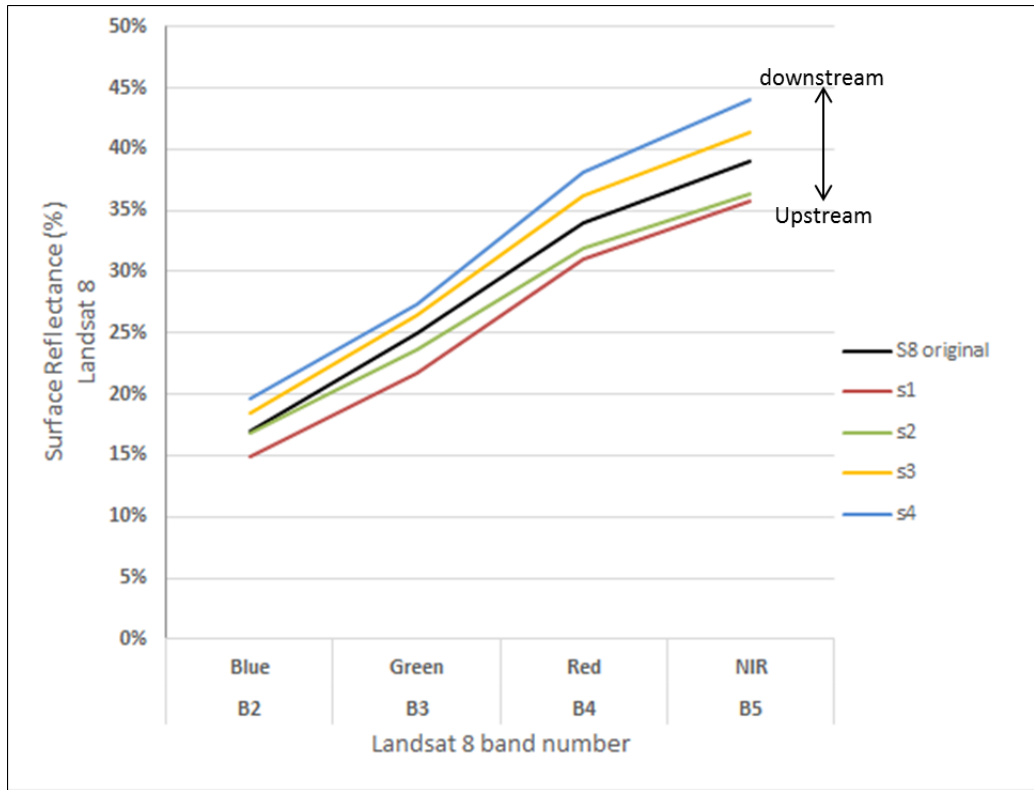
Figure 4.32: Landsat 8 surface reflectance of the four pixel samples along the transect (see Figure 4.31), sample S8 was used as a reference .

4.1.3   Landsat Spectral Data for Mapping

Landsat 8 Image Processing

Landsat-8 Image processing procedures were used to transform multispectral image data into informative images, which exaggerate the spectral contrast between interesting targets, and provide compositional information of certain pixels in the image. The processing techniques used in the current study include colour composites, band ratios, principle component analysis, and supervised classification.

4.1.3.1   Band Composite

Table 4.4: The highest OIF ranked band colour combinations

No.	Band Colour Combination (in RGB)			OIF Rank
	R	G	B	
1	Band 7	Band 6	Band 1	90.94
2	Band 7	Band 6	Band 2	89.32
3	Band 7	Band 5	Band 1	89.24
4	Band 6	Band 5	Band 1	88.41
5	Band 7	Band 4	Band 1	87.71
6	Band 7	Band 5	Band 2	87.67
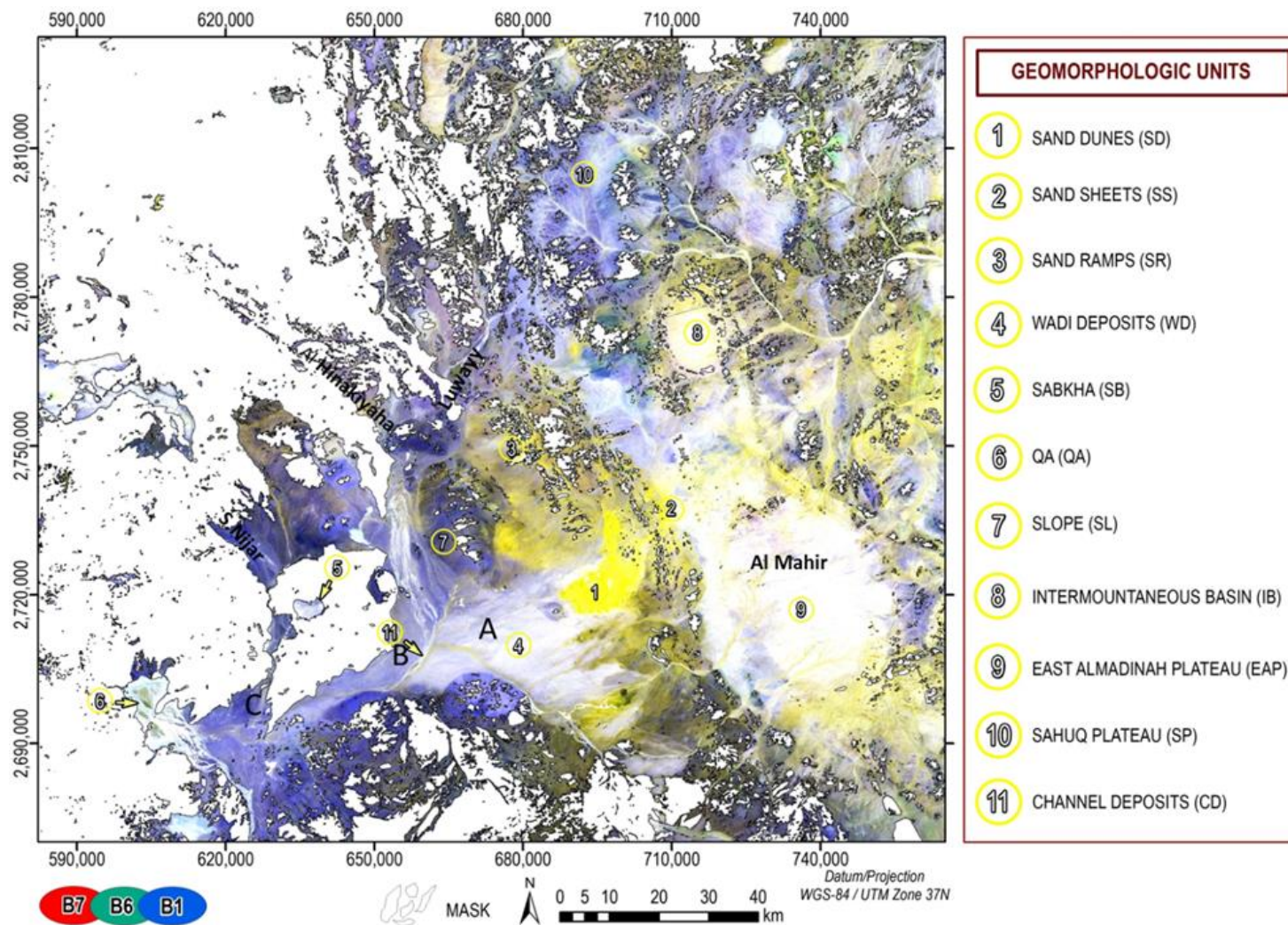
Figure 4.33: False Colour Composites (FCC) in RGB7, 6, 1 and OIF rank 1= 90.94.
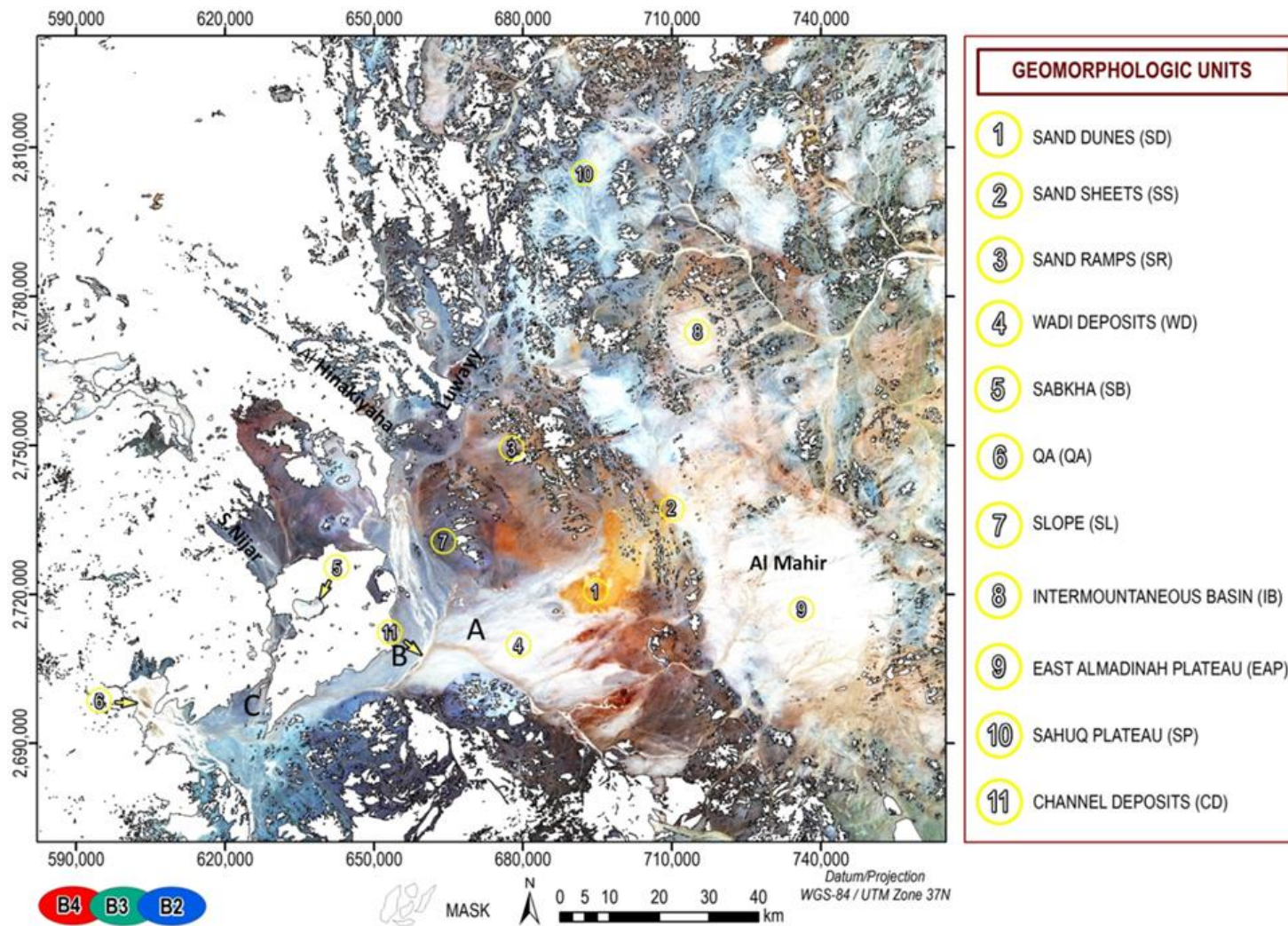
Figure 4.34: True Colour Composites (TCC) in RGB 4, 3, 2.

The OIF algorithm was applied on the Landsat-8, seven reflected bands (VNIR-SWIR). The resultant six highest OIF ranking values were calculated (Table 4.4). The selected False Colour Composites (FCC) image clearly maps the geomorphologic units in the study area with different colour shades (Figure 4.33). This is very clear when both images (TCC and FCC) are compared, as the true colour composite (TCC) bands 432 in RGB colour channels produced a near natural coloured image close to what would observed by the human eye (Figure 4.34). The most prominent geomorphologic units within TCC is sand dunes that appeared in a homogenous pale brown; this is related to its composition (highly sorted aeolian deposits essentially composed of quartz). The pale brown colour of sand dunes in TCC suggests the presence of ferric iron oxides that absorb most of blue and green band wavelengths, and reflect red band ones due to electronic absorption processes.

True colour composite (432 in RGB) could not discriminate between some geomorphological units within the study area. Sabkha, Qa, East Al Madinah plateau, and channel deposits were white in colour, due to a flat reflectance over the three bands. On the other hand, the false colour composite (761 in RGB), the highest OIF rank, distinguished these geomorphological units with crisper colours; sabkha was represented in cyan to lead blue, Qa appeared in cyan, East Al Madinah plateau in white to pale blue, and channel deposits in ghost white to cyan.

All other units took similar tones around bluish to brownish grey, as the visible region of electromagnetic spectrum cannot differentiate between units with subtle spectral characterizations.

The False colour composite (FCC) that had the highest optimum index factor rank (= 90.94) of bands 761 in RGB showed a more colourful appearance. The usage of two SWIR bands supports the differentiation between units of similar mineral composition and consequently spectral behaviour. Sand sheets appeared in olive green, possibly due to a spectral mixing between sand sheets (essentially composed of quartz and feldspars) with the underlying igneous and metamorphic basement complex that contains ferromagnesian minerals (micas, pyroxenes, and amphiboles) that have high reflectance in band 6 (green channel).

Moreover, both grain-size effect and tonal variations appeared to be more obvious in FCC than in TCC, due to the FCC's better colour display. Although dark gravelly surfaces appeared as grey, they took different distinguishable colours in FCC according to the source

rocks of each geomorphological unit. The Sahuq plateau appeared in dark blue whereas slopes took different colours (due to different source rocks) ranging between blue, lead blue, and violet.

4.1.3.2   Band Ratios
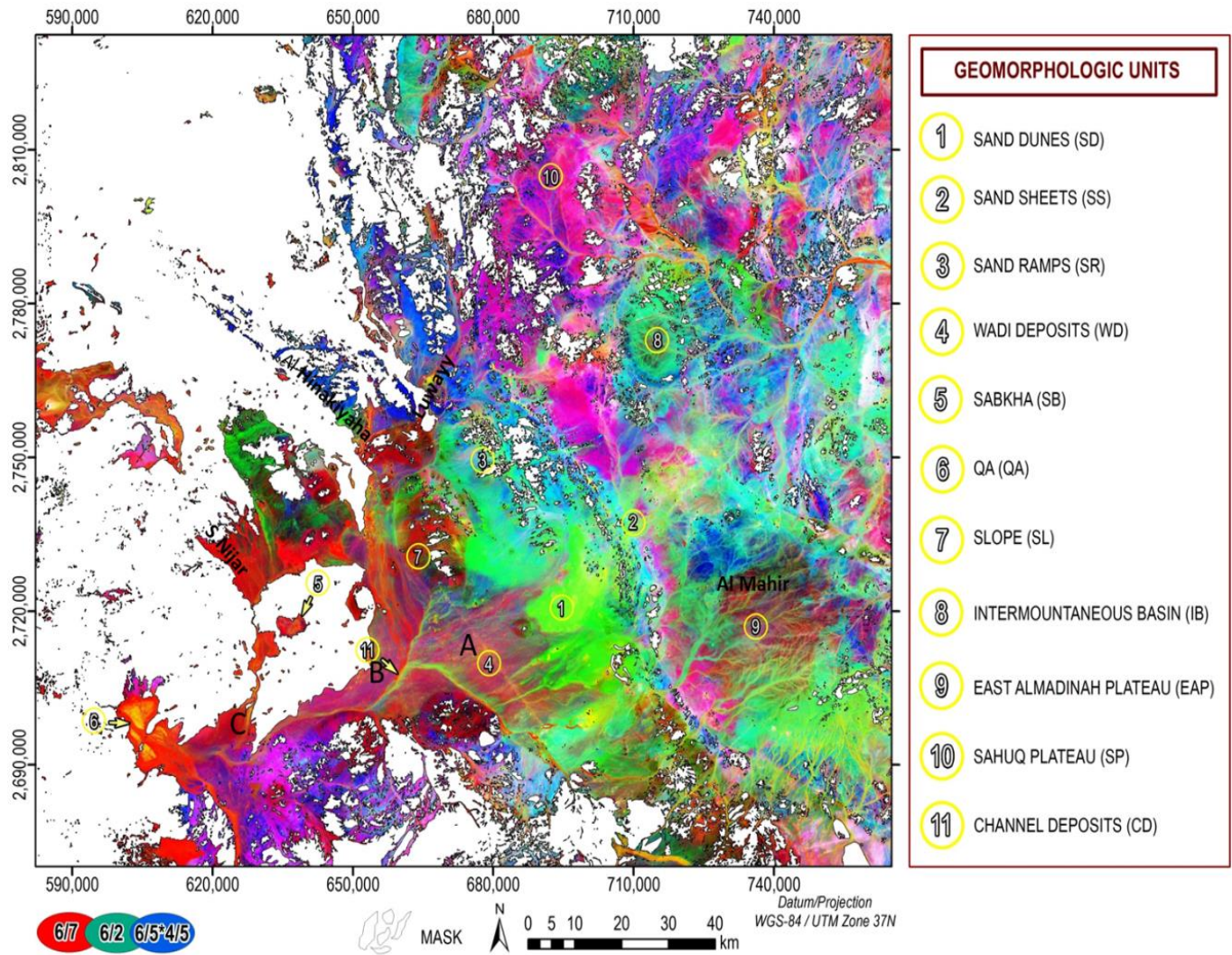
Figure 4.35: FCC of Landsat-8 band ratios 6/7, 6/2, 6/5*4/5 (equivalent to the Landsat-7 Sultan ratio).
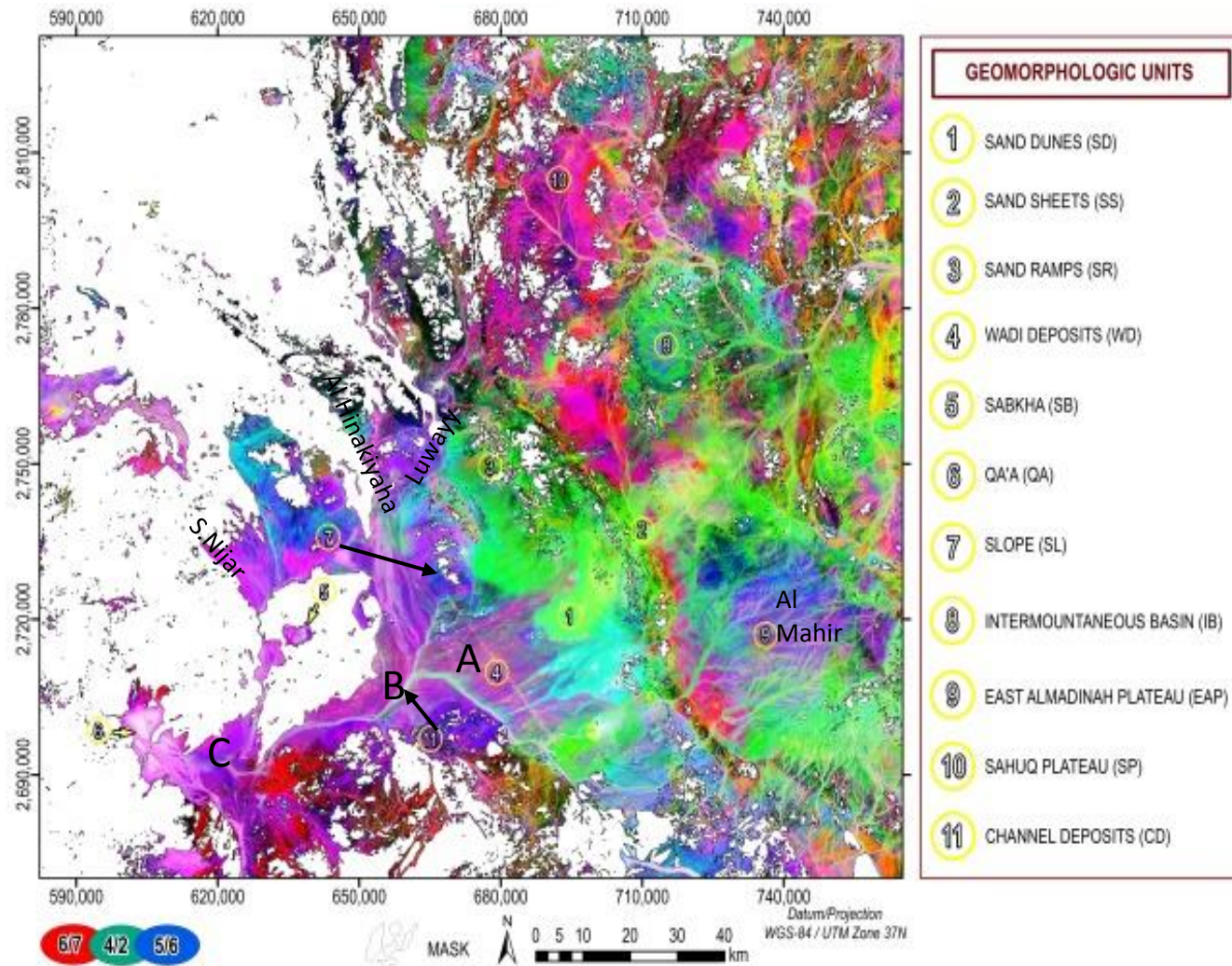
Figure 4.36: FCC of Landsat 8 band ratios 6/7, 4/2, 5/6 in RGB (equivalent to the Landsat-7 Abrams ratio).

Sultan Ratios FCC

Band Ratio 6/2:

Generally, Landsat 8 B6 shows high reflectance values (except for rocks with high contents of mafic minerals (ferromagnesians) like in gabbros and basalts), as it lies between major vibrational absorptions at longer wavelengths (2.11-2.29 µm) related to OH-bearing minerals, and major electronic absorption bands related to Fe-bearing aluminosilicates (quartz & feldspars) at shorter wavelengths (≤1.0µm) (Sultan et al., 1987).

Landsat 8 B2 reflectance is very sensitive to the electronic absorptions in materials with even trace amounts of iron (Hunt, 1977).

Rocks rich in mafic materials have low B6 and B2 reflectance values, whereas other rocks generally should have high B6 and low B2 reflectances.

In the current study, B6/B2 ratio promoted the overall reflectance values of the studied geomorphological units (essentially sand dunes, sand sheets, sand ramps, and partially slopes) that show higher reflectance than that of other units. This could be interpreted by the presence of Fe-oxides (even in trace amounts) within the mineral composition of these units, as Fe-oxides are very common alteration products within ferromagnesian minerals that form essential components in igneous and metamorphic rock complexes - the source of these geomorphological units.

As B6/B2 ratio image falls in the green colour channel; sand dunes, sand sheets, sand ramps, and partially slopes take on green shades in the Sultan ratio false colour composite (Figure 4.35).

Reflectance in landsat-8 band 7 spectral region (2.11 to 2.29 µm) strongly depends on the hydroxyl content of the rocks, and the ratio 6/7 is used to measure the intensity of the hydroxyl absorption in the 2.2 - 2.4 µm region, as band 6 has no specific absorption features related to Fe-bearing aluminosilicates. The ratio B6/B7 highlighted specific geomorphological units within the study area (Qa, sabkha, slopes, and partially East AI Madinah Plateau) appearing as red shades in the Sultan ratio FCC, confirming the presence of hydroxyl minerals (such as clay minerals & gypsum) within these geomorphological units (clay minerals are common alteration products of feldspars that are essential mineral constituents in granites).

B6/B5 * B4/B5

Geomorphologic units rich in Fe -bearing aluminosilicates (essentially feldspars and metamorphic minerals) have a concave-upward spectral reflectance pattern in the B5 wavelength range, which is principally related to the broad absorption associated with ferrous- related absorption near 1µm (principally due to the presence of ferromagnesian minerals like pyroxene and amphiboles in granitic rocks). The overall transformed reflectance values of both B4/ B5 and B6/B5 have the same tendency to highlight geomorphological units rich in ferromagnesian minerals (derived from metamorphic rocks like migmatites). The Sahuq Plateau, in addition to some slopes, appeared with bright reflectance, especially after exaggerating reflectance via multiplication of the two ratios (B6/B5 and B4/B5). Those geomorphological units take bluish shades in the Sultan false colour composite.

Abrams Ratio FCC

(Figure 4.36) The Abrams ratio false colour composite matched with the Sultan ratio, and enhanced the lithologic differences between the geomorphological units. Abrams FCC used the same Sultan's Red (B6/B7), highlighting the OH-bearing minerals with red shades in slopes, wadi deposits, channel deposits, Qa, and sabkha. Abrams green (B4/B2) distinguished Fe-oxides bearing aluminosilicates (quartz and feldspars in sand dunes, sand sheets, sand ramps, and partially slopes) with green shades coinciding with Sultan green (B6/B2) in most places. B5/B6 ratio represents the blue colour channel in Abrams FCC. Geomorphological units rich in ferromagnesian minerals like pyroxenes, amphiboles, and micas, took on blue shades; this mostly appeared in the East Al Madinah plateau, Inter-mountainous basins, some slopes, and the Sahuq Plateau.

Heterogeneous components of some geomorphological units contribute with varying proportions to the RGB colour channels, which provides various intermediate colours.

4.1.3.3 Principal Component Analysis (PCA)

The current study applied PCA analysis on Landsat-8 multispectral reflectance bands (Band 1 to Band 7), obtaining seven principal components, the eigenvector loadings of the PCA transformation as listed in Table 4.5. The first three PCs (PC1, PC2, PC3) have a variance percentage of 99.79% between all output seven PCs (Figures 4.37 a-c). A colour combination of PC1, PC2, PC3 in RGB was used for mapping different geomorphologic units (Figure 4.37 d), for a good contrast between them with crisper colour display. For example, we find sand clearly represented, as it appears pink in colour, while sabkha appears in cyan and yellow, Qa areas as cyan blue, the East Al Madinah plateau appears in yellow as well as in violet, and the Sahuq plateau appears green.
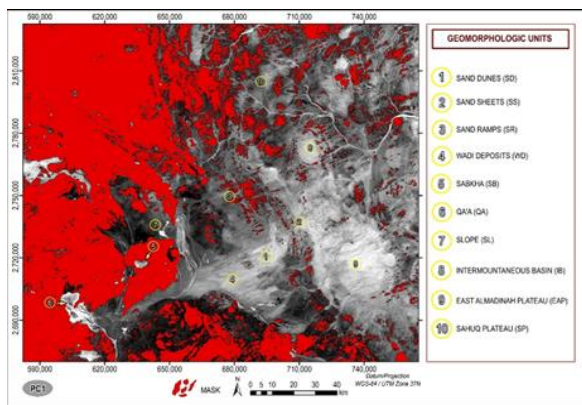
A
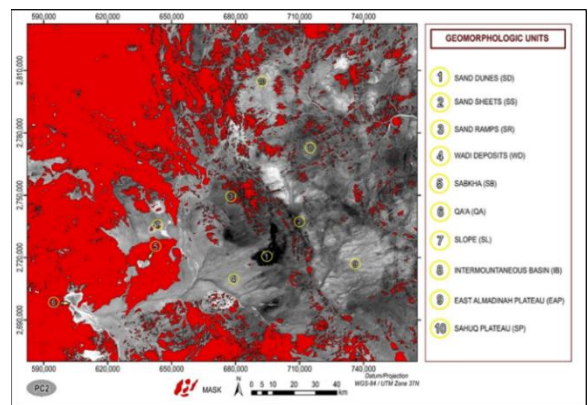
B
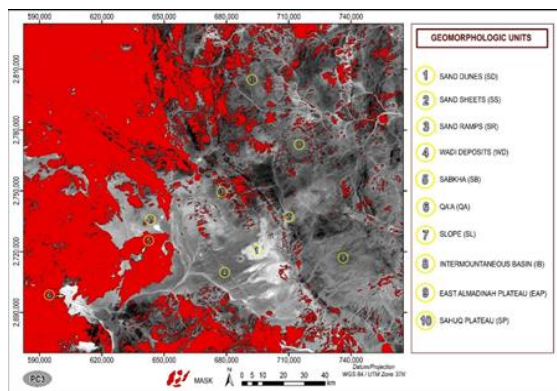
C
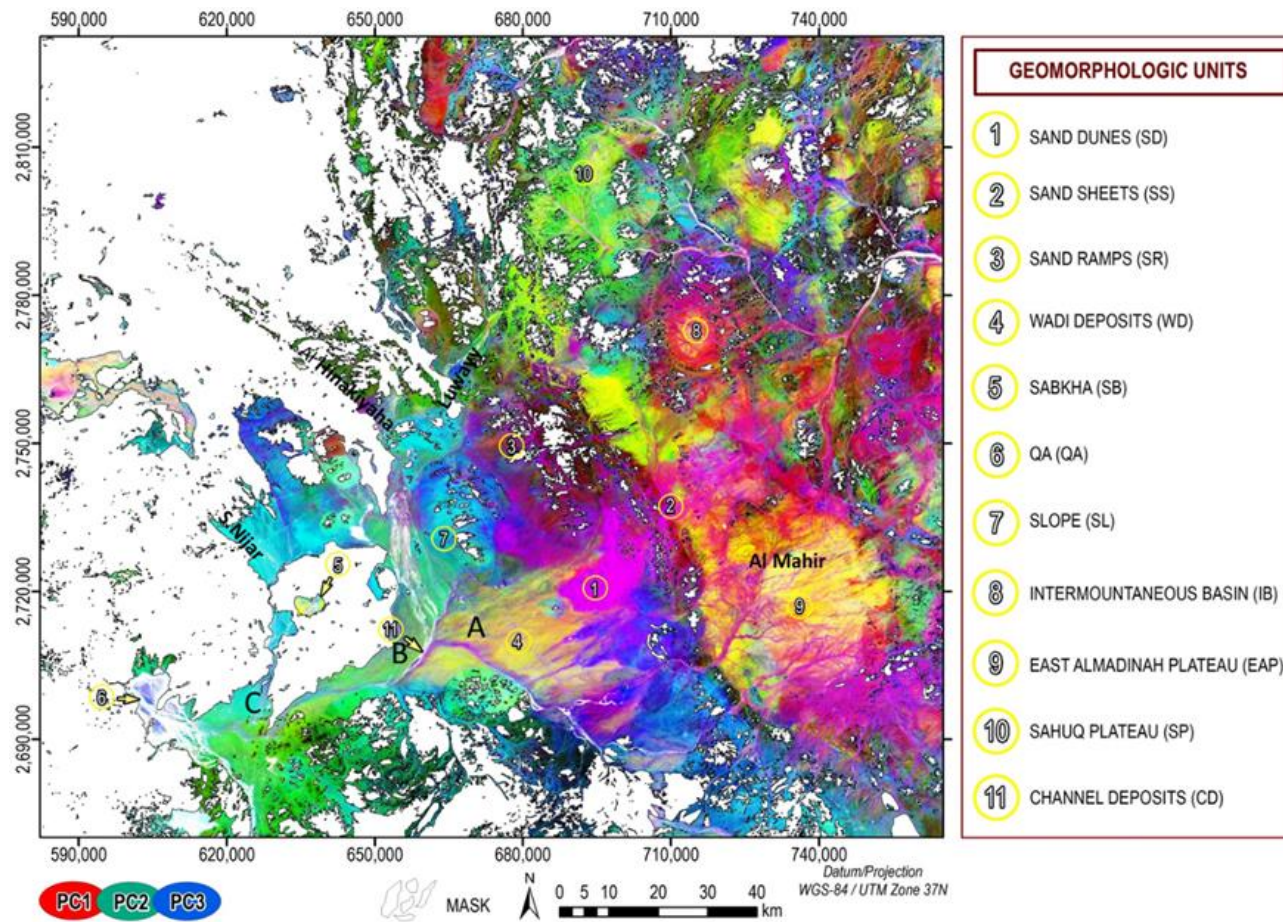
(D)

Figure 4.37: Concentrates Spectral Features; (A) PC1, B) PC2, (C) PC3 and (D) False colour composite of PC1, PC2 and PC3 in RGB.

Table 4.5: Eigenvector loadings and variance of principal components

	B1	B2	B3	B4	B5	B6	B7	Variance	Variance %
PC 1	0.345	0.345	0.367	0.386	0.39	0.407	0.401	40237.51	94.02
PC 2	0.551	0.495	0.25	-0.091	-0.23	-0.375	-0.433	2216.11	5.18
PC 3	0.239	0.132	-0.141	-0.472	-0.571	0.294	0.52	252.8	0.59
PC 4	-0.499	0.066	0.721	-0.029	-0.365	0.257	-0.165	52.48	0.12
PC 5	-0.17	0.02	0.242	0.142	-0.08	-0.731	0.592	24.02	0.06
PC 6	0.088	-0.095	-0.227	0.772	0.573	0.074	-0.049	8.63	0.02
PC 7	0.486	-0.778	0.392	-0.06	0.034	-0.014	-0.002	5.27	0.01

It is clear from PCA that the rock formation on the Al Mahir, Luwayy, Al Hinakiyah and S. Nijar basins feed sediments to the wadi deposits west of the study area. Wadi deposits surfaces (A, B and C) could be identified based on their spectral properties (Figure 4.37d). The differences in the spectral properties of each wadi deposits are related to their different source lithologies in the basin. For example, wadi deposit A (takes on a yellowish colour) is supplied by the Wadi Al Mahir basin dominated by granite. In contrast, area B (in pale green) is supplied by Wadi Luwayy and Al Hinakiyah basins, which are dominated by andesite, basalt and rhyolite. Area C (in yellowish green) is supplied by S. Nijar basins which are dominated by basalts. Also, aeolian deposits sporadically cover the study area, particularly the eastern parts, and come from Nufud Al Qawz, where large bodies of sand dunes occur.

FCC (761 in RGB Figure 4.33) was less effective than PCA in detecting sediments' sources and their depositional sites. This became apparent via the similarity between the B and C regions' wadi deposits, which originated from different sources. Furthermore, sand sheets

within the East Al Madinah plateau did not appear clearly. Abrams ratio provided a good contrast between the geomorphologic units but could not identify the sediments' origins. On the other hand, the Sultan ratio (Figure 4.35) was more efficient in identifying sediments' origins, but less so than PCA. Wind deposits clearly appeared in both the Abrams (Figure 4.36) and Sultan ratios.

4.1.3.4   Image Classification

The current study used the Maximum likelihood supervised classification method based on training sites selected according to previous geologic maps, field investigations, 2D scatter plots of non-correlated reflectance bands, and visual assessment of colour composites.

Eleven geomorphologic units were selected to be classified: sand dunes, sand sheets, sand ramps, wadi deposits, slopes, Qa, sabkha, inter-mountainous basins, the Sahuq Plateau, and East Al Madinah plateau. Each unit is represented by a number of training sites containing a suitable number of pixels. The fact that a geomorphologic unit usually contains materials of different compositions with different spectral characteristics was seen particularly clearly within slopes and wadi deposits. Consequently, a number of training sites were selected as subclasses belonging to the same geomorphologic unit. Therefore, the number of input endmembers increased to 21, reducing the standard deviation of the average reflectance. In this way, the classification results became more reliable (all subclasses then merged to their unit through the post-classification process).

The mean reflectance value of each class was calculated and finally, the end-members spectral library was created (Figure 4.38). Post-classification processes applied to the resulted classification included:

- Sieving; to solve the problem of isolated pixels occurring in classification images.
- Clumping adjacent pixels.
- Majority-Minority analysis; to change spurious pixels within a large single class to that class (Figure 4.40).

- A Confusion matrix was then applied to the classification results to assess the overall accuracy based on an independent validation ground truths (73 sites) representing the different 11 geomorphologic units.

The results of the classification are shown in Figures 4.38 and 4.39.
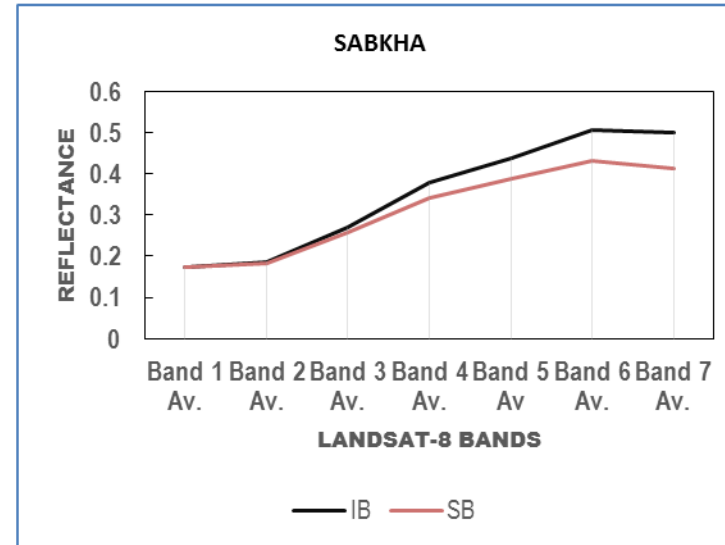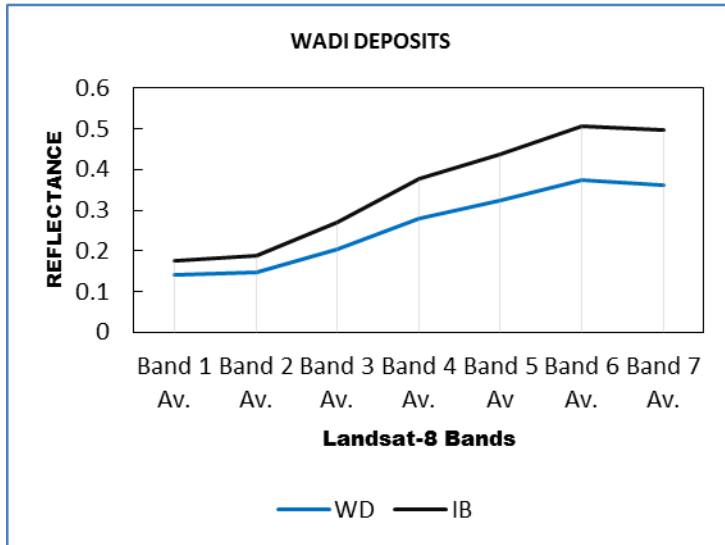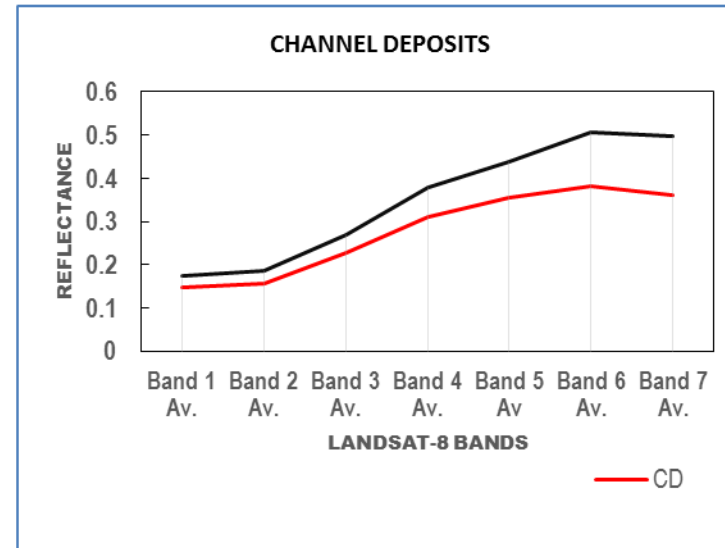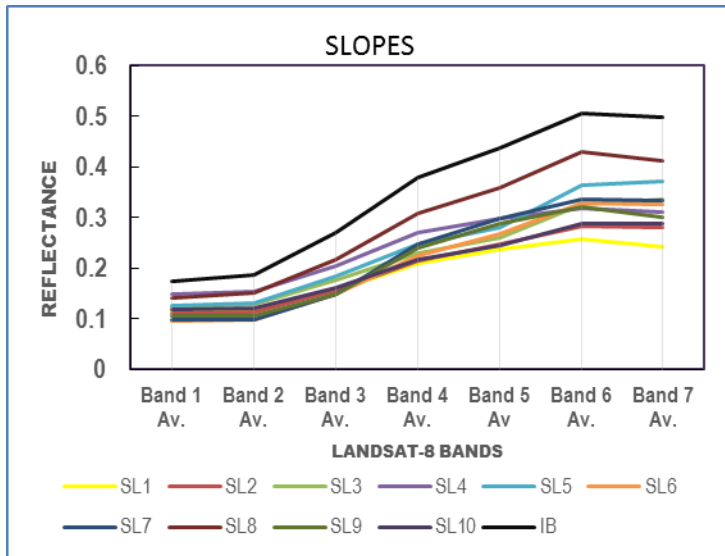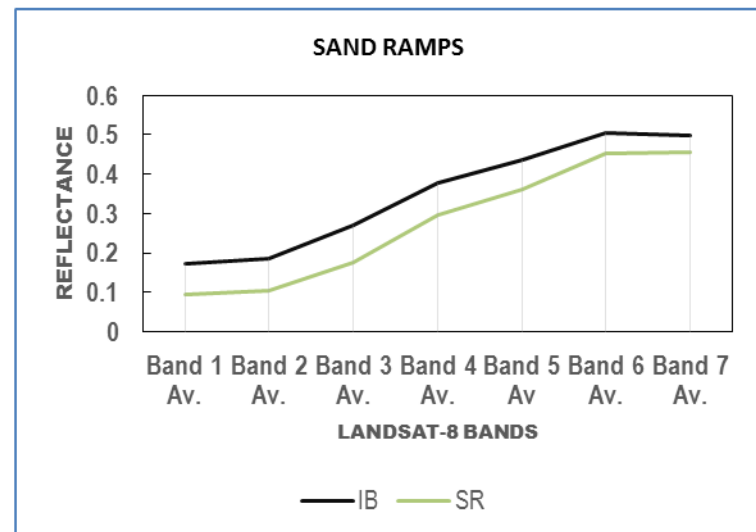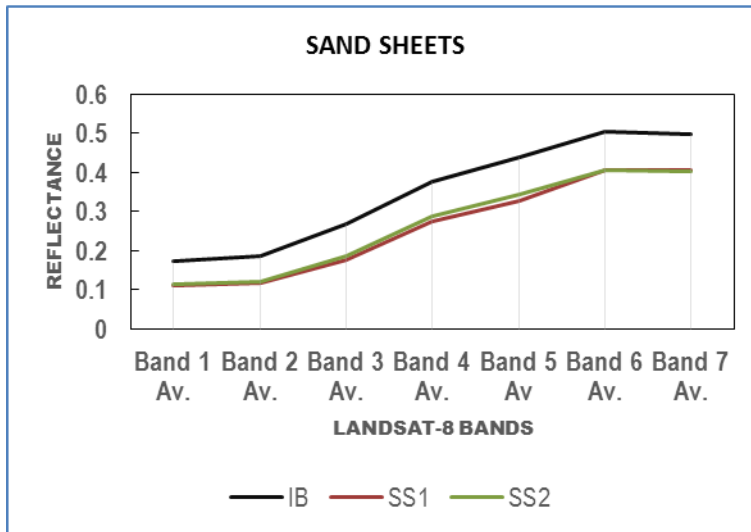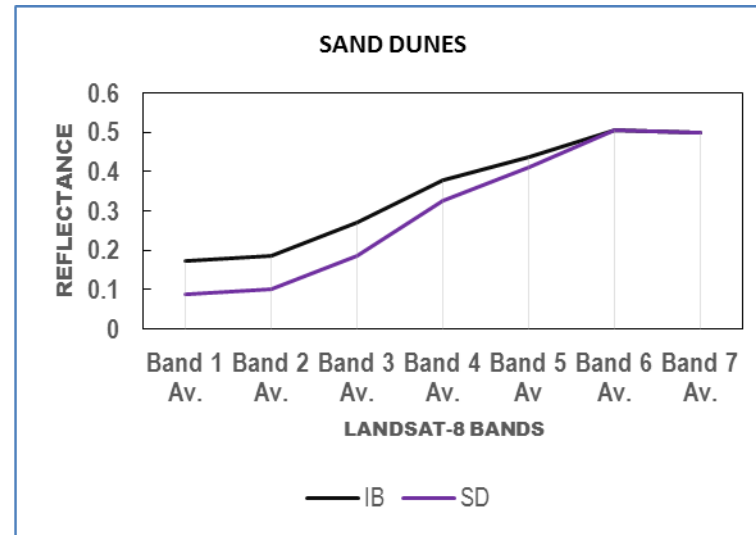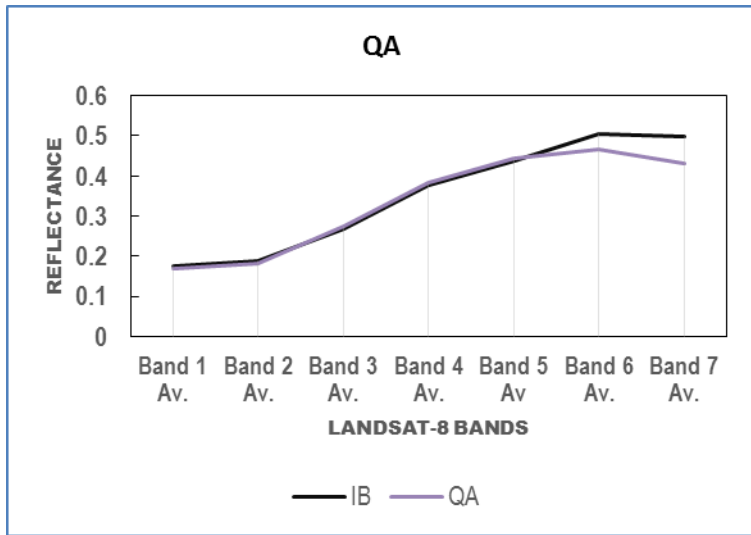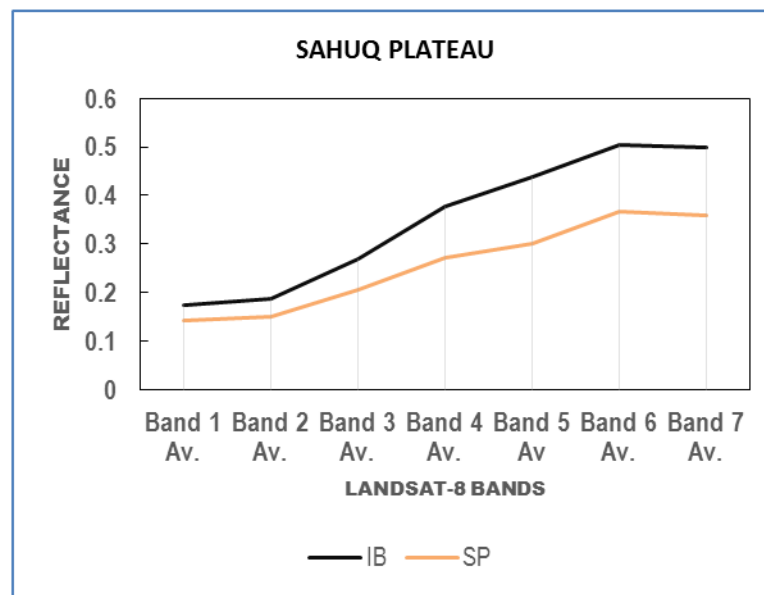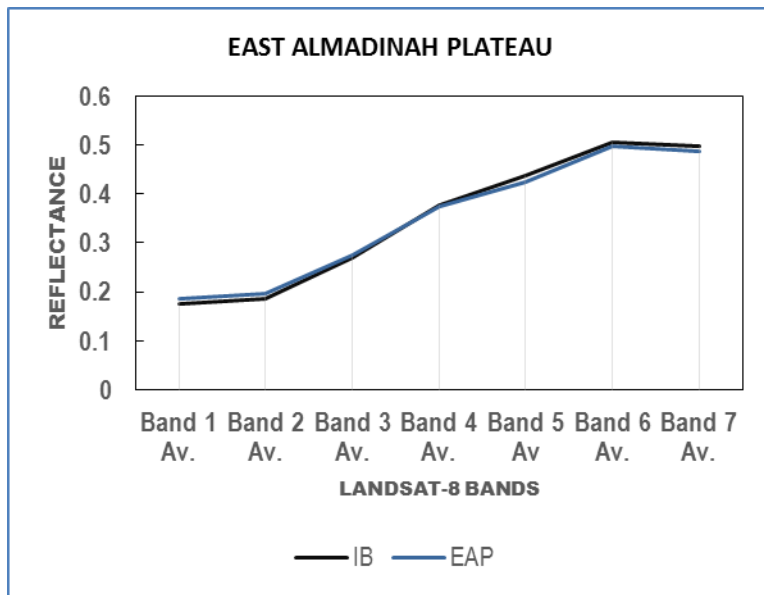
Figure 4.38: Endmembers spectral library used in Maximum likelihood supervised classification: SL (Slope), WD (Wadi Deposits), IB (Intemountanous Basin), SB (Sabkha), SR (Sand Ramps), QA (Qa), SD (Sand Dunes), SP (Sahuq Plateau), EAP (East Al Madinah Plateau), SS (
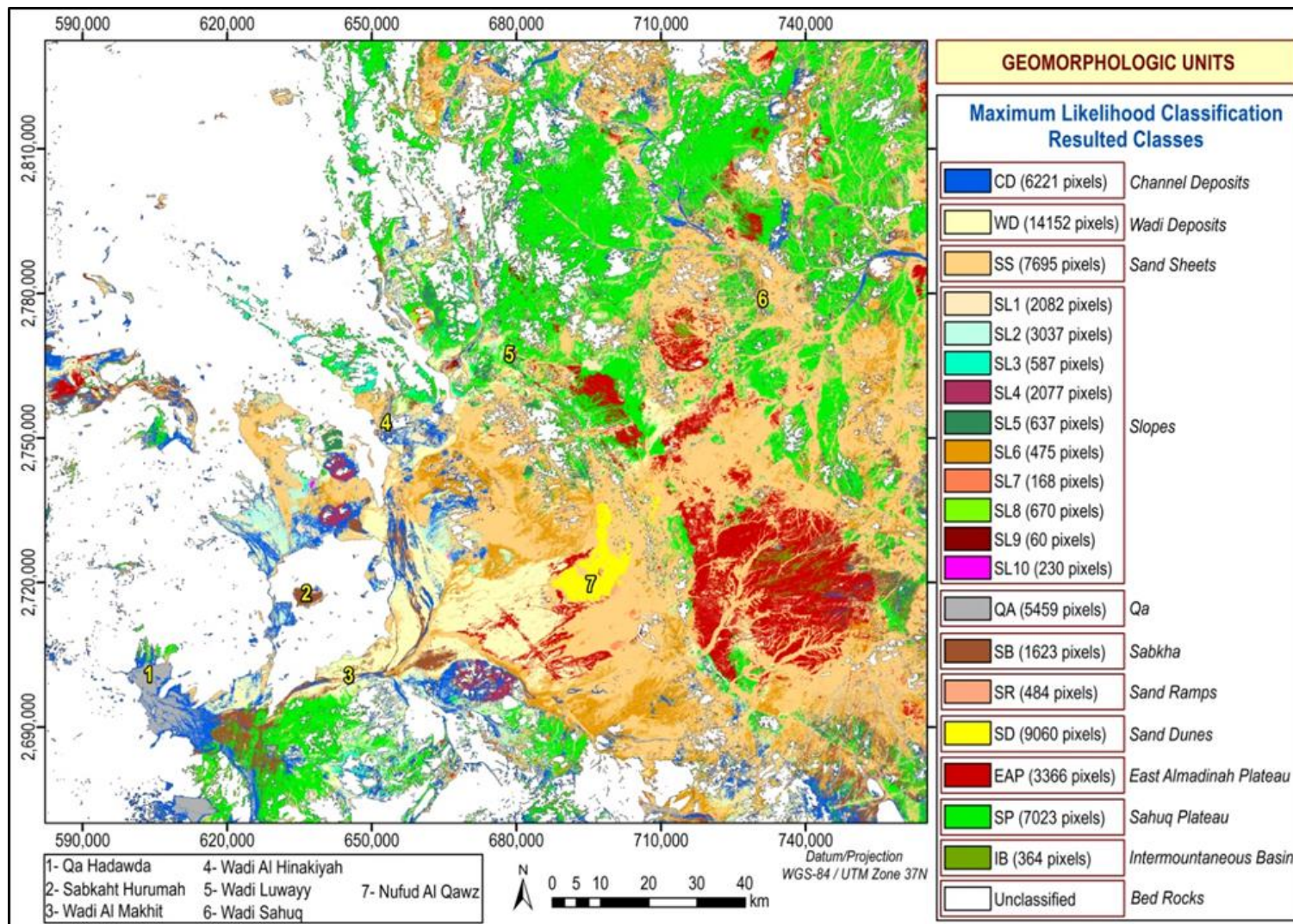
Figure 4.39: Maximum Likelihood classification result (prior to merging subclasses and post-classification processing).
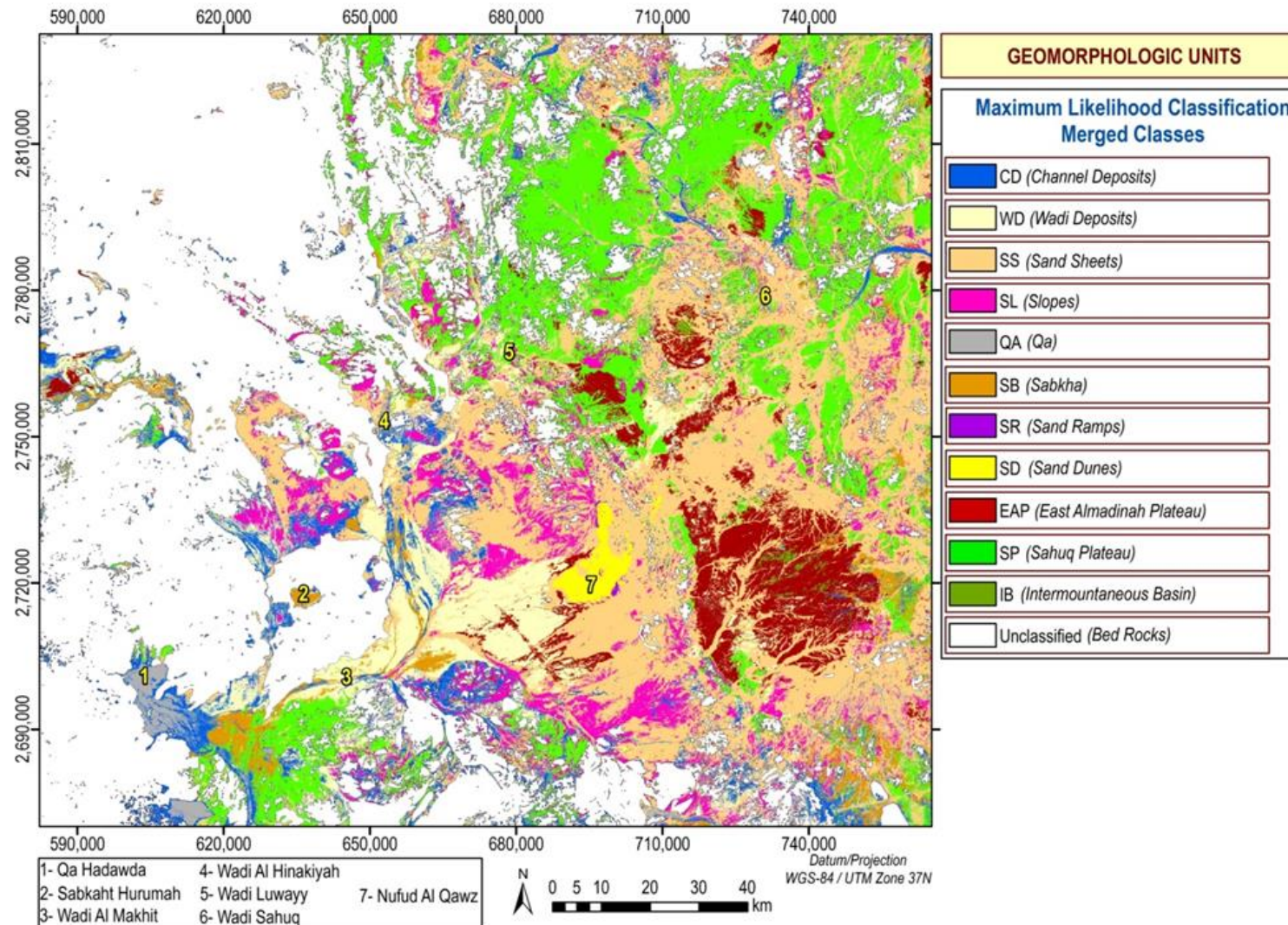
Figure 4.40: Maximum Likelihood classification result (after merging subclasses and post-classification processing).

Accuracy Assessment

The current study used ground truth areas selected from certain locations representing the eleven geomorphologic classes. The ground truth areas were designated using previous maps, field investigations and visual interpretation of higher spatial resolution satellite images (Google Earth). The calculated overall accuracy of the current classification was found to be:

Overall accuracy = (39885/49339) = 80.84%.

Kappa Coefficient = 0.778. This is recognized as 'Very Good' in the classification standard category (Monserud and Leemans, 1992).

Tables 4.6, 4.7, and 4.8 show the confusion matrix used in quantifying the overall accuracy of MLH classification.

Table 4.6: Ground truth areas used in accuracy assessment

Class	Abb.	No. of pixels	Total area (km²)
Sand Ramps	SR	252	226800
Intermountaineous Basins	IB	972	874800
Qa	QA	4791	4311900
Sabkha	SB	1517	1365300
Sand Sheets	SS	3270	2943000
Sand Dunes	SD	5530	4977000
Channel Deposits	CD	1551	1395900
Wadi Deposits	WD	5686	5117400
Slopes	SL	4840	4356000
East Al Madinah Plateau	EAP	13491	12141900
Sahuq Plateau	SP	7439	6695100
	Total	49339	44405100

Table 4.7: Confusion matrix (ground truth pixels) of MLH classification results

Class	Ground Truth Pixels											
	SR	IB	Qa	SB	SS	SD	CD	WD	SL	EAP	SP	Total
Unclassified	0	0	0	0	0	0	0	0	0	0	0	0
SR	156	0	0	0	0	89	0	3	0	0	0	248
IB	0	547	0	0	0	0	0	0	0	2482	0	3029
QA	0	0	3941	0	0	0	0	0	0	0	0	3941
SB	0	0	0	1441	0	0	398	112	0	117	0	2068
SS	44	0	0	25	2856	44	0	93	232	8	5	3307
SD	52	0	0	0	0	5397	0	0	0	0	0	5449
CD	0	0	850	1	0	0	958	210	1143	9	0	3171
WD	0	10	0	50	0	0	28	4599	544	230	0	5461
SL	0	0	0	0	190	0	0	7	1917	0	6	2120
EAP	0	385	0	0	126	0	6	95	26	10645	0	11283
SP	0	30	0	0	98	0	161	567	978	0	7428	9262
Total	252	972	4791	1517	3270	5530	1551	5686	4840	13491	7439	49339

Table 4.8: Confusion matrix (ground truth %) of MLH classification results

Class	Ground Truth %											
	SR	IB	Qa	SB	SS	SD	CD	WD	SL	EAP	SP	Total
Unclassified	0	0	0	0	0	0	0	0	0	0	0	0
SR	61.9	0	0	0	0	1.61	0	0.05	0	0	0	0.5
IB	0	56.28	0	0	0	0	0	0	0	18.4	0	6.14
QA	0	0	82.26	0	0	0	0	0	0	0	0	7.99
SB	0	0	0	94.99	0	0	25.66	1.97	0	0.87	0	4.19
SS	17.46	0	0	1.65	87.34	0.8	0	1.64	4.79	0.06	0.07	6.7
SD	20.63	0	0	0	0	97.59	0	0	0	0	0	11.04
CD	0	0	17.74	0.07	0	0	61.77	3.69	23.62	0.07	0	6.43
WD	0	1.03	0	3.3	0	0	1.81	80.88	11.24	1.7	0	11.07
SL	0	0	0	0	5.81	0	0	0.12	39.61	0	0.08	4.3
EAP	0	39.61	0	0	3.85	0	0.39	1.67	0.54	78.9	0	22.87
SP	0	3.09	0	0	3	0	10.38	9.97	20.21	0	99.85	18.77
Total	100	100	100	100	100	100	100	100	100	100	100	100

Table 4.9: Commission – omission percentage/ pixel of MLH classification results

Class	Commission %	Omission %	Commission Pixels	Omission Pixels
SR	37.1	38.1	92/248	96/252
IB	81.94	43.72	2482/3029	425/972
QA	0	17.74	0/3941	850/4791
SB	30.32	5.01	627/2068	76/1517
SS	13.64	12.66	451/3307	414/3270
SD	0.95	2.41	52/5449	133/5530
CD	69.79	38.23	2213/3171	593/1551
WD	15.78	19.12	862/5461	1087/5686
SL	9.58	60.39	203/2120	2923/4840
EAP	5.65	21.1	638/11283	2846/13491
SP	19.8	0.15	1834/9262	2023384

Table 4.10: Producer's – user's accuracies percentage/ pixel of MLH classification results

Class	Prod. Acc. %	User Acc. %	Prod. Acc. Pixels	User Acc. Pixels
SR	61.9	62.9	156/252	156/248
IB	56.28	18.06	547/972	547/3029
QA	82.26	100	3941/4791	3941/3941
SB	94.99	69.68	1441/1517	1441/2068
SS	87.34	86.36	2856/3270	2856/3307
SD	97.59	99.05	5397/5530	5397/5449
CD	61.77	30.21	958/1551	958/3171
WD	80.88	84.22	4599/5686	4599/5461
SL	39.61	90.42	1917/4840	1917/2120
EAP	78.9	94.35	10645/13491	10645/11283
SP	99.85	80.2	7428/7439	7428/9262

Generally, it should be noted that the supervised classification results are controlled principally by the spectral characteristics of surface components, regardless of the geomorphological units. Field investigations along with principal component analysis, band composite and band ratios, provided a good correlation with supervised classification results and aided the production of the final geomorphological map.

4.1.3.5   Geomorphological Map of the Study Area.

The current geomorphologic map was produced using the following data sources:

1- Previous geological maps (scale 1:250.000) used in preparing the Harrats (Tertiary and Quaternary Basalts) mask, along with the extraction of unmappable dike swarms.

2- Landsat 8 imagery surface reflectance data used in a supervised classification process provided eleven geomorphological units (Sand Dunes (SD), Sand Sheets (SS), Sand Ramps (SR), Wadi Deposits (WD), Channel Deposits (CD), Sabkha (SB), Qa (Qa), Slope (SL), Inter-mountainous Basins (IB), the East Al Madinah Plateau (EAP), and the Sahuq Plateau (SP).). Furthermore, panchromatic band 8 (15m*15m) was used in preparing the mountains mask.

3- ASTER GDEM was used for delineating the drainage systems within the study area.

4- Field visit: This was used for surface samples collecting, investigating regions of interest representing different geomorphological units for Landsat 8 image classification and training sites for later accuracy assessment.

In this section, the geomorphological map of the study area was prepared using the highest OIF ranked combination 761, as well Principal Component Analysis (PCA), and band rationing along with observations from both the field and the laboratory.

The study area contained the following geomorphological features (Figure 4.41).
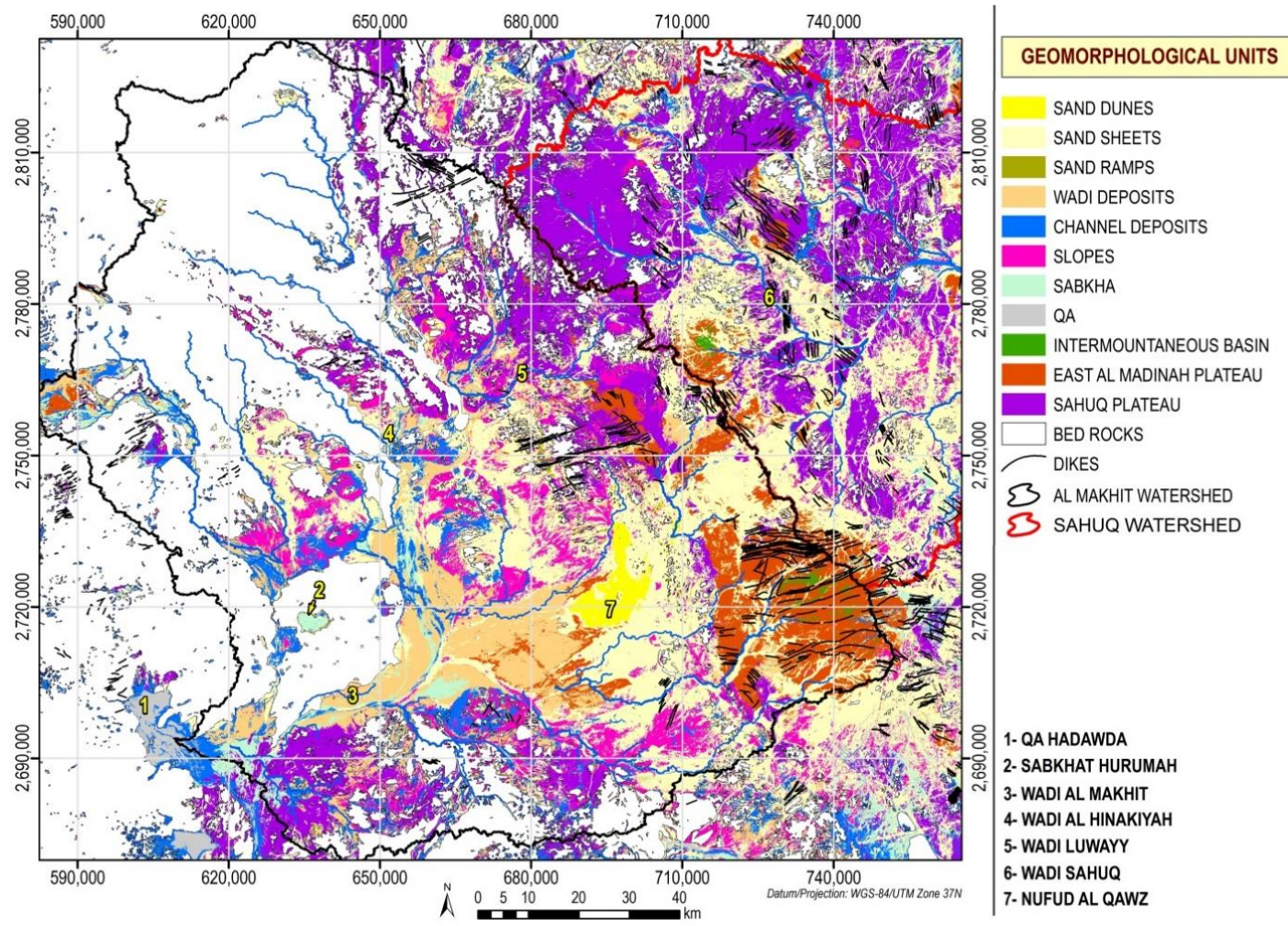
Figure 4.41: Geomorphological map of the study area.

1. Aeolian deposits

These are distinct in that they are formed of quartz grains that are unconsolidated and loose. Moreover, these vary in size, and range from coarse sand to silt particles (Figure 4.42). These aeolian deposits are prevalent in the study area and take several forms, such as star dunes, transverse dunes, crescentic dunes or barchans, interdune areas, and sand sheets.

A. Star dunes

Star dunes appear in Nufud Al Qawz, especially along the boundaries. These are pyramidal in shape and unlike other dune forms, are mounds that grow upwards. They also have arms radiating from the central peak. There are typically four arms, but there may sometimes be as many as five, depending on wind direction and sand supply. In Nufud al Qawz, star dunes range in height from 60-86m.

B. Transverse dunes

These are a common morphological form present in Nufud Al Qawz. A small group of these to the west of Wadi Luwayy, directly below the Marurah mountains. These dunes appear as sand ripples with flat tops varying in height from 15-20m. They are formed perpendicular to the direction of wind. Transverse dunes appear when there is a supply of sand, represented here by wadi deposits and sandstone. They also appear in areas where wind is almost uniformly from one direction.

Interdunes are found among star and transverse dunes, and are the low areas between sand dunes with a layer of sand deposits covering the bedrock underneath. The sand deposits are composed principally of coarse particles which the wind was unable to transport, after having blown away the fine particles (Figure 4.43). These interdunes may sometimes contain sabkha and palaeolake deposits.

Figure 4.42: Transverse dune in Nufud Al Qawz.

Figure 4.43: Interdune appears as the low area between sand dunes.

C. Barchan dunes

These dunes take the form of a crescent, where the points of the horns are oriented in the downwind direction. The broad concave area has a steep face. This type of dune is found in relatively flat areas where sand is limited in supply, while the wind principally blows in one direction. Barchan dunes are present to the west of Nufud Al Qawz, close to Wadi Um Markhah (Figure 4.44).

Figure 4.44: Barchans in the study area.

D. Sand sheet

These are sand-covered plains developed due to wind activity in low angle or flat aeolian stratification. Sand sheets are typically rippled in surface, composed predominantly of coarse sand grains, as such coarse grains cannot be transported by the wind.

Sand sheets appear on the boundary areas surrounding Nufud Al Qawz, barchans, and slope areas. These are also present on the eastern plateau of Al Madinah, and its extension to Sahuq plateau. They are also found in wadi channels, especially run-offs in the lower areas of wadis (Figure 4.45).

Figure 4.45: Sand sheets covering areas close to barchans, with ripple marks appearing on the surface.

E. Sand ramps

Dune scale accumulations of sedimentary sand typically situated at mountain fronts are termed sand ramps. Such accumulations are composed of a combination of aeolian sands and the deposits resulting from hillslope and fluvial activities (Bateman et al., 2012). Sand ramps appear in the mountains close to Nufud Al Qawz, and the inner wall of the Hurumah volcano spout which encloses Sabkhat Hurumah (Figure 4.46).

Figure 4.46: Sand ramps at the front of the inner wall of the Hurumah volcano spout, Sabkhat Hurumah.

2. Dikes

These are a mass of igneous rock that cut longitudinally across rocks that were present earlier. These are typically found in groups parallel to each other, and sometimes intersecting (Weijermars, 1997). They are common in the basin of Wadi Sahuq, and the eastern parts of the Wadi Al Makhit basin (Figure 4.47).

Figure 4.47: Dikes in the study area.

174

3. Wadi deposits and channel deposits

Wadis are distinguished by containing alluvial deposits composed of gravel, sand, silt, clay, and broken rock particles. The main and secondary wadi channel cuts through these deposits, and hold large amounts of these sediments in varying quantities. For instance, we find that Wadi khadra is dominated by fine sediments (Figure 4.48), while the central sector of Wadi Al Hinakiyah is dominated by coarse sediments (Figure 4.49).

Figure 4.48: Fine sediments dominating Wadi khadra.

Figure 4.49: Coarse sediments dominating Wadi Al Hinakiyah.

4. Alluvial fans

Alluvial fans are a type of geomorphological landform that typically form in the exit area of a wadi channel that passes from a mountain highland into a lower and more gentler area situated at a mountain front. Sediment is deposited in the form of a triangular shape or radiating cone. The fan apex contains coarse grain sediment in the area nearer to the mountainous uplands, while the base formed of finer grains is nearer to the low gradient area, at a distance from the mountainous uplands (Thomas, 2011; Karbal, 2011). Alluvial fans appear at the Marurah mountains, which are penetrated by Wadi Luwayy. They are also present in the south of the Dubbah mountains, where Wadi Al Hinakiyah cuts through.

5. Slope

Slope deposits often develop along the foothills of mountains, and are formed from coarse deposits. These are present in the study area around mountains and hills (Figure 4.50.)

Figure 4.50: Slope along the foothill of Abraq al Laaba mountain, near Nufud Al Qawz.

6. Sabkha

Sabkha is a closed depression containing a saline surface in an arid environment, which is composed mainly of sand, silt and clay deposits mixed with evaporites (Mahsoub et al., 1999). Sabkhat Hurumah is considered one of the largest in the study area (Figure 4.51). In addition, small sabkhas are scattered across the Quaternary basalt flows.

Figure 4.51: Sabkhat Hurumah.

7. Qa

Qa is a flat-bottomed, closed depression, containing fine silt and clay, and lacks plant cover or salt evaporites (Saudi Geological Survey, 2012; Edgell, 2006). Qa Hadawda is considered one of the largest depressions in the study area (Figure 4.52). Additionally, small Qa are scattered across the Quaternary basalt flows.

Figure 4.52: Qa Hadawda.

8. Plateaus

These are broad, flat-topped highlands through which wadis sometimes flow. The Al Madinah Eastern plateau appears to the east of the Wadi Al Makhit basin, where the upper sources of Al Madinah eastern wadis flow, such as Wadi Al Hadaqiyah, Al Mahir, and khadra. As for the Sahuq plateau (Figure 4.53), it appears in the basin of Wadi Sahuq in which the upper sources of Wadi Sahuq flow.

Figure 4.53: The Sahuq plateau.

The current study aimed to find a specific relationship between the grain size and spectral behaviour of the detrital sediment. Therefore, harrats and mountains had to be excluded from image processing for more reliable results. Spectral mapping techniques could not separate harrats and mountains effectively, due to the gradational contact between mountains and nearby sediments. Additionally, DEM could not separate these units (harrats and mountains) based on their elevations and/or slopes due to accuracy issues (the vertical accuracy of ASTER GDEM is ± 20meter). Consequently, the manual separation of mountains and

harrats using Landsat 8 panchromatic band 8 was the most effective way to prepare a mask which was applied over all image processing techniques used in the current study.

4.1.4 Factors Influencing the Spectral Reflectance of the Surface Geomorphology

The current study inferred that the main factors potentially affecting surface reflectance in surface geomorphology are:

a. The mineral composition of the geomorphological units under investigation.

b. The grain-size variability present even within the same unit. Generally, the coarser the grain, the lower reflectance.

c. Surface topography; hard topography attenuates the reflected light and consequently leads to lower overall reflectance.

d. Soil moisture reduces reflectance over all reflected wavelengths, especially in SWIR regions.

e. Vegetation cover essentially alters the geomorphological units' reflectance, especially within NIR spectral regions.

f. Atmospheric conditions and diurnal variations within satellite data.

g. Satellite data specifications (spatial, spectral, and radiometric resolutions). Higher resolution of satellite data is the key to classifying geomorphological units with limited spatial extension and/or with subtle spectral differences.

Chapter 5. Results of Quaternary Sediments

This chapter provides a description of the key physical features of the sites selected for study. Moreover, the physical and mineral deposits found in the site sections were described and explained. OSL was employed to determine the dates of such deposits. This allowed for them to be related to the palaeogeomorphic and palaeoenvironmental conditions prevailing in the late Quaternary period in the study area, as well as adjacent regions.

For this purpose, thirteen sections were selected to study the Quaternary landforms spread over the study area (Figures 5.1, 5.18). These comprised sections of fluvial deposits in Wadi Al Hinakiyah, Wadi Sahuq, and alluvial fan deposits in Wadi Luwayy. In Wadi Al Hinakiyah, there are three sections. The first is M7, located in the upper catchment of Wadi Al Hinakiyah, while the other two, M6 and M14, are in the middle catchment of this Wadi. In Wadi Sahuq, two sections are located. One is M8 in Wadi Al Qusayrah, a tributary of Wadi Sahuq, and the other is M13 in the Wadi Sahuq's main channel. In addition, section M1 is located south of Nufud Al Qawz, representing wadi deposits (flood plain) within Nufud Al Qawz. In Wadi Luwayy, there are three sections. The first is M5, located on the eastern part of the Marurah mountains, while the other two, M4 and M3, are on the western part of the Marurah mountains. In addition to these are sections of palaeolake deposits preserved in Sabkhat Hurumah (M10), and the interdune to the west of Nufud Al Qawz (M12). Sections were made in aeolian deposits inside the wall of the crater of Hurumah volcano (M11), and a section in the slope wash deposits in the basin of Shaib Um Markhah west of Nufud Al Qawz (M2).

This chapter focuses on the presentation of the results based on the following structure: 5.1.1. Fluvial deposits in the wadi systems, 5.1.2. Fluvial deposits in the alluvial fans, 5.1.3. Wadi deposits within Nufud al Qawz, 5.1.4. Aeolian sand ramps, 5.1.5. Palaeolake deposits, 5.1.6. Sabkha deposits, and 5.1.7. Slope wash deposits.

5.1   Quaternary Sediments Analysis

The map below (5.1) illustrates the locations of the sections selected for the study of Wadi and alluvial fan sediments. These sections are as follows:
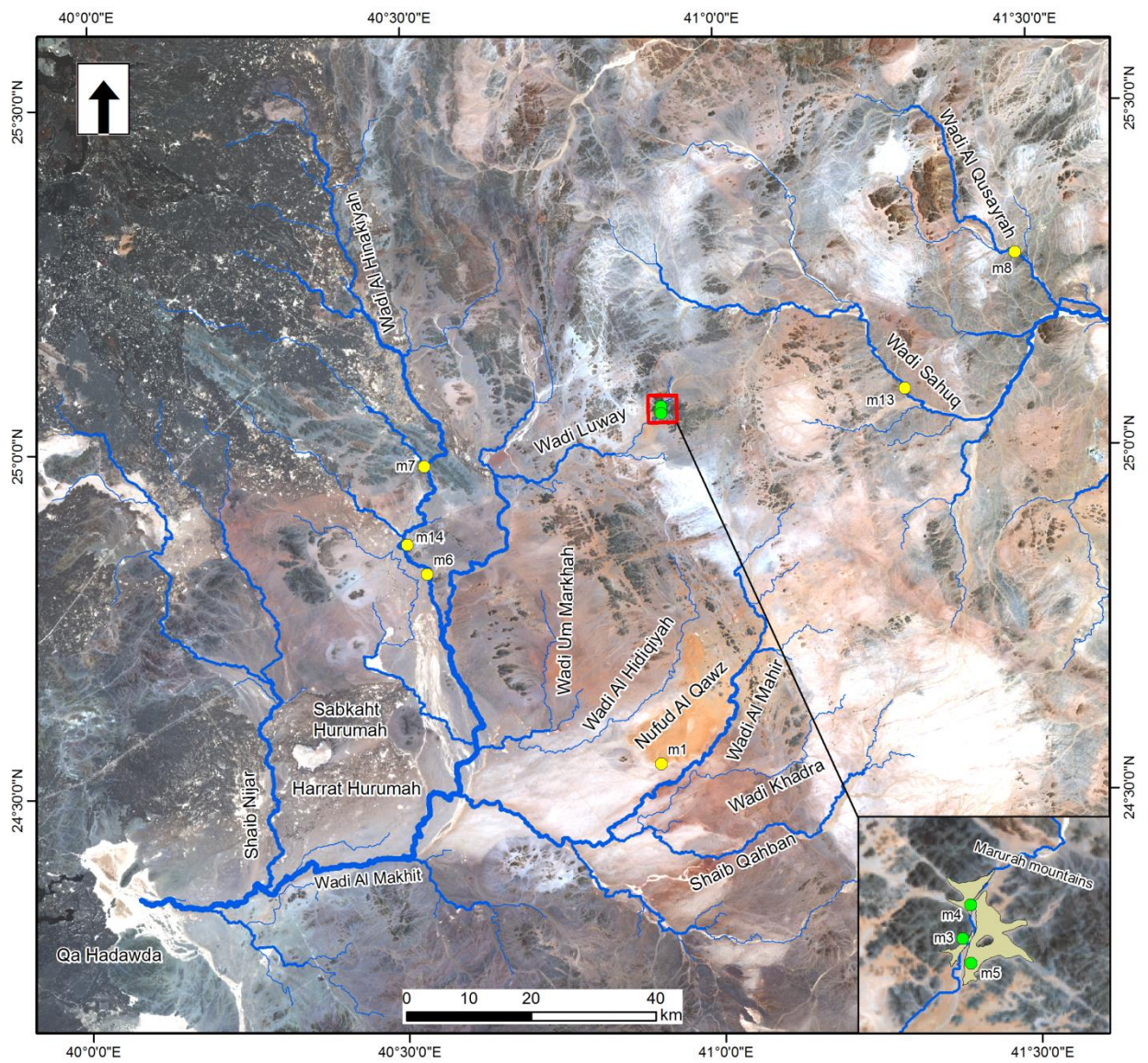
Figure 5.1: This is the study area; the wadis' sample sites are marked with yellow markers, and the alluvial fans are marked with green markers.

5.1.1   Fluvial Deposits in the Wadi Systems

5.1.1.1   Fluvial Deposits in the Upper Catchment of Wadi Al Hinakiyah M7

Wadi Al Hinakiyah on Figure 5.1 is 173.3 km in length, and is considered to be one of the main wadis to the east of Al Madinah. Running from north-east (from the mountains surrounded by Harrats, such as Sumar as Sanfa mountan at an elevation of 1172 m and Hulayyat al Manadah mountain at an elevation of 1826m) to the south, Wadi Al Hinakiyah is linked with Wadi Luwayy, both of which flow into Wadi Al Makhit. This in turn flows into the depression called Qa Hadawda, which lies to the southwest of the Hurumah lava field (Figure 5.1).

Three representative sections were chosen in Wadi Al Hinakiyah to reconstruct the sedimentological history of this wadi, which are sections M7, M6 and M14.

The first section, M7, is situated in the upper catchment of Wadi Al Hinakiyah (N 24°58`49.3"-E 40°31`55.4"), at an elevation of 884m.The channel at the section is 139 m wide, while the flood plain is around 21m –63m wide. Section M7 comprises of 14 sedimentary units as illustrated in Figure 5.2.

The first unit (figure 5.2) is 7.5YR5/4 brown coloured and 10 cm thick, with a pebble foundation at the bottom. The matrix of the first unit is composed of silty sand with a small quantity of clay, as well as a small amount of both sub-angular and sub-rounded pebbles, reaching 19%, of which the majority are very fine, and a small percentage is medium sized. The unit is poorly sorted, and has some carbonates. It is separated from the unit above by a wavy and unconformable boundary.

The second unit is 11 cm thick and 7.5YR6/3 light brown in colour. There is a large quantity of pebbles, reaching 89%, in a sand matrix. Moreover, the pebbles are sub-rounded / rounded and polished, reaching very coarse sizes, indicating that fluvial activity went through a phase of very strong currents. This unit is also very poorly sorted, with the presence of many roots, some carbonates, burrows and wavy bedding; the upper boundary takes on a wavy form.

The third unit is 1 cm thick and composed of 7.5YR5/4 brown coloured silty sand containing a small amount of roots, burrows and carbonates. Its upper boundary is wavy. It is similar to the unit above, which is composed mainly of brown coloured silt sand with clay. XRD shows that the deposit is rich in silicate 75.1% (quartz 55%, plagioclase feldspar 11.1%, and

alkali feldspar 8.8%), clay minerals 13.1% (chlorite 6% and mica 5.9%), and has an extremely small quantity of very fine sub-angular pebbles, indicating that it was transported from a local source in the vicinity. The unit is considered to be very poorly sorted, and contains some roots, burrows, 7.4% calcite and 4.2% amphibole. This unit's upper boundary is wavy.

The fifth unit is 10 cm thick, of a 7.5YR5/4 brown colour, and very poorly sorted, indicating that the energy current was slightly greater than in the unit below, which contributed to the transport of quantities of sands with sub-rounded pebbles, reaching 52%, the majority being medium to fine sized but not exceeding coarse sizes. Quantities of roots, burrows and flat bedding are present, and the unit is separated from the one above by a wavy and unconformable boundary.

The sixth unit is 9 cm thick, 7.5YR6/3 light brown in colour and poorly sorted. Its matrix is composed of coarse to very coarse sand, in addition to around 32% gravel, both sub-angular and sub-rounded, of very fine and medium size. The bedding is wavy and there are a lot of roots and burrows. The unit's upper boundary is wavy and unconformable in nature.

The seventh unit is 7 cm thick, coloured 7.5YR5/4 brown, with evidence that fluvial activity was weaker, as the unit is largely composed of fine sand with very small amounts of silt and clay, interspersed with aeolian sediment (lenses of sand). XRD analysis shows that the deposit contains high amounts of silicate 63.9% (quartz 35.6%, plagioclase feldspar 17.9% and alkali feldspar 10.3%) and clay minerals 17.5% (chlorite 8.4% and mica9%). The amount of silicate has reduced, while the quantity of clay minerals has increased compared to unit 4. This unit is also very poorly sorted, and there can be found some roots and burrows. Furthermore, calcite appears in the upper part of the unit; here, the amount of both calcite (9.2%) and amphibole (9.2%) increase in comparison to unit 4. Finally, the upper boundary in unit 7 is wavy. The characteristics of this unit indicate the sedimentation took place under runoff.

The eighth unit is 12 cm in thickness, and the presence of aeolian sediments is significantly reduced, whereas 7.5YR5/4 brown coloured fluvial sediment is dominant. It is composed of medium to coarse sand, along with small amounts of silt and clay. The unit also contains extremely small quantities of sub-angular pebbles coming from close areas in the vicinity.

The unit is very poorly sorted and contains many roots and some burrows; its upper boundary is wavy.

The pattern of sedimentation changes from the ninth unit and above, with the dominance of fine sediment. The ninth unit is 77 cm in thickness and10YR5/4 yellowish brown in colour. It is composed of silt with some amount of fine sand and clay. XRD analysis shows that the deposit contains high amounts of silicate 60.7% (quartz 37.1, plagioclase feldspar 15.5% and alkali feldspar 8.1%) and high amounts of clay minerals 19.3% (chlorite 9.6% and mica 9.6%). The amount of silicate has reduced, while the quantity of clay minerals has increased compared to units 4 and 7, indicating calmer flow. Its matrix is very poorly sorted; there is no structure to the unit, it is massive, and contains some roots which are concentrated in the upper and lower parts and burrows. In addition to some calcite (11.4%) that has cemented particles weakly, this amount is high in comparison to previous units. Lastly, unit 9 has 8.4% amphibole, and its upper boundary is wavy. This unit is similar in characteristics to the 13th and the 11th units; very small amounts of sub-angular pebbles are present in unit 13. This indicates that these units were formed under similar environmental conditions, even though their thickness is less than that of the ninth unit. The amount of sand begins to increase slightly as does the amount of roots and burrows, and the quantity of carbonates is less than in the unit above, namely the tenth unit; this shares the same characteristics. The sediments in unit 10 are reworked and not cemented. There is alternation appearing in the form of wavy bedding between aeolian sediments that are present in clear and large portions, as well as fluvial deposits. This description also fits the 12th unit. XRD analysis confirms that the amount of silicate is 71.6% (quartz 48.9%, plagioclase feldspar 14.2%, and alkali feldspar 8.4%), whilst the amount of clay minerals is 15.8% (chlorite 7.4% and mica 8.4%) and the amount of calcite is 6.7%. This unit also has some amphibole (5.7%). In this unit, the amount of silicate has increased, while the proportion of clay minerals and calcite has reduced compared to units 7 and 9.

The upper unit is the 14th; it is 14 cm thick and composed of very poorly sorted silty sand matrix, with a little clay, and the presence of roots. In this unit, the sediments are reworked and are not cemented, with alternating aeolian and fluvial deposits, which appear as wavy laminations. Finally, the upper boundary is wavy and unconformable in nature.

Figure 5.2: Schematic and sedimentary log and view of section M7 wadi deposits in the upper catchment of Wadi Al Hinakiyah.

Figure 5.3: Cumulative percentage curve of the grain size composition for section M7 at Wadi Al Hinakiyah.

5.1.1.2 Fluvial Deposits in the Middle Catchment of Wadi Al Hinakiyah M6

This site is located in the middle catchment of Wadi Al Hinakiyah (N 24°49`25.8"-E 40°32`06.7"), at an elevation of 849 m (Figure 5.1). The flow channel at the section is 78m wide, while the flood plain is around 84.7m – 228m wide. The section studied is 2 meters thick and composed of 23 sediment units as illustrated in Figure 5.4.

The first unit is 8cm thick; deposits are a 5YR5/4 reddish brown colour, and its fabric is composed of silty sand with some clay, in addition to a small amount of sub-rounded pebbles, reaching 21%, where overall pebbles does not exceed medium size, and are generally very fine. The unit is very poorly sorted - there are a few burrows and some carbonates present but no roots, and its upper boundary is wavy. The unit is similar to units

2, 3, 5, 6, and 8, with variation in the percentage of pebbles, and the appearance of some roots in the last three units, namely 5, 6, and 8, which indicates that these were formed under quite similar environmental conditions.

The fourth unit is 2 cm thick, a 5YR5/4 reddish brown colour and very poorly sorted. Sediments here are finer than the previous units, where silty medium sand is dominant. There is a little clay and an extremely small quantity of very fine sub-rounded pebbles. It has flat bedding, burrows, and some carbonate, which is evidence of the reduction in the fluvial energy current somewhat compared to the previous units. The upper boundary separating it from the unit above is wavy. The seventh unit is similar to the fourth one in all characteristics, except for colour, as it takes on a 7.5YR 5/4 brown colour, perhaps due to mixing with a small amount of aeolian sediment. The quantity of pebbles increases slightly along with the appearance of some roots. The characteristics of the seventh unit apply to the unit above it, i.e. the ninth, with an increase in the amount of very coarse sand.

Generally, the units 1 to 9 look are similar to one another, with some variation in the fluvial energy current.

The 10th unit is 6 cm thick and 5YR5/4 brown in colour. With this unit, fluvial energy is active once again, and has been able to transport around 60% of sub-angular pebbles, along with a small amount of sub-rounded pebbles. Small sized pebbles are dominant, but none exceed coarse size. In this unit, some carbonates along with a few roots and burrows are present in a sand matrix. It is very poorly sorted with a wavy and unconformable upper boundary. Sediments in the unit above are finer, being composed of silty sand with a very small amount of clay and very fine sub-rounded pebbles. The 12th unit is very similar to the 10th unit, except for the amount of carbonates, which is greater, while the amount of pebbles is reduced to 49%, where they are dominantly medium-sized. A wavy and unconformable boundary separates it from the unit above.

The 13th unit is 2cm thick and of a 7.5YR6/4 light brown colour. This unit is considered a cemented indurated palaeosurface, and is composed of silty sand, a small amount of clay, and very fine sized sub-angular pebbles. The deposits in this unit are strongly cemented together due to the presence of calcite 4.6% with clay minerals 9.3% (chlorite 4.3% and mica 4.9%). XRD analysis shows that the deposits contain high amounts of quartz 58.6% with plagioclase feldspar 11.6%, alkali feldspar 7.11%, and a small number of amphibole

3.5% and pyroxene 5.1%.This unit has wavy bedding, and a small amount of roots and burrows. The upper boundary of this palaeosurface is wavy and unconformable in nature.

Fluvial activity is again strong in the 14th unit, which is 6 cm thick and of a 7.5YR5/4 brown colour. It is very poorly sorted, and composed of 56% sub-rounded pebbles, mainly medium-sized, in a silty sand matrix. There are flat bedding with some amount of carbonates and burrows, while the upper boundary separating it from the unit above is wavy and unconformable in nature.

The 15th and 16th unit are coloured 5YR5/4 reddish brown. These are composed of silty sand and very fine sub-rounded pebbles reaching 25%. This increases in the 16th unit to 40%, with the presence of a small amount of medium-sized pebbles. Both units are poorly sorted with reduced amounts of carbonates, and the appearance of flat bedding. They also have some burrows, and their upper boundaries are wavy and unconformable in nature. The characteristic of units 15 and 16 indicate that the wadi was periodically flooding.

In the 17th unit, which is 24 cm thick, the pattern of sedimentation clearly changes, since the matrix is composed of silt and sand and some clay 12%; the XRD analysis in this unit shows that the deposit contains high amounts of clay minerals (chlorite 5% and mica 7%), in addition to a very small amount of sub-rounded pebbles. This unit is considered very poorly sorted, and has no clear structure, with the amount of calcite (8.5%) has cemented the deposits together but not strongly. The XRD analysis also shows that the deposit is high in quartz 55.6% with plagioclase feldspar 11.2%, alkali feldspar 7.3%, and a small quantity of amphibole 5.2%. There are many roots and burrows present, and this unit's upper boundary is wavy. The 20th and 22nd units are similar to the 17[th]unit in almost all characteristics apart from the small increase in the amount of sand in their matrix. Moreover, the amount of roots and burrows increases significantly in the 22nd unit compared to the other two.

The 18th unit is 5 cm thick and 7.5YR5/4 brown in colour. It is composed of silty sand, in addition to 39% sub-rounded very fine to medium-sized pebbles. The unit is very poorly sorted, with small amounts of carbonates and burrows, and has a wavy upper boundary. The amount of pebbles is greatly increased in the unit above (19th), reaching 65%, the majority coarse in size and sub-rounded, in the presence of a sand matrix. This is evidence of strong fluvial activity, which was able to transport these deposits. This unit is considered very poorly sorted also, and contains some carbonates. Its upper boundary is wavy. The 21st unit

is similar to the 19th in all its characteristics; however, the amount of pebbles is reduced to 44%, and its matrix also contains small amounts of silt and clay.

The upper and last unit, the 23rd, is 11 cm thick, 7.5YR5/4 brown coloured and its matrix is composed of silty sand, and close to 63% sub-rounded pebbles, where medium-size is dominant. This unit is very poorly sorted, which indicates that fluvial activity at the time of sedimentation was quite high. Some carbonates and roots are present, and the unit's upper boundary is wavy and unconformable in nature.
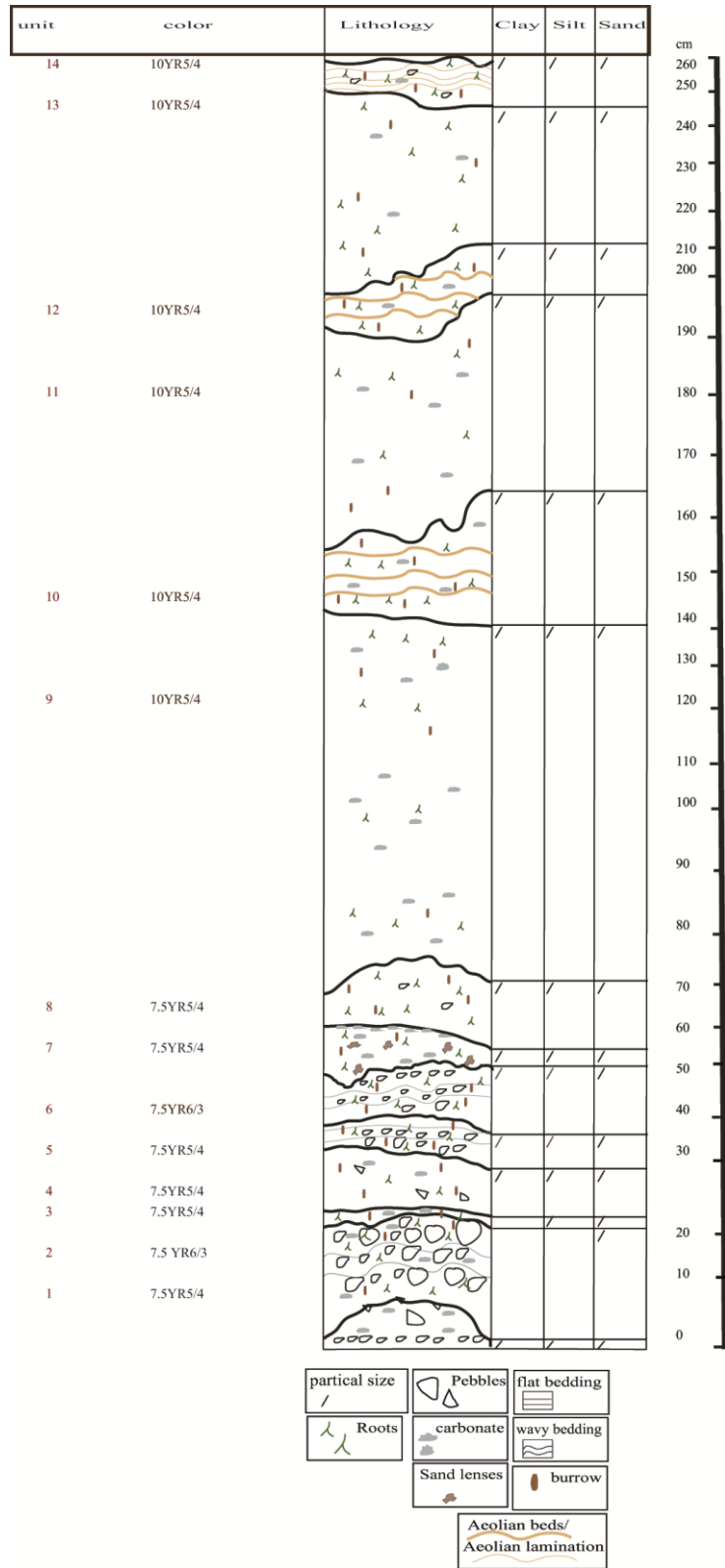
Figure 5.4: Schematic sedimentary log and view of section M6 wadi deposits at the middle catchment of Wadi Al Hinakiyah.
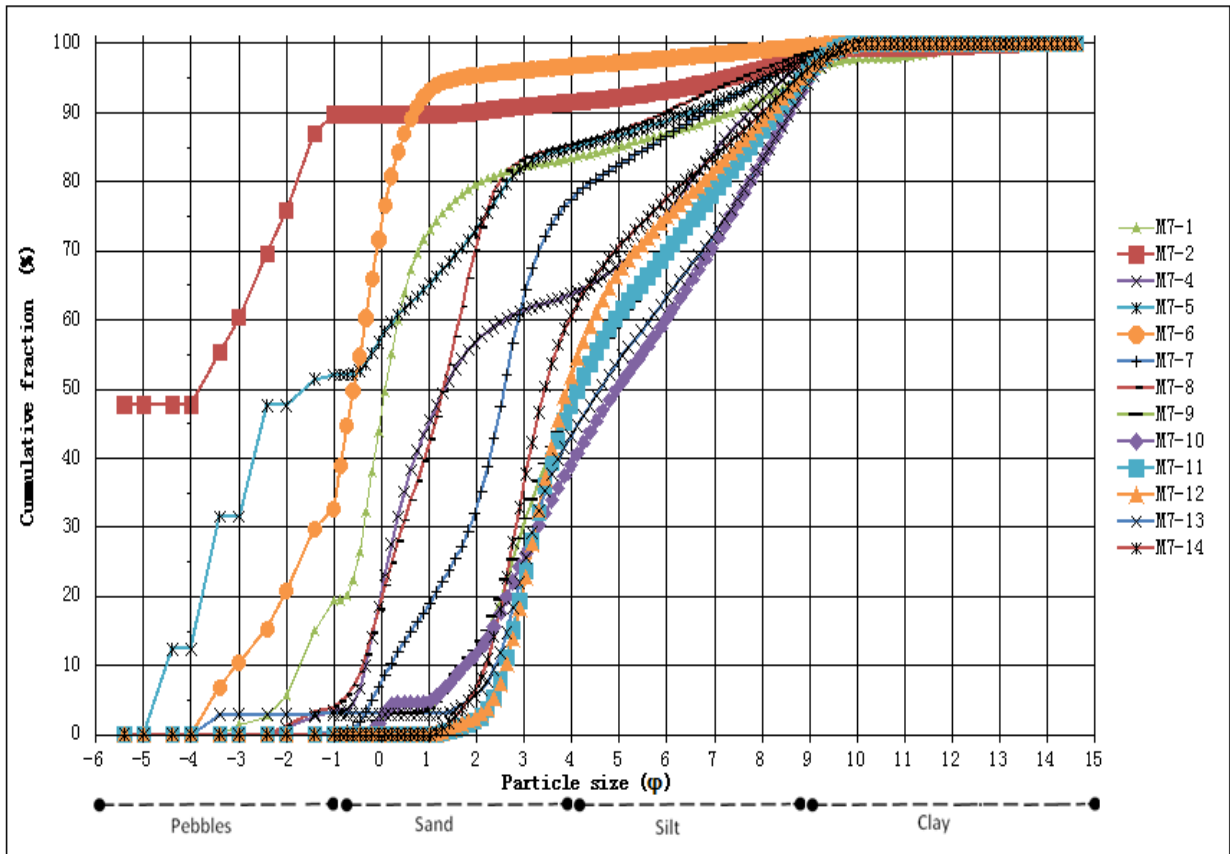
Figure 5.5: Cumulative percentage curve of the grain size composition for section M6 at Wadi Al Hinakiyah.

5.1.1.3 Fluvial Deposits in the Middle Catchment of Wadi Al Hinakiyah M14

This site is located in the middle catchment of Wadi Al Hinakiyah (N 24°52`00.5"-E 40°30`15.2") (Figure 5.1), at an elevation of 857m. The flow channel at the section is 73.1m wide, while the flood plain is around 388m − 478m wide. Here, fluvial terraces do not appear, so this section was freshly excavated. Its thicknessis around 260 cm and comprises of 16 sediment units as illustrated in Figure 5.6.

The first unit is 12cm thick, and is composed of 7.5YR5/4 brown-coloured silty coarse sand, a very small quantity of fine and sub-rounded pebbles, some roots, burrows and a small amount of carbonates. The unit is poorly sorted with a wavy and unconformable boundary separating it from the one above. This unit has an OSL age of 34.2±2.5 ka as shown in table 5.1.

The second unit is 7cm thick, and is 7.5YR6/3 light brown in colour. The amount of pebbles in this unit is significantly greater than in the unit below, reaching 65%, where medium sized pebbles are dominant, but overall, clasts do not exceed coarse size in a silty sand matrix. There is a silicate amount of 77.3% (quartz 49.1%, plagioclase feldspar 20.1% and alkali feldspar 8%) and 12% clay minerals (chlorite 6% and mica 5.9%). The unit is very poorly sorted and has cross bedding. Furthermore, the majority of pebbles are well rounded /sub-rounded and polished due to transport by water over quite large distances. There are some roots, burrows and some calcite nodules 5.7%, and XRD analysis shows 4.9% amphibole. The lower part of unit 2 is a palaeosurface containing a large amount of well-rounded pebbles. This unit is separated from the one above by a wavy and unconformable boundary.

The third unit is 7.5YR7/2 pinkish grey coloured and 9cm thick. It has cross bedding, and the quantity of pebbles is less than in the unit below, reaching 12%; pebbles do not exceed fine size, and are sub-rounded, located in a silty sand. XRD analysis reveals that the deposits are high in silicate 81.9% (quartz 64.6%, plagioclase feldspar 10.8% and alkali feldspar 6.3%), with a very small amount of amphibole (3.2%). Additionally, the deposits in this unit are strongly cemented together due to the presence of calcite (5.8%) with clay minerals 9% (chlorite 4.8% and mica 4.1%). This unit is also poorly sorted. However, the quantity of roots and burrows has increased. Finally, the upper boundary is wavy and unconformable in nature.

The fourth unit is 13 cm thick, and despite resembling the unit below, in terms of colour, beds, is different due to the significantly increased quantity of gravel, reaching 53%. The pebbles do not exceed medium size, and are mostly very fine sized and sub-rounded. The unit is very poorly sorted and contains sand matrix; XRD analysis shows an abundance of silicate 83.4% (quartz 69.7%, plagioclase feldspar 10.4% and alkali feldspar 3.1%), and about 8.3% of clay minerals (chlorite 4.1% and mica 4.1%) with calcite (4.8%), which cemented the deposits together strongly, there is also a small amount amphibole (3.3%). Many roots and burrows are present in this unit and its upper boundary is wavy.

The fifth unit is 8 cm thick, and is similar to the second unit in almost every way; however, its bedding are flat. The unit above is 10 cm thick, and 7.5YR 5/4 brown in colour. The quantity of pebbles reaches 76%, where very coarse sizes are dominant and the majority are rounded. The large sized stones are mainly sub-rounded/ rounded. The unit is very poorly sorted, and has some burrows, roots and carbonate. Its upper boundary appears wavy.

The seventh unit is 16 cm thick and 7.5YR 6/3 light brown in colour. Its matrix is composed of silty sand with a quantity of pebbles reaching 53%, which are both sub-angular and sub-rounded, and dominantly very fine sized, not exceeding coarse size. The majority of coarse sized pebbles are sub-rounded. The unit has wavy bedding, and is poorly sorted; it also has many roots, burrows and some carbonate. It is separated from the unit above by a wavy and unconformable boundary.

The eighth unit is 16 cm thick, 7.5YR 6/3 light brown in colour. It is poorly sorted, and is somewhat similar to the fourth unit, except for the type of bedding it has; unit eight has wavy bedding.

The ninth unit is 3 cm thick, and provides evidence of a clear change in fluvial activity, as its matrix is composed of coarse sand with very small amounts of silt and clay and very small amounts of very fine, sub-angular pebbles, along with some carbonates, roots and burrows. The unit is considered poorly sorted and is also indurated (reworked); its upper boundary is wavy.

Fluvial activity is again strong, given the significant increase in the quantity of pebbles in the 10th unit compared to the ninth unit, reaching 62%. The majority of pebbles are coarse in size and sub-rounded, and not uniformly distributed in the unit. This unit has a silty sand matrix with some carbonates, roots and burrows present. It is separated from the unit above

by a wavy boundary, and is very poorly sorted. The 10th unit is quite similar to the 12th one, but the latter differs in the dominance of very fine and medium-sized pebbles, and the existence of cross bedding. The 12thunit is also considered poorly sorted. With regards to the 11th unit, this is similar in characteristics to the 10th, but the quantity of pebbles is reduced, reaching 33%. The 13th unit is also 7.5YR6/3 light brown in colour, 6 cm thick, and is considered poorly sorted. It is similar to the 12th unit, with a slight increase in the amount of pebbles, and the presence of cross bedding.

The 14th unit is 11 cm thick, and its matrix is composed of silty sand, and a large quantity of sub-rounded pebbles, reaching around 56%, where the medium-sized are dominant, and pebbles do not exceed the coarse size. The pebbles here are not uniformly distributed in the unit, which is very poorly sorted. In this unit, some roots, burrows and a few carbonates appear, meaning that the unit is unconsolidated and mixed with aeolian deposits. The unit is considered quite similar to the last one (16th), with the exception of it having a lesser amount of carbonate, being 5YR 5/4 reddish brown in colour, and reaching 70 cm in thickness. As for the 15th unit, it is 37cm thick, and 5YR5/4 reddish brown in colour. It differs slightly from the previous two units in that it has a sand matrix, and the quantity of pebbles reaches 77%, with the very coarse size being dominant. Pebbles of this size can only be transported by a stronger energy flow than the previous two units. XRD analysis shows that the deposit contains high amounts of silicate 82.8% (quartz 65.6%, plagioclase feldspar 11.8% and alkali feldspar 5.3%) while clay minerals reach 9.7% (chlorite 5.1% and mica 4.5%), the sediment in this unit is weakly cemented (unconsolidated) as the amount of calcite is very low (3.7%), there is also a small amount of amphibole (3.6%). This unit has many roots and burrows.

Table 5.1: Dates determined using OSL of sedimentary section M14 Fluvial deposits in the middle catchment of Wadi Al Hinakiyah

sample	location	Lab code	Altitude (m)	Radioactivity Data			Dosimetry Data			Water (%)	Age Data	
				U (ppm)	Th (ppm)	K (%)	Beta (µGy a^{-1})	Gamma (µGy a^{-1})	Cosmic (µGy a^{-1})		Dose rate (Gya^{-1})	Age (Ka)
M14-unit1	Wadi Al Hinakiyah	MAD13/14/1	856	0.84	2.8	2.1	1501±112	739±40	204±10	1.4±2	2.44±0.12	34.2±2.5

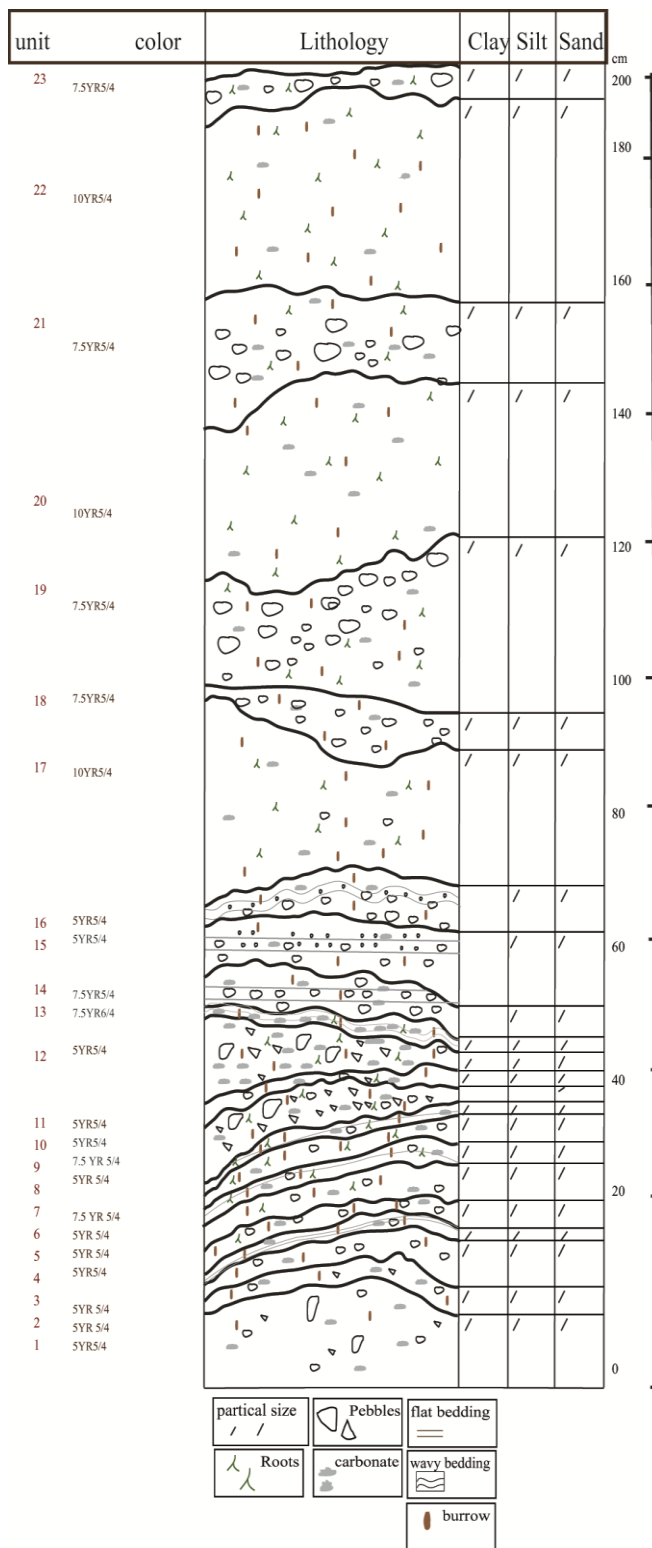Source: Luminescence dating report, Department of Geography, Leicester.

Figure 5.6: Schematic sedimentary log and view of section M14 wadi deposits in the middle catchment of Wadi Al Hinakiyah.
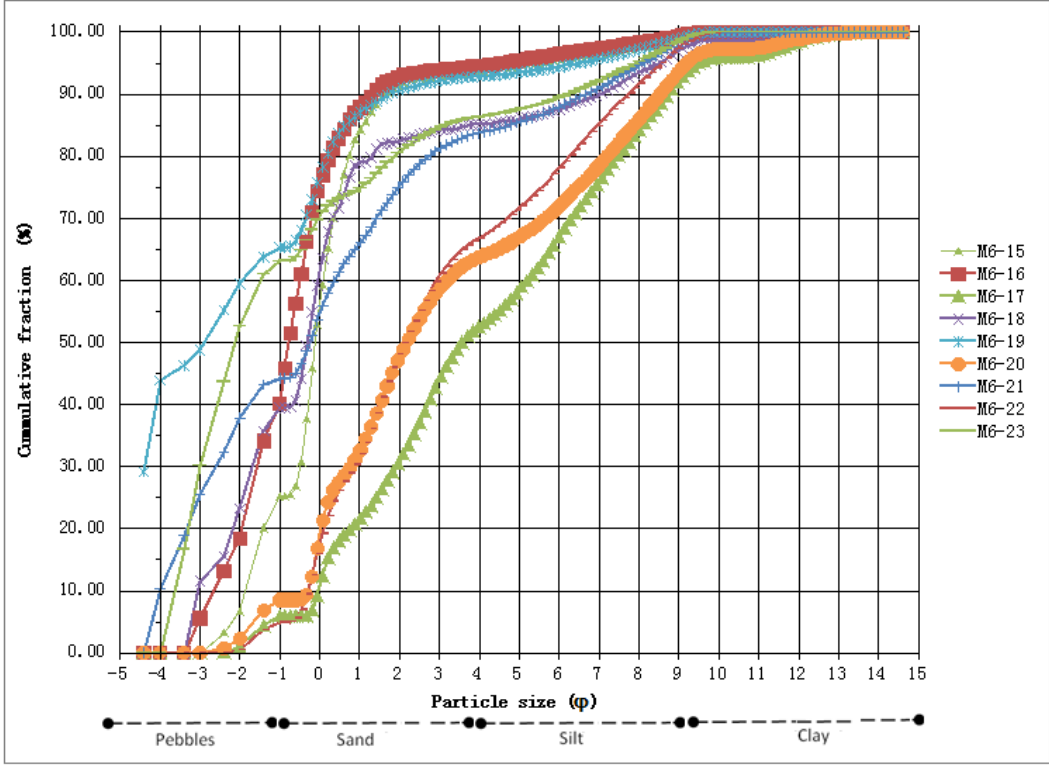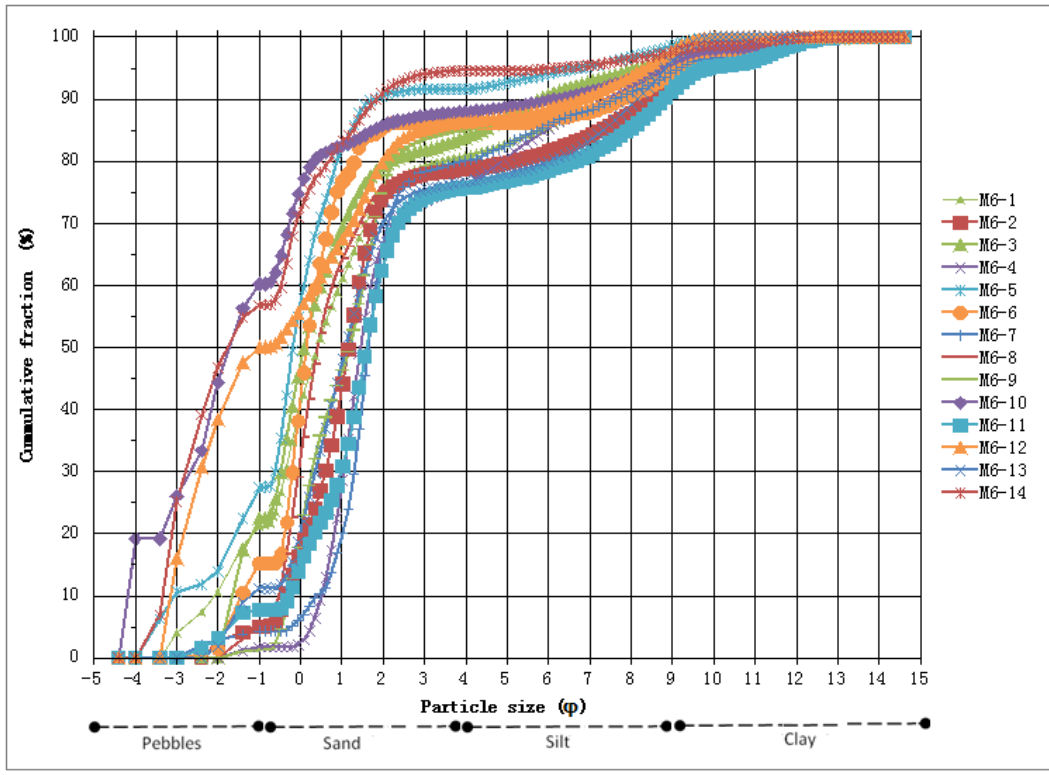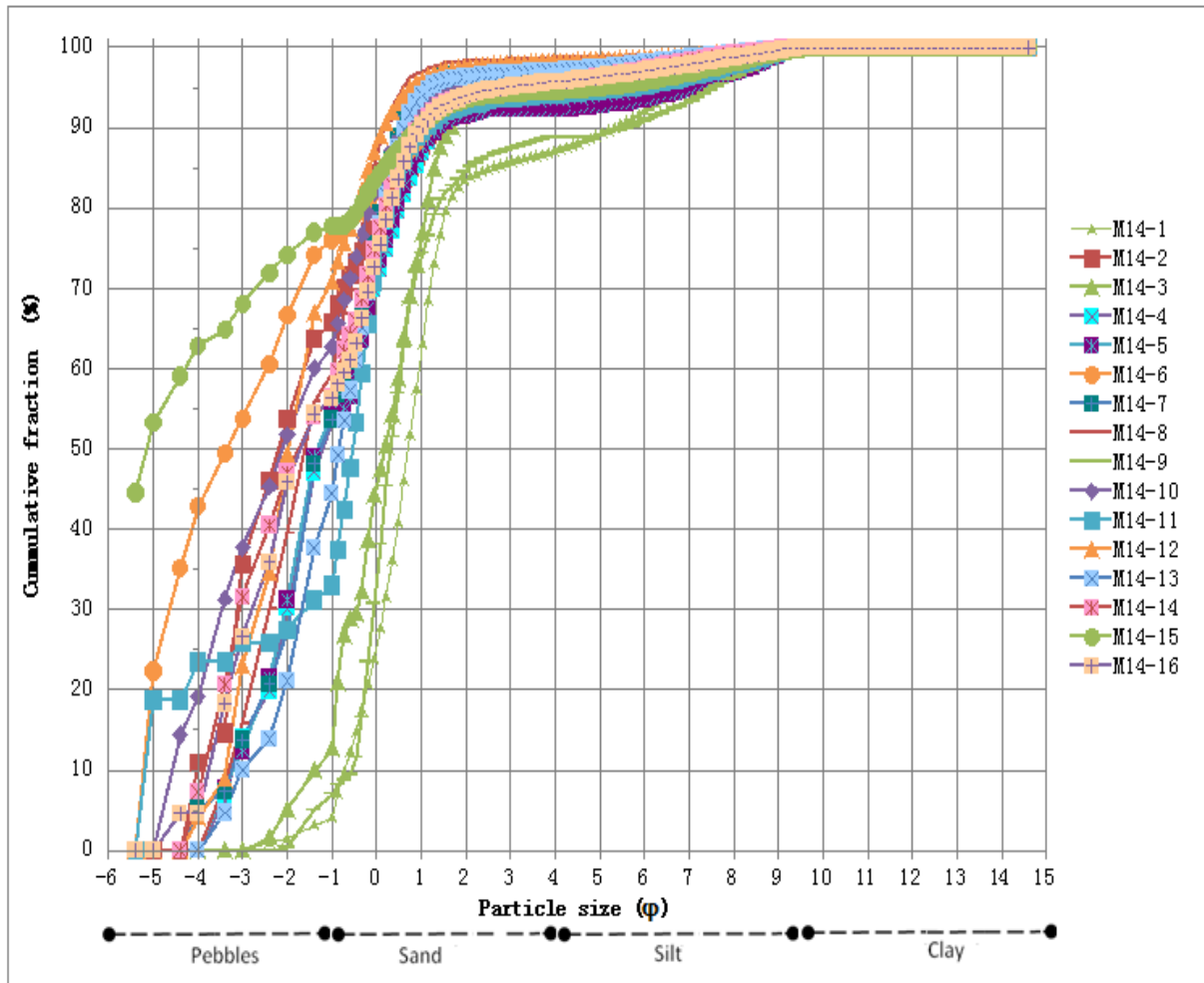
Figure 5.7: Cumulative percentage curve of the grain size composition for section M14 at Wadi Al Hinakiyah.

5.1.1.4   Fluvial Deposits in the Main Channel of Wadi Sahuq M13

Wadi Sahuq is km in length, it is considered to be one of the key wadis in the area east of Al Madinah. Running from the north west where al Buwaybat mountain is situated at an elevation of 1187m, the wadi then flows to the south east, turning to the north east, and then east to connect with Wadi Al-Rimah (Figure 5.1).

Section M13 is located in the main channel of Wadi Sahuq (N 25°05`04.5"-E 41°17`56.7"), at an elevation of 979 m. The flow channel at the section is 17.8m wide, while the flood plain is around 475m wide. The section studied is 120 cm thick and is composed of thirteen sediment units as illustrated in Figure 5.8.

The first unit is 27cm thick, 7.5YR6/4 light brown in colour and contains very poorly sorted matrix, alternating between silty, very coarse sand and sub-angular pebbles. These reach 55%, and are predominantly very fine in size, but do not exceed the coarse size, of which some pebbles are sub-rounded in shape, and increase in size towards the unit's upper part. In the unit can be found wavy bedding with some roots, burrows as well as carbonates that have strongly cemented together the deposits, giving the unit a 7.5YR6/4 light brown colour. A wavy boundary separates this unit from the one above, which is similar in characteristics, but with less coarser, sediment a greater amount of coarse and medium sand, and less pebbles, reaching 17%, compared to the first unit. The colour of the second unit is 7.5YR5/4 brown, and its boundary is wavy and unconformable in nature.

The third unit is 8cm thick, and composed of very poorly sorted matrix consisting of an alternation between silty medium sand with minor amount of clay, and 8% sub-angular and very fine sized pebbles with a smaller amount of medium sized ones. The pebbles are horizontally distributed (flat bedding). There are some roots, burrows and carbonates, with a wavy boundary separating it from the fourth unit above, which is similar, but with a slightly greater amount of silt and an extremely small amount of pebbles.

The fifth unit is 12cm thick, massive, 7.5YR5/4 brown in colour and poorly sorted. It is composed mainly of coarse sand, and a very small amount of silt and very fine sized, sub-angular pebbles. The unit contains some roots, burrows and carbonates and has a wavy upper boundary.

The sixth unit is 19cm in thickness, massive, 7.5YR5/4 brown in colour, and made up of very poorly sorted silty sand matrix with a small amount of clay and very fine sub-angular pebbles. There are many roots, burrows, some carbonates and lenses of sand. A wavy boundary separates it from the seventh unit, which is similar, but with slightly less silt in comparison to the sixth. Moreover, the amount of very fine pebbles is slightly greater, where the majority is concentrated at the base of the unit. Here, wavy layers of gravel deposits are found followed by sand deposits along with silt and clay. The upper boundary is wavy.

The eighth unit is 18cm thick, massive, 10YR5/4 yellowish brown coloured, and consists of a very poorly sorted matrix of silty fine sand, and some amounts of clay and very fine angular pebbles. XRD analysis shows that the deposit contains high amounts of silicate 79.8% (quartz 60.7%, plagioclase feldspar 14.2% and alkali feldspar 4.9%) as well as clay minerals

10.7% (chlorite 5.2% and mica 5.4%), a little calcite 5% and amphibole 4.3%. In this unit, the amount of silt is higher than in the units below. Moreover, the unit contains a large amount of silt lenses, which are originally silt desiccation cracks which formed when the Wadi dried out. On the upper part, fine laminations of silt appear, alternating with sand. In this unit, there are some roots and burrows which are more concentrated in the upper part. The unit is separated from those above by a wavy boundary. These units clearly differ in type of sedimentation, with an increased amount of sand, and a lesser amount of silt and clay in the upward direction, except for the tenth unit.

The ninth unit is 9cm thick, 7.5YR5/4 brown and very poorly sorted, with a dominance of medium and fine sand in its matrix. XRD analysis shows that the deposit contains silicate 80.2% (quartz 54.1%, plagioclase feldspar 16% and alkali feldspar 9.9%), and small amounts of silt, clay (chlorite 3.8% and mica 4%), and very fine sub-angular pebbles. This unit also has 4.6% amphibole. There is an abundance of roots and burrows, and the presence of fine laminations of silt in the central area. The colour of this unit differs from the previous units, and is similar to that of the three top units. The boundary of the ninth unit is wavy and unconformable in nature.

The 10th unit clearly differs in the pattern of sedimentation, as it is 10YR6/4 light yellowish brown in colour, and composed of sandy silt, some clay, and very fine sub-angular pebbles. XRD analysis shows that in comparison to units eight and nine, the deposit contains higher amounts of clay minerals (16.4%) (chlorite 7.7% and mica 8.6%) and higher amounts of calcite (10.2%) and (amphibole 7.5%); however, the unit contains lower amounts of silicate 65.7% (quartz 47.1, plagioclase feldspar 12.1% and alkali feldspar 6.4%). Fine laminations appear at the top of the unit; sand is mixed with these laminations in some parts, but not all. There are some roots and burrows in the 10th unit, which has a wavy upper boundary.

The 11th and 12th units are similar; both are formed of a silty sand matrix, with a very small amount of clay and very fine sub-angular pebbles, which increase slightly in the 12th unit. Carbonates are few, while roots and burrows are abundant. The upper boundaries of both units are wavy and unconformable; however, at the top of the eleventh unit, there is a fine wavy strip of silt, topped by gravelly sediments that appear cut off in some parts. These are fluvial deposits that were exposed to different erosion processes, which caused some parts to be removed.

The 13thunit is 3cm thick, with poorly sorted matrix comprising of very coarse and medium sand, and a very small amount of silt, with very small sub-angular pebbles. There are some roots, burrows and carbonate, and the upper boundary is wavy and unconformable in nature.
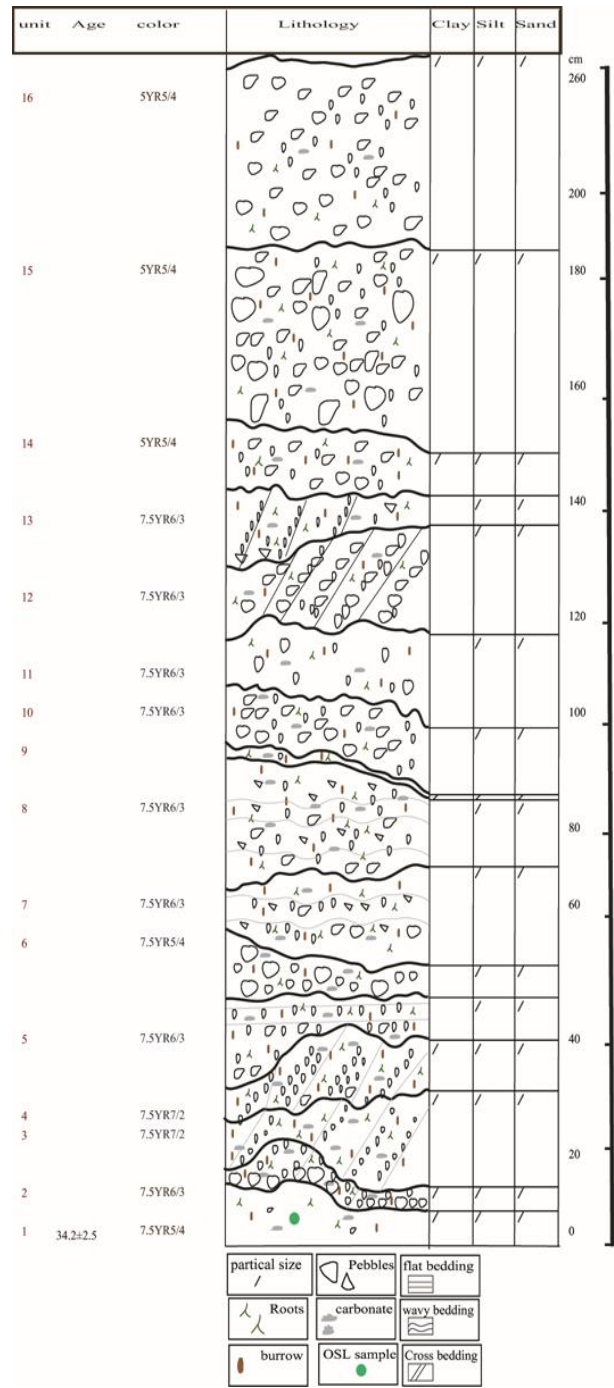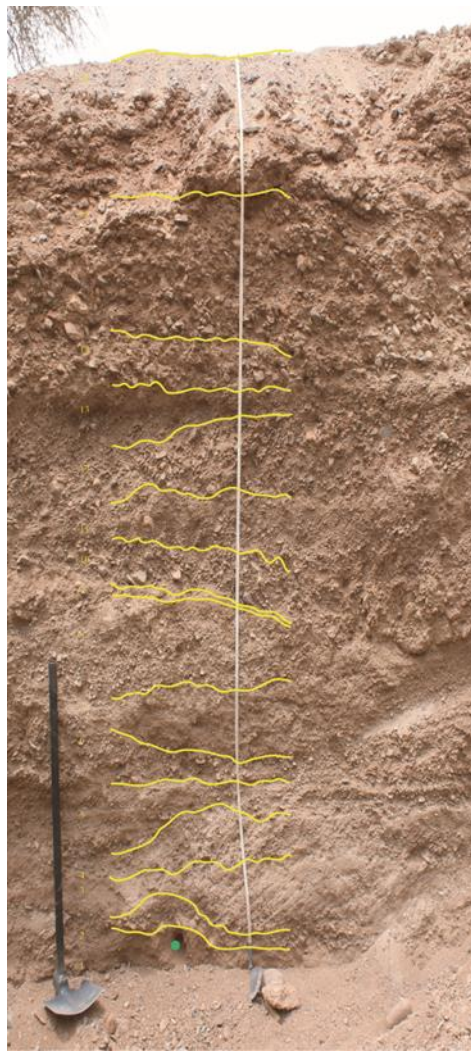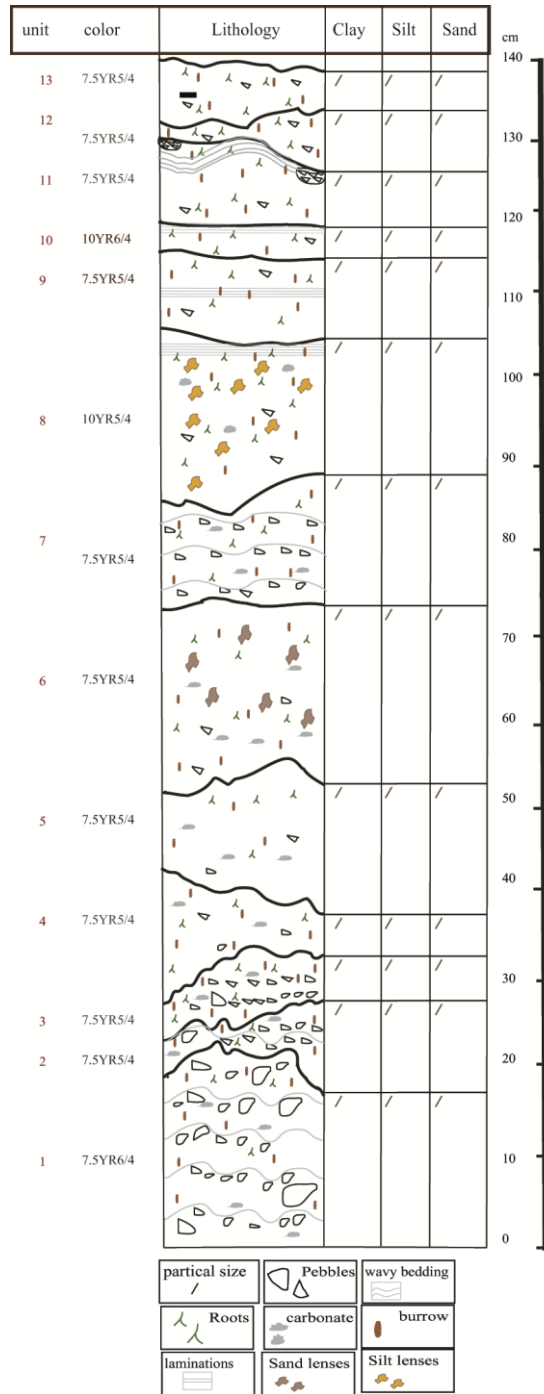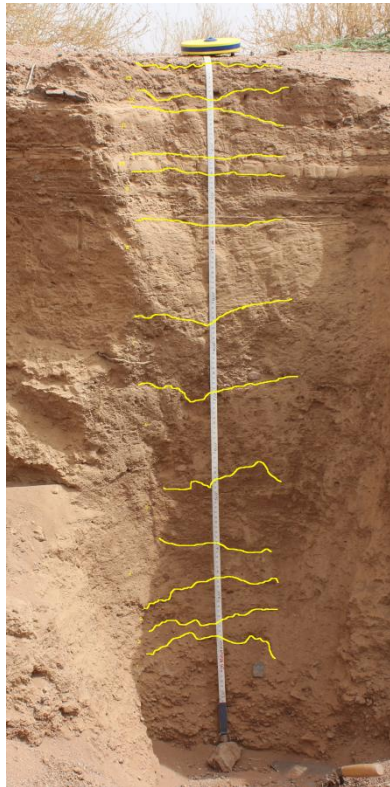
Figure 5.8: Schematic sedimentary log and view of section M13 wadi deposits in the main channel of Wadi Sahuq M13.
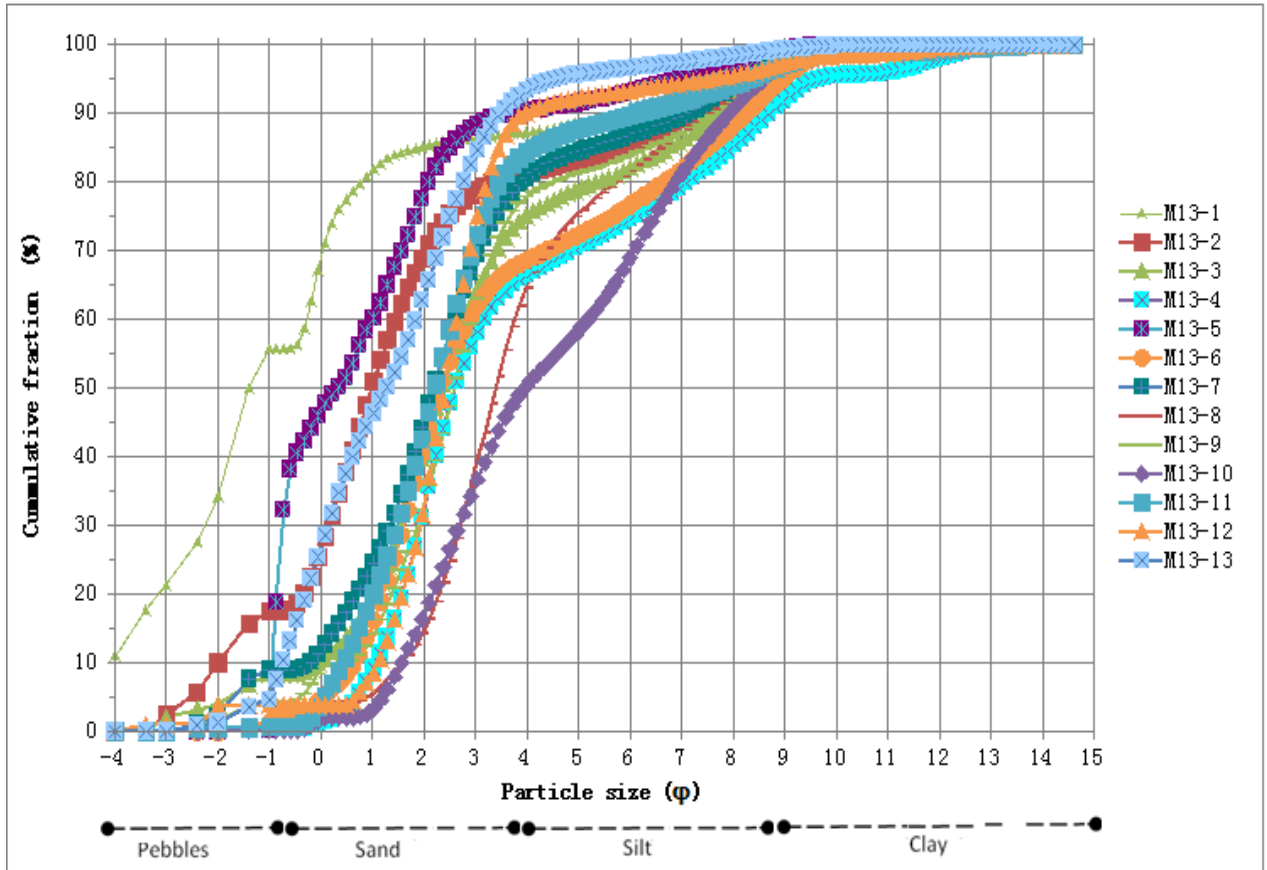
Figure 5.9: Cumulative percentage curve of the grain size composition for section M13 in the main channel of Wadi Sahuq.

5.1.1.5 Fluvial Deposits in the Wadi Al Qusayrah M8

Wadi Al Qusayrah is 102.1 km in length, it is one of the main tributaries of Wadi Sahuq. Wadi Al Qusayrah begins from the north west, at the Al Alam mountains at an elevation of 1276m, and flows to the south east into Wadi Sahuq, near the Mawan mountain (Figure 5.1).

Section M8 is located in the Wadi Al Qusayrah (N 25°16`45.1"-E 41°28`41.5"), at an elevation of 934m. The flow channel at the section is 55m wide, while the flood plain is 598 m wide. The section studied is 120 cm thick and is composed of thirteen sediment units as illustrated in Figure 4.10.

The first unit is 21cm thick, 5YR5/4 reddish brown in colour, and composed of sand matrix with around 40% sub-angular pebbles, the majority of which are very fine in size. Medium sized pebbles are concentrated at the bottom of the unit; most are sub-rounded, and size

reduces as we proceed upwards. This unit is poorly sorted, and there is an alteration between fluvial sand and pebbles, with wavy bedding containing some amounts of carbonates, roots and burrows. The upper part of the unit appears wavy and unconformable in nature.

The second unit is 4cm thick, 5YR5/4 reddish brown in colour, and poorly sorted. The amount of pebbles in this unit is greater than in the unit below, occupying nearly three-quarters of unit two, while the rest is sand. The pebbles are distributed in layers; coarse pebbles at the bottom, whilst those in the main section are sub-rounded, indicating that they were transported from a distance. The pebbles' size decreases as we move upwards. In this unit, there are small amounts of carbonate, and no roots and burrows are present; it is separated from the one above by a wavy and unconformable boundary.

The third unit is 2cm thick and 7.5YR6/4 light brown in colour. Its matrix is composed of sand, along with 43% sub-angular pebbles, and small amounts of carbonates. It is poorly sorted with flat bedding, there are no roots or burrows, and its boundary with the unit above is wavy and unconformable in nature.

The fourth unit is 13cm thick, and 7.5YR6/4 light brown in colour. It is similar in all characteristics to the second unit, except for the structure, as pebbles size increases as we move upwards, in contrast to the second unit. On the other hand, pebbles are dominantly fine sized, and do not exceed medium size. Some roots and burrows are also present. The unit is separated from the one above by a wavy and unconformable boundary. The similarity between the units indicates that they were formed under largely similar environmental conditions.

The fifth unit is 2 cm thick and of a 7.5YR6/4 light brown colour. Its matrix is composed of sand, and up to 51% very fine sub-angular pebbles, with a lack of roots and carbonates. The unit is moderately sorted, where the range of particle sizes demonstrates a river flow of moderate energy. In addition, fine wind-borne sand is present in small quantities. Its upper boundary is wavy and unconformable in nature.

In the sixth and seventh units, the pattern of sedimentation begins to change, with the dominance of 7.5YR6/4 light brown coloured sand in the matrix of both units. The sixth unit is 16 cm thick, and also contains a small percentage of very fine sub-angular pebbles in a coarse sand matrix, not exceeding 16%, concentrated in some of the upper parts of the unit,

which is separated by a wavy boundary from the one above. Unit six is moderately sorted, and has some roots, burrows and carbonates.

As for the seventh unit, which is 12 cm thick, the sand here is finer than in the previous units, and the quantity of sub-angular pebbles decreases to only 9%; they are generally very fine in size, and do not exceed medium size, appearing sporadically in the middle part of the unit. This unit is poorly sorted and has roots and burrows. The upper boundary of this unit is wavy and unconformable.

The eighth unit is 4 cm thick, and is composed of 7.5YR5/4 brown coloured silty sand matrix, in addition to very minor amounts of very fine, sub-angular pebbles. XRD analysis reveals that the deposit contains high amounts of silicate 82% (quartz 61.1%, plagioclase feldspar 14.5% and alkali feldspar 6.4%) and some clay minerals 9.2% (chlorite 4.1% and mica 5%) as well as a small amount of calcite and amphibole (4.4%). This unit has a few roots and burrows, and is poorly sorted. It is separated from the unit above by a wavy and unconformable boundary.

The ninth unit is 8 cm thick, and is similar in all its characteristics to the seventh unit, with the presence of more burrows and a small amount of carbonate. A wavy boundary separates it from the 10th unit, which it resembles in all characteristics, but the presence of small quantities of aeolian sediments in the tenth unit distinguishes it from the ninth unit.

The deposits in the remaining units begin to take on the same 7.5YR5/4 brown colour. The 11th and 12th units are 6 cm and 10 cm thick respectively, and are both poorly sorted. These two units are similar in matrix, and are composed mainly of sand and a very small quantity, not exceeding 3%, of sub-angular, very small sized pebbles. However, in the 12th unit, some pebbles reach medium size. Some roots, burrows, and a small amount of carbonates are present, and the upper boundaries of both units are wavy. The characteristics of these units (11-12) indicate a notable low energy in fluvial activity, and clear contributions of aeolian activity. XRD analysis in unit 11 shows that the deposit contains higher amounts of silicate 88.6% (quartz 60.9%, plagioclase feldspar 17.1% and alkali feldspar 1.5%), but lower amount of clay minerals 6% (chlorite 2.8% and mica 3.2%), calcite and amphibole (2.6%).

The 13th unit is 13 cm thick, and its matrix is composed of sand with a quantity of pebbles reaching 41%, and not exceeding coarse size; the pebbles are sub-angular in shape, while for the coarse size pebbles, some are sub-rounded, due to being transported from a distance.

The unit is considered very poorly sorted, and contains some roots, burrows and a small amount of carbonate, while clasts are non-uniformly distributed.
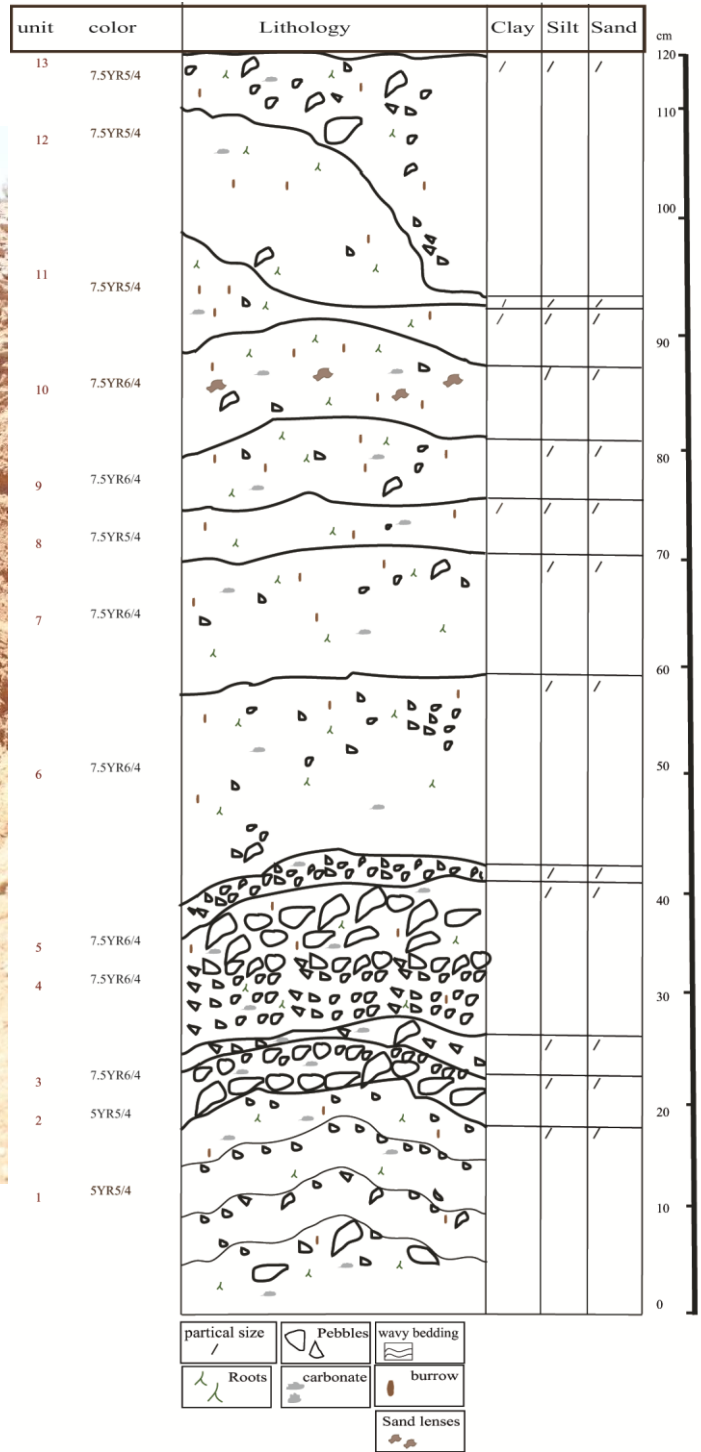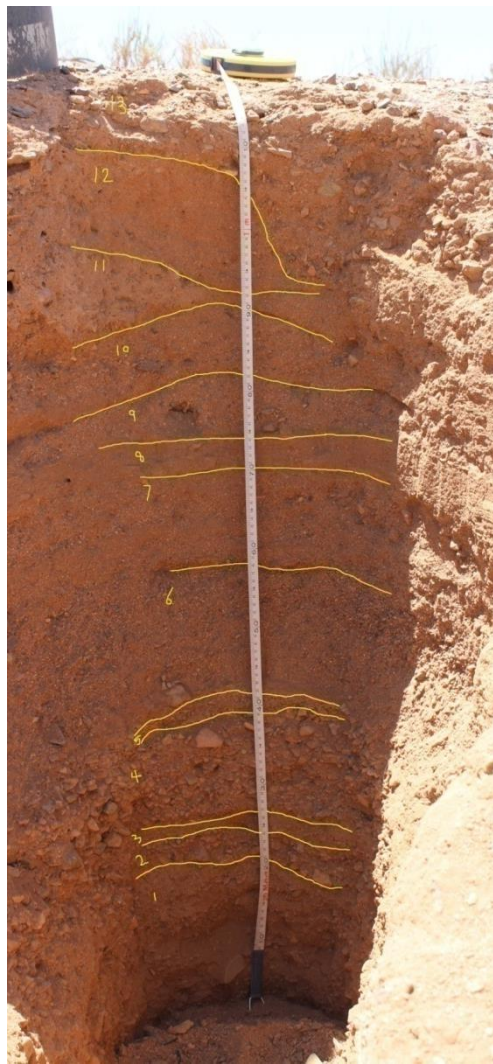
Figure 5.10: Schematic sedimentary log and view of section M8 wadi deposits at Wadi Al Qusayrah.
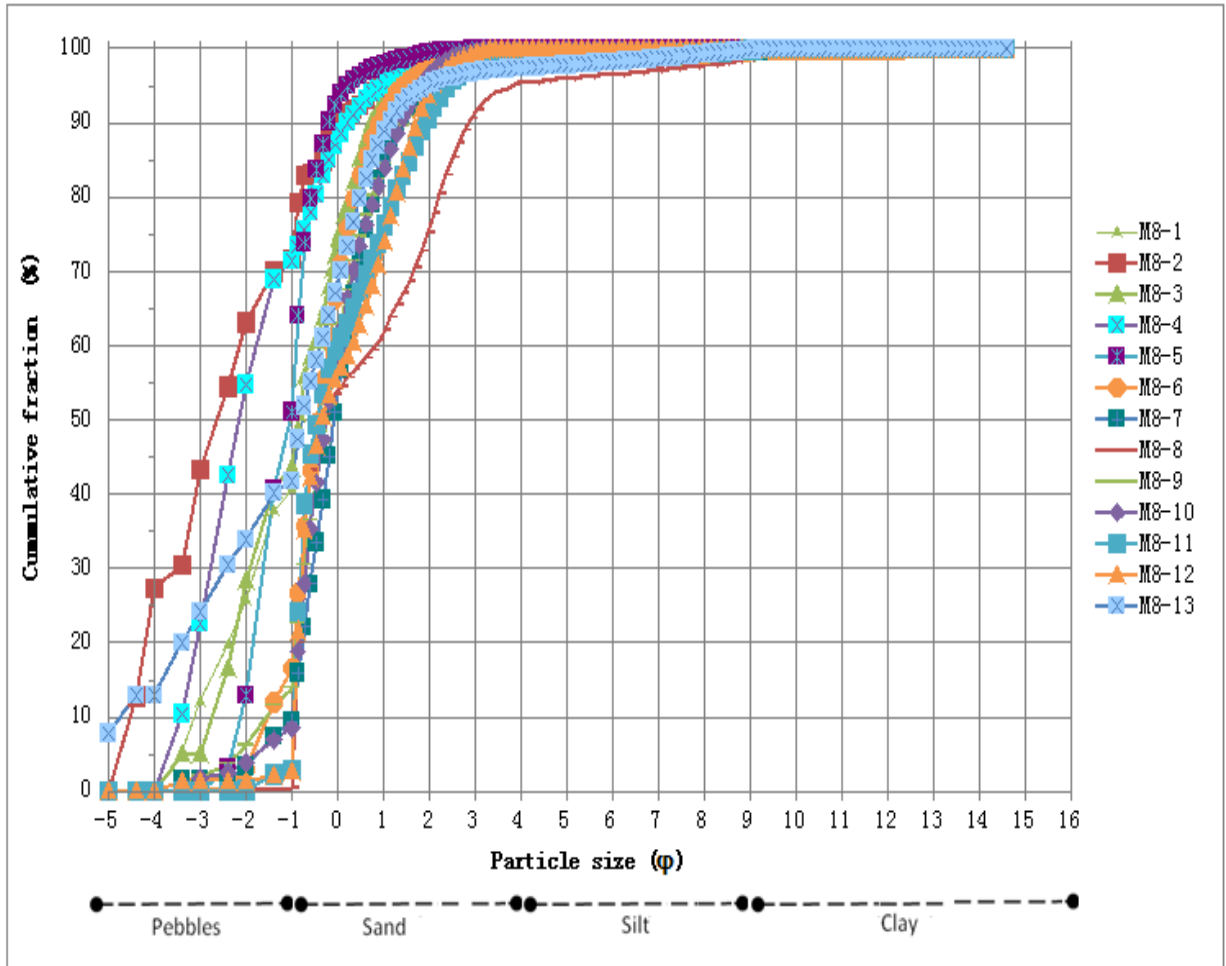
Figure 5.11: Cumulative percentage curve of the grain size composition for section M8 at Wadi Al Qusayrah.

5.1.2 Fluvial Deposits in the Alluvial Fans

5.1.2.1 Fluvial Deposits in the Alluvial Fan in the West of Wadi Luwayy M3

Wadi Luwayy is considered to be one of the main Wadis in the area east of Al Madinah. It is 106.9 k m in length, and receives water from highland sources, starting with Al Jihfah mountains to the east, passing through Marurah mountains and al Khishaybiyat mountains to the north at an elevation of 1094 – 1168 m. Wadi Luwayy connects with Wadi Al Hinakiyah then Wadi Al Makhit, ending at Qa Hadawda (figure 5.1).

Interconnected alluvial fans are present on the western part of Marurah mountains. These were formed from the deposits of a set of wadis sloping from the western part of Marurah mountains. These wadis flow into Wadi Luwayy, which cuts across the alluvial fan. Section M3 is part of the alluvial fan cut by Wadi Luwayy (25°03`26.2`N- 40°54` 31.7`), at an elevation of 1034m. The section studied is 130cm thick and is composed of four sediment units as illustrated in Figure 5.12.

The first unit is 41cm thick, and is a 7.5YR4/6 strong brown in colour, formed principally of silty sand, and with only around 29% of angular and sub-angular pebbles ranging in size from 2-16mm; the majority of pebbles are coarse in size. All the pebbles are comprised of local lithologies as gabbro and chert, originating from the surrounding slopes such as Marurah mountains that make up this catchment. This unit is very poorly sorted, which indicates that the fluvial sedimentation was subject to slightly strong energy currents. This unit has some roots, burrows and a few carbonate nodules. The boundary between this unit and the one above is wavy.

The second unit is 49 cm thick, 7.5YR 5/4 brown in colour, very poorly sorted, with locally derived, angular cobbles and pebbles in a sand matrix. The quantity of coarser particles in this unit increases noticeably compared to the unit below. It is notable in this unit that the large pebbles and cobbles are imbricated and dip down flow at an angle of around two to three degrees away from the mountain. There is some evidence of coarser clasts armouring finer sediment beneath, but also some areas show pebbles building up behind the larger cobbles. In this unit, some roots, burrows and a small amount of carbonate is present, and the upper boundary layer appears wavy and unconformable in nature.

Unit three is 20cm thick and is 7.5YR 6/3 light brown in colour. This deposit is similar to the unit below it in terms of lithology, texture, structure and carbonates. However, the number of roots and burrows here is higher compared to the previous units, which indicates that they were, to a large extent, formed under similar environmental conditions. The junction with the overlying bed is wavy and unconformable in nature.

The uppermost fourth sediment unit is 20cm thick, and is 7.5YR 5/4 brown in colour. It is extremely poorly sorted, and is largely composed of a matrix of silty sand, with around 28% angular and sub-angular pebbles; no clasts larger than coarse pebbles are present. In this unit, the pebbles are less abundant than in the two units below; these originate locally from neighbouring high slopes such as Marurah mountains, based on the shape characteristic and lithology of the pebbles. They are present as angular and sub-angular particles, indicating that they are local in origin, containing gabbro and chert that constitute most of the neighbouring slopes. Few roots, burrows and carbonates are present in this unit, and its upper boundary is wavy. Recently reworked sediments cap this unit.
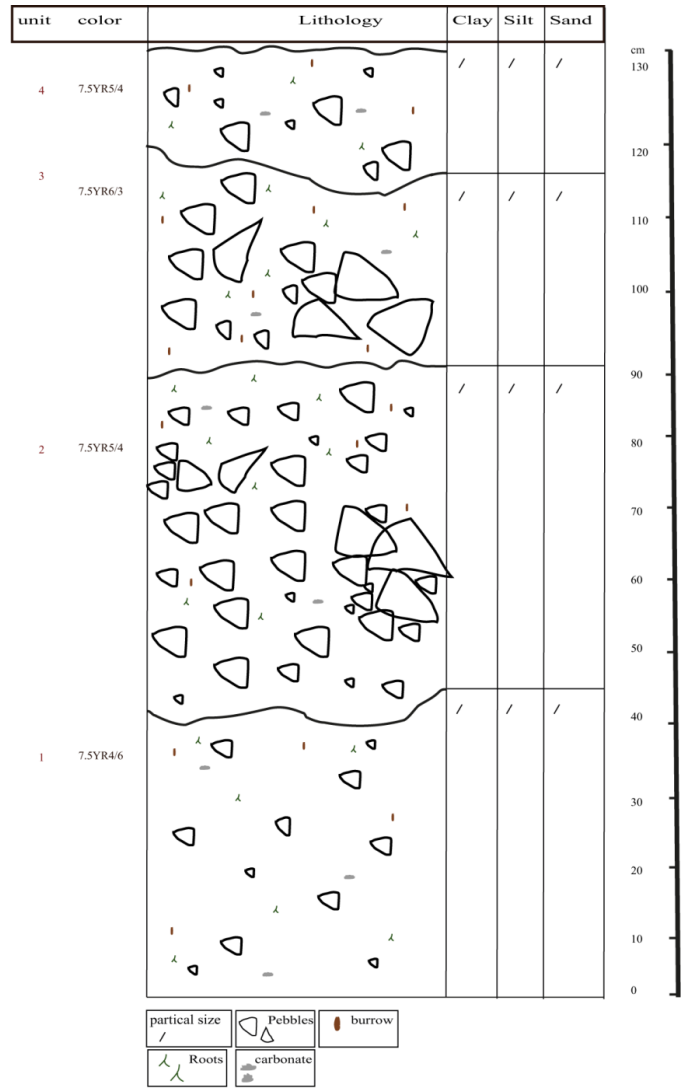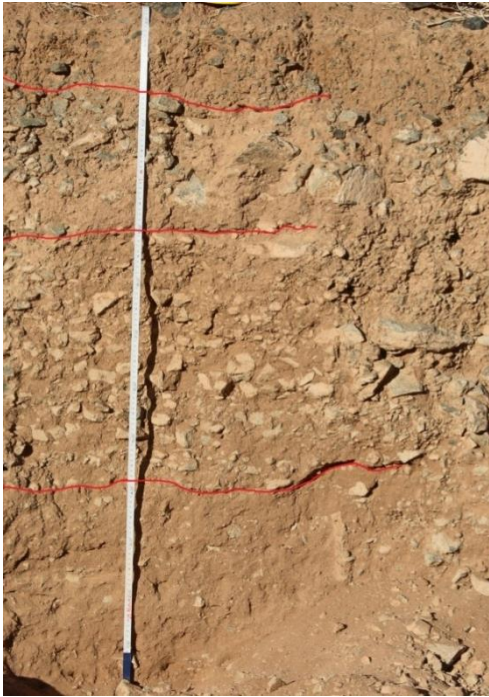
Figure 5.12: Schematic sedimentary log and view of section M3 alluvial fan deposits at Wadi Luwayy.

5.1.2.2   Fluvial Deposits in the Alluvial Fan in the West of Wadi Luwayy M4

On the western part of the Marurah mountains, interconnected alluvial fans are present. These were formed from the deposits of a set of wadis sloping from the western part of the Marurah mountains. These Wadis flow into Wadi Luwayy, which cuts across the alluvial fan (Figure 5.1). Section M4 was chosen in this location, within the alluvial fan cut by wadi Luwayy (25°03ʾ48.1ʾʾN- 40°54ʾ 36.7ʾʾE), at an elevation of 1025m. This section is north of M3 by about 693.93 m. The section studied is 155cm thick and is composed of three sediment units as illustrated in Figure 5.13.

The first unit is 29cm thick, 7.5YR5/4 brown in colour, and composed of silty sand, with very small amounts of very fine pebbles. The sand here ranges from medium to coarse, with small quantities of carbonates as well as roots and burrows. This unit is moderately sorted, and its upper boundary, which separates it from the second unit, appears wavy in form. This unit has an OSL age of 11.6±1.0 ka, as shown in table 5.2.

The second unit is 113cm thick and 7.5YR5/4 brown coloured. Sand is coarser in this unit and contains quantities of angular and sub-angular pebbles, not exceeding 10% of its composition. All the pebbles are from the same source - the local high slopes situated behind (such as Marurah mountains) because the clasts share the same lithology as the rocks forming the mountains situated behind represented in gabbro and chert and pebbles are angular and sub-angular in shape. A small amount of carbonates, some burrows and roots are also present. The unit is poorly sorted, and is generally composed of alternating layers of coarse to medium sand beds, and pebbles beds, which are distinct in the upper parts of the unit; there is a distinct gravel bed, with some lenses of pebbles within it. The upper boundary of this unit is wavy in form and unconformable in nature. This unit has an OSL age of 9.9±0.6 ka as shown in table 5.2.

The third unit is 13cm thick, and is a 7.5YR4/6 strong brown colour, composed of aeolian medium sand with cross bedding. Some roots and burrows appear in this unit, which is considered moderately well sorted, giving a clear indication that the fluvial deposit was subject to relatively weak current, as nabkahs appear on the surface.

Nabkahs appear on the surface, furthermore, a layer of pebbles is found on the upper part of the section, which may have resulted from recent transport from the high slopes in the vicinity.

Table 5.2: Dates determined using OSL of sedimentary section M4 alluvial fan deposits at Wadi Luwayy.

				Radioactivity Data			Dosimetry Data				Age Data	
sample	Location	Lab code	Altitude (m)	U (ppm)	Th (ppm)	K (%)	Beta (μGy a^{-1})	Gamma (μGy a^{-1})	Cosmic (μGy a^{-1})	Water (%)	Dose rate (Gya^{-1})	Age (Ka)
M4-unit1	Wadi Luwayy	MAD13/ 4/1/1	1027	1.04	3.2	1.7	1293±92	682±36	226±11	1.4±2	2.20±0.1	11.6±1.0
M4- unit2	Wadi Luwayy	MAD13/ 4/1/2	1027	0.84	3.2	1.4	1079±77	589±31	215±11	1.0±2	1.88±0.08	9.9±0.6

Source: Luminescence dating report, Department of Geography, Leicester.
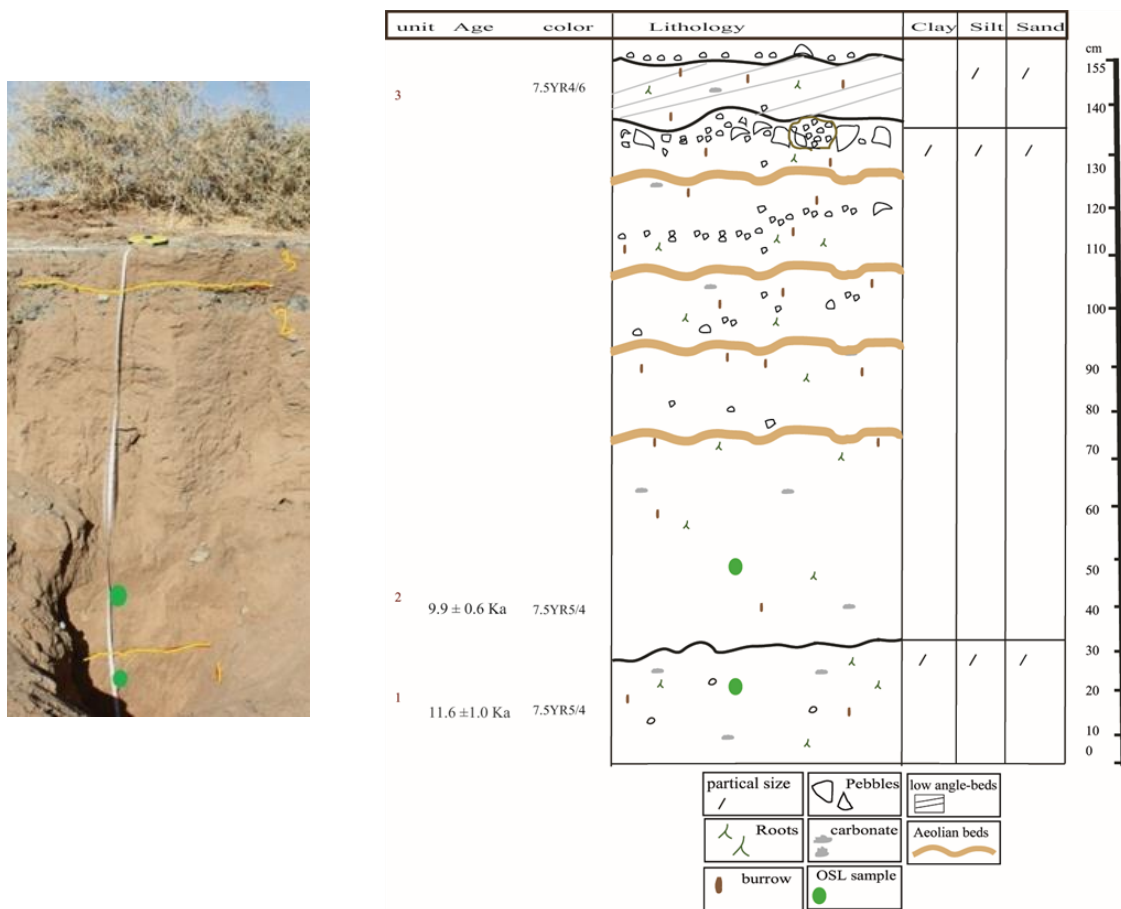
Figure 5.13: Schematic sedimentary log and view of section M4 alluvial fan deposits at Wadi Luwayy.
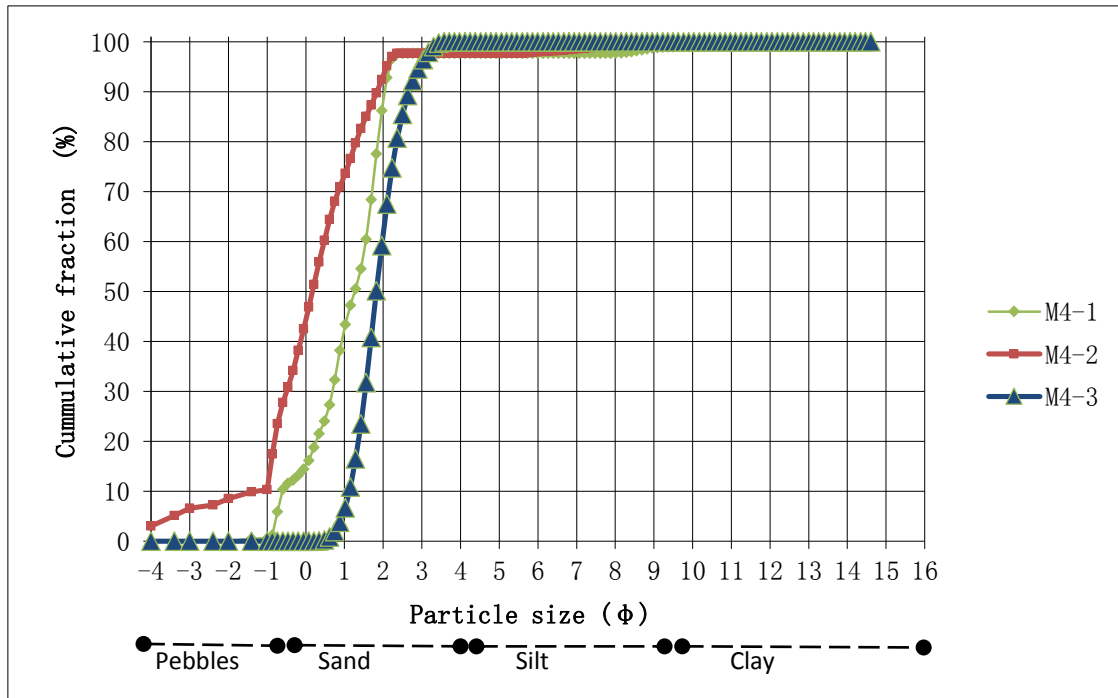
Figure 5.14: Cumulative percentage curve of the grain size composition for section M4 alluvial fan deposits at Wadi Luwayy.

5.1.2.3 Fluvial Deposits in the Alluvial Fan in the East of Wadi Luwayy M5

On the eastern part of the Marurah mountains, interconnected alluvial fans are present. These were formed from the deposits of a set of wadis sloping from the eastern part of the Marurah mountains. These wadis flow into Wadi Luwayy, which cuts across the alluvial fan (figure 5.1). This section was chosen to lie on the alluvial fan in Wadi Luwayy, to the east of M3 (25° 03` 10.1``N - 40° 54` 37.0``E), at an elevation of 1028m. The section was freshly excavated, it is 136cm thick and composed of two sediment units as illustrated in Figure 5.15.

The first unit is 29cm thick, a 7.5YR4/6 strong brown colour, and has a pebble foundation at the bottom. The unit's texture is composed mainly of clayey silt with sand, along with very small amounts of fine pebbles. The unit is poorly sorted, with particles cemented together by carbonates. Wavy laminations which alternate between carbonates and aeolian (windblown fine orange sand) sediments appear, in addition to some roots and burrows. The

214

upper boundary is wavy in form. This unit has an OSL age of >83 ka as shown in table 5.3. The second unit is 94cm in thickness, and is 7.5YR5/4 brown in colour. A foundation of angular and sub-angular pebbles can be found at the bottom. The unit is very poorly sorted, and its texture is made up of silty sand. XRD analysis shows that the deposit contains high amounts of silicate 71.5% (quartz 57.3%, plagioclase feldspar 4.4% and alkali feldspar 9.6%) and some clay minerals 8.1% (chlorite 4.4% and mica 3.6%), in addition to the quantity of pebbles making up 36% of its composition. The majority of pebbles are fine sized (around 16.65%), but with quantities of coarse (5.89%) and very coarse (6.75%) pebbles, as well as cobbles, which are concentrated in layers in the middle of the unit. This suggests a sudden change in fluvial current strength. Subsequently, the amount of pebbles reduces as we move upwards; starting from 1m to 120 cm, there is less gravel, and no clear structure for sediments. These are mixed with each other. The upper parts of the section, from around 120cm and up, consist of non-cemented, fine sediments, intermixed with significant amounts of aeolian deposits. All of the clasts share the same lithology as the rocks forming the mountains situated behind the fan represented in gabbro and chert. In this unit, roots and burrows are present, and the unit has a small amount of calcite (3.7%), amphibole (5.9%). and serpentine (10.6%). Its upper boundary is unconformable, and the amount of calcite, roots and burrows decreases as we move upwards.

Table 5.3: Dates determined using OSL of sedimentary section M5 alluvial fan deposits at Wadi Luwayy.

sample	Location	Lab code	Altitude (m)	Radioactivity Data			Dosimetry Data			Water (%)	Age Data	
				U (ppm)	Th (ppm)	K (%)	Beta (μGy a^{-1})	Gamma (μGy a^{-1})	Cosmic (μGy a^{-1})		Dose rate (Gya^{-1})	Age (Ka)
M5- unit1	Wadi Luwayy	MAD13/ 5/1/1	856	0.98	2.7	1.5	1133±81	597±31	218±11	2.3±2	1.95±0.09	>83

Source: Luminescence dating report, Department of Geography, Leicester.
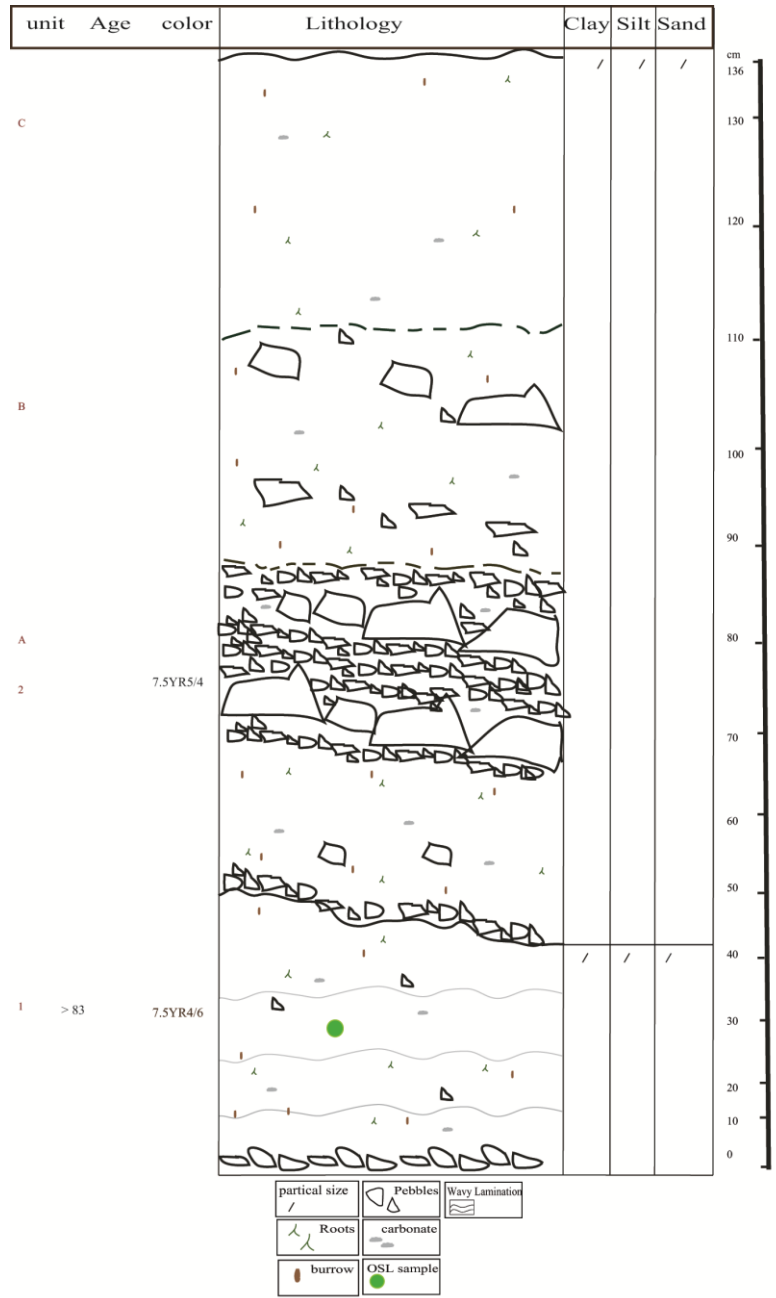
Figure 5.15: Schematic sedimentary log and view of section M5 alluvial fan deposits at Wadi Luwayy.
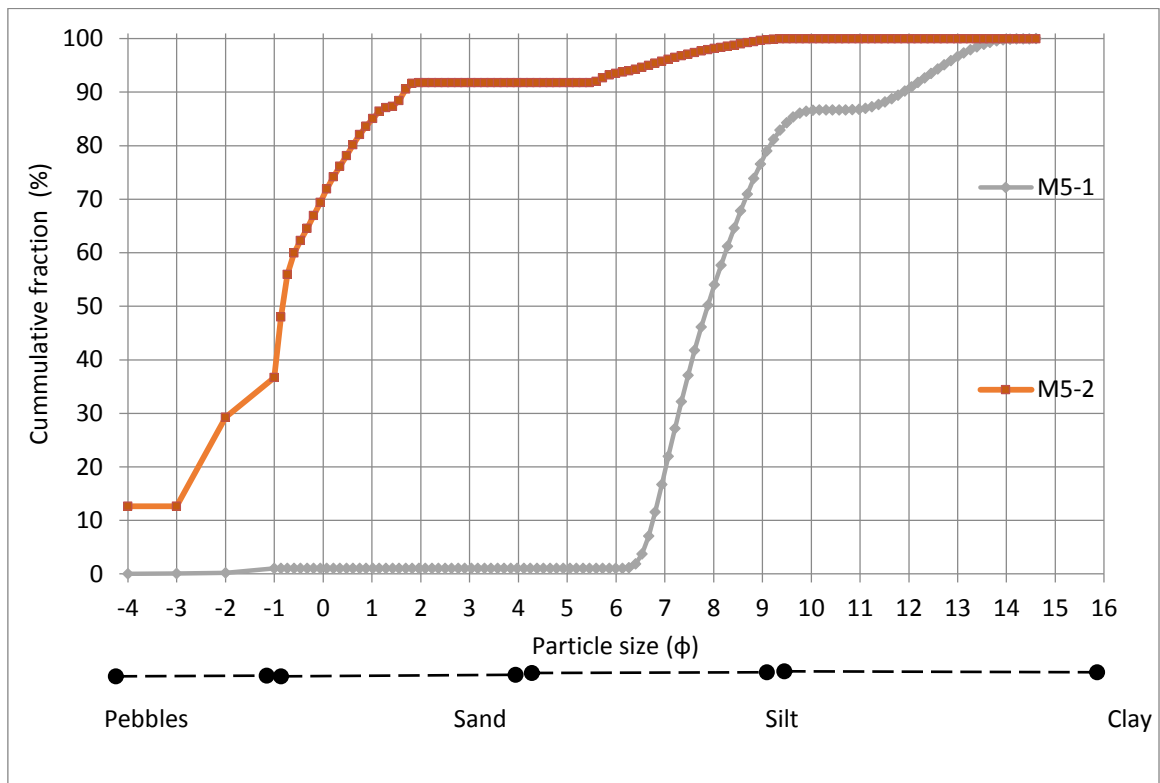
Figure 5.16: Cumulative percentage curve of the grain size composition for section M5 alluvial fan deposits at Wadi Luwayy.

5.1.3   Wadi Deposits within Nufud Al Qawz

5.1.3.1   Wadi Deposits within Nufud Al Qawz, Southern Boundary of Nufud Al Qawz M1

This area is where palaeowadis meet; the most prominent of those are Wadi Al Mahir, Wadi Al Hidiqiyah and Wadi Khadra. These come from the eastern plateau of Al Madinah, where Sinaf Umm Arte (at an elevation of 1085m), Hadabat al Musayikah (at an elevation of 1106m), Dilan Umm Asim (at an elevation of 1118m) and others are situated (Figure 5.1).

Section M1 is situated at (N 24°32`39.5"-E 40°54`10.6"), at an elevation of 855m. Section M1 was selected in this area, given that it is the meeting area of Wadis, which were buried

217

after drying out. Its sediment characteristics can be determined by studying this section. The section was excavated, and is composed of 7 sediment units as illustrated in Figure 5.17.

The first unit is 13cm thick, 5YR6/4 light reddish brown coloured and composed of silt clay. XRD analysis shows that the deposit contains 36.5% silicate (quartz 17.1%, plagioclase feldspar 5.2% and alkali feldspar 14.1%) as well as high amounts of clay minerals - around 11.7% (chlorite 5.6% and mica 6%). There is also a high amount of calcite 19.7%, with around 31.9% of gypsum, which cuts across into the upper unit. There are some roots, burrows and a few spots of possible organic material such as (algae). The boundary separating it from the second unit above is wavy and unconformable. The second unit is similar to the 1st in almost every way, except for the fact that gypsum is concentrated only at the base, with a small amount of very fine size pebbles, which increases as we move upwards in the unit.

The third unit is 15cm thick, and is similar to the first unit, although the amount of calcite and clay minerals present is less here than in unit 1, while the amount of silicate is higher. XRD analysis shows that the deposit is high in silicate 71.8% (quartz 59.2%, plagioclase feldspar 4.2% and alkali feldspar 8.4%), with high amounts of clay minerals present 10% (chlorite 4.8% and mica 5.1%). There are some roots and burrows, also some spots of possible organic material such as (algae) are present, and there is no evidence of gypsum.

The fourth unit is 12cm thick, 5YR5/4 reddish brown in colour and composed of silt some clay, and some carbonates nodules. In this unit, some roots and burrows are present. There is no evidence of gypsum nor pebbles.

The fifth unit is 12cm thick, and composed of 5YR5/6 yellowish and red coloured silty sand with a small amount of very fine pebbles. XRD analysis shows an abundance of silicate 74% (quartz 54.8%, plagioclase feldspar 10.9% and alkali feldspar 8.2%), and about 9.9% of clay minerals chlorite 3.9% and mica 5.9%). This unit also has some amount of calcite (11.7%) and amphibole (4.2%). Additionally, it is clear from the analysis that the deposit contains low amounts of clay and calcite, but higher amount of silicate in comparison to the previous units. Many roots and burrows are present, and there is no evidence of gypsum nor of spots of possible organic material such as (algae). The sixth unit is quite similar, but the roots and burrows are clear at the base, and are less in number than in unit 5. Aeolian sediments are

clearly apparent here, especially in the upper parts of unit 6. Finally, the upper boundary is wavy.

The seventh unit is 6cm thick and composed of 5YR5/6 yellowish red coloured fine sand, with a small amount of very fine pebbles. Whilst some roots are present, there is very little evidence of carbonates, with very fine wavy laminations of sand present, which represent seasonal flow in current times, while the upper boundary is wavy and unconformable in nature.

In the upper part of the section, a layer is formed of pebbles, sand, carbonates, and some of roots.
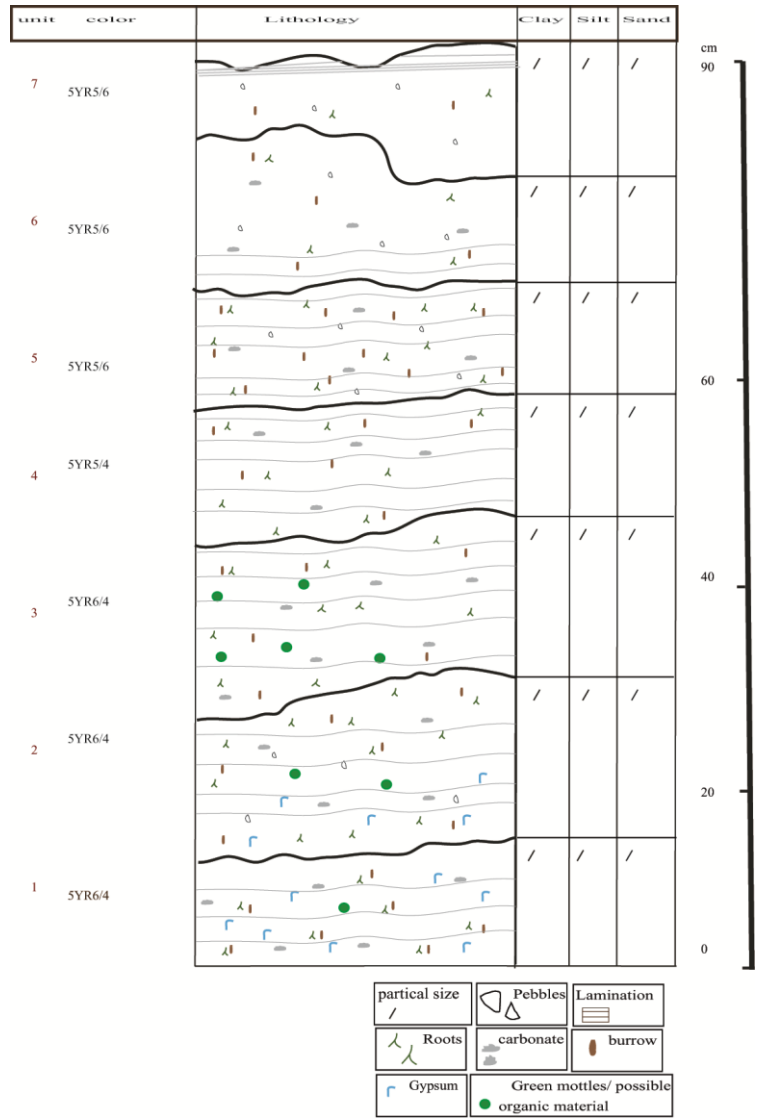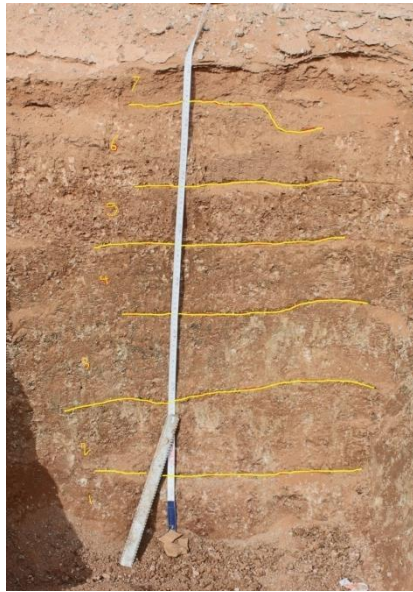
Figure 5.17: Schematic sedimentary log and view of section M1 Wadi deposits within Nufud Al Qawz, southern boundary of Nufud Al Qawz.

The map below (5.18) illustrates the locations of the sections selected for the study of aeolian (sand ramps), sabkha, palaeolake and slope wash deposits. These sections are as follows:
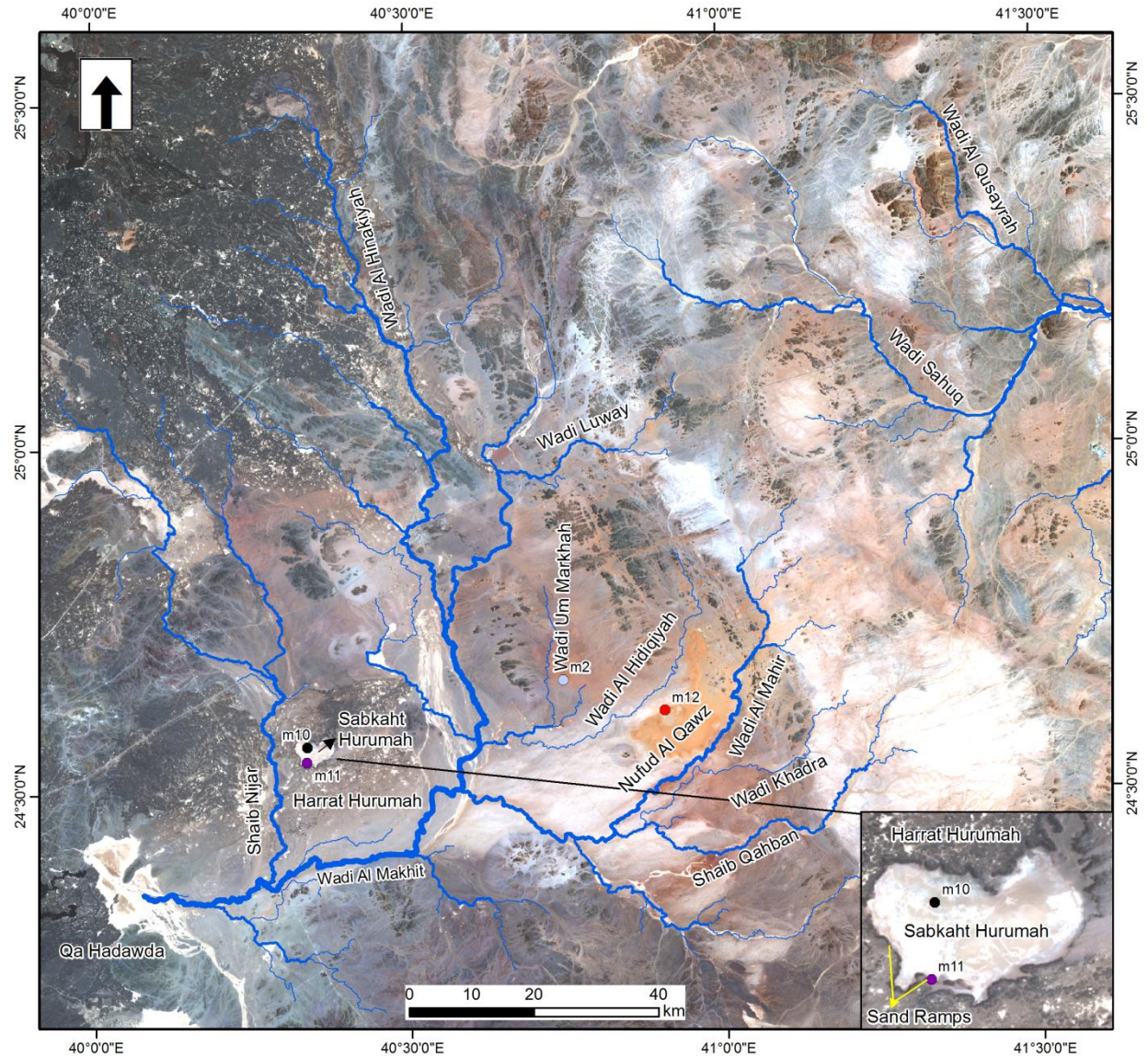
Figure 5.18: This is the study area, the sand ramps' sites is marked with purple marker, the sabkha with black marker, the palaeolake with red marker, and the slope wash with blue marker.

5.1.4 Aeolian Sand Ramps

5.1.4.1 Aeolian Deposits in the Sand Ramps inside the Wall of the Crater of Hurumah Volcano M11

The crater of the Hurumah volcano extends over an area around of 25.3 km^2 within the Hurumah lava field. Sand ramps are found on the majority of the inner walls/edges of the volcano spout. The height of the crater walls is around 57.7m. Section M11 is located on these sand ramps and was cut through the sand ramp deposits on the inside wall of the Hurumah volcano's crater (N 24°32`43.4"-E 40°20`11.0"), at an elevation of 798m (figure 5.18). The section studied is 185cm thick and is composed of seven sediment units as illustrated in Figure 5.19.

The units ranging from 1 to 5 are all composed of 5YR 4/6 yellowish red, silty medium sand, with around 86.7% of silicate in unit 1 and 2, whilst a very small quantity of sub-angular pebbles are present in the 2nd and 3rd units; these pebbles originate locally from the volcanic rocks forming the volcanic crater. Slightly wavy bedding appear in the 1st unit, with a small quantity of carbonates (4%) and ash, where sediments are cemented. The amount of carbonates increases in the three units above, as XRD shows that unit 2 contains 4.5%, in addition to the presence of roots and burrows. XRD analysis also shows that unit 1 has 6.1% clay minerals and 3.11% amphibole, while unit 2 has 8.7% clay minerals without any amphibole. The fifth unit is thicker compared to the previous units, reaching 56cm, and contains some roots. Carbonates are concentrated in the central part, with a slightly higher number of burrows compared to the fourth unit. Moreover, the size of burrows is greater in unit 5 than in other units. All previous units are poorly sorted, except for the second, which is moderately sorted.

The sixth unit is composed of poorly sorted, medium to coarse sand, with a small amount of silt. Roots are abundant, and there can be found some burrows and carbonates. In the seventh unit, the size of sand particles increases. It is composed of moderately sorted, 5YR 5/4 reddish brown, coarse sand. XRD analysis shows that silicate 88% (quartz 74.7%, plagioclase feldspar 6.5% and alkali feldspar 6.7%) and small amounts of silt and clay minerals (mica 4.4%) are present, along with fine laminations at the top, with some roots from the surface. Roots are abundant in this unit, while burrows are absent. This unit has some carbonates (7.4%), in higher amounts than previous units, and its upper boundary is wavy and unconformable in nature.
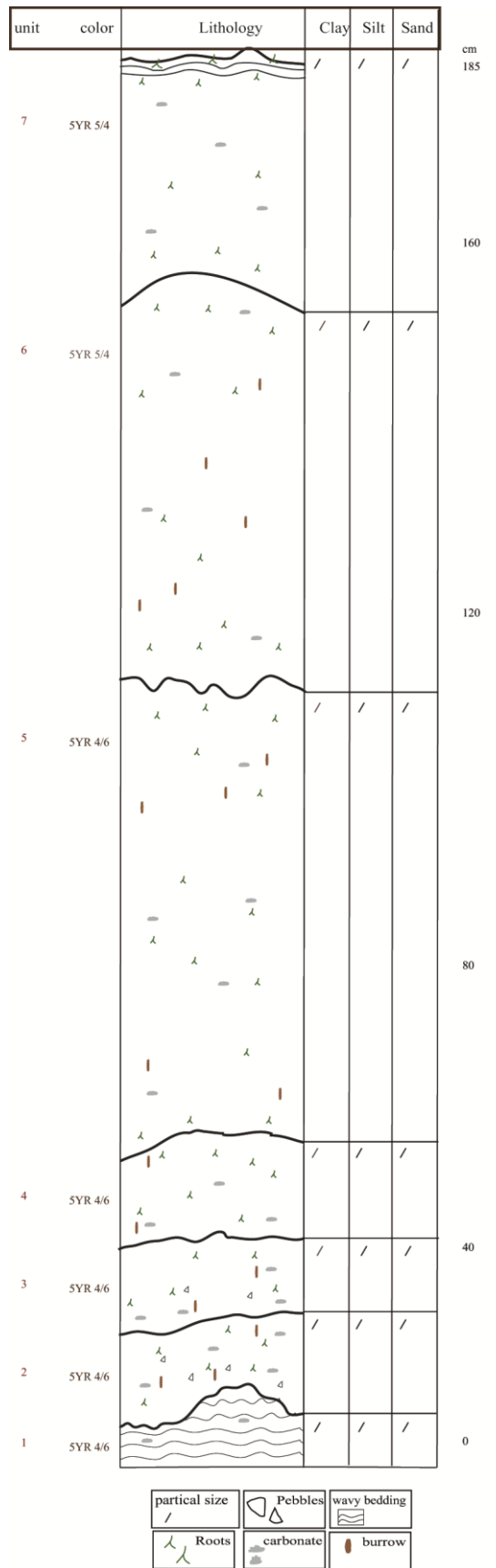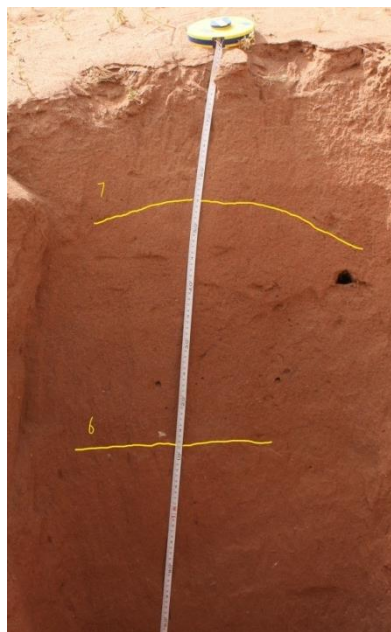
Figure 5.19: Schematic sedimentary log and view of section M11 Aeolian deposits in the sand ramps deposits, on the inside wall of the crater of Hurumah volcano.
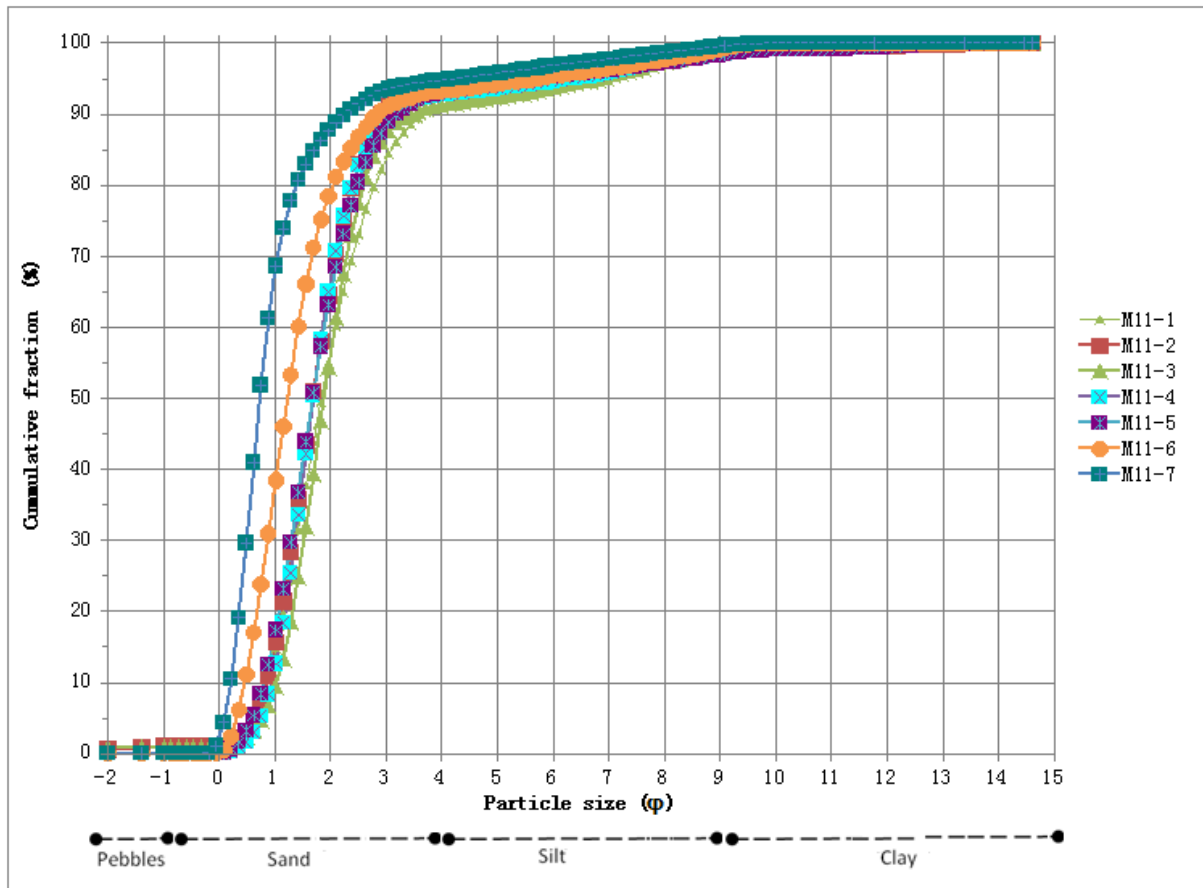
Figure 5.20: Cumulative percentage curve of the grain size composition for section M11 in the sand ramps deposits, on the inside wall of the crater of Hurumah volcano.

5.1.5   Palaeolake Deposits

5.1.5.1   Palaeolake Deposits in the Interdunes, in Western Nufud Al Qawz M12

This area consists of a palaeolake over which Nufud Al Qawz was deposited. Section M12 was nominated, and is situated in an interdune in the western part of Nufud Al Qawz (N 24°36`59.5"-E 40°54`19.6"), at an elevation of 872 m (Figure 5.18). The section was excavated; it is composed of 7 sediment units and is 105 cm thick as illustrated in Figure 5.21.

The first unit is 17cm thick, and composed of GLEY1 7/1light greenish gray silty clay with minor amounts of sand. XRD analysis shows that the deposit is high in silicate 84.9% (quartz 68%, plagioclase feldspar 9.9% and alkali feldspar 6.9%), with a high amount of clay 9% (just mica) and some amphibole (5.9%). It has wavy bedding, and many roots and burrows are present, as well as a few yellow spots of iron oxide. The unit is separated by a wavy and unconformable boundary from the 2nd unit above, which is similar in all its characteristics but some amount of carbonate and burrows present in unit 2, along with sand lenses concentrated in the upper part of this unit.

The third unit is 2.5Y 6/3 light yellowish brown in colour, and 16cm thick. It is composed of silty clay and minor amounts of sand, with a small quantity of very fine, and fine sized sub-angular pebbles. Sediments are cemented by carbonates, roots are abundant, some burrows and sand lenses can be found, and the number of yellow spots here is greater than in the units below. A wavy boundary separates this unit from the fourth unit above, which is similar in colour and the presence of roots. The amount of burrows is however greater in the fourth unit, whilst the amount of pebbles is significantly less, and of a very fine size, only in a clayey silt with minor sand matrix. As the XRD analysis in this unit shows, the deposit contains high amounts of clay minerals 13.6% (chlorite 7.4% and mica 6.2%), and silicate 74.2% (quartz 58.1%, plagioclase feldspar 7.6% and alkali feldspar 8.4%). Additionally, the number of yellow spots present is much less in unit 4. The fourth unit is distinguished by the presence of large, non-uniformly shaped masses of carbonates that cement the deposits together. It also has some fossils (leaf impressions), as the amount of calcite is around 8.2%. Moreover, there are desiccation cracks filled with sand, separating the layers of carbonic sediment. Unit 4 also has 3.8% amphibole.

The fifth and sixth units are composed of a 10YR6/4 light yellowish brown silt and sand matrix, with minor amounts of clay, and a very small amount of very fine sub-angular pebbles. The amount of sand increases towards the sixth unit. XRD analysis shows that the deposit in unit 6 contains higher amounts of silicate and lower clay minerals in comparison to unit 4, with there being 76.4% silicate (quartz 60.6%, plagioclase feldspar 7.7% and alkali feldspar 8%), and about 10% of clay minerals (chlorite 4.9% and mica 5.1%). Roots, burrows and carbonates (13.5%) are spread across the units. The carbonates have cemented the deposits together, but not strongly, and the units have desiccation cracks.

The seventh unit is 14cm thick and composed of 7.5YR5/6 strong brown coloured, fine sand, and minor amounts of silt, with a very small amount of very fine sized sub-angular pebbles. The properties of the sediments, in terms of size of grain, and high proportion of fine, uncemented sand are characterised by a strong brown colour, which all indicates evidence of windblown activity. There are some roots present, and the upper boundary is wavy and unconformable in nature.
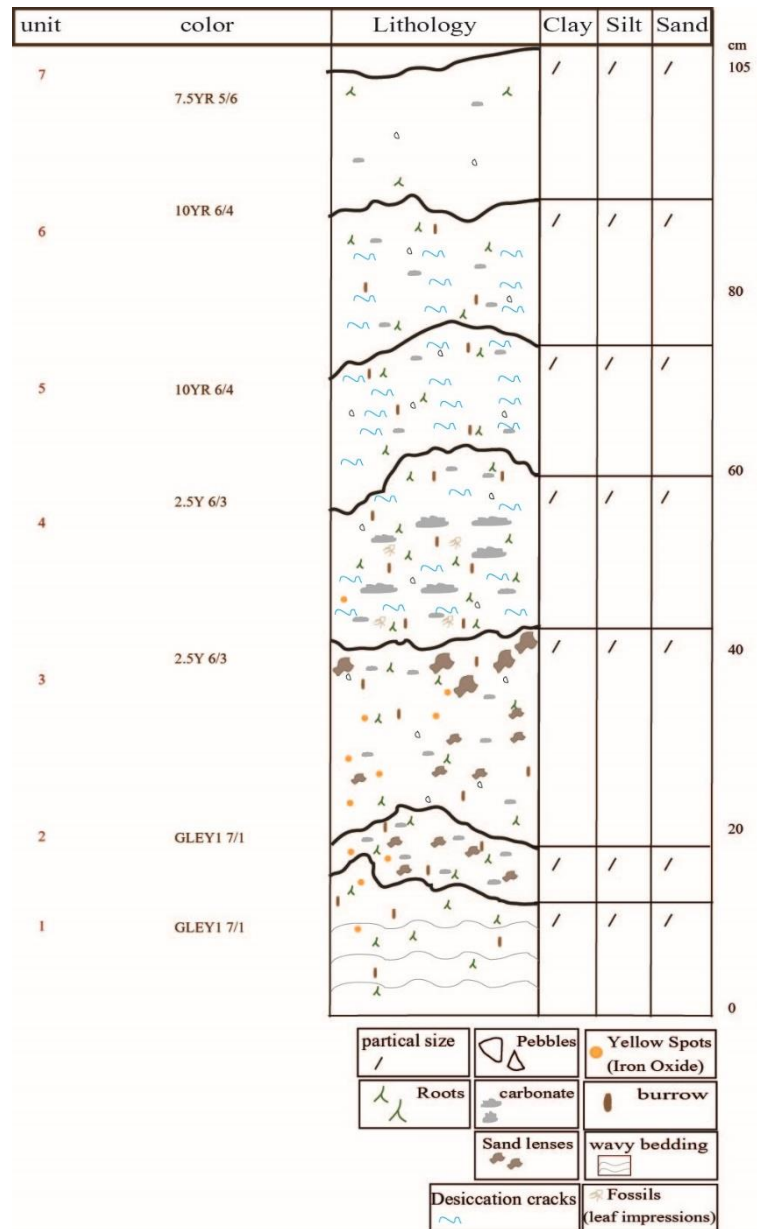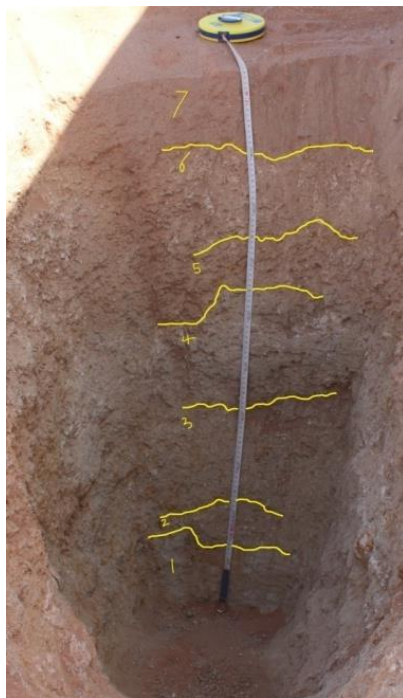
Figure 5.21: Schematic sedimentary log and view of section M12 palaeolake deposits in the interdunes, in western Nufud Al Qawz.

5.1.6 Sabkha deposits

5.1.6.1 Sabkhat Hurumah deposits Section M10

Sabkhat Hurumah is situated in the crater of the Hurumah volcano situated in the south west of the study area. Sabkhat Hurumah extends over the entire crater, an area of 25.3 km^2, with a mean elevation of 758.9 m. The height of the crater walls /edges that surround the Sabkhat is 57.7m (Figure 5.18).

Section M10 lies in the deposits inside the crater of the Hurumah volcano (N 24°34`04.0"- E 40°20`14.6"). The section was excavated, and is composed of 13 sediment units, as illustrated in Figure 5.22.

The first unit is 51cm thick, composed of 7.5YR 5/3 brown clay with a little sand. XRD analysis in this unit shows that the deposit contains amounts of silicate 58.4% (quartz 37.15%, plagioclase feldspar 13.65%, alkali feldspar 7.63%) and high amounts of clay minerals 14.9% (chlorite 7.55%, mica 7.43%). The unit also has some calcite (10.20%), halite (9.64%) and amphibole (6.75%). The unit is massive, contains some burrows and roots, and is separated by a wavy boundary from the 2nd unit above, which is considered to be mostly similar, although the amount of sand is significantly less than in the 1st unit. XRD analysis in unit 2 shows that the deposit contains 43.5% silicate (quartz 27.59%, plagioclase feldspar 9.91%, alkali feldspar 6.08%). Moreover, the proportion of halite increases in the second unit, reaching 24.76%. In addition, there are more roots and burrows in unit 2 compared to unit 1.

The third unit is 2cm thick, and is a palaeosurface, which is strongly cemented due to the presence of calcite and gypsum. XRD analysis shows that the deposit contains high amounts of gypsum (43.63%), with some amount of silicate 49.5% (quartz 23.01%, alkali feldspar 17.11%, plagioclase feldspar 9.41%) and calcite (6.84%), indicating conditions of a high level of dryness. The pattern of sedimentation begins to differ compared to the two lower units. Indeed, sand deposits are predominant. The fourth unit contains a 7.5YR 6/4 light brown coloured matrix of silty sand in the form of fine laminations. It also contains some carbonates, burrows, roots, organic matter, and a wavy upper boundary.

Units 5 to 8 are composed of a 7.5YR5/4 brown, silty sand matrix, with an extremely small quantity of clay in the form of laminations, except for the seventh unit, which does not

contain laminations, and has more roots than the others. They contain carbonates, a lot of organic matter, roots and burrows.

The ninth unit is 9cm thick and 7.5YR5/3 brown coloured. Its matrix is composed of clay, and a very small amount of silt, massive. The XRD analysis shows that the deposit contains some amount of silicate 39.6% (quartz 19.82%, plagioclase feldspar 10.11%, alkali feldspar 9.73%) with high amounts of clay minerals 18.3% (mica 9.73%, chlorite 8.64%). Furthermore, this unit has some amount of halite (8.06%), calcite (6.72%), amphibole (7.74%) and bassanite (19.45%). Its matrix contains some roots and burrows, and the unit is separated from the one above by a wavy boundary.

The 10th unit is a 2cm thick strip containing a large quantity of halite mixed with a little clay. This halite also spread to the 11th unit above, which contains quantities of clay with silt and a very small amount of medium to coarse sand. XRD analysis shows that the deposit is rich in silicate 72.6% (quartz 52.05%, plagioclase feldspar 14.12%, alkali feldspar 6.47%) with some amount of clay minerals 13.5% (chlorite 6.06%, mica 7.46%). In addition, halite, comprising of 8.28%, appears in the unit as cemented desiccation cracks, which indicates dry conditions. Amphibole (5.55%) can also be found. The upper part of the 11th unit contains some roots and burrows.

The amount of sand begins to increase as we move upwards; the 12th unit, which is 14cm thick, is composed of 7.5YR4/4 brown coloured matrix of indurated silty clay with sand; XRD analysis in unit 12 shows that the deposit contains some amount of silicate 26.6% (quartz 10.05%, plagioclase feldspar 11.27%, alkali feldspar 5.37%) with 12.3% of clay minerals (chlorite 6.76%, mica 5.55%). In this unit, the proportion of gypsum (33.2%) and halite (22.5%) rises compared to previous units, and appears as cemented desiccation cracks. This unit is devoid of carbonates, while amphibole (5.20%) is present, indicating dry conditions. Unit 12 also has some burrows and roots, and its upper boundary is wavy in form. The unit above is of the same colour, but the amount of fine sand present is greater, with some silt and clay present. XRD analysis in unit 13 demonstrates that the deposit contains 54.4% silicate (quartz 37%, plagioclase feldspar 3.42%, alkali feldspar 13.96%) and 12.2% of clay minerals (chlorite 7.69%, mica 4.56%), as well as amphibole (5.13%). Moreover, the unit contains gypsum (28.2%), while calcite and halite are not present. Roots and burrows are absent. From this, the presence of dry conditions is very clear; these conditions are similar to the present day's dry condition.

At the top of the section, large amounts of gypsum and quartz mixed with clay and sand are spread across, which further indicates very dry conditions.
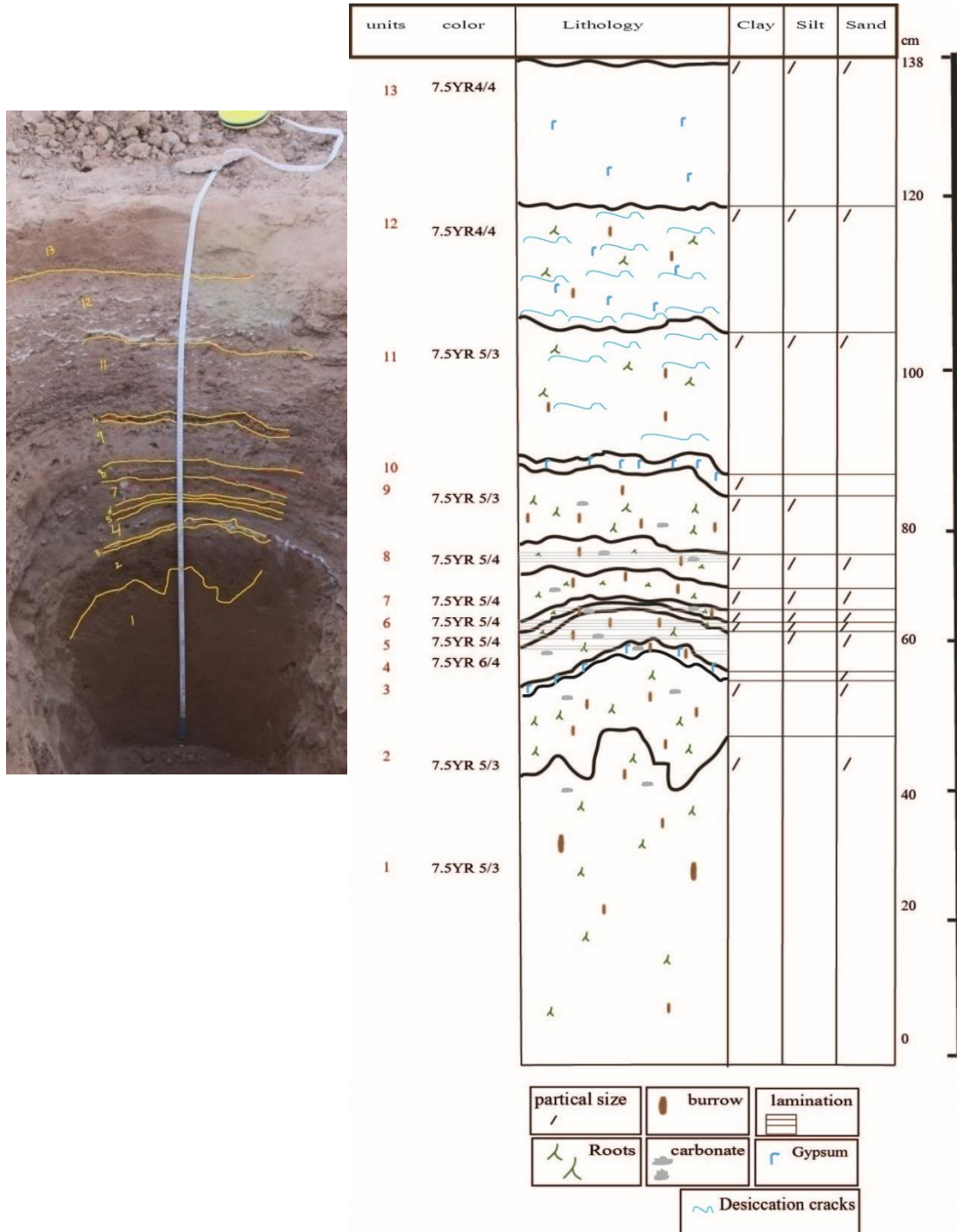
Figure 5.22: Section M10 in the deposits inside the crater of the Hurumah volcano and schematic representation of the strata.

5.1.7 Slope Wash Deposits

5.1.7.1 Slope Wash Deposits in the Reg Surface M2, Western Nufud Al Qawz

Section M2 lies in the basin of Wadi Um Markhah west of Nufud Al Qawz. This Wadi flows from Jada Mountain at an elevation of1180m, and proceeds south, then west to end up feeding into Wadi Al Makhit. The section is located in the slope wash area of the surrounding mountains (Dayin Mountain, Huwayqat Mountain, Jada Mountain, Dilan Umm Uruq and Dilan as Sifr). Here, water deposits sediments, which accumulate to form different types of level surfaces and small hills. One of these hills was selected (M2) to determine its characteristics. The M2 section was cut through a reg slope surface on a bedrock adjacent to a barchan, to the west of Nufud Al Qawz (24° 39` 43.9`` N - 40° 44` 42.6`` E), at an elevation of 843 m (Figure 5.18). The section studied is 50 cm thick and is composed of four sediment units as illustrated in Figure 5.23.

The first unit is 22cm thick and is 2.5YR5/4 reddish brown in colour, with a layer of cobbles at the base. Its texture is principally composed of silty sand, with 14% angular and sub-angular fine to medium sized pebbles. This unit is very poorly sorted, and the particles are cemented together by carbonates. There is evidence of some wavy sub-beds within this unit, but there is no change in texture between them. Some roots and burrows are present. The unit's upper boundary has a wave form and is unconformable in nature.

The second unit is10cm thick, and is 7.5YR5/4 brown coloured. Pebbles represent around 44% of its composition, and thus, they are more abundant than in the unit below. The pebbles are angular and sub-angular in shape, and very fine to medium sized. The unit has some quantities of very coarse sand, and is very poorly sorted, with small cemented clasts. Some roots and burrows are present, and the upper boundary is wavy.

The third unit is 8cm thick and is similar to unit 2 in terms of lithology, colour, and structure. However, the pebbles composition is greater than in the second unit, reaching about 52%, and so is the unit with the highest pebbles content. The pebbles are angular to sub-angular in shape, mainly medium sized, with small quantities of sub-rounded cobbles. In addition, this unit contains some very coarse sand and some carbonates. It is very poorly sorted, and has some roots and burrows. The upper boundary of this unit is unconformable.

The fourth unit is 10cm thick, 2.5YR5/4 reddish brown coloured, and extremely poorly sorted. Its texture is generally composed of silty sand, but in contrast to the two units below

it, the percentage of medium sand is greater than that of very coarse sand. The unit also contains quantities of angular and sub-angular pebbles (35%), where coarse size is dominant, with small quantities of cobbles. Some roots and burrows are present; on the unit's upper part is a small amount of root. Lastly, its boundary is unconformable.

The surface layer of the section is composed of sand, pebbles, cobbles, and very few roots.

Figure 5.23: Schematic sedimentary log and view of section M2 at slope deposits in the reg surface, western Nufud Al Qawz.
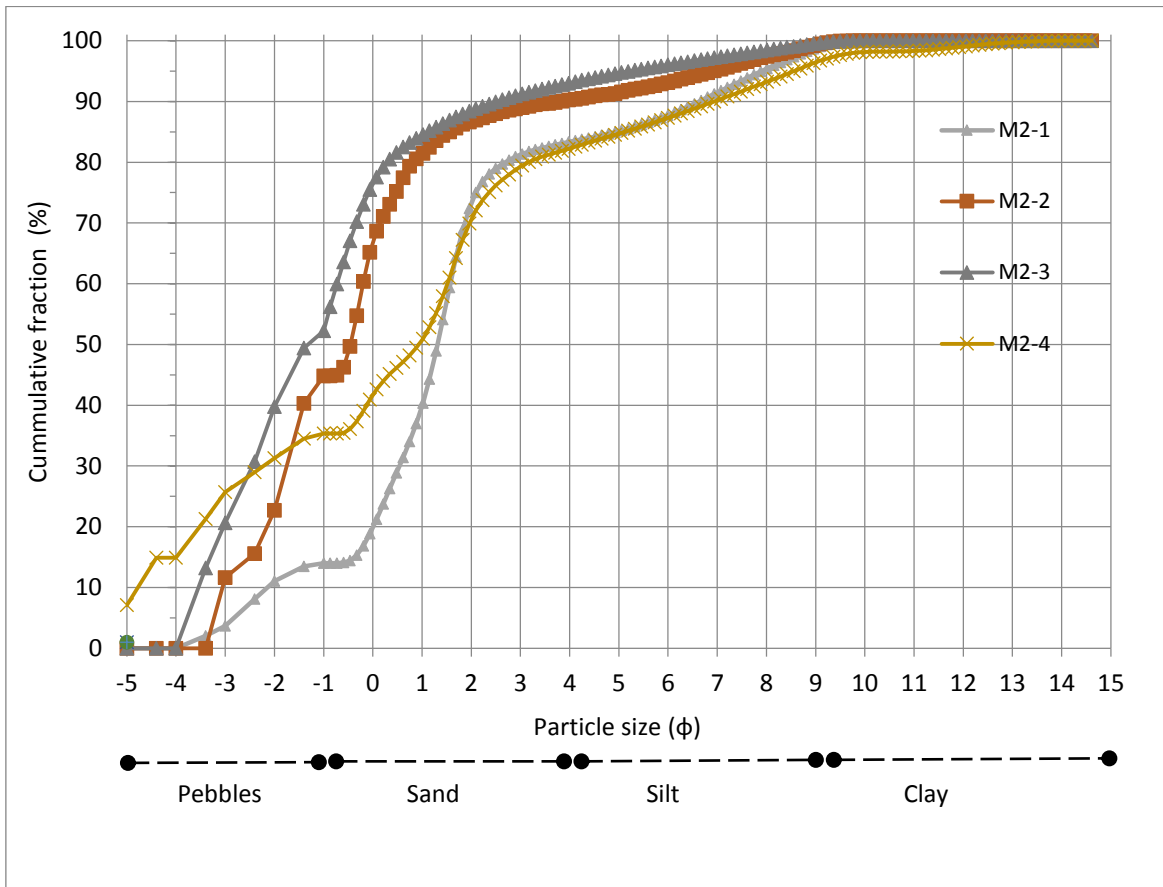
Figure 5.24: Cumulative percentage curve of the grain size composition for section M2 at slope deposits in the reg surface, western Nufud Al Qawz.

Chapter 6. Discussion

In this chapter, the study results are discussed as follows:

6.1. Remote sensing for geomorphological mapping.

6.2. Evolution of the study area and late Quaternary sediments: an interpretation.

6.3. Provisional correlation of the palaeogeomorphology /palaeoenvironment events during the late Quaternary period, in the Al Madinah province and surrounding areas.

6.1   Remote Sensing for Geomorphological Mapping

The results of this study revealed that remote sensing data has contributed to mapping and interpreting the landscape in the Al Madinah region. This region has not been studied before, and knowledge on this area is very limited. In this study, remote sensing data provided valuable information about this region.

The ASTER GDEM has contributed to extracting the drainage network (wadis and basins), as well as identifying the characteristics of the landscape, such as elevation and slope. With the ASTER GDEM, it was possible to divide the Al Madinah region into two large drainage basins containing a set of sub-drainage basins (Figure 4.4):

1. Wadi Sahuq drainage basin: the elevation and slope gradually decreases eastwards towards Al Qassim then outlets to the Arabian Gulf (Figures 4.1 and 4.2).
2. Wadi Al Makhit drainage basin that takes a westward direction and outlets to Qa Hadawda, where elevation and slope reduce going westward (Figures 4.1 and 4.2).

Processing Landsat 8 multispectral data using PCA, band ratios and false colour composite, contributed to a better understanding of the distribution of different sediments within Al Madinah region (Figures 4.12-4.28). Highlighting these spectral changes helped in the interpretation of the landscape of the East Al Madinah region (emphasising sediment source, transport pathways and depositional locations that formed the principal geomorphological features in the area).

234

Accordingly, the maximum likelihood supervised classification followed by majority-minority filtering successfully mapped the eleven geomorphological units (Figure 4.40), sand dunes, sand sheets, sand ramps, wadi deposits, slope, Qa, sabkha, intermountainous basins, Sahuq plateau, and the East Al Madina plateau. Based on randomly selected regions of interest, these geomorphic units were confirmed during field visits. The classification's overall accuracy is 80.84% (kappa coefficient= 0.778); this differs from the classification accuracy achieved in the Al dughairi and Al Jaddani (2016) study on the Wadi Al Fuwayliq basin in central KSA, reaching 93.50%. This may be attributed to their limited study area, with highly spectral contrasted classes, which increased the overall accuracy.

Using image analysis, the major geomorphological features and their distribution within the study area (Figures 4.41, 6.1) are as follow; tributaries (wadis) branching off wadi Al Makhit flow to Qa Hadawda to the west, carrying very fine sediments (silt and clay) due to the low slope $0 - 2°$ (Figure 4.2). The Qa appears in cyan blue within the PCA colour composite (Figure 6.1), and sabkhas deposits were found to be concentrated within harrat area (lava flows), to the west of the study area. The largest is Sabkhat Hurumah, which appears in cyan yellow within the PCA colour composite (Figure 6.1), which is situated in the crater of the Hurumah volcano. In Figure 6.1, aeolian deposits appear in pink; sand dunes are clearly concentrated in Nufud Al Qawz, and to the west of Nufud Al Qawz can be found barchans dunes. Sand sheets were recorded within the study area, particularly to the east. Slope deposits are also present close to the mountain areas.

The spectral variation is quite complex, therefore, the focus will be on two sub-basins, and describe how the image analysis can be used to describe composition and mixing of sediments, and infer the geomorphic processes playing out in this area. The sub-basins used are Um Markhah and Al Mahir sub-basins (as an example):
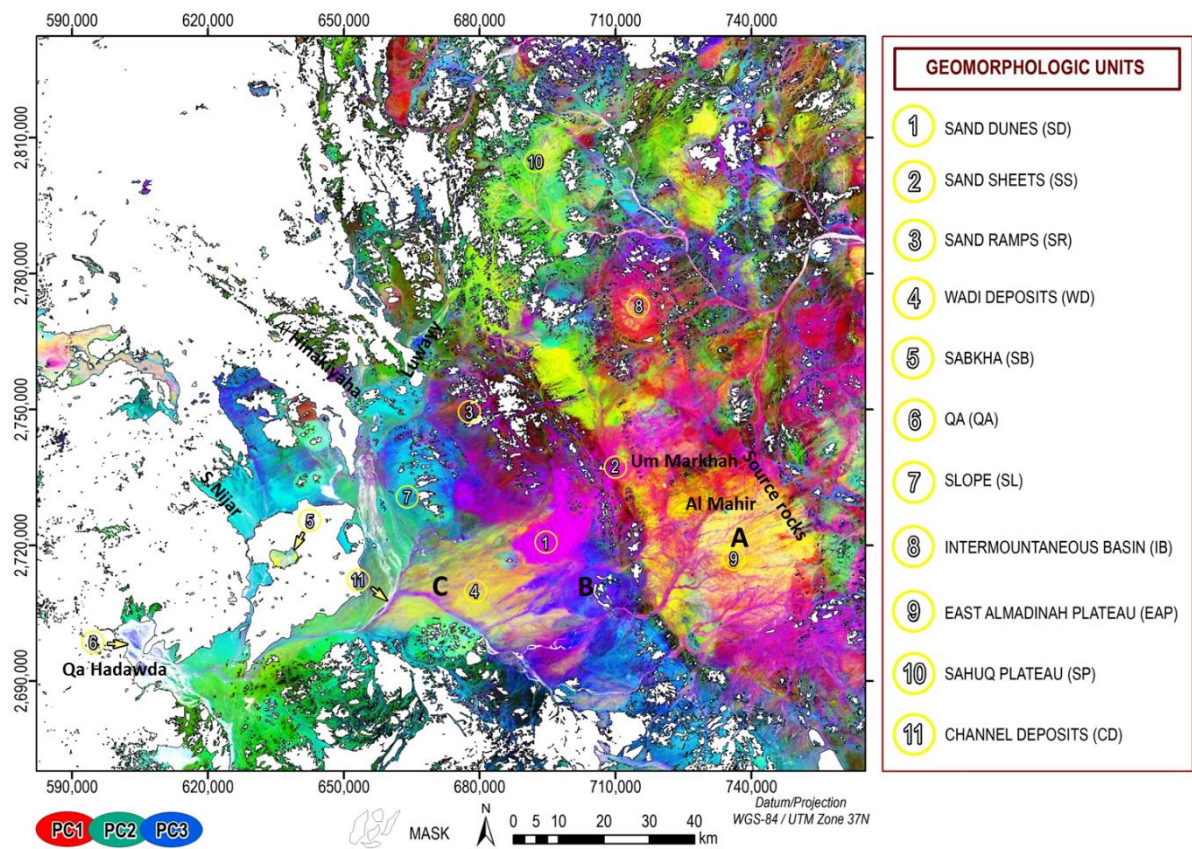
Figure 6.1: Spectral characteristics of Um Markhah and Al Mahir sub-basins, in Principal Component Analysis (PCA).

The Wadi Um Markhah and Al Mahir sub-basins (Figure 4.4) situated in Wadi Al Makhit basin were selected for a detailed description of their spectral characteristics. The purpose was to use the spectral differences to identify and discuss the source of deposits found in the landscape. This included deposit location and transport processes, which led to the principal geomorphological features currently present. PCA (Figure 6.1) shows that Wadi Al Mahir and Um Markha sub-basins contain three parts:

1. The first part (A) is situated within East of Al Madinah plateau, appearing in yellow violet colour, and is composed of granite.

2. The second part (B) is situated in the central area as slope deposits, appearing in blue, and is composed of basalt, andesite, and rhyolite.

3. The third part (C) is situated to the west, there are wadis deposits appearing in yellow violet to bluish colour, essentially composed of granitic mineral.

Considering the colour differences between deposits in the PCA colour composite (Figure 6.1), sediments seem to be transported from the heights of East Al Madinah plateau area (A), westwardly passing between the heights in area (B), and mixing with the deposits there. These then proceed to area (C), appearing in a yellow violet to bluish colour as a result of passing through the heights in the central area. However, these continue to possess the same characteristics as the source, and this can be distinguished quite clearly from the image. Here, some of the deposits from area (C) are dropped from the load due to the low slope of the area (Figures 4.1 and 4.2). Therefore, wadi sediments are deposited here, while the remaining fine sediment such as silt and clay, continue their journey to Qa Hadawda. It is also apparent from the PCA (Figure 6.1) that aeolian deposits, appearing in pink, are concentrated largely in Nufud Al Qawz (as shown in number 1 in Figure 6.1). Sand sheets are spread quite clearly to the east and north-east of Nufud Al Qawz, originating from there. This is in agreement with the prevailing direction of wind in Al Madinah, where it is subjected to winds coming from the west. Due to the dominance of dry conditions and wind activity in the present day, aeolian deposits (pink colour) are found on the features. This interpretation of spectral differences can be applied to the remaining basins in the area to interpret the sediment source, movement, and locations where deposited.

In the current study, an attempt was made to assess the ability of Landsat 8 data in mapping the relative proportion of fine and coarse materials in one part of the East Al Madinah

plateau. This was possible as the current study's results revealed a good correlation between both image and laboratory measurements of the reconstructed surfaces (Figure 4.29). This demonstrates the suitability of Landsat 8 data in mapping the geomorphological units based on their spectral behaviour in visible-NIR spectral regions.

A transect spectral profile was made within the East Al Madinah Plateau (Figures 4.31, 4.32), and effectively used to estimate the grain size distribution. It found that upstream, the surface was predicted to be more coarse grained, while downstream, the surface was predicted to be more fine grained (Figures 4.31, 4.32). With more research, this shows a potential to spatially map the relative proportions of fine to coarse grain sediments over large areas, and work out some geomorphic processes. In future work, other surface samples transects can be done in several other areas to find out whether the results are applicable to these other locations. The results of the current study have also illustrated that the mineral composition and grain size of the deposits are the most effective elements on their spectral behaviour (Figures 4.12-4.28). This was also indicated by both Al-Juaidi (2003), Bullard and White (2002).

6.2   Evolution of the Study Area and Late Quaternary Sediments: An Interpretation.

Given that the present is the key to the past, thirteen sections were selected to find out whether there are differences between the environment today and the palaeoenvironment. The remote sensing data acquired points to the dominance of wind activity due to the spread of sand sheets in the area, appearing in pink colour (Figure 6.1). Moreover, the all upper parts of the stratigraphic sections (Figures 5.2 to 5.23) also support the dominance of this wind activity. Figure 6.2 illustrates the huge accumulation of sand sheets in the wadi channels, alluvial fans, and on the slopes of the mountains, largely due to the activity of the Shamal wind. This activity is evidenced and confirmed by the effects on the rock surfaces, which are smooth, as in Figure 6.2b, in Wadi Luwayy. In addition, the presence of black basaltic sand covering parts of the sand dunes, concentrated in the west of Nufud Al Qawz confirms wind activity. Dark sand has been transported through wind erosion from the mountains in the vicinity of Al Nufud to the north and west, as in Figure 6.3.

The evidence from the stratigraphic sections supports the idea that the area was subject to wet periods, during which Nufud Al Qawz was a palaeolake (Figure 5.21), and area C was

a large flood plain (Figures 6.1, 5.17). Remote sensing also points to remnants of this palaeoloake. The effects of this palaeolake are represented by the presence of bright sands (light white evaporites and calcium carbonate) on the surface, as shown in Figure 6.3. These sands are concentrated significantly in the east of the Nufud and the interdune areas.

Figure 6.2: (a) Dominance of sand sheets and nabkahs in the alluvial fans of Wadi Luwayy, (b) Ventifacts: the effect of wind on rocks in Wadi luwayy, (c and d) sand sheets and nabkahs cover the channel and terraces of the lower catchment of Wadi Al Hinakiyah, (e) sand sheets are prevalent on the slopes, as shown in number 2 in Figure 6.1.
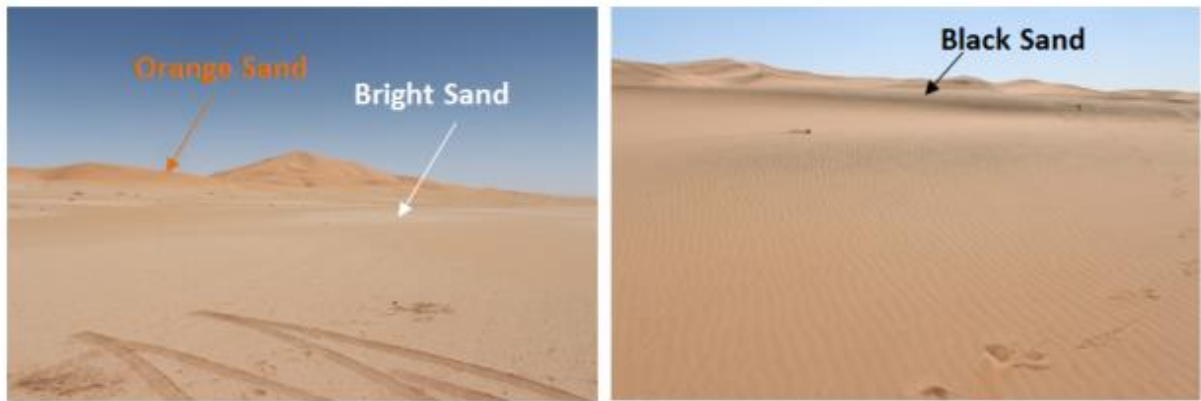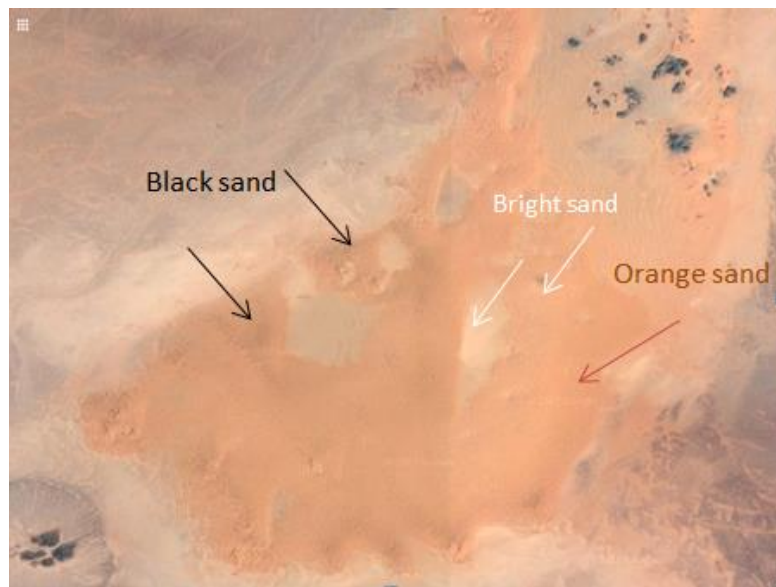
Figure 6.3: Contrasting sand colour in Nufud Al Qawz. (A and B) field photos, (C) satellite image.

The palaeolake perhaps received water from two principal sources; the first being nearby springs/wells, an assumption supported by the abundance of springs (wells) near Nufud Al Qawz (east of Nufud Al Qawz) (Figure 6.4). The second source are the wadis coming from the Al Madinah eastern plateau (such as Wadis Al Mahir, Al Hidiqiyah, and Khadra), as well as smaller wadis originating in the mountain slopes encircling Nufud Al Qawz to the east and west, such as Kihlah, Dilan al Qunfudhi, and Barqa al

Fuhud heights. These small wadis flow down and supply the palaeolake with water, then continue to Qa Hadawda, which was also a body of water. This is supported by the hydrologic network extracted from the ASTER GDEM, as in Figure 6.7. These wadis contributed to the formation of flood plains in the area surrounding Nufud Al Qawz due to the shallow slope; hence, the wadis would deposit their sediments in this area (the white area east of south of Nufud Al Qawz in Figure 6.7; area C in Figure 6.1). These formed flood plains according to the evidence found in section M1 (Figure 5.17).

The formation of sand dunes on top of the palaeolake was due to the change of the palaeolake from a wet to a muddy environment with the onset of dry conditions, and reduced water level (Figure 5.21). This, along with other factors, helped in capturing and holding the accumulation of sand, leading to the formation of Nufud Al Qawz in this location. These factors are:

   a. the presence of large amounts of wadi sediments that were deposited in the area of the flood plains surrounding Nufud Al Qawz, which are considered an important source providing dunes with sand.
   b. The bedrock, where there are exposed sandstone formations near to Nufud Al Qawz, which are considered an important source supplying sand to the dunes, as shown in the geology map (Figure 1.6).
   c. The activity of the Shamal wind during dry periods contributed to the transport of sediments (whether from the sandstone bedrock, flood plain or wadi deposits), and deposited these at the palaeolake bottom.
   d. The presence of nabkahs and mountains to the east and north of Nufud Al Qawz and environment for building and accumulation rather than one of erosion and transport (Figures 6.4, 6.8).

The star-shaped dunes in Nufud Al Qawz may have been the first phase around which Nufud Al Qawz was formed. These star dunes were formed as deposits, either on top of rock surfaces or springs, where water flows from the springs, led to the growth of the star dune; particularly since one of the star shaped dune which is situated to the north of Nufud Al Qawz, around which there are white surfaces. This supports the argument that it was perhaps the influence of springs that led to the initial formation of Nufud Al Qawz (Figure 6.5). However, these dunes grew to varying heights, and the wadis were unable to penetrate, and were forced to flow parallel to the Nufud Al Qawz dune field; for example, as in Wadi Al Mahir and Wadi Al Hidiqiyah (Figures 6.7, 6.8).

Similarly, sand ramps surrounding Sabkhat Hurumah, as in section M11 (Figure 5.19), which was formed because of the local wetness of the palaeolake that covered the volcano crater during wet periods. This in addition to wind activity and the availability of sediments

whether due to wind scavenging the surface of the sabkha during dry periods or from outside the sabkha from the surrounding areas. All these helped the slopes of the volcano spout to be a good place to capture and hold sand, hence leading to significant growth during dry periods. Indeed, Sabkhat Hurumah was a lake full of water, according to the evidence in section M10 (Figure 5.22). It perhaps attracted inhabitants to the area, as there are remains of an abandoned village today (Figures 6.6, 6.7), which consisted of cultivated areas, wells, a cemetery, and homes on the edge of the sabkha, next to the slope of the Hurumah volcano crater.

Regarding barchans found close to Nufud Al Qawz to the West, the presence of small, scattered hills, which were formed due to the wash from the slopes during old flows, led to the capture and holding of sand and so the growth of barchan dunes in the area. Also, the presence of the bedrock near to Nufud Al Qawz and the mountains enclosing the area to east and west contributed to the wind blowing from one direction only, leading to formation of these barchan dunes.
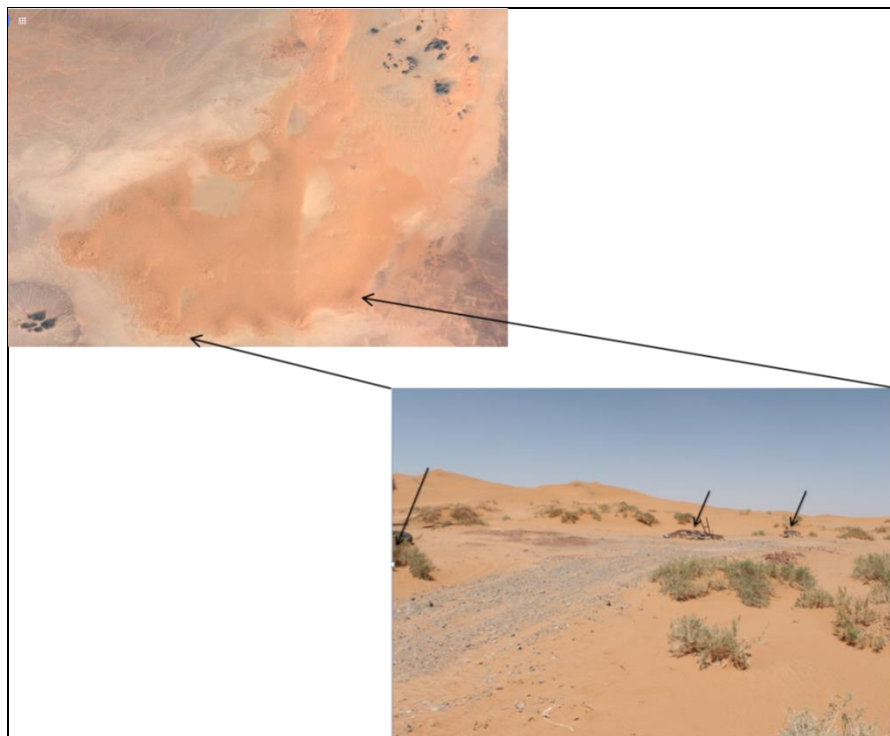
Figure 6.4: Abundance of wells around Nufud Al Qawz.

Figure 6.5: White surfaces and star dune north Nufud Al Qawz.

Figure 6.6: The currently abandoned village in Hururmah volcano crater.
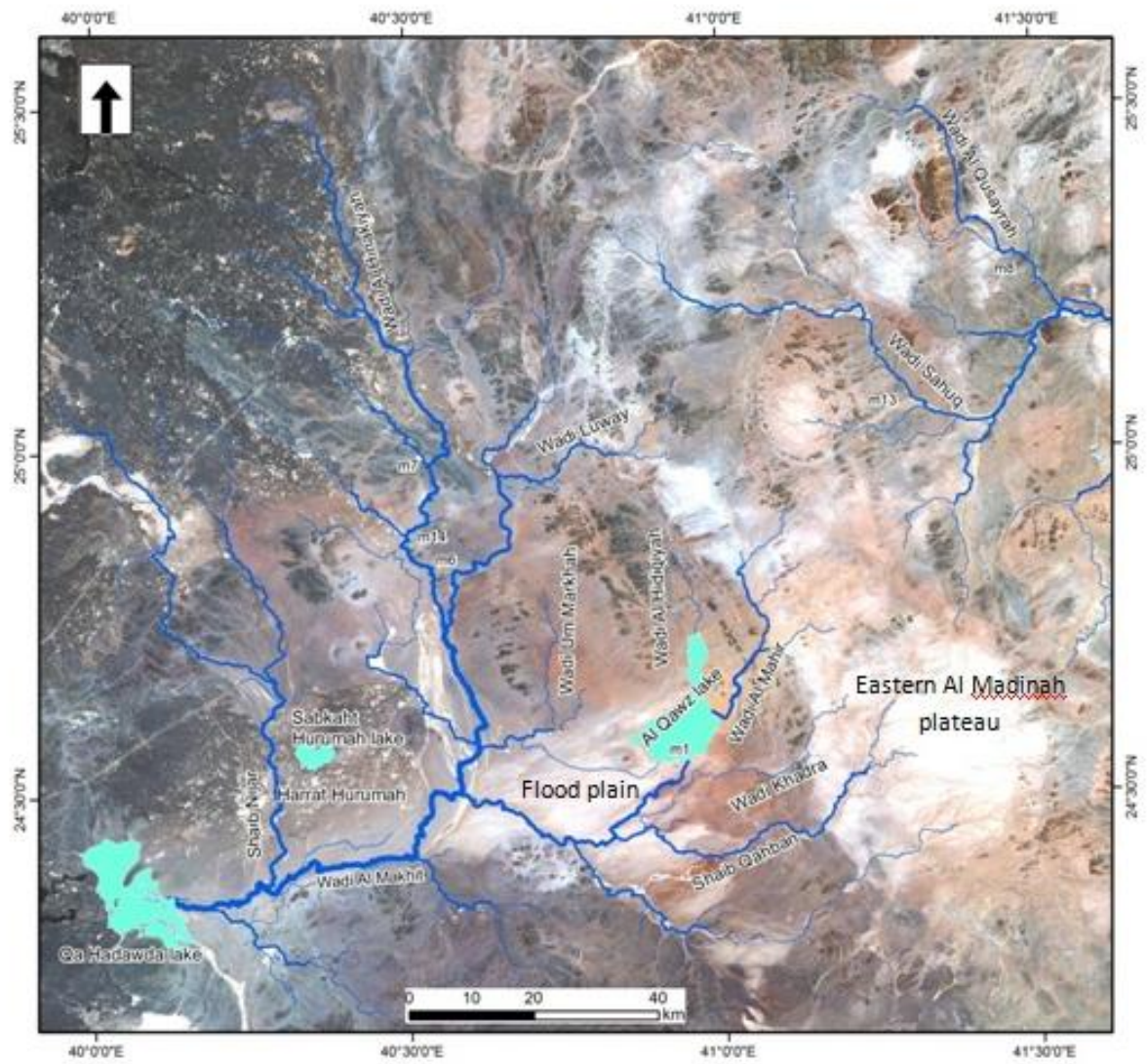
Figure 6.7: Palaeogeographic map of Al Madinah during the early Holocene.
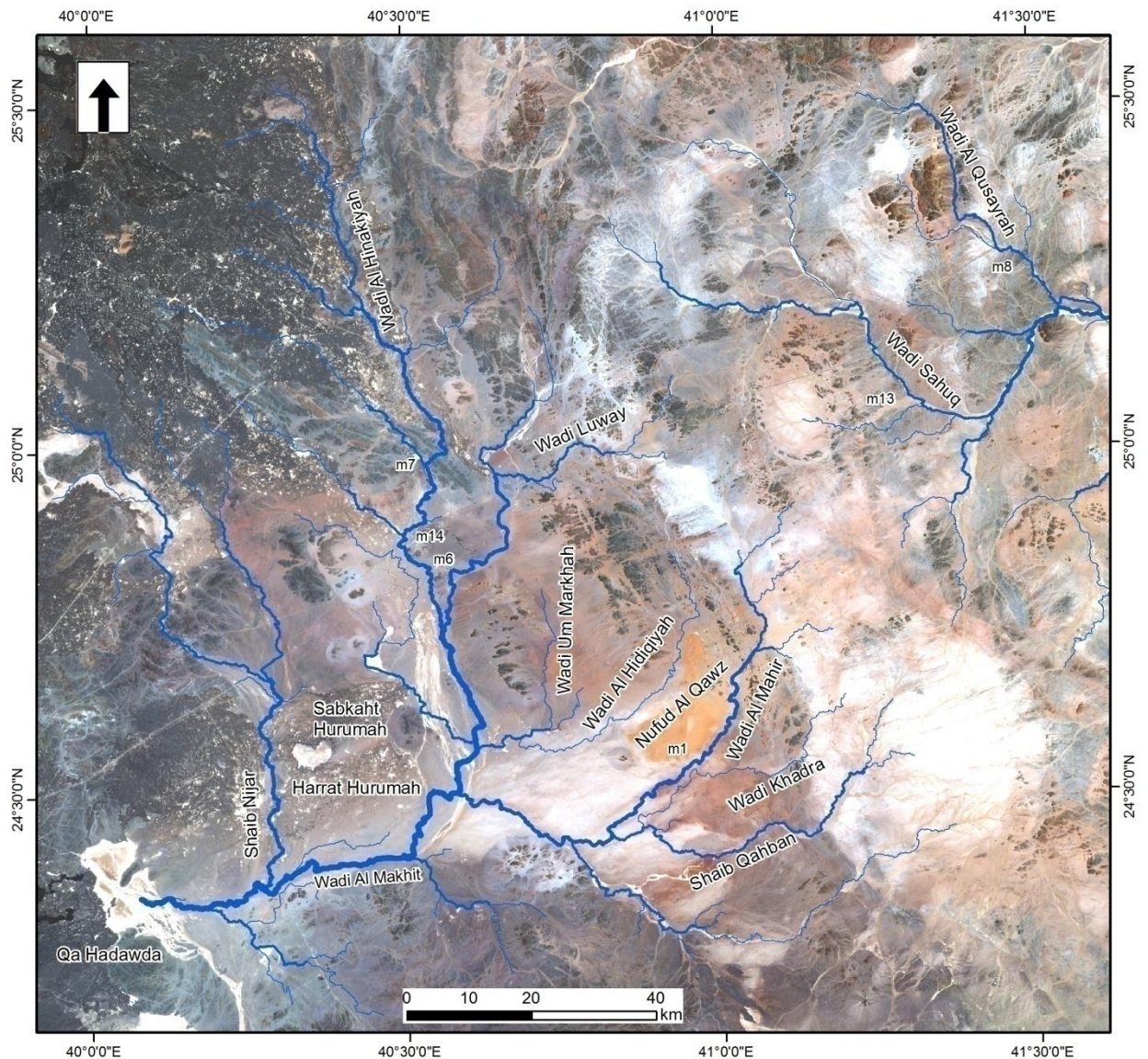
Figure 6.8: Map of Al Madinah during the late Holocene.

A general and comprehensive insight into the palaeoenvironment and palaeogeomorphology prevailing in the Al Madinah region in the late Quaternary period is derived from a discussion of the results acquired from evidence preserved in the sections of the study areas. These results are linked to those reported by Al Dughairi (2011), whose investigation was conducted close to the current study area. Indeed, the upper catchment of wadis in Al Madinah are near to the upper catchment of Wadi Al-Rimah in Al Qassim. Hence, it is expected that these witnessed the same palaeoenvironmental conditions. Therefore, they may be relied upon in approximate dating of deposits in Al Madinah, which have only been

dated in a limited way (figures 6.12, 6.13). The findings acquired from evidence preserved in study area sections are discussed below:

6.2.1. Interpretation of origins and development of wadis and alluvial fans in Al Madinah

The origin of alluvial fans has been linked to the flows of those wadis that descend from the east and west of the Marurah mountains. As such, their origin is addressed combined with that of wadis. The Al Madinah wadis witnessed low energy flows that were followed by a sedimentation cycle corresponding to the flow ceasing for a limited time. This period may have been quite short, due to the presence of a palaeosurface rich in quartz and sodium. These flows occurred prior to 83ka, based on OSL analysis of samples taken from the alluvial fan in Wadi Luwayy (Figure 5.15). Moreover, the characteristics of these deposits match the description reported by Al dughairi (2012) for Wadi Al Tarfiyah, dating back to 105.5 ka. Therefore, the activity of Al Madinah wadis may be attributed to 105.5 ka. The activity of such flows in Al Madinah and Wadi Al Tarfiyah during this time coincided with Wadi Al Bathah in Oman, such that fluvial sands in the wadi terrace bear the indications of a significant flow that dominated the phase MIS5c (Juyal et al., 1998). Fluvial sand accumulation was also quite apparent in the alluvial fans in Ras Khaimah in UAE, during 108 ka (Stokes and Bray, 2005).

The lower parts of Al Madinah wadis also witnessed flows varying between gentle and medium strength flow, such that fine to coarse grain sand with gravel fluvial deposits are dominant (Figure 5.10). Subsequently, the wadis witnessed flows where fluvial sand deposits were dominant during wet periods. These flows are interrupted by periods when flows ceased, as evidenced by the presence of aeolian deposits. This agrees with the description for Wadi Al Butaun deposits given by Al dughairi (2011), which he dated at 77.2-85.5 ka, as in Figure 6.9a. Al Madinah Wadis continued to flow in subsequent periods dating back to 34.2±2.5ka, as was the case of Wadi Al Hinakiyah, based on OSL analysis (Figure 5.6). Deposits indicate that flows were strong, accompanied by floods, as evidenced by the dominance of fluvial deposits that are fine to coarse grained, along with sub-rounded gravel. In addition, the presence of roots and burrows preserved within these deposits indicates the existence of plants and organisms, corresponding to wet conditions. The

strength of these floods increases moving towards the top of these deposits. This is supported by the presence of cross-beds formed of fluvial deposits with well-rounded gravel, as well as the presence of roots, burrows, and carbonates reflecting wet conditions. This explains how Wadi Al Hinakiyah and other Wadis of the eastern Al Madinah plateau were able to arrive at Qa Hadawda (Figure 5.1). Moreover, the size of Qa Hadawda supports the view that the Al Madinah region witnessed significantly heavy rainfall of such a scale that it allowed wadis to cover these large distances to reach Qa Hadawda.

The massive activity in this wadi is concurrent with the activity in a number of other lakes in the same timeframe, such as those found in Al Qassim, as reported by Al dughairi (2011), pointing to them having been full of water before 34.5 – 33.2 cal Bp. This is also concurrent with the palaeolake in Al-Rub Al-Khali (McClure, 1976), and the activity in Al Khayzaran palaeolake in the Rub Khali during 35.9 – 36.4 cal Bp (Al dughairi, 2016). Additionally, this is similar to the findings by McLaren et al. (2009), Al-Juaidi (2003) in terms of the dominance of floods during the Pleistocene period (38.8 – 54 ka), which occurred at the same time as the formation of alluvial fans in Al-Quwaiayh, in central KSA.

In the subsequent phase, Al Madinah Wadis continued to flow, and contributed to the formation of alluvial fans in Wadi Luwayy in the early Holocene during 9.9±0.6-11.6±1.0ka, based on OSL analysis (Figure 5.13). The evidence observed points to active flows, reflecting the relatively wetter conditions than those at present, as evidenced by fluvial sand, allied to roots, burrows, and carbonate nodules preserved in the deposits. These flows also contributed to the formation of fluvial terraces, as in Wadi Al Hinakiyah. There, fluvial silt and sand deposits were encountered, containing roots, burrows, and carbonates. In addition, flows varied intermittently between gentle and high, as evidenced by the presence of flat and wavy beds.

These observations are in broad agreement with the description made by Al dughairi (2011) for deposits in Wadi Al Watah, which he dated to 10 ka, as in Figure 6.9b. He inferred this to be indicative of higher humidity. The fan activity examined in this study coincided with lacustrine deposits that were reported by Parker et al. (2006), Lézine et al. (1998), which developed in Yemen at approximately 11 ka. In the area of Al Qassim, situated in central Saudi Arabia, the upper area of Wadi Al-Rimah provides evidence of a humid climate prevailing in the period from 13 to 11 ka. Humid conditions during this period of 11.2 to 10.7 and 9.9 ka, is also evidenced by the presence of tufa in this area (Al dughairi, 2011).

This supports the conclusion that in the early Holocene, humid conditions were dominant. Moreover, according to Hötzl and Zötl (1978), the period around 9-9.5 ka cal BP, Wadi Al Luhy (21°N) was active. This is most likely a response to the strong penetration of monsoon winds (Fleitmann et al., 2004).

In the subsequent phase, Al Madinah Wadis' activity began to decrease based on the upper parts of Al Madinah wadi terraces; characteristic as shown in Figures 5.2, 5.4, 5.6, 5.8 and 5.10), coinciding with aeolian deposition, leading to growth of sand sheets, dunes, and nebaks (as in Figure 6.2, and the upper parts of the study sections in the results chapter). This is quite apparent in the characteristics of deposits in Al Madinah wadi terraces. Indeed, the upper parts of Al Madinah wadi terraces imply a clear reduction in the proportion of clay, silt, and carbonates, coinciding with a higher proportion of quartz (aeolian deposits), and the spread of nebaks. This supports the idea of a gradual change to arid conditions and weaker wadi flows. These may perhaps date back to the mid-Holocene. These deposits that were noted in Al Madinah are comparable to those described by Al dughairi (2012), which he dated to the mid-Holocene. He found that the early beginnings of weak flow in Wadi Al Tarfiyah date back to earlier than 5.1ka. This was accompanied by a notable increase in sand deposition in Wadi Raghwah, east of Nafud Al Sirr before 5.3ka, aeolian sand deposition activity in Nafud Uyun Al Jiwa before 4.7ka, and complete blockage of Wadi Al-Rimah flow channel by Nafud Al Thuwayrat sand before 4.8ka (Al dughairi, 2011). This coincides with Shamal wind activity, which was most influential in the formation of sand in central KSA, 5000 years before the present day (Edgell, 2006; Fleitmann et al., 2007). Nebaks proliferated rapidly before 2.1 ka and 5.3 ka, as in the Wadi Raghwah in Al Qassim (Al dughairi, 2011).

However, despite the change to more arid environment in Al Madinah Wadis, especially in the late Holocene, the period was also distinguished by some sudden flash floods. This is clearly apparent from the characteristics of deposits in the upper parts of Al Madinah wadi terraces. These are distinctly uncemented, due to the low amounts of carbonates, with higher proportion of silicates (83%), and the dominance of coarse gravel (as is the case in the upper parts of Wadis Al Hinakiyah [Figure 5.6], and Sahuq [Figure 5.10], and the alluvial fans in Wadi Luwayy at M3 and M4). These perhaps date back to 800 years. Al Juaidi (2003) pointed to these types of deposits, and stated that they occurred during a wet period in Nafud Al Sirr in central KSA, during 800 years, as shown in Figure 6.9c.
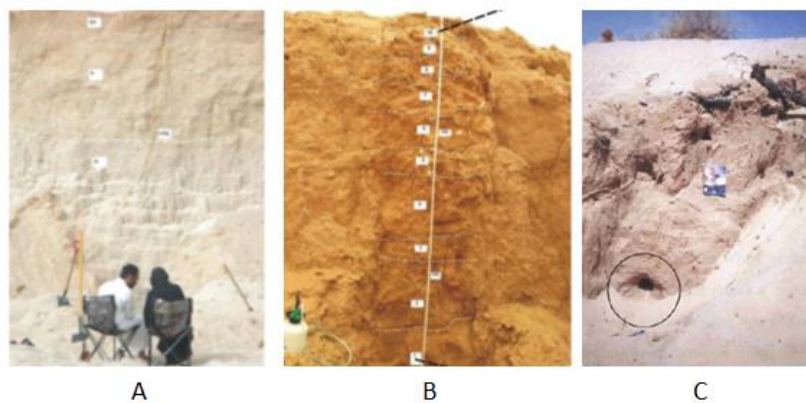
Figure 6.9: A) Wadi Al Butaun , B) Wadi Al Watah in Al Qassim, Al dughairi (2011). C) Nufud Al Sirr, Al-Juaidi (2003).

6.2.2.   Interpretation of origins and development of palaeolakes in Al Madinah

Deposits in the lower parts of palaeolakes in Al Madinah, as in section M10 in sabkhat Hurumah (Figure 5.22) and M12 (Figure 5.21) in the interdune in the west of Nufud Al Qawz, support the view that Al Madinah contained palaeolakes. This is because these contain roots and burrows that indicate dominance of plant life and organisms, in addition to clear presence of clay and carbonates. This is in agreement with the description given by Al Moqren (2016), relating to the lower sections of the Nafud Ash-Shuqayyiqah palaeolake, as in Figure 6.10c. These date back to 6.1ka and coincide with wet periods in the early and mid-Holocene. At the time, monsoon wind effects significantly influenced the central parts of KSA (Fleitmann et al., 2007).

Palaeolake water levels dropped due to scarce rainfall related to (wet) periods, or even a brief halt, which were considered a reflection of brief and intermittent semi-arid periods within this wet period (Al Moqren, 2016). This is confirmed by the characteristics of deposits in the middle parts of palaeolake sections (M10 and M12), which clearly show aeolian deposits and sand lenses. These aeolian deposits represent the early beginnings of

the formation of both Nufud Al Qawz and the sand ramps around sabkhat Hurumah (Figure 5.18). This perhaps coincided with volcanic activity in neighbouring areas. This idea is supported by the presence of some dark deposits, as in units 5 and 8 in sabkhat Hurumah M10 (Figure 5.22). Deposits in the upper parts of palaeolakes support the idea that water levels began to recede, coinciding with a period of gradual drying that began in the late Holocene. Hence, palaeolakes dried out and transformed into sabkha, which were filled in. This is supported by the presence of desiccation cracks as a result of higher levels of evaporation, accompanied by aeolian deposition processes indicative of the dominance of dry climatic conditions. These continue to increase proceeding upwards, where wind activity is dominant, and completely filled the shallow palaeolake basin. The remnant of these palaeolakes is a white layer of evaporites, representing the final phases. This is in agreement with the description given by Al Moqren (2016) of the upper sections of the deposits in the Nafud Ash-Shuqayyiqah palaeolake, dating back to 4.6- 4.7 ka. This coincides with the accumulation of wind-borne sand in Nafud Uyun Al Jiwa before 4.7 ka (Al dughairi, 2011).
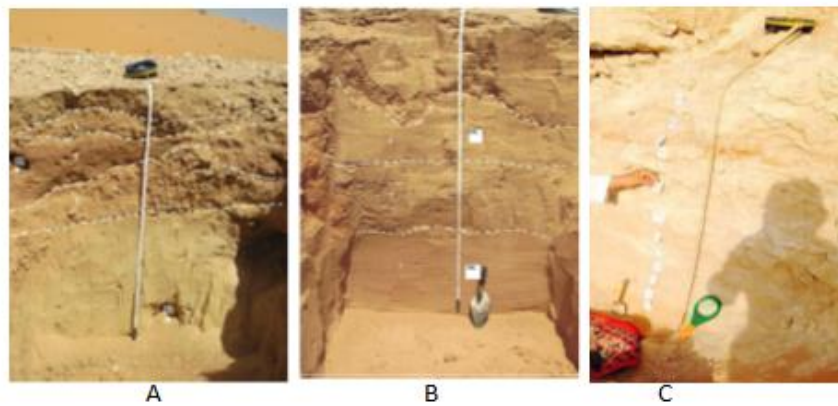
Figure 6.10: A) Nafud Dasmah in Nafud Al Thuwayrat, B) Wadi Al-Rimah within Nafud Al Thuwayrat, Al dughairi (2011). C) Deposits of the palaeolake in Nafud Ash-Shuqayyiqah, Al Moqren (2016).

6.2.3. Interpretation of origins and development of aeolian deposits in Al Madinah

The lower parts of aeolian deposits in Al Madinah, as in the sand ramps (Figure 5.19), confirm that these are borne of aeolian deposition processes that were dominant during wet climatic conditions. This is evidenced by the clear presence of roots, burrows, and carbonates. This is in agreement with the description given by Al dughairi (2011) for Nafud Dasmah in nafud Al Thuwayrat, as in Figure 6.10a, dating back to 11.3 ka, and Nafud Uyun Al Jiwa at 9.8 ka, coinciding with wet periods during the early and mid-Holocene. At that time, monsoon wind effects were highly influential on the central parts of KSA (Fleitmann et al., 2004, 2007). Aeolian processes increased at Al Madinah, and from the characteristics of the grain sizes, it is deduced that these deposits were wind-borne. This is in addition to the higher proportion of water-free haematite iron oxide coating the surfaces of these deposits, granting these 5YR5/4 colour. This supports the idea that deposition coincided with arid periods due to Shamal wind activity that was most influential in sand formation in KSA, during the mid-Holocene until the present time. These aeolian deposits in Al Madinah are similar in characteristics to those present in Al Qassim. Hence, these two regions may be in agreement regarding period of deposition, which for Al Qassim was dated by Al dughairi (2011) at 4.7 ka in Nafud uyun Al Jiwa, and Nafud Al Thuwayrat at 4.8 ka.

It is recommended for future work to perform dating on samples from sand ramps and sections of Nufud Al Qawz, to determine the conditions relating to origin and deposition in Nufud Al Qawz. This may then be compared to other deposits from the Arabian Peninsula, such as Al-Rub Al-Khali, and others.

6.2.4. Interpretation of origins and development of slope wash deposits in Al Madinah

From the results, it appears that slope wash deposits originated and developed during wet climatic conditions. The lower parts of these deposits (Figure 5.23) confirm the incidence of gentle successive flows that washed the slopes, resulting in wavy beds of wash deposits coinciding with wet periods. This is supported by red deposits affected by oxides, and the presence of roots, burrows, and carbonates that cemented the deposits. Al dughairi (2011) described similar deposits in the lower parts of the Al Mistawi plateau in Al Qassim, as in Figure 6.11a, dating back to 221.7 ka. He inferred that these red deposits were associated

with wetter conditions. Moreover, Petraglia et al. (2010) found deposits in Al Dawadmi similar to those of Al Madinah, and confirmed the presence of vegetation growth coinciding with wet periods, and human settlement prevailing before 204 ka. This evidence of wet periods is in agreement with other evidence of wet periods (ca. 230 – 220 ka) which were due to the influence of Mediterranean cyclones in the Black Desert, Jordan (32°N) (Frumkin et al., 2008). Indeed, high temperature and sufficient moisture are argued to be required for haematite formation (Schwertmann, 1993).

Sediments in the middle parts of the slope deposits confirm the incidence of strong flows that transported angular and sub-angular gravel sourced from surrounding slopes. In the upper parts, deposits confirmed the dominance of dry conditions, with a significant increase in silicate, and a large reduction in carbonates, with uncemented deposits. This is in agreement with those aforementioned deposits in Al Madinah found in the upper parts of the study sections. It is also notable that in the current general perspective, as in Figure 6.11b, wadis and wind worked at eroding and cutting large swathes of slope wash deposits. However, small hills continued to exist, as a very small part of massive transported deposits. On the other hand, in low areas around these hills, these were eroded and transported due to wind and wadis.
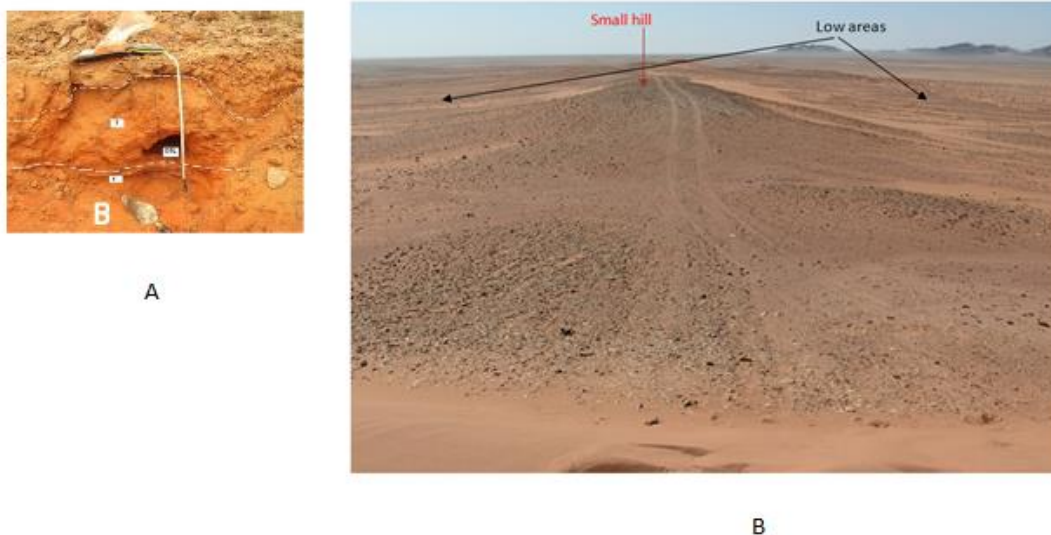
Figure 6.11: A) Weathered deposit, situated at Al Mistawi Plateau, in Al Qassim, Al dughairi (2011). B) General view of slope deposits.

6.3 Provisional Correlation of the Palaeogeomorphology/ Palaeoevironment Events During the Quaternary Period. in the Al Madiah Province and Surounding Areas:

The palaeoenvironmental and palaeogeomorphological changes will be presented over a wide area that includes Al Madinah and regions and countries in its vicinity. This allows for a general and comprehensive perspective of the prevailing conditions during some parts of the Pleistocene and Holocene periods, up to the present day (Figure 6.12, 6.13).
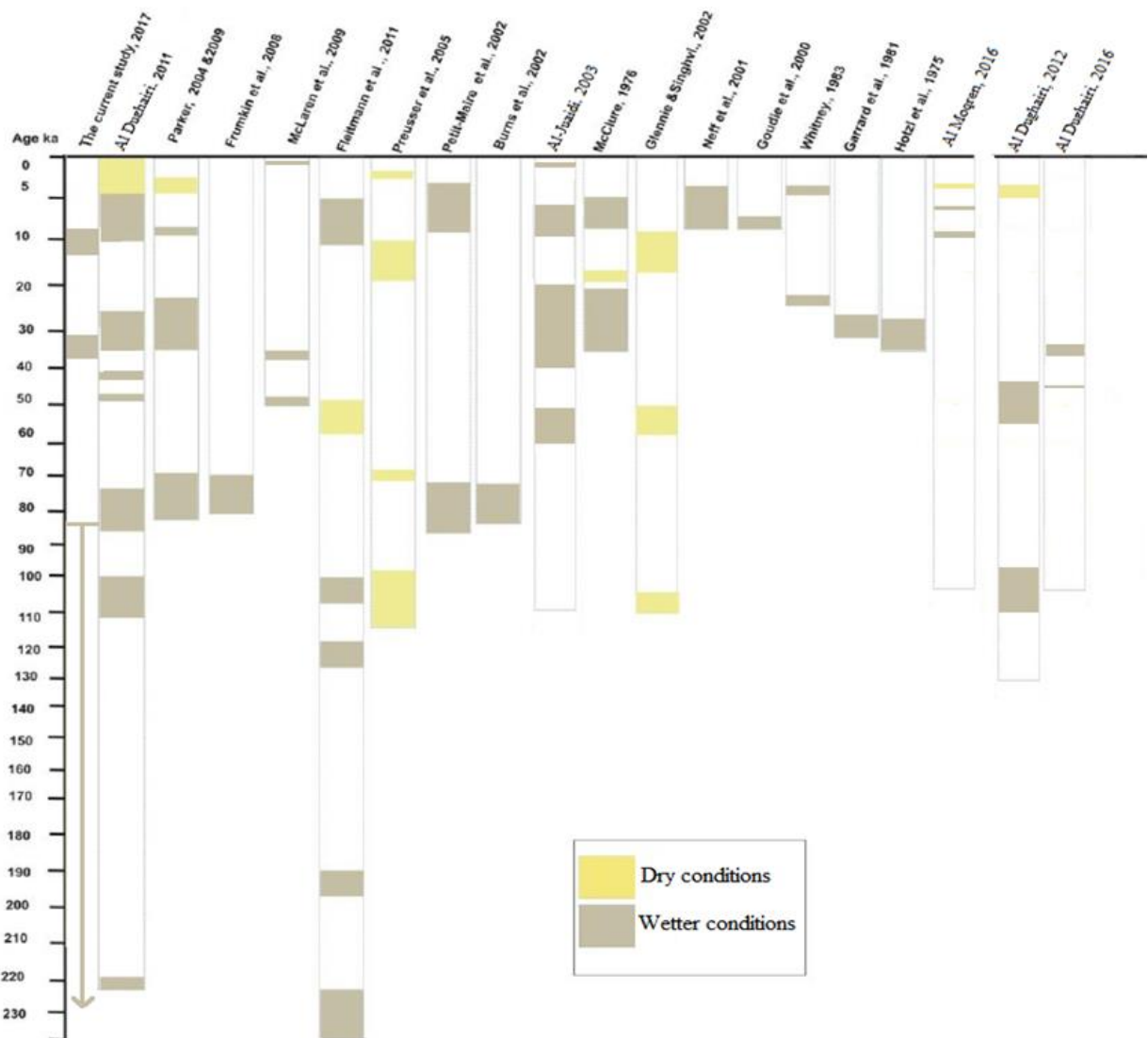
Figure 6.12: Summary of the late Quaternary palaeoenvironments in Al Madinah (in central western KSA) and surrounding areas- modified after Al dughairi (2011).

A. Marine Isotope Stage 5c (95-105 ka)

This was a period of high precipitation (Fleitmann et al., 2011), where the area witnessed large amounts of rainfall, leading to gentle flows in the Al Madinah wadis. These flows contributed to the geomorphological changes in Al Madinah, where they deposited terraces and alluvial fans. It is highly likely that these were caused by the penetration of monsoon winds into central KSA (Fleitmann et al., 2004, 2011). Particularly given that this coincided with activity in the Bathah Wadi in Oman, where fluvial sand in the wadi terrace bears indications of a significant flow prevailing during the MIS 5c phase (Juyal et al., 1998). It also coincided with the growth of speleothems in Yemen during 105 ka, and increased human migrations to the Arabian Peninsula during this wet phase (Fleitmann et al., 2011). In addition, the Dahna desert in that period was characterised by thick vegetation cover (Anton, 1984).
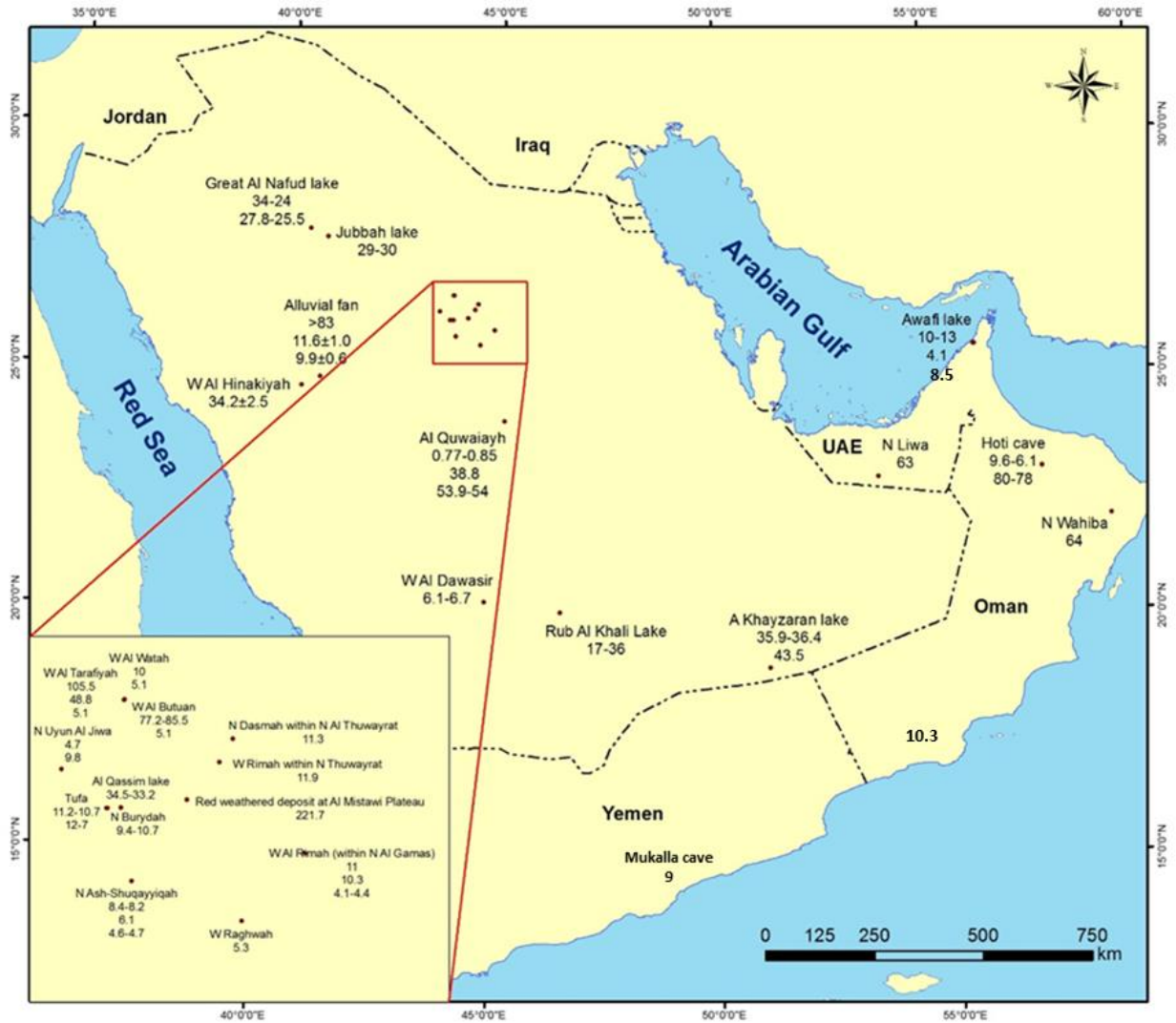
Figure 6.13: Location of the features dated in the current research and others surrounding areas.

Source: Current study (2017), Al dughairi (2016, 2012, 2011), Al Moqren (2016), McLaren et al. (2009), Parker et al. (2004, 2006), Stokes and Bray (2005), Al-Juaidi (2003), Burns et al. (2002, 1998), Preusser et al. (2002), Fleitmann et al. (2011, 2007), Neff et al. (2001), Goudie et al. (2000), Schulz and Whitney (1987), Whitney et al. (1983), Garrard and Harvey (1981), Hötzl and Zötl (1978), McClure (1976).

257

B. **Marine Isotope Stage 5a (75-85 ka)**

This wet period witnessed large amounts of precipitation. Indeed, the activity in Wadi Al Qusayrah, which is a tributary of Wadi Sahuq, in the lower parts of the terrace correspond to this period. This is similar to the evidence found by Al dughairi (2011) in the lower and middle parts of the Wadi Al Butaun terrace, dating back 77.2 – 85.5 ka. This is in agreement with the evidence found by Burns et al. (1998, 2002, 2003, 2001) in Hoti Cave in Oman, where they inferred increased precipitation in 82-78 ka from speleothem evidence. They concluded that this was associated with northward movement of Indian monsoon rainfall. On the other hand, Petit-Maire et al. (2010) discovered Mudawwara Lake in Jordan, situated to the north of KSA. They established that the palaeolake had been active due to precipitation from Indian monsoon and Mediterranean systems in MIS5b (ca.91.1 ka, 88 ka) and MIS5a (ca.77 ka). Furthermore, the influence of Indian monsoon rainfall and Mediterranean cyclones was linked to the growth of speleothem between MIS5b and MIS5a (ca.80 and 70ka) in Jordan (Frumkin et al., 2008).

However, it must be mentioned that the matter requires further studies to be undertaken in the future to determine the date of deposits in Wadi Sahuq, and confirm dating accurately.

C. **Marine Isotope Stage 4 (64-75 ka)**

This period was distinguished by increasing dryness until 50 ka (Fleitmann et al., 2007). Sand accumulated in Al-Rub Al-Khali (KSA), Liwa region in UAE, and Wahiba Sands (Stokes and Bray, 2005; Preusser et al., 2002). This period may perhaps have contributed to wadi activity ceasing in the Al Madinah area, as well as the formation of parts of the sand dunes, especially the huge star dunes in Nufud Al Qawz in the study area are similar in size to dunes in the Al-Rub Al-Khali.

D. **Marine Isotope Stage 3 (32-64 ka)**

During this period, wadis in the Al Madinah region were at peak activity. Indeed, Wadi Al Hinakiyah witnessed powerful flows during 34.2±2.5ka. At the same time, there is no evidence of aeolian activity. Indeed, wadi activity led to the deposition of fluvial terraces and alluvial fans. This may be attributed to the probability of heavy rainfall in the area. This

very high precipitation is likely due to the effects of the monsoon. This is inferred from the fact that such activity was not limited to the Al Madinah area, but was witnessed in other parts of the Arabian Peninsula, such as the flooding during the period 38.8-54 ka, which formed the alluvial fans in Al-Quwaiayh (McLaren et al., 2009; Al-Juaidi, 2003), and the activity of other lakes in Al Qassim, as reported by Al dughairi (2011) having been full of water before 34.5 – 33.2 ka. This is also concurrent with the palaeolake in Al-Rub Al-Khali (McClure, 1976), and the activity in the Al Khayzaran palaeolake in the Al-Rub Al-Khali during 35.9 – 36.4 ka (Al dughairi, 2016). According to Schulz and Whitney (1986), lakes in N. KSA, specifically in the Great Al Nufud, may be linked to wet periods during ca. 34-24 ka. Similarly, north of KSA, in eastern Jordan, a large lake was discovered within Lake Al Jafr, dating to 29.3-32.7 cal year BP (Huckreide and Wieseman, 1968). In Egypt, Warne and Stanley (1993) established that the Lake in Alexandria had been active ca. 35 ka.

It is worth pointing out that previous studies have reported that this period witnessed some dry spells (ca. 40- 47 ka) (Al-Juaidi, 2003) according to the evidence collected in parts of the Arabian Peninsula, such as in Wadi Al Tarfiyah in central KSA. By 48.8 ka, the flow in Wadi Al Tarfiyah had changed, distinguished by medium flows interspersed by brief periods where these flows ceased (Al dughairi, 2012). Also, sand accumulated in Liwa region in UAE at 45ka, under the effect of Shamal winds (Stokes and Bray, 2005).

E. Marine Isotope Stage 2 (13-32 ka)

The influence of wet monsoon winds in the early beginnings of this period up to 19 ka is quite notable. Indeed, the palaeolakes in Nufud Jabbah in the North of KSA filled during 29-30 ka (Whitney et al., 1983; Garrard and Harvey, 1981; Garrard et al., 1981). Also, the palaeolake in the Great Al Nafud indicated that conditions were wetter during 27.8-25.5ka (Schulz and Whitney, 1987). Several studies have affirmed that the end of this period witnessed huge droughts across the entire Arabian Peninsula, reaching a peak in the period of 18 ka, when sand dunes formed (Whitney et al., 1983; Edgell, 2006; Juyal et al., 1998). Fleitmann et al. (2004) mentioned that the aridity was more common due to the weakened monsoon system and the extent of the ice sheet over most northern parts of the world. In addition, a large lake in North of KSA in Jordan, disappeared during the LGM (Huckreide and Wieseman, 1968).

F. Marine Isotope Stage 1 (13 ka to the present time)

The discussion of previous works compared with the evidence found in Al Madinah region revealed that the beginning of this period until ca. 5 ka was characterised by wetness as a result of monsoon and Mediterranean cyclones, which discharged heavy rains on Al Madinah. The wadis in the region were at peak activity. Indeed, Wadi Luwayy witnessed powerful flows during 11.6±1.0ka and 9.9±0.6ka. This activity was not limited to the Al Madinah region, but coincided with wet conditions that dominated most of the Arabian Peninsula (Goudie et al., 2000; Parker et al., 2006; Lézine et al., 1998; Al dughairi, 2011).

The wadi and alluvial fan activity examined in this study coincided with lacustrine deposits reported by Parker et al. (2006), Lézine et al. (1998), which developed in Yemen at approximately 11 ka. In the area of Al Qassim, situated in central Saudi Arabia, the upper area of Wadi Al-Rimah provides evidence of a humid climate prevailing in the period from 13 to 11 ka. Humid climate in the period 11.2 to 10.7 ka is also evidenced by the presence of tufa in this area (Al dughairi, 2011).

There is also evidence that in this period, sand accumulated in different parts of the Arabian Peninsula and Africa. In Al Qassim, ca. 11.9 ka, sand accumulated in Wadi Al-Rimah's lower channel at Nafud Al Thuwayrat. In addition, significant amounts of burrows, roots, and some carbonate were found in Nafud Dasmah within Nafud Al Thuwayrat, in the part corresponding to ca. 11.3 ka. This seems to indicate that the water table rose in a wetter phase, leading to accumulation of sand (Al dughairi, 2011). Also, Awafi dune was active in the period between 10 - 13 ka (Goudie et al., 2000).

The results of the current study indicate that the wadi and alluvial fans' activity continued throughout 9.9±0.6ka in Wadi Luwayy. This is in agreement with the evidence gathered by Al dughairi (2011) in Al Qassim, in the form of tufa deposits. This supports the conclusion that in the early Holocene, humid conditions prevailed (Parker et al., 2004). Similar findings have been reported relating to Africa. In this respect, in southern Egypt, the effect of the enhanced monsoon led to the rise of Umm Akhtar Lake in the two periods, ca. 9.9 to 9.5 cal yr BP and 7.8 to 6.7 cal yr BP (Nicoll, 2001). On the other hand, both Nafud Uyun Al-Jiwa and Nafud Burydah were formed by deposits occurring in the periods 9.8 ka and 9.4 – 10.7 ka, respectively (Al dughairi, 2011). These reinforce the hypothesis that in the Arabian

Peninsula, the incidence of arid conditions does not directly correlate with aeolian deposition. Indeed, it is suggested that in Liwa (UAE), the preservation of sand dunes took place during wetter periods (Stokes and Bray, 2005). Also in the UAE, the Awafi linear dunes were shown to have developed in the period 9.1 − 10.7 ka, leading to a conclusion that arid conditions are not a critical factor in sand accumulation. Rather, sand accumulation may be driven by the destabilisation of vegetation cover arising from human activity, such as herding, or supply of sediment during the late Pleistocene and early Holocene periods (Goudie et al., 2000).

By the mid-Holocene, there was a decline in the penetration of monsoon winds effects, and the Shamal wind became active (Glennie and Singhvi, 2002; Fleitmann et al., 2007). As a result, dry conditions prevailed in Al Madinah, accompanied by wind deposition activity leading to the accumulation of sand sheets, dunes, and nebaks. This coincided with the accumulation of aeolian sand in Nufud Uyun Al Jiwa at 4.7 ka also, in Wadi Raghwah east of Nafud Al Sirr at 5.3 ka (Al dughairi, 2011). The flow channel of Wadi Al-Rimah was closed by Nufud Al Thuwayrat sand before 4.8ka. This also coincided with weakened wadi flow activity in Al Qassim, such as Wadi Al Tarfiyah (Al dughairi, 2012) and Wadi Al Butaun before 5.1ka. Nebaks expanded rapidly before 5.3 and 2.1 ka, as in Wadi Raghwah in Al Qassim (Al dughairi, 2011). This was concurrent with the accumulation of aeolian sand in the Awafi palaeolake in UAE ca. 4.1 ka (Parker et al., 2004), and ceased activity in the Selima palaeolake in the eastern desert of Egypt ca. 3-4ka (Stokes et al., 1997). Additionally, this ceased activity in the Ash-Shuqayyiqah palaeolake in Al Qassim ca. 4.6-4.7 ka (Al Moqren, 2016). There was also sand accumulation activity in Oman around 5.4ka (Preusser et al., 2005), as well as in the Liwa region in UAE ca. 6 ka (Stokes and Bray, 2005).

There exists a strong agreement between a number of studies supporting the hypothesis that the mid-Holocene is the actual beginning of the dry period and gradual change to arid conditions. This is due to the general decline in monsoon wind activity at ca. 6-5ka. The effects of these winds did not penetrate beyond the southern fringes of the coast of Oman (Neff et al., 2001; Fleitmann et al., 2007). This was accompanied by a general decline in monsoon activity, huge sand accumulations, and drying out of most of the palaeolakes in the Al-Rub Al-Khali and the deserts of Oman before 5ka (Goodall, 1995; Al dughairi, 2016; Stokes and Bray, 2005).

Despite the dominance of arid conditions, especially in the late Holocene, some flows and flash floods are evident, as is the case in Nufud Al Sirr in central KSA, during 800 years (0.85 ka) (Al-Juaidi, 2003).

G. Findings about the history of monsoon precipitation in Saudi Arabia

Since the study area is located in the central western part of KSA (25° N), linking the results of the current study to those of other studies conducted in other areas of the Arabian Peninsula has provided data on monsoon precipitation over a larger spatial area than previously. This allowed some facts to be deduced that have confirmed the error in the conclusions drawn by both Fleitmann et al. (2004), Parker (2009). Based on the results presented in sections 6.2 and 6.3, and Figure 6.13, it is demonstrated that wet conditions prevailed in Al Madinah (central western KSA) before 34.2±2.5 ka.

Also, results of the investigation support the argument that wet periods prevailed in the study area in the early Holocene (9.9±0.6 ka to 11.6±1.0 ka). This is most likely a response to the strong penetration of monsoon winds (Fleitmann et al., 2004). This meant that most of the environment in the Kingdom was subjected to wet conditions during the early Holocene, as established by previous studies. Monsoon precipitation had reached latitude 25° N, where the study area is situated. Yet, it had also reached the area of Al Qassim (central Saudi Arabia) situated on latitude 26° N further north, as was reported by Al dughairi (2011). This is in disagreement with the conclusion by Fleitmann et al. (2004), who argued that in Saudi Arabia, the monsoon precipitation belt was static and situated near 23-24°N.

Moreover, the results of this study contradict Parker's (2009) conclusions, as Al dughairi's (2011) results did. Parker mentioned that during the early Holocene the migration of monsoon winds from the south of the Arabian Peninsula (latitude 15° N) at 10.3 ka to the north of the Peninsula (latitude 25° N) at 8.5 ka took 1800 years. The current results have shown that monsoon precipitation had also penetrated, around the same time, into the south, west, central and east of the Arabian Peninsula. This is supported by the results of the current study as well as other studies demonstrating the prevalence of wet conditions in Al Madinah (central western KSA) during 9.9±0.6 ka. Also, Fleitmann et al. (2011) studied the stalagmites in which Mukalla Cave (southern Arabian Peninsula), and found that wetter conditions existed during 9ka. Moreover, according to workers Hötzl and Zötl (1978),

during the period around 9-9.5 ka cal BP, Wadi Al Luhy 21°N (near Al-Quwaiayh) was active. Speleothems were found in the northern Hoti Cave, Oman, which lead to the conclusion that the period 9.6 – 6.1 ka of the early to mid-Holocene witnessed a wetter climate, because of enhanced rainfall in the monsoon (Neff et al., 2001). Tufa was found in the area of Al Qassim in central Saudi Arabia, which indicates that humid climate existed in the period 9.9 ka (Al dughairi, 2011).

Chapter 7. Conclusion and Recommendations

In this chapter, the main findings of this research, and the recommendations for future work are presented. This work covers two principal aims:

Firstly, to employ data from remote sensing and field research to identify the provenance of sediments in the landscape, sediment transport pathways and depositional locations, and to then identify and map the key geomorphological features and understand how they are distributed in the study area.

Secondly, to employ the maps produced, field observations, as well as laboratory results relating to the deposits preserved in the study area, to determine the palaeogeomorphic and palaeoenvironmental conditions during the late Quaternary period that have prevailed in the area, and which have contributed to the development of the geomorphological features.

7.1 Key Findings

Key Findings of Remote Sensing for Geomorphological Mapping

The current study integrated between multiple data resources including elevation data (ASTER GDEM), multispectral satellite imagery (Landsat 8), laboratory hyperspectral data, in addition to field investigations in order to assess the spectral characteristics of different geomorphological units and consequently to map these units on a spectral base.

Multispectral image processing techniques (false colour composites, principle component analysis, band ratioing, and supervised image classification) have been applied alongside with field and laboratory reflectance measurements (using ASD HH2 spectrometer). The current study found that mineral composition and grain size are influential factors in the variations of surface reflectance of deposits.

Moreover, the results provided by this work have helped towards a better interpretation of the landscape east of Al Madinah including provenance, sediment movement, and locations of deposition that have contributed to the principal geomorphological features found in the area. PCA colour composite provided a good summary of sediments transportation, mixing,

and deposition from East Al Madinah plateau towards Qa Hadawda (Figure. 6.1) as formerly discussed in section 6.1.

As the drainage network plays an important role in shaping geomorphological features, the digital elevation model (ASTER GDEM) was used efficiently in determining the drainage system, as well as identifying the general characteristics of the landscape such as altitude and slope within the study area. Accordingly; the study area contains two main basins; Wadi Sahuq basin that flows towards the northeast, and Wadi Al Makhit that flows towards the southwest pouring to Qa Hadawda. The delineation of drainage basins helped in tracing sediments sources, movements, and deposition over the study area.

Collected field sediment samples from different geomorphological units were used to demonstrate the relationships between laboratory spectral reflectances and that of Landsat 8 imagery, showing a strong positive correlation (R^2=0.84 to 0.89). Subsequently, Landsat 8 surface reflectance data was used effectively in mapping different geomorphological units (sand dunes, sand sheets, sand ramps, wadi deposits, slopes, Qa, sabkha, intermountaneous basins, Sahuq plateau, and East Al Madinah plateau) on spectral bases using maximum likelihood supervised classification with overall accuracy of 80.84%.

In order to put these results in practice; a spectral transect composed of four pixel samples (1, 2, 3, 4) with a monitoring well defined sample (S8) (Figure 4.17), passing through East Al Madinah Plateau showed that there is an obvious relation between the sediments grain size and their surface reflectance values; the coarser and the nearer to upstream the lower the reflectance and vice versa. In addition, Landsat 8 PCA colour composite was found to be the most effective for visual interpreting and describing the composition and mixing of sediments, and inferring the geomorphological processes within the study area.

In some cases, field spectral measurements might be more effective than laboratory measurements in giving reliable spectral signatures that are more comparable with satellite imagery, especially for dikes and similar longitudinal features. Dikes are longitudinal bodies of mafic to felsic mineral composition partly covered by sand sheets and sparsely distributed vegetation cover, which alter their surface reflectance within Landsat imagery. Conversely, the laboratory samples of dikes did not contain these components, and this explains the weak correlation between Landsat 8 and HH2 lab reflectance (Figure 4.21).

Key Findings of Evolution of the Study Area and Late Quaternary Sediments: An Interpretation.

Remote sensing and stratigraphic sections were used to find out whether there are differences between the environment today and the palaeoenvironment. Data acquired through remote sensing has indicated that wind activity dominated, given the major presence of sand sheets in the study area. These are represented by the pink colour (Figure 6.1). Moreover, stratigraphic sections provide evidence that supports the idea that wet conditions prevailed in the area in the past, as seen in Figures 5.2, 5.4, 5.6, 5.17 and 5.22. Indeed, at times, Nufud Al Qawz was itself a palaeolake (Figure 5.21), while a flood plain covered area C (Figures 6.1, 5.17). The remains of this palaeolake are captured by remote sensing, with bright sand appearing on the surface, comprising of light white evaporates and calcium carbonate (Figure 6.3). These are concentrated significantly in the east of the Nufud, and the interdune areas.

Change in the palaeolake environment from wet to muddy allowed the formation of sand dunes on the palaeolake surface with the onset of dry conditions, where water levels dropped significantly (Figure 5.21). As a result, and with other influencing factors, sand was captured and accumulated, leading to Nufud Al Qawz being formed at this location. These contributing factors were:

1.   The availability of sand supply from the sediments of large amount of wadis and exposed sandstone formations close to Nufud Al Qawz with Shamal wind activity that contributed to the transport of these sediments and their deposition at the bottom of the palaeolake.

2.   The existence of mountains surrounding the north and east of Nufud Al Qawz in addition to the nabkahs that contributed to making Nufud Al Qawz the place for deposition of sand and formation of sand dunes.

Similarly, from section 11, and Figure 5.19, sand ramps surrounds Sabkhat Hurumah. This formed due to the wetness of the palaeolake within the volcano crater resulting from wet periods. Moreover, the availability of sediments along with wind activity also contributed. Indeed, during dry periods, wind would transport sediments from the sabkha surface or the areas surrounding the sabkha. As such, the volcano crater slopes where ideal for capturing and retainbing this sand. In turn, the sand ramps grew significantly during dry periods.

According to the evidence in section M10 (Figure 5.22), Sabkhat Hurumah had been a palaeolake filled with water.

Key Findings of Evidence of Provisional Correlation of the Palaeogeomorphology and Palaeoenvironment Events during the Late Quaternary Period, in the Al Madinah Province and Surrounding Areas.

Evidence of the palaeogeomorphic and palaeoenvironmental conditions during the late Quaternary period that have prevailed in Al Madinah, gathered during this work, were presented. Key evidence comprised a sequence of sediments in the terrain around Al Madinah. As part of the investigation, these sediments were dated using OSL, thus supporting the view that a wet period had prevailed in Al Madinah at 34.2±2.5 ka as in (Figure 5.6). Deposits indicate that flows were strong, accompanied by floods. The massive activity in this wadi was concurrent with the activity in a number of other lakes in the same timeframe, such as that found in Al Qassim (Al dughairi, 2011) and Al-Rub Al-Khali (McClure, 1976). Also, this is similar to the findings by McLaren et al. (2009), Al-Juaidi (2003) in terms of the dominance of floods during the 38.8–54 ka in Al-Quwaiayh in central KSA. OSL analysis performed in the current research also showed that wet periods prevailed in the study area in the early Holocene (9.9±0.6 – 11.6±1.0 ka) Figure 5.13. This is in agreement with the evidence gathered by Goudie et al. (2000), Hötzl and Zötl (1978). This is most likely as a result of the monsoon (Fleitmann et al., 2004). The current study confirmed that the influences of monsoon winds had reached Al Madinah at latitude 25°N. This finding is contrary to that of Fleitmann et al. (2004), who argued that in Saudi Arabia, the monsoon precipitation belt was static and situated near 23-24°N. Also, the current study and others on central Saudi Arabia have shown that penetration of monsoon winds took place at the same time, in southern, western, eastern and central Saudi Arabia. This differs with Parker (2009) who claimed that it moved from Southern Arabia (15°N) to Northern Arabia (25°N) over a period of 1,800 years.

In addition, linking the results of the current study with other research works conducted on the Arabian Peninsula allowed a general and comprehensive picture to emerge of the conditions prevailing in the late Quaternary period. It appears that wet conditions prevailed in 105.5 ka (Al dughairi, 2012). Moreover, the period 75-85 ka witnessed large amounts of

precipitation, likely due to the influence of the ITCZ, as it reached the highest position north wards. Hence, moisture was transported from the Indian Ocean by monsoon winds, with north westerly Mediterranean systems also contributing (Petit-Maire et al., 2010; Burns et al., 1998, 2002, 2001). The period between 64-75 ka was distinguished by increasing dryness until 50 ka (Fleitmann et al., 2007). Moreover, a long and wetter period quite likely prevailed at around 34.2 ka. However, the period ca. 40-47 ka witnessed some dry spells (Al-Juaidi, 2003), while the period ca. 19-13ka was hyper-arid. The latter situation is thought to have prevailed, with strong consensus among workers, due to the extensive aridity in the period ca.18 ka, i.e. in the last glacial maximum (LGM) (Whitney et al., 1983; Edgell, 2006; Juyal et al., 1998). On the other hand, in the Arabian Peninsula, 10-5 ka was wetter, as supported by plenty of evidence. This latter evidence may indicate that during the Holocene, monsoon activity had prevailed, along with contributions from winter Mediterranean rainfall systems (Fleitmann et al., 2004; Al dughairi, 2011). However, from 5 ka to the present time, deposits of sand sheets predominated. This indicates that the climate was relatively arid (as is the case currently), with very brief periods of precipitation. This has been attributed to the gradual reduction in monsoon effects, as the northern hemisphere summer solar insolation underwent change (Al dughairi, 2011; Al Moqren, 2016; Parker et al., 2004). In contrast, wetter conditions prevailed ca. 0.8 ka (Al-Juaidi, 2003).

7.2   Future Recommendations

Finally, the following are recommended as avenues of future work:

1- To more thoroughly conduct OSL dating throughout the study area to be able to link environmental changes throughout other areas in the Arabian Peninsula.

2- The development of unit 1 in the sand ramps and units 5 and 8 in Sabkhat Hurumah may have coincided with volcanic activity in neighbouring areas. This idea is supported by the evidence of darker coloured deposits compared to other units. Therefore, this seems to offer another interesting area which warrants further investigation.

3- Describing and interpreting spectral reflectance of deposits in other basins in the area east of Al Madinah.

4- Performing transects in a number of other locations in the study area to determine whether the results are applicable to these other places. Subsequently, verifying the correctness of the transect results by undertaking field work for this purpose.

References:

ABRAMS, M. J., BROWN, D., LEPLEY, L. & SADOWSKI, R. 1983. Remote sensing for porphyry copper deposits in southern Arizona. *Economic Geology,* 78**,** 591-604.

ADAM, E. & MUTANGA, O. 2009. Spectral discrimination of papyrus vegetation (Cyperus papyrus L.) in swamp wetlands using field spectrometry. *ISPRS Journal of Photogrammetry and Remote Sensing,* 64**,** 612-620.

ADAMS, J. B., SMITH, M. O. & GILLESPIE, A. R. 1993. Imaging spectroscopy: interpretation based on spectral mixture analysis. In: Pieters, C.M., Englert, P.A.J. (Eds.), Topics in Remote Sensing IV: Remote Geochemical Analysis: Elemental and Mineralogical Composition. *Cambridge University Press, Cambridge***,** 145-166.

AGGARWAL, S. 2004. Principles of remote sensing. *Satellite remote sensing and GIS applications in agricultural meteorology,* 23.

AITKEN, M. J. 1998. *Introduction to optical dating: the dating of Quaternary sediments by the use of photon-stimulated luminescence,* Oxford, Oxford University Press.

AL- HUSBAN, U. & ZRAGAT, D. 2011. The Role of the Digital Elevation Model in the Geomorphological Analysis in Pirayn Region, Jordan. *Humanities and Social Sciences,* 38**,** 1-26.

AL-JUAIDI, F. 1997. *The role of remotely sensed data for geomorphological mapping: wadi Al-Harmaliah drainage basin, central Saudi Arabia.* MSc thesis, King Saud University, Riyadh, Saudi Arabia.

AL-JUAIDI, F. 2003. *The utilisation of merged remotely sensed data for geomorphological investigations in the desert of central Saudi Arabia.* PhD, University of Leicester, UK.

AL-SAHARIF, A. 1998. Biological environment (soil, plants, animals). *In:* AL-RUWAYTHI, M. & KHOGALI, M. (eds.) *Man and his Environment in Al-Madinah Al-Munawwarah.* 1st ed. Al-Madinah: Dar Al Waha Al Arabiah, 83-102.

AL-SALEH, M. 1999. The Application of Landsat-TM Enhanced Images and Topographic Maps for Morphometric Analysis in Wadi Muzayriah and Wadi Inan, Central Saudi Arabia. *King Saud University,* 2**,** 287-304.

AL-SAQQA, A. 2004. *physical Geography of the Kingdom of Saudi Arabia,* Jeddah, Darkonoz Almarefa.

AL-SHANTI, A. 1993. *Geology of the Arabian Shield,* Jeddah, Center for Scientific Publishing, King Abdulaziz University.

AL-WASH, M. A., ZAIDI, S. M. & TERHALLE, U. 1986. Description of arid geomorphic features using Landsat-TM data and ground truth information (Wadi Fatima, Kingdom of Saudi Arabia). *Catena,* 13**,** 277-293.

AL-WELAIE, A. 1997a. *Geomorphology and Geomorphology of Saudi Arabia,* Riyadh, Al Obeikan Library.

AL-WELAIE, A. 1997b. *Sand Seas in Saudi Arabia,* Riyadh, King Fahd National Library.

AL-WUHABI, A. 2013. Using Remote Sensing Techniques in Assessing the Flood of Wadi Al-Nisa in Al Qassim *First Saudi International Conference on Crisis and Disaster Management.* Riyadh.

AL -AZMI, N. 2009. *Measure the Creeping of the Barkan Dunes in Dahana Desert using Remote Sensing Imagery.* PhD, Al-Imam Mohammad Ibn Saud Islamic University, Riyadh, Saudi Arabia.

AL DUGHAIRI, A. 2011. *Late Quaternary Palaeoenvironmental Reconstruction in the Burydah Area, Central Saudi Arabia.* PhD, University of Leicester, UK.

AL DUGHAIRI, A. 2012. Evidences of Wadi Al Turfiyah Flooding , Tributary of Wadi Al Rimah.in Al Qassim Region, Central Saudi Arabia. *Kuwait Geographical Society,* 377**,** 1-48.

AL DUGHAIRI, A. 2016. The Evolution of Paleolakes and Hydrological Systems in the Rub Al Khali Desert over the Last 43ka. *Kuwait Geographical Society,* 395**,** 1-49.

AL DUGHAIRI, A. & AL JADDANI, A. 2016. Integration of Geospatial and Radiocarbon Techniques in Study of Geomorphology and Vegetation Cover in The Basin of Wadi Al-Fuwayliq ، Al- QassimArea. *King Saud University,* 2**,** 1-35.

AL DUGHAIRI, A. & AL MOQREN, K. 2016. Nafud Ash-Shuqayyiqah in Al-Qassim. *Kuwait Geographical Society,* 397**,** 1-15.

AL MOQREN, K. 2016. *Nafud Ash-Shuqayyiqah, in Al Qassim, Central Saudi Arabia "Geomorphology Study".* Master, Al Qassin University, Saudi Arabia.

AL SEHRI, L. 2011. *Using Remote sampling in the detection of spatial variations and temporal changes of the surface properties of the internal sabkat AlRagda and the coastal sabkat Al Maslamyah on the eastern coast of the Kingdom.* Master King Saud University, Riyadh, Saudi Arabia.

AL SHAIK, A., MOHAMMAD, A. & AL WELAIE, A. 2000. *Studies in Geography of Saudi Arabia,* Riyadh, Saudi Arabia, Al Obeikan Library.

ANDERSON, D., GOUDIE, A. & PARKER, A. 2007. *Global environments through the Quaternary: exploring environmental change,* Oxford, UK, Oxford University Press.

ANDERSON, K. & CROFT, H. 2009. Remote sensing of soil surface properties. *Progress in Physical Geography,* 33**,** 457-473.

ANTON, D. 1984. Aspects of geomorphological evolution; paleosols and dunes in Saudi Arabia. *In:* JADO, A. & ZOTL, J. (eds.) *Quaternary Period in Saudi Arabia.* Springer, Vienna.

ASD INC 2014. HandHeld 2: Hand-held VNIR Spectroradiometer.

ATKINSON, O. A., THOMAS, D. S., GOUDIE, A. S. & BAILEY, R. M. 2011. Late Quaternary chronology of major dune ridge development in the northeast Rub'al-Khali, United Arab Emirates. *Quaternary Research,* 76**,** 93-105.

BATEMAN, M. & CATT, J. 1996. An absolute chronology for the raised beach and associated deposits at Sewerby, East Yorkshire, England. *Journal of Quaternary Science,* 11**,** 389-395.

BATEMAN, M. D., BRYANT, R. G., FOSTER, I. D., LIVINGSTONE, I. & PARSONS, A. J. 2012. On the formation of sand ramps: A case study from the Mojave Desert. *Geomorphology,* 161**,** 93-109.

BELL, W. 1979. Thermoluminescence dating: radiation dose-rate data. *Archaeometry,* 21**,** 243-245.

BEN-DOR, E., CHABRILLAT, S., DEMATTÊ, J., TAYLOR, G., HILL, J., WHITING, M. & SOMMER, S. 2009. Using imaging spectroscopy to study soil properties. *Remote Sensing of Environment,* 113**,** S38-S55.

BISHOP, M. P., JAMES, L. A., SHRODER, J. F. & WALSH, S. J. 2012. Geospatial technologies and digital geomorphological mapping: concepts, issues and research. *Geomorphology,* 137**,** 5-26.

BOWERS, S. & HANKS, R. 1965. Reflection of radiant energy from soils. *Soil Science,* 100**,** 130-138.

BRADY, N. C. 1983. Nature and soil properties. *Natureza e propriedades dos solos.* Freitas Bastos.

BREUNIG, F. M., GALVÃO, L. S. & FORMAGGIO, A. R. 2008. Detection of sandy soil surfaces using ASTER-derived reflectance, emissivity and elevation data: potential for the identification of land degradation. *International Journal of Remote Sensing,* 29**,** 1833-1840.

BROWN, G. F., LAYNE, N., GOUDARZI, G. H. & MACLEAN, W. H. 1963. Geologic map of the northeastern Hijaz quadrangle, Kingdom of Saudi Arabia: U.S. Geological Survey Miscellaneous Geologic Investigations Map I-205A, scale 1:50,000.

BULLARD, J. E. & WHITE, K. 2002. Quantifying iron oxide coatings on dune sands using spectrometric measurements: An example from the Simpson-Strzelecki Desert, Australia. *Journal of Geophysical Research: Solid Earth,* 107.

BURNS, S., MATTER, A., MANGINI, A. & MUDELSEE, M. 1998. The history of the monsoon in southern Arabia: results based on stable isotopes and U/Th dating of speleothems. *Mineralogical Magazine A,* 62**,** 261-262.

BURNS, S. J., FLEITMANN, D., MATTER, A., KRAMERS, J. & AL-SUBBARY, A. A. 2003. Indian Ocean climate and an absolute chronology over Dansgaard/Oeschger events 9 to 13. *Science,* 301**,** 1365-1367.

BURNS, S. J., FLEITMANN, D., MATTER, A., NEFF, U. & MANGINI, A. 2001. Speleothem evidence from Oman for continental pluvial events during interglacial periods. *Geology,* 29**,** 623-626.

BURNS, S. J., FLEITMANN, D., MUDELSEE, M., NEFF, U., MATTER, A. & MANGINI, A. 2002. A 780-year annually resolved record of Indian Ocean monsoon precipitation from a speleothem from south Oman. *Journal of Geophysical Research: Atmospheres,* 107.

CAMP, V. E. & ROOBOL, M. J. 1991. Geologic Map of Cenozoic Lava Field of Harrat Rahat, Kingdom of Saudi Arabia, Directorate General of Mineral Resources, Geosciences Map GM-123,Scale 250,000 with text.

CHANG, C.-W., LAIRD, D. A., MAUSBACH, M. J. & HURBURGH, C. R. 2001. Near-infrared reflectance spectroscopy–principal components regression analyses of soil properties. *Soil Science Society of America Journal,* 65**,** 480-490.

CHAVEZ, P. S. J., BERLIN, G. L. & SOWERS, L. B. 1982. Statistical methods for selecting Landsat-MSS ratios. *Journal of Applied Photogrammetric Engineering* 8**,** 23-30.

CLARK, R. N. 1999. Spectroscopy of rocks and minerals, and principles of spectroscopy. *Manual of remote sensing,* 3**,** 3-58.

COLEMAN, R. G., GREGORY, R. T. & BROWN, G. F. 1983. Cenozoic volcanic rocks of Saudi Arabia. *Saudi Arabian Deputy Ministry for Mineral Resources Open-File Report* USGS-OF-03-93.

COLEMAN, T., AGBU, P. & MONTGOMERY, O. 1993. SPECTRAL DIFFERENTIATION OF SURFACE SOILS AND SOIL PROPERTIES: IS IT POSSIBLE FROM SPACE PLATFORMS? *Soil science,* 155**,** 283-293.

COOKE, R. & DOORNKAMP, J. C. 1990. *Geomorphology in environmental management: a new introduction*, Oxford University Press (OUP).

COOKE, R. U., WARREN, A. & GOUDIE, A. S. 2006. *Desert geomorphology*, CRC Press.

CROUVI, O., BEN-DOR, E., BEYTH, M., AVIGAD, D. & AMIT, R. 2006. Quantitative mapping of arid alluvial fan surfaces using field spectrometer and hyperspectral remote sensing. *Remote sensing of environment,* 104**,** 103-117.

CURRAN, P. J. 1985. *Principles of remote sensing*, Longman Inc.

DELFOUR, J. 1966. Report on the mineral resources and geology of the Hulayfah-Musayn'ah region (sheet 78, Zone 1 North) SG-JED. *French Bureau de Recherches Geologiques et Minieres Technical Record,* 66(A8).

DELFOUR, J. 1967. Report on the mineral resources and geology of the Hulayfah-Musayna'ah region (Sheet 78, Zone 1 North). *French Bureau de Recherches eologiques et Minieres open file,* 66(A8)**,** 138p.

DELFOUR, J. 1970. Le Group de J'Balah, une nouvelle unite du Bouclier Arabe. *french Bureau de Recherches eologiques et Minieres Bulletin,* Ser(2)**,** 19-32.

DEMATTÊ, J. A., FIORIO, P. R. & ARAÚJO, S. R. 2010. Variation of routine soil analysis when compared with hyperspectral narrow band sensing method. *Remote Sensing,* 2**,** 1998-2016.

DHELLEMMES, R. & DELFOUR, J. 1980. Geologic map of the Khybar quadrangle, sheet 25D, Kingdom of Saudi Arabia (with text): Saudi Arabian Directorate General of Mineral Resources Geologic Map GM-50A, scale 1:250,000.

DRAMIS, F., GUIDA, D. & CESTARI, A. 2011. Nature and aims of geomorphological mapping. *Developments in earth surface processes.* Elsevier.

DULLER, G. 2003. Distinguishing quartz and feldspar in single grain luminescence measurements. *Radiation measurements,* 37**,** 161-165.

DULLER, G. 2007. Assessing the error on equivalent dose estimates derived from single aliquot regenerative dose measurements. *Ancient TL,* 25**,** 15-24.

DULLER, G. A. 2008a. *Luminescence Dating: guidelines on using luminescence dating in archaeology*, English Heritage.

DULLER, G. A. 2008b. Single-grain optical dating of Quaternary sediments: why aliquot size matters in luminescence dating. *Boreas,* 37**,** 589-612.

EDGELL, H. S. 2006. *Arabian deserts: nature, origin and evolution*, Springer Science & Business Media.

ERDAS TUTORIAL 2010.

EXELIS E.N.V.I 2012. Exelis ENVI Manual.

FARR, T. G. & CHADWICK, O. A. 1996. Geomorphic processes and remote sensing signatures of alluvial fans in the Kun Lun Mountains, China. *Journal of Geophysical Research: Planets,* 101**,** 23091-23100.

FLEITMANN, D., BURNS, S. J., MANGINI, A., MUDELSEE, M., KRAMERS, J., VILLA, I., NEFF, U., AL-SUBBARY, A. A., BUETTNER, A. & HIPPLER, D. 2007. Holocene ITCZ and Indian monsoon dynamics recorded in stalagmites from Oman and Yemen (Socotra). *Quaternary Science Reviews,* 26**,** 170-188.

FLEITMANN, D., BURNS, S. J., PEKALA, M., MANGINI, A., AL-SUBBARY, A., AL-AOWAH, M., KRAMERS, J. & MATTER, A. 2011. Holocene and Pleistocene pluvial periods in Yemen, southern Arabia. *Quaternary Science Reviews,* 30**,** 783-787.

FLEITMANN, D. & MATTER, A. 2009. The speleothem record of climate variability in Southern Arabia. *Comptes Rendus Geoscience,* 341**,** 633-642.

FLEITMANN, D., MATTER, A. & PINT, J. 2004. The speleothem record of climate change in Saudi Arabia. Open-File Report. *Open-File Report, SGS-OF-2004-8, Saudi Geological Survey*.

FRANKLIN, J. 1995. Predictive vegetative mapping: geographic modeling of biospatial patterns in relation to environmental gradients. *Progress in Physical Geography,* 19(4)**,** 474-499.

FRUMKIN, A., BAR-MATTHEWS, M. & VAKS, A. 2008. Paleoenvironment of Jawa basalt plateau, Jordan, inferred from calcite speleothems from a lava tube. *Quaternary Research,* 70**,** 358-367.

GAFFEY, S. 1986. Spectral reflectance of carbonate minerals in the visible and near infrared (035–2.5 μm): calcite, aragonite and dolomite. *American Mineralogist,* 71**,** 151-162.

GARRARD, A. & HARVEY, C. 1981. Environment and settlement during the Upper Pleistocene and Holocene at Jubba in the Great Nefud, northern Arabia. *Atlal. The Journal of Saudi Arabian Archaeology Riyakd,* 5**,** 137-148.

GARRARD, A., HARVEY, P. & SWITSUR, V. 1981. Environment and settlement during the Upper Pleistocene and Holocene at Jubbah in the Great Nefud, northern Arabia. *Atlal, Journal of Saudi Arabian Archaeology,* 5**,** 137-148.

GASSE, F. & VAN CAMPO, E. 1994. Abrupt post-glacial climate events in West Asia and North Africa monsoon domains. *Earth and Planetary Science Letters,* 126**,** 435-456.

GLENNIE, K. 1987. Desert sedimentary environments, present and past—a summary. *Sedimentary Geology,* 50**,** 135-165.

GLENNIE, K. & SINGHVI, A. 2002. Event stratigraphy, paleoenvironment and chronology of SE Arabian deserts. *Quaternary Science Reviews,* 21**,** 853-869.

GOETZ, A. F. & ROWAN, L. C. 1981. Geologic remote sensing. *Science,* 211**,** 781-791.

GOETZ, A. F. H. 2009. Three decades of hyperspectral remote sensing of the Earth: A personal view. *Remote Sensing of Environment,* 113, Supplement 1**,** S5-S16.

GOODALL, T. M. 1995. *The geology and geomorphology of the Sabkhat Matti region (United Arab Emirates): a modern analogue for ancient desert sediments from north-west Europe.* University of Aberdeen.

GOUDIE, A. S., COLLS, A., STOKES, S., PARKER, A., WHITE, K. & AL-FARRAJ, A. 2000. Latest Pleistocene and Holocene dune construction at the north-eastern edge of the Rub Al Khali, United Arab Emirates. *Sedimentology,* 47**,** 1011-1021.

GUÉRIN, G., MERCIER, N. & ADAMIEC, G. 2011. Dose-rate conversion factors: update. *Ancient TL,* 29**,** 5-8.

GUPTA, R. P. 2003. *Remote Sensing Geology.* 2nd edition ed. Berlin: Heidelberg, Springer.

HAMAD, S. 2010. Spatial and morphometric analysis of the wadi Al Lawlab basin areas using RS and GIS techniques. *Journal of remote sensing***,** 1-9.

HAMDAN, S. & ABU AMRAH, S. 2010. Some Morphometric Properties of the Upper Part of the Basin In Jordan Using Traditional Methods and GIS Software. *Journal of Al - Azhar University,* 12**,** 620-959.

HERVÁS, J., BARREDO, J. I., ROSIN, P. L., PASUTO, A., MANTOVANI, F. & SILVANO, S. 2003. Monitoring landslides from optical remotely sensed imagery: the case history of Tessina landslide, Italy. *Geomorphology,* 54**,** 63-75.

HIVELY, W. D., MCCARTY, G. W., REEVES, J. B., LANG, M. W., OESTERLING, R. A. & DELWICHE, S. R. 2011. Use of airborne hyperspectral imagery to map soil properties in tilled agricultural fields. *Applied and Environmental Soil Science,* 2011.

HOOGHIEMSTRA, H. 1988. Changes of major wind belts and vegetation zones in NW Africa 20,000–5000 yr BP, as deduced from a marine pollen record near Cap Blanc. *Review of Palaeobotany and Palynology,* 55**,** 101-140.

HÖTZL, H. & ZÖTL, J. 1978. Climatic changes during the Quaternary period. *Quaternary Period in Saudi Arabia.* Springer.

HUCKREIDE, R. & WIESEMAN, G. 1968. Der jungpleistozäne pluvial-see von El-Jafr und weitere daten zum Quartär Jordaniens. *Geologica et Palaeontologica,* 2**,** 73–95.

HUGENHOLTZ, C. H., LEVIN, N., BARCHYN, T. E. & BADDOCK, M. C. 2012. Remote sensing and spatial analysis of aeolian sand dunes: A review and outlook. *Earth-Science Reviews,* 111**,** 319-334.

HUNT, G. & SALISBURY, J. 1970. Visible and Infrared Spectra of Minerals and Rocks. II: Carbonate. *Modern Geology,* 2**,** 23-30.

HUNT, G. R. 1977. Spectral signatures of particulate minerals in the visible and near infrared. *Geophysics,* 42**,** 501-513.

HUNT, G. R. & SALISBURY, J. W. 1971. Visible and near infrared spectra of minerals and rocks. II. Carbonates. *Modern Geology,* 2**,** 23-30.

ILWIS TUTORIAL.

JOHNSON, T. C., KELTS, K. & ODADA, E. 2000. The holocene history of Lake Victoria. *AMBIO: A Journal of the Human Environment,* 29**,** 2-11.

JUYAL, N., SINGHVI, A. & GLENNIE, K. 1998. Chronology and paleoenvironmental significance of Quaternary desert sediment in southeastern Arabia. *Quaternary Deserts and Climatic Change: Rotterdam, The Netherlands, Balkema***,** 315-325.

KARBAL, A. 2011. *Science of earth forms, geomorphology,* Beirut, Al Dar Al namouthajiyah Publishing, Beirut, Lebanon.

KINGDOM OF SAUDI ARABIA DEPUTY MINISTRY FOR MINERAL RESOURCES. 1981. *Al Madinah Geological maps*, 1:250,000 KSA: Kingdom of Saudi Arabia Deputy Ministry for Mineral Resources,

.

KOGALY, M. & AL BESHI, M. 1998. Climte. *In:* AL RWATHI, M. & KOGALY, M. (eds.) *Man and his Environment in Al-Madinah Al-Munawwarah.* Al-Madinah: Dar Alwaha Al Arabia.

LANDSAT, U. 2016. 8 (l8) data users handbook. LSDS-1574.

LEVERINGTON, D. W. 2010. Discrimination of sedimentary lithologies using Hyperion and Landsat Thematic Mapper data: a case study at Melville Island, Canadian High Arctic. *International Journal of Remote Sensing,* 31**,** 233-260.

LÉZINE, A.-M., SALIEGE, J.-F., ROBERT, C., WERTZ, F. & INIZAN, M.-L. 1998. Holocene lakes from Ramlat as-Sab'atayn (Yemen) illustrate the impact of monsoon activity in southern Arabia. *Quaternary Research,* 50**,** 290-299.

LÉZINE, A.-M., TIERCELIN, J.-J., ROBERT, C., SALIÈGE, J.-F., CLEUZIOU, S., INIZAN, M.-L. & BRAEMER, F. 2007. Centennial to millennial-scale variability of the Indian monsoon during the early Holocene from a sediment, pollen and isotope record from the desert of Yemen. *Palaeogeography, Palaeoclimatology, Palaeoecology,* 243**,** 235-249.

LILLESAND, T. M., KIEFER, R. W. & CHIPMAN, J. W. 2008. *Remote Sensing and Image Interpretation,* New Jersey, John Wiley & Sons, Inc.

LIU, J. G. & MASON, P. J. 2016. *Image Processing and GIS for Remote Sensing: Techniques and Applications*, Wiley.

MADANI, A. A. 2011. Spectral properties of carbonatized ultramafic mantle xenoliths and their host olivine basalts, Jabal Al Maqtal basin, South Eastern Desert, Egypt, using ASD FieldSpec spectroradiometer. *The Egyptian Journal of Remote Sensing and Space Science,* 14**,** 41-48.

MAHSOUB, M., ARBAB, M. & AL GHAMDI, A. 1999. *Studies in the Geography of the Kingdom, Natural Aspects,* Cairo, Dar Elfikr Alarabi.

MANN, L. M., GOOD, S. M., NICHOLSON, A. M. & WOODARD, M. A. 2012. Landsat Data Continuity Mission (LDCM) Safe Operations Ascent Design.

MANTOVANI, F., SOETERS, R. & VAN WESTEN, C. J. 1996. Remote sensing techniques for landslide studies and hazard zonation in Europe. *Geomorphology,* 15**,** 213-225.

MATHIEU, R., CERVELLE, B., RÉMY, D. & POUGET, M. 2007. Field-based and spectral indicators for soil erosion mapping in semi-arid mediterranean environments

(Coastal Cordillera of central Chile). *Earth Surface Processes and Landforms,* 32**,** 13-31.

MCCARTY, G., REEVES, J., REEVES, V., FOLLETT, R. & KIMBLE, J. 2002. Mid-infrared and near-infrared diffuse reflectance spectroscopy for soil carbon measurement. *Soil Science Society of America Journal,* 66**,** 640-646.

MCCLURE, H. 1976. Radiocarbon chronology of late Quaternary lakes in the Arabian Desert. *Nature,* 263**,** 755-756.

MCCLURE, H. A. 1984. *Late Quaternary palaeoenvironments of the Rub'Al Khali.* University College London (University of London).

MCLAREN, S. J., AL-JUAIDI, F., BATEMAN, M. D. & MILLINGTON, A. C. 2009. First evidence for episodic flooding events in the arid interior of central Saudi Arabia over the last 60 ka. *Journal of Quaternary Science,* 24**,** 198-207.

MEJDAHL, V. 1979. Thermoluminescence dating: Beta-dose attenuation in quartz grains. *Archaeometry,* 21**,** 61-72.

MILLINGTON, A. & TOWNSHEND, J. 1987. The potential of satellite remote sensing for geomorphological investigations: an overview. *International Geomorphology, Wiley, Chichester***,** 331-342.

MINISTRY OF AGRICULTURE AND WATER 1984. *The soils atlas of Saudi Arabia,* Saudi Arabia, Ministry of Agriculture and Water.

MOHAMMAD, R. 2008. *Geographical Information System Based Analysis of Paleofluvial Systems in the Kuwait Region.* University of Pittsburgh.

MONSERUD, R. A. & LEEMANS, R. 1992. Comparing global vegetation maps with the Kappa statistic. *Ecological modelling,* 62**,** 275-293.

MULDER, V., DE BRUIN, S., SCHAEPMAN, M. & MAYR, T. 2011. The use of remote sensing in soil and terrain mapping—A review. *Geoderma,* 162**,** 1-19.

MURRAY, A. S. & WINTLE, A. G. 2000. Luminescence dating of quartz using an improved single-aliquot regenerative-dose protocol. *Radiation measurements,* 32**,** 57-73.

MURRAY, A. S. & WINTLE, A. G. 2003. The single aliquot regenerative dose protocol: potential for improvements in reliability. *Radiation measurements,* 37**,** 377-381.

MUSHKIN, A. & GILLESPIE, A. 2005. Estimating sub-pixel surface roughness using remotely sensed stereoscopic data. *Remote Sensing of Environment,* 99**,** 75-83.

MUZEIN, B. S. 2006. Remote sensing & GIS for land cover/land use change detection and analysis in the semi-natural ecosystems and agriculture landscapes of the Central Ethiopian Rift Valley.

NADERI KHORASGANI, M. & DE DAPPER, M. 2010. Evaluation of the capability of Landsat MSS data for mapping landforms in arid regions: a case study in the centre of Iran. *Journal of Agricultural Science and Technology,* 11**,** 67-80.

NANNI, M. R. & DEMATTÊ, J. A. M. 2006. Spectral Reflectance Methodology in Comparison to Traditional Soil Analysis. *Soil Science Society of America Journal,* 70.

NASA. 2013. Available: https://landsat.gsfc.nasa.gov/landsat-8/landsat-8-bands/ [Accessed 30 February , 2013 2013].

NASH, D. J., BATEMAN, M. D., BULLARD, J. E. & LATORRE, C. 2018. Late Quaternary coastal evolution and aeolian sedimentation in the tectonically-active southern Atacama Desert, Chile. *Palaeogeography, Palaeoclimatology, Palaeoecology,* 490**,** 546-562.

NATHAN, R. & MAUZ, B. 2008. On the dose-rate estimate of carbonate-rich sediments for trapped charge dating. *Radiation Measurements,* 43**,** 14-25.

NEFF, U., BURNS, S., MANGINI, A., MUDELSEE, M., FLEITMANN, D. & MATTER, A. 2001. Strong coherence between solar variability and the monsoon in Oman between 9 and 6 kyr ago. *Nature,* 411**,** 290-293.

NICOLL, K. 2001. Geoarchaeology of Umm Akhtar playa: early holocene palaeoenvironments of South Egypt. *Archaeological Geology NO125*.

O'NEIL, N. T., ZAGOLSKI, F., BERGERON, M., ROYER, A., MILLER, J. R. & FREEMANTLE, J. 1997. Atmospheric correction validation of CASI images acquired over the BOREAS Southern Study Area. *Canadian Journal of Remote Sensing (Special Issue: BOREAS),* 23 (2)**,** 143-162.

ORTIZ, J., GUILDERSON, T., ADKINS, J., SARNTHEIN, M., BAKER, L. & YARUSINSKY, M. 2000. Abrupt onset and termination of the African Humid Period:: rapid climate responses to gradual insolation forcing. *Quaternary science reviews,* 19**,** 347-361.

OTTO, J.-C. & SMITH, M. J. 2013. Geomorphological mapping. *Geomorphological techniques*.

PARKER, A. 2009. Pleistocene climate change in Arabia. Developing a framework for Hominin dispersal over the last 350 kyr. *Springer Science +Business Media*, 39-49.

PARKER, A., ECKERSLEY, L., SMITH, M., GOUDIE, A., STOKES, S., WARD, S., WHITE, K. & HODSON, M. 2004. Holocene vegetation dynamics in the northeastern Rub'al-Khali desert, Arabian Peninsula: a phytolith, pollen and carbon isotope study. *Journal of Quaternary Science,* 19**,** 665-676.

PARKER, A., PRESTON, G., WALKINGTON, H. & HODSON, M. 2006. Developing a framework of Holocene climatic change and landscape archaeology for the lower Gulf region, southeastern Arabia. *Arabian archaeology and epigraphy,* 17**,** 125-130.

PELLATON, C. 1981. Geologic Map of the Al Madinah Quadrangle, Sheet 24D,Kingdom of Saudi Arabia Deputy Ministry for Mineral Resources Geologic Map GM-52C,Scale 250,000, with text.

PETIT-MAIRE, N., CARBONEL, P., REYSS, J.-L., SANLAVILLE, P., ABED, A., BOURROUILH, R., FONTUGNE, M. & YASIN, S. 2010. A vast Eemian palaeolake in Southern Jordan (29 N). *Global and Planetary Change,* 72**,** 368-373.

PETRAGLIA, M. D., DRAKE, N. & ALSHAREKH, A. 2010. Acheulean landscapes and large cutting tools assemblages in the Arabian Peninsula. *The evolution of human populations in Arabia.* Springer.

PRESCOTT, J. R. & HUTTON, J. T. 1994. Cosmic ray contributions to dose rates for luminescence and ESR dating: large depths and long-term time variations. *Radiation measurements,* 23**,** 497-500.

PRESIDENCY OF METEOROLOGY AND ENVIRONMENT PROTECTION 2014. *The annual climatological elements in the Study Area for the Period 1970 to 2014,* Jeddah, Presidency of Meteorology and Environment Protection

PREUSSER, F., RADIES, D., DRIEHORST, F. & MATTER, A. 2005. Late Quaternary history of the coastal Wahiba sands, Sultanate of Oman. *Journal of Quaternary Science,* 20**,** 395-405.

PREUSSER, F., RADIES, D. & MATTER, A. 2002. A 160,000-year record of dune development and atmospheric circulation in southern Arabia. *Science,* 296**,** 2018-2020.

QARI, M. & BASYOUNI, M. 2003. *Using Landsat-TM Images in Mapping. Al-Majnonah, Sabkaha Distribution Along the Red Sea Coast, Southeast of Al-Lith, Kingdom of Saudi Arabia,* Jeddah, King Abdulaziz University.

RAO, D. 2002. Remote sensing application in geomorphology. *Tropical Ecology,* 43**,** 49-59.

RIVARD, B., ARVIDSON, R., DUNCAN, I., SULTAN, M. & EL KALIOUBY, B. 1992. Varnish, sediment, and rock controls on spectral reflectance of outcrops in arid regions. *Geology,* 20**,** 295-298.

ROBERTSON, K. M., MILLIKEN, R. E. & LI, S. 2016. Estimating mineral abundances of clay and gypsum mixtures using radiative transfer models applied to visible-near infrared reflectance spectra. *Icarus,* 277**,** 171-186.

ROMKENS, M. & WANG, J. 1987. Soil roughness changes from rainfall. *Transactions of the ASAE,* 30**,** 101-0107.

ROSKIN, J., PORAT, N., TSOAR, H., BLUMBERG, D. G. & ZANDER, A. M. 2011. Age, origin and climatic controls on vegetated linear dunes in the northwestern Negev Desert (Israel). *Quaternary Science Reviews,* 30**,** 1649-1674.

ROSSEL, R. V., WALVOORT, D., MCBRATNEY, A., JANIK, L. J. & SKJEMSTAD, J. 2006. Visible, near infrared, mid infrared or combined diffuse reflectance spectroscopy for simultaneous assessment of various soil properties. *Geoderma,* 131**,** 59-75.

ROWAN, L. C., ANTON-PACHECO, C., BRICKEY, D. W., KINGSTON, M. J., PAYAS, A., VERGO, N. & CROWLEY, J. K. 1987. Digital classification of contact metamorphic rocks in Extremadura, Spain, using Landsat thematic mapper data. *Geophysics,* 52**,** 885-897.

SAFI, M. & QARI, M. 1996. Application of Landsat Thematic Mapper Data in Sabkha Studies at the Red Sea Coast. *Remote Sensing Magazine,* 1**,** 63-74.

SAHWAN, W. 2007. *Geomorphological Studies Using GIS and Remote Sensing with Considering Some Hydrological Issues.* PhD.

SALAMA, H. 2013. *principles of geomorphology,* Jordan, Dar Al Massira.

SALISBURY, J. W. & D'ARIA, D. M. 1992. Infrared (8–14 μm) remote sensing of soil particle size. *Remote Sensing of Environment,* 42**,** 157-165.

SAUDI GEOLOGICAL SURVEY 2012. *Kingdom of Saudi Arabia Facts and Figures*

jeddah, Saudi Geological Survey.

SCHOWENGERDT, R. 2007. Remote sensing, models and methods for image processing., Elservier Inc. *New York, USA*.

SCHOWENGERDT, R. A. R. A. 1983. *Techniques for image processing and classification in remote sensing*.

SCHULZ, E. & WHITNEY, J. 1986. Vegetation in north-central Saudi Arabia. *Journal of arid environments*.

SCHULZ, E. & WHITNEY, J. W. 1987. Upper pleistocene and holocene lakes in the an Nafud, Saudi Arabia. *Paleolimnology IV*. Springer.

SCHWERTMANN, U. 1993. Relations between iron oxides, soil color, and soil formation. *Soil color*, 51-69.

SELIGE, T., BÖHNER, J. & SCHMIDHALTER, U. 2006. High resolution topsoil mapping using hyperspectral image and field data in multivariate regression modeling procedures. *Geoderma,* 136, 235-244.

SHAW, G. A. & BURKE, H. K. 2003. Spectral imaging for remote sensing. *Lincoln Laboratory Journal,* 14, 3-28.

SHEPHERD, K. D. & WALSH, M. G. 2002. Development of reflectance spectral libraries for characterization of soil properties. *Soil science society of America journal,* 66, 988-998.

SLAYMAKER, O. 2001. The role of remote sensing in geomorphology and terrain analysis in the Canadian Cordillera. *International Journal of Applied Earth Observation and Geoinformation,* 3, 11-17.

SMITH, M. & PAIN, C. 2009. Applications of remote sensing in geomorphology. *Progress in Physical Geography,* 33, 568-582.

SMITH, M. O., JOHNSON, P. E. & ADAMS, J. B. 1985. Quantitative determination of mineral types and abundances from reflectance spectra using principal components analysis. *Journal of Geophysical Research: Solid Earth,* 90.

SOLOMON, J. & ROCK, B. 1985. Imaging spectrometry for earth remote sensing. *Science,* 228, 1147-1152.

SORIANO-DISLA, J. M., JANIK, L. J., VISCARRA ROSSEL, R. A., MACDONALD, L. M. & MCLAUGHLIN, M. J. 2014. The Performance of Visible, Near-, and Mid-

Infrared Reflectance Spectroscopy for Prediction of Soil Physical, Chemical, and Biological Properties. *Applied Spectroscopy Reviews,* 49**,** 139-186.

SPINETTI, C., MAZZARINI, F., CASACCHIA, R., COLINI, L., NERI, M., BEHNCKE, B., SALVATORI, R., FABRIZIA, B. & PARESCHI, M. 2009. Spectral properties of volcanic materials from hyperspectral field and satellite data compared with LiDAR data at Mt. Etna. *International Journal of Applied Earth Observation and Geoinformation,* 11**,** 142-155.

STOKES, S. & BRAY, H. E. 2005. Late Pleistocene eolian history of the Liwa region, Arabian Peninsula. *Geological Society of America Bulletin,* 117**,** 1466-1480.

STOKES, S., THOMAS, D. S. & WASHINGTON, R. 1997. Multiple episodes of aridity in southern Africa since the last interglacial period. *Nature,* 388**,** 154.

STONER, E. R. & BAUMGARDNER, M. 1981. Characteristic variations in reflectance of surface soils. *Soil Science Society of America Journal,* 45**,** 1161-1165.

STRAHLER, A. H. & JUPP, D. L. B. 1990. Geometric-optical modelling of forests as remotely sensed scenes composed of threedimensional, discrete objects. In: Myneni, R., Ross, J. (Eds.), Photon-Vegetation Interactions: Applications in Optical Remote Sensing and Plant Ecology. *Springer, Heidelberg, Germany***,** 162-190.

SUBRAMANIAN, S., GAT, N., RATCLIFF, A. & EISMANN, M. Real-time hyperspectral data compression using principal components transformation. In Proceedings of the AVIRIS Earth Science & Applications Workshop, 2000. Citeseer.

SULTAN, M., ARVIDSON, R. E., STURCHIO, N. C. & GUINNESS, E. A. 1987. Lithologic mapping in arid regions with Landsat thematic mapper data: Meatiq dome, Egypt. *Geological Society of America Bulletin,* 99**,** 748-762.

TALBAH, S. 2002. *The Climate of Al Madinah and its Economic Effects,* Jeddah, Al Madinah Press institution (Dar Al Alam).

THOMAS, D. S. 2011. *Arid zone geomorphology: process, form and change in drylands*, John Wiley & Sons.

TOOTH, S. 2000. Process, form and change in dryland rivers: a review of recent research. *Earth-Science Reviews,* 51**,** 67-107.

TOOTH, S. & MCCARTHY, T. S. 2007. Wetlands in drylands: geomorphological and sedimentological characteristics, with emphasis on examples from southern Africa. *Progress in Physical Geography,* 31**,** 3-41.

TSOAR, H. & PYE, K. 2009. *Aeolian sand and sand dunes*, Springer Berlin Heidelberg.

TUCKER, M. 1988. *Techniques in sedimentary,* London, Blackwell Science Ltd.

USGS. 2013. Available: https://landsat.usgs.gov/using-usgs-landsat-8-product [Accessed 30 May, 2013.

VICENTE, L. E. & DE SOUZA FILHO, C. R. 2011. Identification of mineral components in tropical soils using reflectance spectroscopy and advanced spaceborne thermal emission and reflection radiometer (ASTER) data. *Remote Sensing of Environment,* 115**,** 1824-1836.

VINCENT, R. K. 1997. Fundamentals of Geological and Environmental Remote Sensing: Upper Saddle River, NJ: Prentice-Hall, Inc.

WARNE, A. G. & STANLEY, D. J. 1993. Late Quaternary evolution of the northwest Nile delta and adjacent coast in the Alexandria region, Egypt. *Journal of Coastal Research***,** 26-64.

WEIJERMARS, R. 1997. *Structural geology and map interpretation*, Alboran Science Publishing.

WHITE, K., GOUDIE, A., PARKER, A. & AL-FARRAJ, A. 2001. Mapping the geochemistry of the northern Rub'Al Khali using multispectral remote sensing techniques. *Earth Surface Processes and Landforms,* 26**,** 735-748.

WHITE, K., WALDEN, J. & GURNEY, S. D. 2007. Spectral properties, iron oxide content and provenance of Namib dune sands. *Geomorphology,* 86**,** 219-229.

WHITNEY, J. W., FAULKENDER, D. & RUBIN, M. 1983. *The environmental history and present condition of the northern sand seas of Saudi Arabia*, Ministry of Petroleum and Mineral Resources, Deputy Ministry for Mineral Resources.

WINTLE, A. G. & MURRAY, A. S. 2006. A review of quartz optically stimulated luminescence characteristics and their relevance in single-aliquot regeneration dating protocols. *Radiation measurements,* 41**,** 369-391.

YE, H., CHEN, C. & YANG, C. 2017. Atmospheric Correction of Landsat-8/OLI Imagery in Turbid Estuarine Waters: A Case Study for the Pearl River Estuary. *IEEE Journal of Selected Topics in Applied Earth Observations and Remote Sensing,* 10**,** 252-261.

ZANI, H., ASSINE, M. L. & MCGLUE, M. M. 2012. Remote sensing analysis of depositional landforms in alluvial settings: method development and application to the Taquari megafan, Pantanal (Brazil). *Geomorphology,* 161**,** 82-92.